A Study of Pronephric-Glomerular Morphogenesis in Zebrafish

Chiu-Ju Huang

2009

Declaration

I hereby declare that this thesis is entirely my own composition. The experimental work described in this thesis had been exclusively performed by myself, unless stated in the text. I also declare that the contents of this thesis have not been submitted for any other degree of professional qualification.

Chiu-Ju Huang

30 March 2009

'I would say that in my scientific and philosophic work, my main concern has been with understanding the nature of reality in general and of consciousness in particular as a coherent whole, which is never static or complete, but which is in an unending process of movement and unfoldment.'

David Bohm, Wholeness and the Implicate Order

Acknowledgements

It was a great opportunity for me to join this incredible Institute, Centre for Cardiovascular Science, on the Wellcome Trust 4-Year PhD program. Edinburgh is a wonderful place to live and work. These four years of doing my PhD were a truly great period in my life. First of all, I am grateful to Professor John Mullins for recruiting me to the program and for the support from the Wellcome Trust. I would like to thank you all whom I worked with during this time, for giving me good suggestions and making it so special. In addition I would like to give special thanks to Dr Val Wilson and Dr Sari Pennings for help with my matriculation.

I am grateful to those people listed in Table 231 who shared helpful plasmids and to Ms Ellen Scott for assistance in preparation of personal license-mouse & rat. Many thanks to Dr Carl Tucker and Mr Sanjay Thakrar for the help in preparation of personal license-fish and for transporting the mutant zebrafish embryos from Sheffield. Many thanks to the Zebrafish Facility in the MRC Centre for DBG at the University of Sheffield for providing the mutant zebrafish embryos.

I would like to thank Ms Ching-Wen Cheng, Heck's Lab for her help and giving good suggestions in the immunostaining work. My thanks also go to all the present, and former, members of the Molecular Physiology Lab for creating a warm and pleasant atmosphere, for encouraging me, for listening, when I needed to talk about work, for giving good suggestions and for all the fun we had in and out of the laboratory. Special thanks to Ms Patricia Smart for lots of help in the Lab and in the zebrafish facility. Many thanks to Dr Xiaojun Liu and Mrs Nina Kotelevtseva for

their suggestions on the molecular biology experiments. Special thanks to Mr Mike Miller, Ms Arantza Esnal and Ms Shila MacPheron, MRC Human Reproductive Sciences Unit, Histology and Imaging Facility, for their help with confocal imaging.

Many thanks to all the friends inside and outside of the CVS for the great time we had together. I will miss you all! Very special thanks to Dr Chih-Ying Su, Yale University and Ms Carol Bassett, Cambridge, for cheering me up when things did not work and helping me with my English language study.

I dedicate this thesis to my family, who are always there for me.

Contents

List Of Figures

List Of Tables

Abbreviations

§: Chapter
E: days post coitum (dpc, mouse embryo)
EMT: epithelial-mesenchymal transition
Epo: *erythropoietin* (gene)
EVL: enveloping layer
FGF: *fibroblast growth factor* (gene; signalling pathway)
Flh: *floating head* (gene)
Flk1: *vascular endothelial growth factor receptor* 2 (*vegr*2, gene)
FISH: fluorescence *in situ* hybridization
Gli2a: *GLI-Kruppel family member 2a* (gene)
hpf: hour-post fertilization (zebrafish embryo)
dpf: day-post fertilization (zebrafish embryo)
dph: day-post hatching (medaka embryo)
IM: immunostaining
JAK-STAT: *Janus kinase-signal transducers and activators of transcription* (gene; signalling pathway)
LIM: *lens intrinsic membrane protein* (gene)
Lim1: *LIM-class* homeobox 1 (*lhx*1, gene)
Mesendoderm: mesoderm and endoderm
MZ*oep*$^{-/-}$: lack of both maternal and zygotic Oep activity
Odd1: *odd-skipped related* 1 (*osr*1, gene)
Oep*: one-eyed pinhead* (gene)
Pax2: *paired-box* 2 (gene)
Pax8: *paired-box* 8 (gene)
PGP: pronephric glomerular primordium
Shha: *sonic hedgehog a* (gene)
Sim1: *single-minded* 1 (gene)
Spt*: spadetail* (gene)
Sqt: *squit* (gene)
Syu/Shha: *sonic you/sonic hedgehog a* (gene)
TRAP230/MED12: *mediator of RNA polymerase II transcription, subunit 12 homolog* (gene)
WISH: whole-mount *in situ* hybridization
Wnt: *wingless* (gene; signaling pathway)
Wt1: *Wilms' tumour* 1 (gene)
Yot/Gli2a: *you-too/GLI-Kruppel family member 2a* (gene)
YSL: yolk syncytial layer
Zoep$^{-/-}$: lack of zygotic Oep activity

Abstract

Midline convergence of organ primordia is an important mechanism for shaping the vertebrate body-plan at various stages of development, such as the morphogenesis of the heart and endoderm. Down regulation of *wnt* or noncanonical *wnt* signalling components, such as *dishelleved* (*Dvl*) or *RhoA GTPase* (*RhoA*), impairs midline convergence of the heart primordia and endoderm in zebrafish. This suggests that *wnt* signaling plays an important role in regulating midline convergence. At the early patterning stage of the zebrafish kidney, the two pronephric-glomerular primodia (PGP), which derive from intermediate mesoderm, converge towards the midline and fuse to form a functional pronephros. In contrast, during development of the mammalian kidney, the pronephros degenerates as the mesonephros develops without midline convergence. The hypothesis is thus that there is/are mechanisms underlying midline convergence of PGP in zebrafish, which is/are in addition to the control of the non-canonical *wnt/Dvl/RhoA* pathway and specific to kidney morphogenesis. In this study, the aim was to identify genetic factors that are specifically involved in the mechanism of PGP midline convergence by establishing a cell lineage tracing transgenic system with Cre-loxP, followed by the analysis of selected mutant embryos using the cell lineage tracing system, whole-mount *in situ* hybridization (WISH) and immunostaining.

The cell lineage tracing system was generated, and tested. Constructs, in which β-*actin* promoter drives the transcription of the reporter genes, were microinjected

into zebrafish embryos at 1- to 4-cell stages. The mRNAs in microinjected embryos (5 dpf) were analyzed by RT-PCR. The results show that the constructs induced indiscriminate alternative splicing. RNA splicing mechanisms were not affected by transcription termination when the polyA signal was located in *introns*.

To provide an alternative approach, three mutants were selected after screening of available ENU zebrafish mutants. These mutants were chosen not only because of their genetic importance in cell adhesion and motility but also because of their respective developmental defects in tissues surrounding the PGP, such as the notochord (*no tail, ntl*), somite (*spadetail, spt*), and endodermal tissues (zygotic *one-eyed pinhead, Zoep*). *Spt* and *ntl* are key targets of *fibroblast growth factor* (FGF) signalling in the trunk and tail respectively. EGP-CFC gene *oep* is a Nodal signalling cofactor.

Firstly, a rapid genotyping technique was developed, which was applied in identifying the mutant alleles. Since the tools for tracing PGP using transgenes were unavailable, the three mutants were analyzed by WISH and immunostaining. Zygotic mutation of *Zoep* causes a PGP midline convergence phenotype of variable severity due to maternal Oep effects. In more than 90% of $Zoep^{-/-}$ embryos, PGP midline convergence was impaired. Even though the abnormality could be observed as early as 15 hpf, the differentiation of the PGP was not affected. Heart primordial phenotypes were also observed but they did not correlate with that of the PGP phenotypes. Embryos homozygous for mutations in T-box transcription factors, *ntl* or *spt* had normal heart midline convergence phenotypes. PGP midline convergence abnormality was observed in $spt^{-/-}$ but not in $ntl^{-/-}$ prior to 36 hpf. In addition the extracellular matrix (ECM) might play a key role in the mechanisms of PGP midline

convergence.

Furthermore, PGP midline convergence proceeds from 10 hpf (the specification of intermediate mesoderm) to 48 hpf (fused pronephric glomerulus) in wild type zebrafish embryos. The process was quantified by 2D image analysis of the PGP distance. Prior to 18 hpf, PGP midline convergence is closely correlated with the midline convergence of mesoderm but not at later stages in *Zoep*$^{-/-}$. *Spt* is essential for PGP but not for cardiac primordium midline convergence. Data from this research suggests that there is not one universal mechanism, which controls all the midline convergence of organ primordia. Indeed, specific factors, which depend on tissues and development stages, are also required.

1. Introduction

1.1 Diversity In Kidney Morphology

The Head Kidney in Zebrafish

The kidney is an important organ. The main functions of kidneys, in the body, are firstly filtration of blood in order to excrete the toxic metabolic products and maintain homeostasis of body fluid and electrolytes, secondly the secretion of *erythropoietin* (Epo) to control the rate of formation of red blood cells and finally the secretion of Renin, an important enzyme in the control of blood pressure. Kidney morphology, however, is more diverse than kidney function between species. In adult zebrafish, the kidney consists of a fused head kidney (Fig 111, Fig 631), regarded as pronephros (Calderwood, 1891), and a trunk kidney (Fig 111, Fig 631), regarded as mesonephros (Lametschwandtner, 1995; Reimschussel, 2001). This differs from the morphology of two metanephric kidneys present in adult mammals (Fig 111). Interestingly another small fresh water teleost fish, medaka (*Oryzias latipes*) has the morphology of two separate kidneys (Fig 111).

Even though kidney morphology in zebrafish is strikingly different from that in mammals, the main functions of the kidney in zebrafish are similar to their mammalian counterparts. The vertebrate kidney is composed of numerous functional units, the nephrons, which are supported by connective tissue containing blood vessels, nerves and lymphatic vessels and arranged into the dedicated kidney architecture precisely (Guyton and Hall, 1996; Ross et al., 1996). Segmentation of the nephrons into distinct units is critical for kidney function (Fig 112). The zebrafish pronephric nephrons consist of multiple tubular segments similar to metanephric nephrons in the mouse (Wingert and Davidson, 2008; Wingert et al., 2007). The

pronephros in zebrafish is a functional blood filtration organ (Drummond et al., 1998). The gill and kidney share osmoregulatory functions in zebrafish (Nakada et al., 2007). Epo signalling is also functionally conserved in zebrafish (Chu et al., 2007; Paffett-Lugassy et al., 2007). Despite the functions of Renin in zebrafish being unclear (Nishimura et al., 1973), the *renin* gene has been characterized in this species (Liang et al., 2004). Renin mRNA expression in response to environmental salinity has been demonstrated (Hoshijima and Hirose, 2007). Furthermore, the zebrafish mutant from the *renin receptor* displayed reduced head size, central nervous system necrosis, hypopigmentation, and a lethal phenotype in early development (Amsterdam et al., 2004; Schefe et al., 2008).

Evolution of the Head Kidneys (Teleost Fish)

Kidney morphology in the *teleostei* shows even wider variety. The zebrafish (*Danio*), goldfish (*Carassius auratus*), pike (*Esoxlucius*) and anglerfish (*Lophius piscutorius*) have a fused head kidney (Balfour, 1882; Hall et al., 2007; Hsu et al., 2003; Sakai, 1985). The medaka (*Oryzias latipes*) and cichlid fish (*Cichlidae*) develop bilateral head kidneys (Fedorova et al., 2008; Fishelson, 1996). The Puffer fish (Tetraodontidae) is a type of aglomerular fish, with kidneys lacking glomeruli (Beyenbach, 2004). The evolution relationships for these six species are shown in Fig 114. Zebrafish and medaka both derived from their last common ancestor approximately 175 million years ago (mya) (Furutani-Seiki and Wittbrodt, 2004; Wittbrodt et al., 2002). This common ancestor most likely has the fused head kidney, for example pike and anglerfish that develop fused head kidney are more ancient

(125 and 90 mya) divided species (Muller, 2005) than medaka, 50 mya (Furutani-Seiki and Wittbrodt, 2004). The bilateral head kidney could have evolved from an apparently fused head kidney.

Embryological Renal Fusion Malformation in Humans

Remarkably, during evolution humans have not lost the genes for developing the single-body kidney, namely a type of renal congenital anomaly, regarded as a fusion anomaly, in which the two kidneys are fused together in early embryonic life. These congenital fusion anomalies can generally be categorized into two varieties (O'Brien et al., 2008): horseshoe kidneys (Fig 113) and crossed fused ectopia. The 'horseshoe' kidney refers to the morphology of a fusion of the lower poles of both kidneys at midline giving rise to a U-shaped kidney (Oktem et al., 2008). In crossed fused ectopia, the fused kidney lies on one side of the midline (Patel and Singh, 2008). Horseshoe kidney is the most common renal fusion malformation, occurring in approximately 1 in 500 persons (Yakeishi et al., 2007) and is more common in men (Yoshinaga et al., 2002). The causes of the horseshoe kidney are still to be elucidated. No genetic determinant has been reported, and cases of discordance of horseshoe kidney in identical twins (Hoyme et al., 1981; Kalra et al., 1985; Leiter, 1972) suggest the causes of the horseshoe kidney are not simply genetic.

This research project aims to discover the reason for the morphogenesis of the single head in zebrafish. The study of pronephric-glomerulus morphogenesis in zebrafish could provide a new insight into the formation of the renal anomalies in humans.

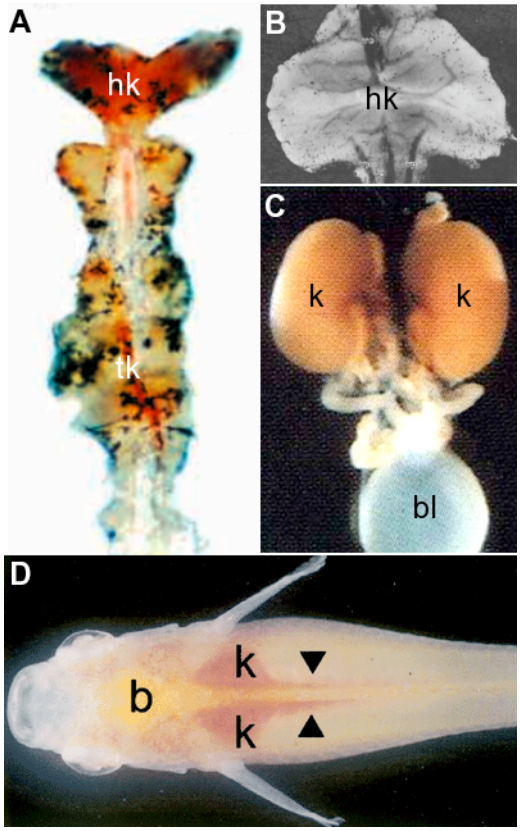

Figure 1-111. Diversity in adult kidney morphology.

(A) The zebrafish head kidney (hk) is located at the anterior of the kidney. The image is adapted from (Hsu et al., 2003). (B) Goldfish (*Carassius auratus*) is a species that is categorized in the same order, Ostariophysi, as zebrafish (classification scheme, Carolus Linnaeus). It also has the fused head kidney. A surface view of the head kidney of the goldfish is seen from the ventral side. The image was adapted from (Sakai, 1985). (C) The urinary rudiment of a 19 days p.c. mouse. The image was adapted from (Dudley et al., 1995). (D) This image is a dorsal view of a transparent madaka (adult female). The bilateral kidney structure is demonstrated (k). The image was adapted from (Mochizuki et al., 2005). Abbreviations are: b, brain; bl, bladder; hk, head kidney; k, kidney; tk, trunk kidney. Arrowheads show cylindric caudal parts of the kidney (trunk kidney). The images are not to scale.

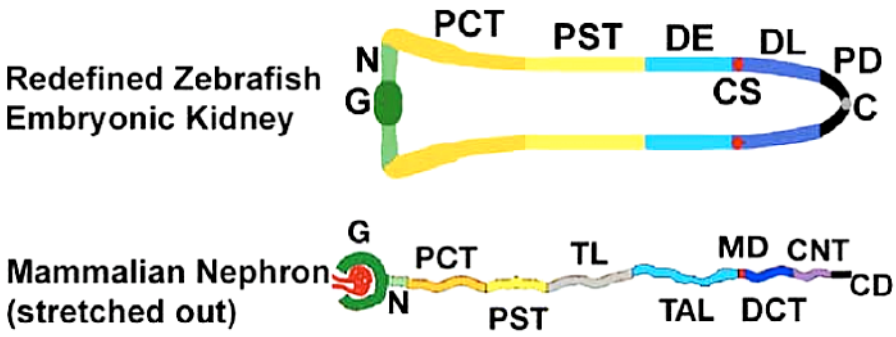

Figure 2-112. Segmentation of nephrons during embryonic development.

Nephrons possess a segmental organization where each segment is specialized for the secretion and reabsorption of particular solutes. Diagram of a recent model of the 48 hpf zebrafish pronephros (top), and a mammalian nephron stretched to compare segmentation of the metanephric nephron (bottom). Mammalian segments are colour coded according to observations of shared solute transporter expressions with respective zebrafish pronephros segments. Additional abbreviations are: C, cloaca; CD, collecting duct; CNT, connecting tubule; CS, corpuscle of Stannius; DCT, distal convoluted tubule; DE, distal early; DL, distal late; G, glomerulus; MD, macula densa; N, neck; PCT, proximal convoluted tubule; PD, pronephric duct; PST, proximal straight tubule; TAL, thick ascending limb and TL, thin limb. This figure was adapted from (Wingert et al., 2007).

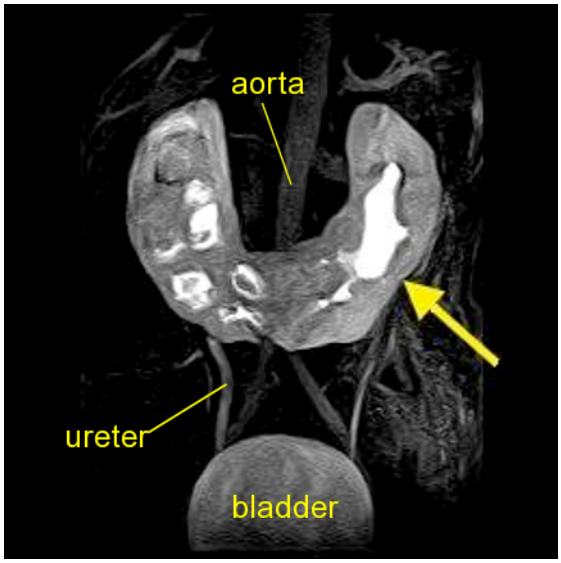

Figure 3-113. Horseshoe kidney.

This is an MRI image (coronal post-gadolinium, 3D-GRE image, maximum intensity projection) that depicts a horseshoe kidney. A horseshoe kidney is a congenital anomaly. In this condition, the kidneys are fused together in early embryonic life. The term “horseshoe kidney” is derived from the appearance of the fused kidneys (arrow). The ureters and the collecting system may develop normally.The image was adapted from the Progressive MRI website (http://progressivemri.com/case/horseshoe.htm).

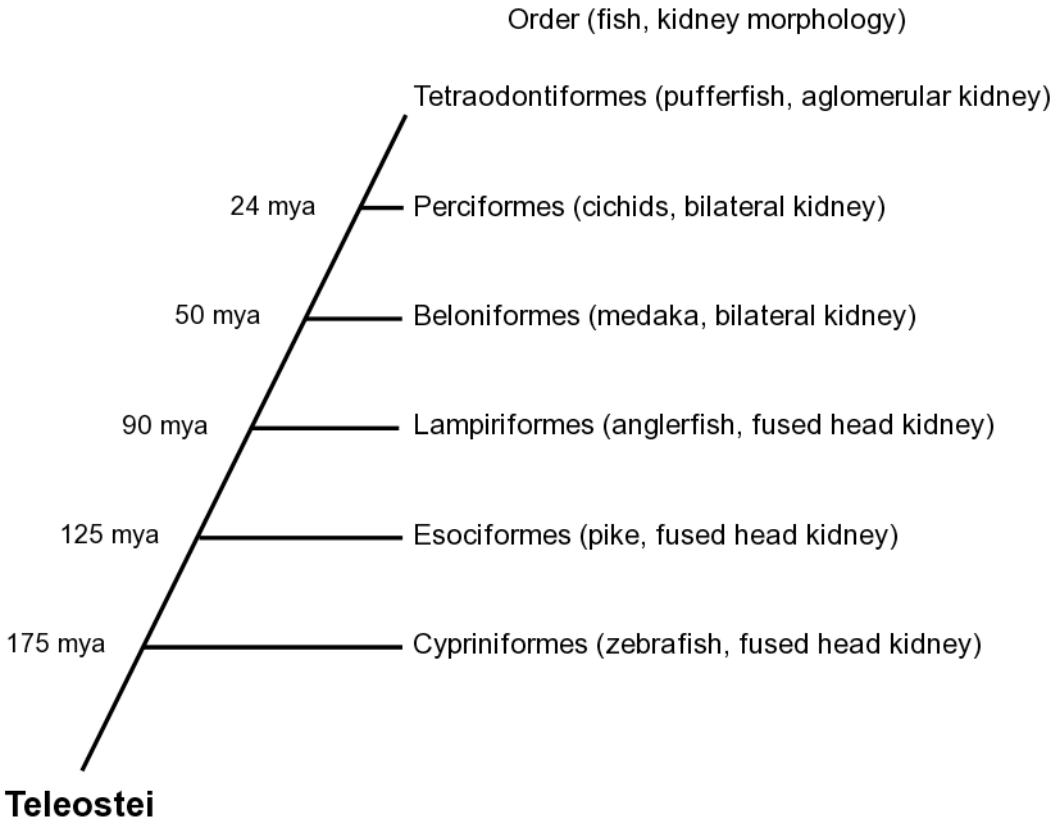

Figure 4-114. Evolutionary relationship between teleostei.

Six selected species, zebrafish, pike, anglerfish, medaka, cichids, and puffer fish, in teleostei are displayed by their order respectively (bold). This evolutionary tree illustrates that the common ancestor of the puffer fish and the cichids lived approximately 24 million years ago (mya). These six species have common ancestor more than approximately 175 mya. The diagram was edited from (Beyenbach, 2004; Diogo and Abdala, 2007; Furutani-Seiki and Wittbrodt, 2004; Muller, 2005; Wittbrodt et al., 2002)

1.2 Zebrafish As A Model For Vertebrate Development

The zebrafish (*Danio rerio*), a small fresh water teleost fish, has emerged as one of the eminent model systems for understanding embryonic development. Zebrafish have a relatively short generation time of 3 months. Hundreds of eggs are produced once per week for every mating pair. Zebrafish embryos, which are approximately 0.7 mm diameter chorion-shelled transparent eggs, develop outside the mother and hatch at 48 to 72 hpf, allowing easy visualization even of internal tissues. Furthermore, organogenesis occurs rapidly in zebrafish, major organs being present in larvae by 5 to 6 dpf (Rubinstein, 2003). These characters of zebrafish allow mutagenesis and screening strategies on a large scale, which is both economic and allows high-throughput, thus increasing the potential for zebrafish to model human diseases and aid drug discovery.

1.3 Embryonic Development of Zebrafish

Cleavage & Blastulation

During fertilization, the calcium wave initiated at fertilization stimulates the contraction of the cytoskeleton to squeeze yolk-free cytoplasm (blastodisc) into the animal pole of the egg (Leung et al., 1998). At this stage, regarded as 1-cell stage (Fig 131A), the egg is mostly yolk. The egg then undergoes meroblastic cleavages. Cleavage occurs only in the blastodisc, which then gives rise to blastoderm, but does not completely divide the egg. During cleavage, all the cells maintain an open connection between cells and also with the underlying yolk so that nutrition

molecules can pass freely (Kimmel and Law, 1985a; Kimmel and Law, 1985b). Blastula arises at the 128-cell stage. From approximately the tenth cell division, zygotic gene transcription begins and cell divisions slow down and loose synchronicity (Kane and Kimmel, 1993). Theoretically, prior to gastrulation, the blastoderm is a ball of a mixture of cells, any one blastomere can give rise to any types of tissue (Helde et al., 1994; Kimmel and Warga, 1987).

At the sphere stage (late blastulation, Fig 131B), the embryo can be divided into three distinct cell populations: the enveloping layer (EVL), the yolk syncytial layer (YSL) (Kimmel and Law, 1985b; Trinkaus, 1993) and the cells between these two layers, called deep cells. The fate of the blastoderm cells is fixed shortly before gastrulation begins. It means cells in specific regions of the embryo give rise to a certain tissue in a highly predictable manner (Kimmel et al., 1990) thus allowing a fate map (lineages of the germ layers) to be made. Arguably, a more recent report suggests that the zebrafish dorsal axis is determined at the 4-cell stage, based on the observation of asymmetrical *squit* (*sqt*) RNA expression and loss of dorsal structures by removal of cells containing transcripts from 4- to 8-cell embryos (Gore et al., 2005).

Gastrulation

Lewis Wolpert has been quoted, as saying “It is not birth, marriage or death, but gastrulation which is truly the most important time in your life.” During vertebrate gastrulation, massive cellular movements and rearrangement lead to the differentiation of the three germ layers, ectoderm, mesoderm and endoderm. The

movement is due to the expansion of the YSL, which joins tightly with EVL. It severing the attachment between the EVL and the yolk, the EVL and deep cells stay on the top of the yolk while the YSL expands (Chen and Kimelman, 2000; Trinkaus, 1992). Microtubules are shown essential for the expansion of the YSL, while the inactivation of polymerization of tubulin only partially inhibits the vegetal expansion of the EVL and deep cells (Solnica-Krezel and Driever, 1994). In addition, microfilaments are shown playing a key rule in the late epiboly (Cheng et al., 2004).

The shield stage (Fig 131C) is considered equivalent to amphibian organizer formation, which is critical in the regulation of dorsal-ventral axis formation (Koshida et al., 1998; Mizuno et al., 1999; Shinya et al., 1999). Interestingly, the anterior-posterior axis is specified during oogenesis. The animal cap marks the anterior of the embryo and directs central nervous system development (Houart et al., 1998; Thisse et al., 2000; Woo and Fraser, 1997).

Gastrulation movements in zebrafish can be classified into three categories, epiboly, internalization plus convergence and extension, based on the morphogenetic changes they produce. In epiboly the blastoderm thins and spreads to cover the yolk at the vegetal pole (Fig 131B, C). Radicl cell intercalations are thought to contribute to epibolic movements (Warga and Kimmel, 1990; Wilson et al., 1995). Cell internalization at the blastoderm margin separates prospective mesoderm and endoderm (mesendoderm) cells from the blastula surface (prospective ectodermal layer) and leads to the formation of distinct germ layers. At the margin, cells move internally from the outer blastodernal layers towards the yolk (Warga and Kimmel, 1990). The major cell behaviour driving internalization is involution (Fig 131C).

Subsequently, mesendoderm and neuroectoderm narrow towards, and extend along, the developing dorsal midline in the process of convergence and extension (Fig 131C, D). Cells at the ventral side of the embryo however do not converge on the dorsal side. They move towards the vegetal pole to eventually contribute to the tail bud (Myers et al., 2002a; Sepich et al., 2000). The YSL exhibits similar movement of mesendodermal and neuroectodermal cells (D'Amico and Cooper, 2001). Depending on location along the anterior-posterior axis, movement of lateral mesendoderm is subdivided into tissue giving rise to the head moving anterior and tissue giving rise to the trunk/tail moving posterior (Heisenberg and Tada, 2002; Sepich et al., 2005).

The last stage of gastrulation is the bud stage (Fig 131D), in which the yolk is completely covered by blastoderm and the dorsal axis (notochordal region) takes shape. A tail bud forms on the posterior of the dorsal axis 10-15 minutes after the yolk is completely covered by blastoderm (Kimmel et al., 1995). At this stage, the zebrafish embryo is ready for formation of somites.

Molecular Control of Gastrulation

Large-scale mutagenesis screening in zebrafish has been conducted to identify genes essential for embryonic or early development (Amsterdam et al., 2004; Haffter et al., 1996; Mullins et al., 1994). Mutants have been identified which exhibit morphogenic defects during gastrulation. For instance mutation of the *one-eyed pinhead* (*oep*) gene produces defects in endodermal cell specification and internalization movement (Carmany-Rampey and Schier, 2001). Another example, mutation of the *spadetail*

(*spt*) gene exhibits defects in paraxial mesoderm specification and convergence movement (Ho and Kane, 1990; Kimmel et al., 1989). Wnt signalling has been demonstrated which regulates convergent extension movements during zebrafish gastrulation (Heisenberg et al., 2000; Sepich et al., 2005). JAK/STAT and FGF signalling are also thought to be crucial for gastrulation (Griffin et al., 1998; Sepich et al., 2005; Smith et al., 1991; Yamashita et al., 2002).

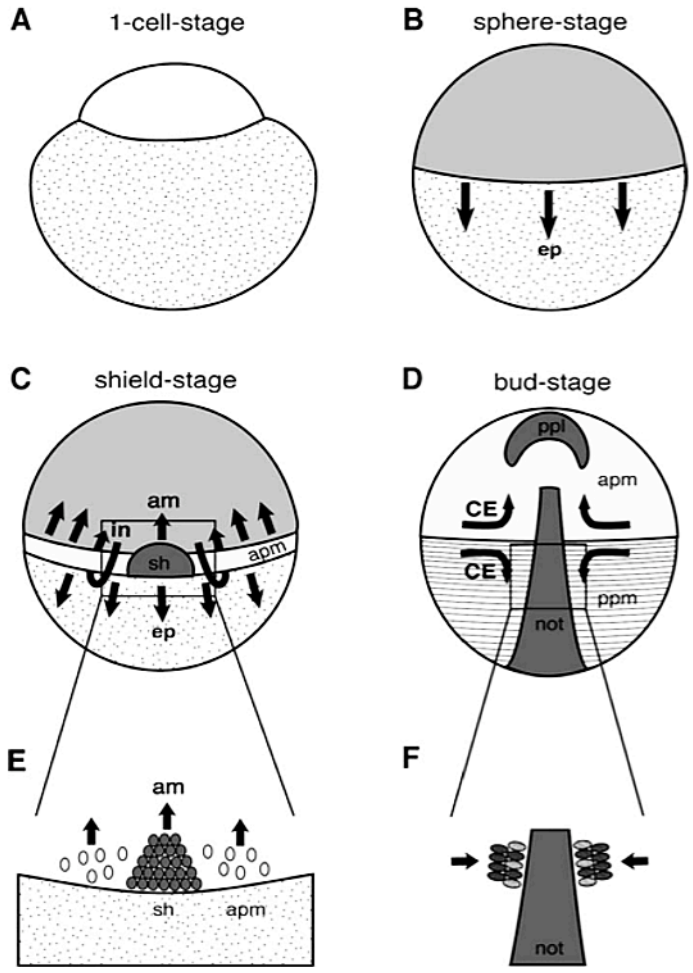

Figure 5-131. Cellular movements at different developmental stages in zebrafish embryos.
(A) After fertilization of the egg, cytoplasmic streaming leads to the formation of the first cell at the animal pole of the yolk sac. (B) At sphere stage, the cells of the epiblast (grey) start epibolic movements (ep) that cause a progressive spreading of the epiblast over the yolk sac. (C) At shield stage, involution (in) of the first prospective mesendodermal cells leads to the formation of axial (shield, sh) and anterior paraxial mesendodermal (apm) tissue, the cells of which migrate anteriorly (am) towards the animal pole. (D) At bud stage, convergent extension movements (CE) of both ectodermal and mesendodermal cells drive the progressive medio-lateral narrowing and anterior-posterior extension of the emerging embryonic body axis. The mesendoderm has been tentatively subdivided into anterior (apm) and posterior domains (ppm) based on their distinct cellular and molecular characteristics. (E) Close-up of the shield region shown in (C) illustrating the anterior migration (am) of axial (sh) and paraxial (apm) mesendodermal cells. (F) Close-up of the notochordal region (not) shown in (D) depicting medial-lateral cell intercalations of paraxial mesendodermal cells (ppm) that undergo convergent extension (CE) movements. This figure was adapted from (Heisenberg and Tada, 2002).

1.4 Considering The Early Development Of Vertebrates In A Comparative Context

Pre-gastrulation & Gastrulation

Patterns of pre-gastrulation in vertebrates are bewilderingly diverse. Zebrafish, *Xenopus* and chick embryos develop externally. Cleavage and early blastulation of these embryos rely on yolk energy supply and on maternally stored mRNA and proteins, prior to the activation of endogenous genes (Kane and Kimmel, 1993; Newport and Kirschner, 1982b; Zagris et al., 1998). After midblastula transition, the zygotic genome takes control. In contrast, mammalian embryos develop in the uterus. The yolk energy supply is minimal. Embryonic genome activation can be as early as the 2-cell stage (Kanka, 2003).

Cleavage cell divisions only take place on the animal cap and do not completely divide the egg in zebrafish and chick embryos (Fig 141A, C). Cleavage in frog embryos is holoblastic, completely dividing the egg (Fig 141B). The divisions begin at the animal pole and extend down into the vegetal region. The yolk is concentrated vegetally (Heasman, 2006; Lee et al., 2007). Mammalian embryos are the smallest among the vertebrates. The human zygote is less than one-thousandth the volume of a frog egg (Gilbert et al., 2000). Their cell divisions, named rotational holoblastic cleavage, are a relatively slow process and completely cleave blastomeres (Fig 141D) (Piotrowska and Zernicka-Goetz, 2002).

Vertebrate gastrulation transforms the unstructured blastula into the highly distinct architecture of ectoderm, mesoderm and endoderm between organisms (Fig 142). Subsequently, a cell's fate corresponds more to its location in the embryo and can be predicted by lineage tracing (Schoenwolf, 2001). Despite the bewildering

diversity of the history of pre- and gastrulation, there are three stereotyped morphogenetic movements shared by all vertebrates: epiboly, internalization, and convergence and extension. The main cell behaviours contributing to epiboly are radial cell intercalation (Warga and Kimmel, 1990; Wilson et al., 1995) and directed cell movement (Lin et al., 2005). The mesendoderm internalization is the major event defining gastrulation (Stainier, 2002; Warga and Stainier, 2002). Mesendodermal precursors move inside an embryo via the blastopore lip in frogs, the plastoderm margin in zebrafish and the primitive streak in birds and mammals (amniotes) (Fig 142). The cells move as a coherent sheet (involution or invagination) or move in an individually coordinated manner (ingression) through the blastopore (Trinkaus, 1996). This is thought to involve an epithelial-mesenchymal transition (EMT) (Solnica-Krezel, 2005). The convergence and extension narrow the embryo axis and elongate the vertebrate body. Convergence and extension movement can be independent or can be linked as convergence extension in terms of their underlying mechanisms (Keller et al., 2000; Myers et al., 2002b). The movements involve directed migration and mediolateral cell intercalations (Myers et al., 2002b; Warga and Kimmel, 1990).

Conserved Segmental Patterning of the Vertebrate Embryonic Axis

Unlike the huge diverse morphological patterns of pre- and gastrulation, segmental patterning of the body axis is relatively conserved in vertebrates (Fig 143A, B, C). Vertebrate body development is composed of repeating and non-repeating organ primordia (Cooke, 1975). Segmentation is a process of producing the series of

repeating segmental pattern, regarded as somites, from paraxial mesoderm (Fig 143D). The somites are produced from anterior to posterior, bilaterally and rhythmically (Dequeant and Pourquie, 2008). The total number of somites vary widely between species, approximately 30 pairs in zebrafish, 50 in chicks, 65 in mice or several hundreds in snakes (Richardson et al., 1998; Stickney et al., 2000).

The Major Lineages of the Mesoderm

The basis of studies in developmental biology is the evolution of anatomy during development. Which parts of the embryo form the kidney? The mesoderm of a neurula stage amniote (or segmental stage zebrafish) embryo further differentiates into five regions (Fig 143D). The body axis landmark, notochord, is derived from the chordamesoderm (axial mesoderm)(Glickman et al., 2003). The somites are derived from paraxial mesoderm (Barnes et al., 1997; Iimura et al., 2007). The kidneys are derived from intermediate mesoderm (Barak et al., 2005; James and Schultheiss, 2003). The heart, circulation system and lining of the body cavities are derived from lateral plate mesoderm (Abu-Issa and Kirby, 2008; Funayama et al., 1999). Finally, the head mesoderm forms the connective tissue and musculature of the head (Kiecker and Niehrs, 2001; Tzahor et al., 2003). As shown in Fig 144, the bilateral intermediate mesoderm (expressing *pax*2) is on both sides of the somites (expressing *paraxis*) in an 8-somite stage (31 hours) chick embryo (Denkers et al., 2004). This morphological pattern is similar among vertebrates at their comparable stages, i.e. 8-somite, 13 hpf in zebrafish; 8-12 somite pairs, E8.5 in mice (Serluca and Fishman, 2001; Tsang et al., 2000).

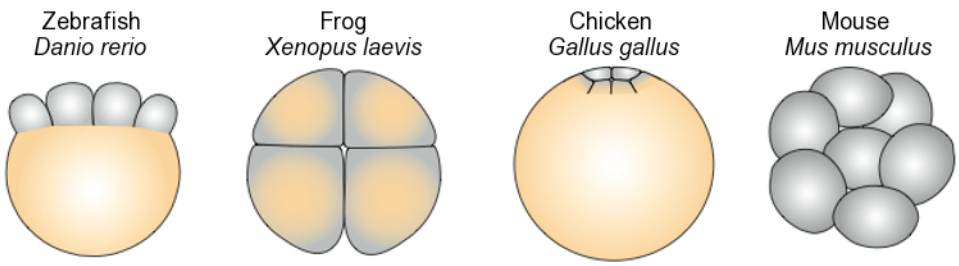

Figure 6-141. Cleavage stages of four vertebrate model organisms.
Zebrafish (A), frog (B), and chick (C) embryonic development relies on energy stored in the yolk (beige) and on maternal determinates deposited in the cytoplasm (grey) until the onset of utilization of zygotic genome. In contrast, mouse embryos (D) develop in the uterus, their zygotic genome is active at the 2-cell stage (Kanka, 2003). Zebrafish and chicken embryos undergo incomplete cleavage during cleavage stages. In the frog, the embryos divide completely with different sizes of blastomeres. In the mouse, the embryos undergo complete cleavage with uniformly sized blastomeres. Colours: grey, cytoplasm; beige, yolk. This figure is adapted from (Solnica-Krezel, 2005)

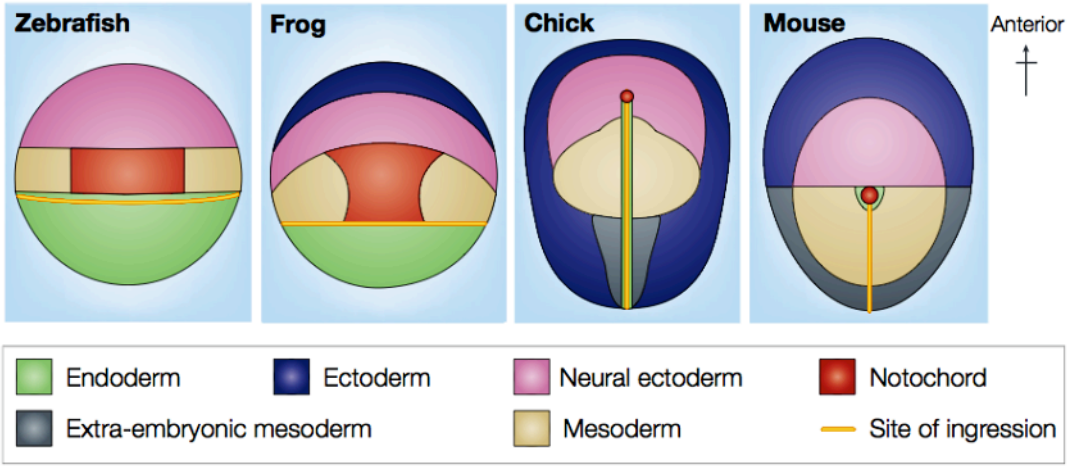

Figure 7-142. Prospective fate maps of gastrula stages of four vertebrate model organisms.
These prospective fate maps have been generated by a combination of many techniques, such as injection of vital fluorecent dyes into early embryos (Hatada and Stern, 1994) and transplantation of cells between embryos (Garcia-Martinez et al., 1993; Lopez-Sanchez et al., 2001). More recently, temporarilly and spatially targeted electroporation of cells in whole embryos was developed (Lopez-Sanchez et al., 2001; Timmer et al., 2001). This diagram is adapted from (Schoenwolf, 2001).

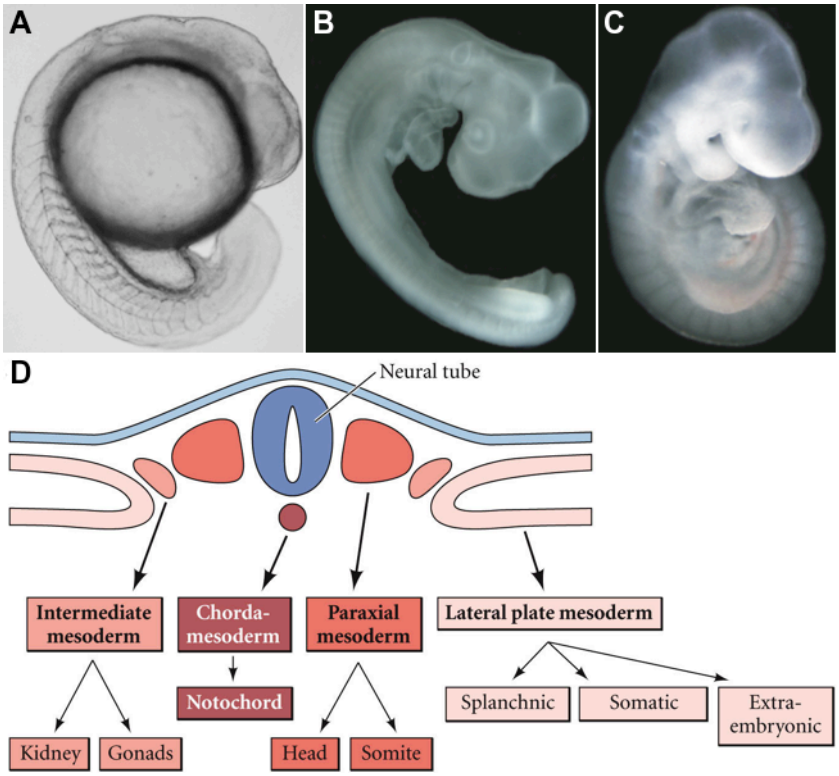

Figure 8-143. The major lineage of the mesoderm of a neurula stage embryo.

Lateral views of zebrafish (A), chick (B), and mouse (C) pharyngula. These images were adapted from (Solnica-Krezel, 2005). (D) A cross-section of a vertebrate embryo at neurula stage. The mesoderm of a neurula stage embryo can be divided into five regions: cordamesoderm/axial mesoderm (dark red), paraxial mesoderm (red), head mesenchyme (red), intermediated mesoderm (pink), and lateral plate mesoderm (light pink). The Kidney is derived from intermediate mesoderm. The heart is derived from lateral plate mesoderm. This illustration was adapted from (Gilbert et al., 2000).

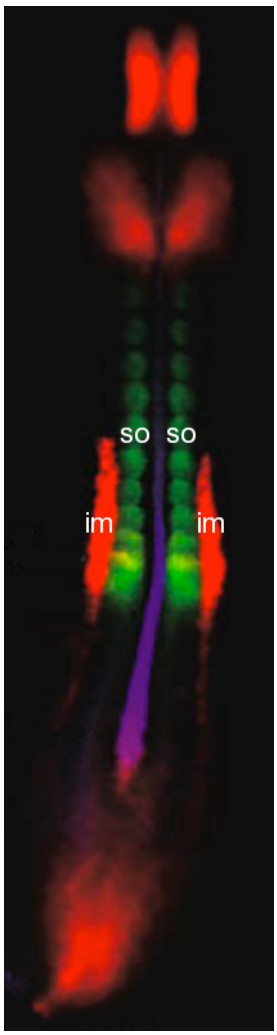

Figure 9-144. Intermediate mesoderm, somites and notochord in the neurula stage embryo. Triple-label whole-mount fluorescent *in situ* hybridization of an 8-somite chick embryo. Images were obtained with an inverted fluorescence microscope in a dorsal view. *Paraxis* (green) was expressed in the somites (so)/paraxial mesoderm. *Pax*2 (red) was expressed in several tissues including pronephros/intermediate mesoderm (im). *Chordin* (blue) was expressed in the notochord. This figure was edited from (Denkers et al., 2004).

1.5 Kidney Morphogenesis

Patterning of the Intermediate Mesoderm

Prior to any morphological indication of kidney development, several marker genes are expressed in the intermediate mesoderm (Fig 143D). The mRNA expression of these markers is an indication that the intermediate mesoderm is differentiated from surrounding cells. In the amniote embryos, the transcription factor *odd-skipped related* 1(*odd*1), previously known as *osr*1 (So and Danielian, 1999), is the earliest marker of the intermediate mesoderm so far. Transcription of *odd*1 is detectable by WISH in the intermediate mesoderm immediately after gastrulation. Its expression pattern extends to include the medial lateral plate mesoderm in later stages (James et al., 2006; James and Schultheiss, 2005). During gastrulation, neurulation, and organogenesis, the *homeobox* gene, *lim*1 is expressed in the visceral endoderm, the anterior mesoderm, the lateral plate and the intermediate mesoderm (Shawlot and Behringer, 1995; Tsang et al., 2000). The *paired-box* gene, *pax*2, is expressed in the intermediate mesoderm at later stages than *odd*1 and *lim*1 but in a more restricted manner. The expression of *pax*2 does not extend into the lateral plate mesoderm (Bouchard et al., 2002; Patel and Dressler, 2004). The *Wilms' tumour* 1 (*wt*1) gene encodes a zinc-finger transcription factor (Call et al., 1990; Mrowka and Schedl, 2000) that is deleted or disrupted in 10-15% Wilms' tumour cases (Hastie, 1994). In the developing mouse, *wt*1 is first expressed in the metanephrogenic mesenchyme at the E9 stage. By E10 it is widely expressed in many organ primordia (Armstrong et al., 1993; Rackley et al., 1993).

During pronephros morphogenesis in zebrafish, *wt*1 mRNA expression is restricted to the anterior intermediate mesoderm at early stages and to the fused

pronephric glomerulus at 48 hpf. The intermediate mesoderm regions are defined by the mRNA expression of *wt*1, *pax*2.1, and *single-minded* 1 (*sim*1) (Serluca and Fishman, 2001). Sim1 is a basic helix-loop-helix (bHLH) transcription factor that regulates development of neuroendocrine lineages (Michaud et al., 1998). It is also recognized as a marker for intermediate mesoderm in avian embryos (Obara-Ishihara et al., 1999; Pourquie et al., 1996).

Metanephric Nephron Formation in the Developing Mammalian Kidney

Mammalian kidney development undergoes two transient stages, the pronephros and the mesonephros, prior to the formation of metanephric/adult kidney. All three forms of the kidney are derived from the intermediate mesoderm. The first morphological indication of kidney development is the pronephric duct, which differentiates from the anterior intermediate mesoderm (Obara-Ishihara et al., 1999). The pronephric duct contributes to the formation of the pronephros. Mammalian pronephros is not functional and degenerates when the mesonephros forms (during E8 in the mouse). The duct elongates caudally and forms the Wolffian duct which is a signalling centre for the interaction with both meso- and metanephric mesenchyme (Kuure et al., 2000; Vize et al., 1997).

Mammalian mesonephros consists of glomeruli-like structures (Tiedemann and Egerer, 1984). In the pig, mesonephric nephrons are functional excretory organs whereas the murine mesonephros is non-secretory (Egerer et al., 1984; Smith and Mackay, 1991; Tiedemann and Egerer, 1984). The mesonephros regresses by E15 in

the mouse due to apoptosis (Sainio et al., 1997; Smith and Mackay, 1991). In female embryos the degeneration is complete but in males the Wolffian duct develops further into male genitals (Kuure et al., 2000). Previous research, however, suggests the mesonephros might also be involved in the development of the ovary (Vainio et al., 1999).

The metanephros is the permanent kidney of amniotes. It begins to develop when an aggregation of the metanephric mesenchyme (E12.75) and an outgrowth of the ureteric bud invades the surrounding metanephric mesenchyme at approximately E11.5 in mice (Bard et al., 2001). As the ureteric bud enters the metanephric mesenchyme, the mesenchyme induces the bud to branch. At the tips of the branches, the epithelium induces the mesenchyme to aggregate and to form renal tubules and glomeruli (Saxen and Sariola, 1987) (Fig 151B). This process of nephrogenesis (know as reciprocal induction) that is interaction between the epithelial ureteric bud and metanephric mesenchyme is repeated a million times during formation of the functional adult kidney in humans (Kuure et al., 2000; Vize et al., 1997). Many gene products have been shown to be important in the process (Dressler, 2006; Yu et al., 2004). Switching of metanephric mesenchyme from the apoptosis pathway is *wt*1 dependent. In *wt*1 null mice, at day 11 of gestation, the cells of the metanephric blastema undergo apoptosis, the ureteric bud fails to grow out from the Wolffian duct. (Kreidberg et al., 1993). Glial cell-line derived neurotrophric factor (Gdnf), synthesized in the metanephric mesenchyme, is critical for the ureteric bud to grow from the nephric duct (Moore et al., 1996; Pichel et al., 1996).

Fused Pronephric Glomerulus in Zebrafish

Considering the progression of the three kidney types during mammalian kidney development, pronephros in zebrafish is regarded as similar to mammalian metanephros rather than to mammalian pronephros.

Mammalian pronephros and mesonephros are transient tubule structures. The nephrons, with a glomerulus at one end, are not formed until metanephric induction has taken place. The mammalian metanephric nephron (Fig 151B) consists of a glomerulus integrated into the tip of a kidney tubule, known as Bowman's capsule, which is vascularized by a folded arteriole (Vize et al., 1997). In zebrafish, transient tubule structures are not observed during kidney morphogenesis. The bilateral pronephric-glomerulus which primordia adjacent to the anterior tip of the pronephric tubules migrates towards the midline of the embryo. The two pronephric-glomerulus primordia then fuse into a single glomus that is vascularized by the dorsal aorta (Drummond et al., 1998; Serluca and Fishman, 2001; Vize et al., 1997). In contrast to the structure of a mammalian metanephric nephron, the zebrafish pronephric nephron structure consists of a pair of pronephric tubules connecting the central glomerulus to the paired pronephric ducts, which extend caudally and are fused at the cloaca (Drummond, 2005) (Fig 151A). Remarkably, the morphology of these pronephric nephrons looks like the horseshoe kidney (Fig 113) as in cases of embryological renal fusion malformation in humans. The cause of horseshoe kidney may be a type of ectopic induction of tissue migration during kidney development.

Differences in pronephros between zebrafish and mammals are also evident in several markers of gene expression. Most notably, *wt*1 is expressed first in the

metanephrogenic mesenchyme in mouse embryos (Armstrong et al., 1993; Rackley et al., 1993) however is expressed in the intermediate mesoderm in zebrafish. There are three commonly used intermediate mesoderm markers in the mammalian model, *odd*1/*osr*1, *lim*1/*lhx*1 and *pax*2. *Pax*2 expresses in the intermediate mesoderm at a later stage than *odd*1/*osr*1, *lim*1/*lhx*1 (Bouchard et al., 2002; James et al., 2006; James and Schultheiss, 2005; Patel and Dressler, 2004; Shawlot and Behringer, 1995; Tsang et al., 2000). In the zebrafish model, *pax*2.1 along with *lim*1/*lhx*1, *wt*1 and *sim*1 are markers for intermediate mesoderm in zebrafish (Serluca and Fishman, 2001; Tena et al., 2007). All these markers express in the intermediate mesoderm at the same developmental stages. Furthermore, *odd*1/*osr*1 is a lateral, but not an intermediate, mesoderm marker in zebrafish (Mudumana et al., 2008). This comparison suggests that the duration of embryogenesis increases concurrently with the increase in molecular complexity during evolution.

It is unclear whether the reciprocal induction is also the mechanism for developing mesonephros in zebrafish. Formation of the pair of pronephric nephrons in zebrafish does not involve the mechanisms, which proceeds tubule branching and formation of multiple metanephrons from the collecting duct in mammals. Functional and persistent pronephros could be evolved to meet the needs of rapid embryonic development in zebrafish. Despite these special attributes, the zebrafish pronephros is a simple model approachable to investigate the establishment of nephron functions during embryonic development.

The Genetic System for Pronephric-glomerular Morphogenesis in Zebrafish

During the last two decades, wide genetic screening carried out in zebrafish (Amsterdam et al., 2004; Solnica-Krezel et al., 1994) has identified several mutants in which pronephric-glomerular morphogenesis is disrupted. In *spt*;*ntl*, and *spt*;*Zoep* double mutants, *wt*1 expressed cells are severely reduced or absent (Weidinger et al., 2002). In other words, genetic interaction of *spt* and *ntl* or interaction of *spt* and *Zoep* are essential for the specification of the anterior intermediate mesoderm. Pronephric-glomerular precursor cells are specified but kidney morphogenesis fails in *kohtalo* (*kto*) mutants (Hong et al., 2005). The genetic locus, *kto,* encodes the Mediator component thyroid hormone receptor-associated protein, TRAP230/MED12 (Fondell et al., 1996) which is required for the development of the zebrafish pronephric kidney (Hong et al., 2005).

In *floating head* (*flh*), *sonic you* (*syu*), and *you-too* (*yot*) mutants, glomeruli differentiate at ectopic lateral positions and contain differentiated podocytes and endothelial cells. These studies suggest that midline signals are required for formation of the fused central glomus but not for the differentiation of functional glomeruli (Liu et al., 2000; Majumdar and Drummond, 2000). Matrix metalloproteinase-2 (MMP-2) is thought to relay hemodynamic forces to endothelial signalling, in order to direct the formation of the midline pronephric glomerulus. Mutants locked in circulation, such as *island beat* (*isl*), *valentine* (*vtn*), and *silent heart* (*sih*), exhibit bilateral pronephric glomeruli (Serluca et al., 2002). Arguably, contradictory evidence that is provided by the mutant, *cloche* (*clo*) suggests that a central fused glomerulus is able to develop in the absence of endothelia or endothelial- derived signals (Majumdar and Drummond, 1999). The *col* locus

encodes an acyltransferase, Lycat, which acts upstream of *vascular endothelial growth factor receptor* 2 (*vegr2*/*flk*1) to regulate endothelial cell differentiation (Liao et al., 1997; Xiong et al., 2008).

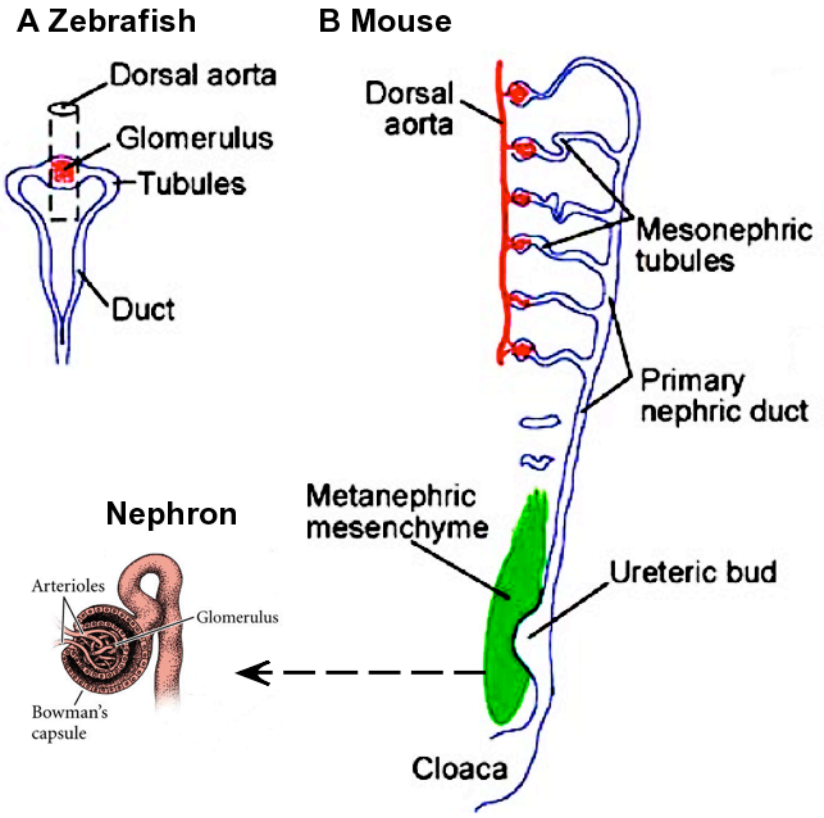

Figure 10-151. Early patterning of kidneys.

(A) The zebrafish pronephric nephron at 48 hpf. The zebrafish pronephric nephron has a single midline glomerulus (pronephric glomerlulus) filtering from the dorsal aorta. Two bilateral pronephric tubules direct the filtrate laterally and caudally to the duct. (B) One side of the developing mouse intermediate mesoderm is shown at approximately E10.5. Towards the anterior, the primary nephric duct connects to a series of mesonephric tubules, and towards the posterior it exhibits a single ureteric bud. The induction between the metanephric mesechyme and ureteric buds generates the metanephric nephrons that compose the adult kidney. This diagram is adapted from (Dressler, 2006) and (Gilbert et al., 2000).

1.6 Hypothesis & Aims

Post-gastrulation Midline Convergence

Passing through the almost unified segmentation patterning during early embryonic development in vertebrate, renal morphogenesis in zebrafish and amniotes starts diverse processes from the organogenesis stages. In zebrafish, the group of cells in the anterior intermediate mesoderm, which express genetic markers of the nephric glomerulus, is referred to as the pronephric-glomerular primordium (PGP). The bilateral PGP continue moving toward the midline of the embryo (regarded as post-gastrulation midline convergence) and eventually forms a fused head kidney adjacent to dorsal aorta (Fig 161). In contrast, the mammalian kidneys are differentiated and induced from intermediate mesoderm to form a left-right pair without involving postgastrulation midline convergence.

The heart is the most notable organ in which the primordia undergo post-gastrulation midline convergence during organogenesis (Fig 162). In all vertebrates, the heart tube develops from anterior lateral plate mesoderm (McFadden and Olson, 2002). During somitogenesis, the myocardial precursors migrate coordinately toward the midline of the embryo in zebrafish (Stainier, 2001; Trinh and Stainier, 2004). Screening of large-scale mutagenesis in zebrafish has identified different loci that disrupt the midline migration process, resulting in a phenotype with two hearts developed on both sides of the embryo regarded as cardia bifida (Alexander et al., 1998; Chen et al., 1996; Stainier et al., 1996). Analyzing these mutants, such as *hands off*, *casanova*, *bonnie and clyde*, *miles apart*, and *natter*, reveals the importance of lysosphingolipids, transcriptional controls, endodermal tissue formation, the YSL and extracellular matrix, in regulating cardiac precursor midline

migration during organogenesis of the heart (Kikuchi et al., 2000; Kupperman et al., 2000; Sakaguchi et al., 2006; Trinh and Stainier, 2004; Yelon et al., 2000).

Hypothesis & Aim

Midline convergence of organ primordia is an important mechanism for shaping the vertebrate body plan at various stages of development (Ober et al., 2004; Sakaguchi et al., 2006). Wnt signalling not only plays crucial roles in regulating gastrulation movement (Nelson and Nusse, 2004; Tada et al., 2002) but also in post-gastrulation midline convergence of cardiac primordia (Fig 162). Down regulation of noncanonical Wnt signalling components, such as *dishelleved* (Dvl) or *RhoA GTPase* (RhoA), exhibits the phenotype of cardia bifida in zebrafish (Fig 163). This suggests that Wnt signalling plays an important role in regulating the post-gastrulation midline convergence during heart morphogenesis (Matsui et al., 2005).

If the post-gastrulation midline convergence of PGP were regulated by the same mechanism as post-gastrulation midline convergence of cardiac primordia, higher vertebrates should develop two hearts bilaterally when the mechanism of the post-gastrulation midline convergence of PGP was remodelled during evolution. The fact is that, in higher vertebrates, normal kidney morphogenesis does not involve further midline convergence mechanisms in order to develop the two bilateral kidneys (Sainio and Raatikainen-Ahokas, 1999). In contrast, cardia bifida is a lethal developmental malformation in higher vertebrates (Aiello and Xavier-Neto, 2006; Compernolle et al., 2003; Schulte et al., 2007).

I, therefore, hypothesize that there is/are mechanism(s) underling midline convergence of PGP in zebrafish, which is/are in addition to the control of the non-canonical *wnt/Dvl/RhoA* pathway and specific to kidney morphogenesis. In this research on pronephric-glomerula morphogenesis, the aim was to identify the signaling pathways additional to the one regulating general midline convergence (i.e. noncanonical *wnt* signaling) and specific to kidney morphogenesis.

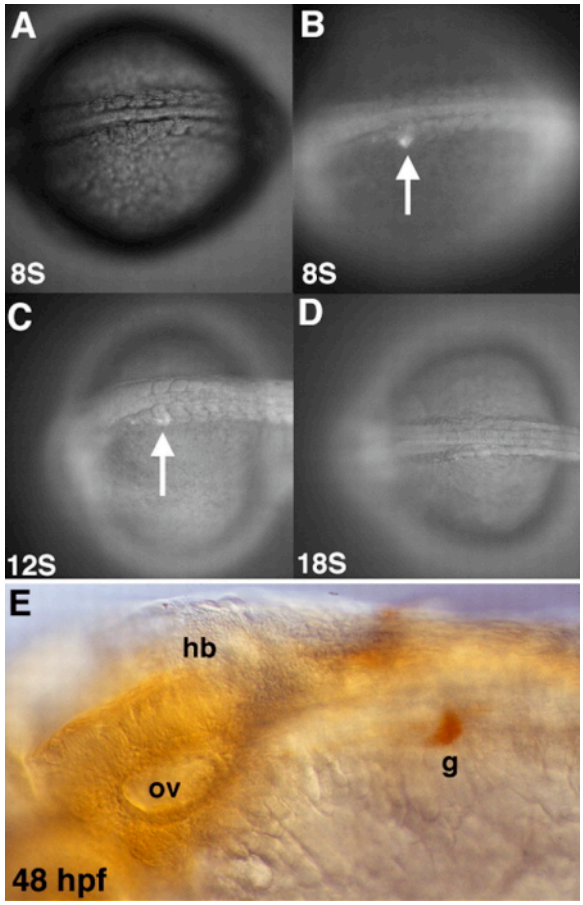

Figure 11-161. Origin of the medial pronephric glomerulus.

(A-D) images are time lapse analyses of a single embryo labelled at the 8-somite stage at the anterior intermediate mesoderm (first somite region). (A) An image taken by phase contract microscope is shown to verify the location of the fluorescence patch relative to somite. (B) & (C) Arrows indicate the labelled patch on the corresponding fluorescence image of the labelled embryo. The intermediate mesoderm migrates towards the midline of the embryo during 8- to 12-somite stages. (D) However, by 18-somite stage, the labelled cells have become difficult to observe using fluorescence microscopy. (E) the Whole-mount DAB-stained 48 hpf embryo showing that the labelled anterior intermediate mesoderm gives rise to the pronephric glomerulus in the midline of the embryo. In other words, like the heart primordia, PGP undergo post-gastrulation midline convergence to form the medial pronephric glomerulus during zebrafish embryonic development. Abbreviations are: g, pronephric glomerulas; hb, hindbrain; ov, otic vesicle**.** The figure was adapted from (Serluca and Fishman, 2001).

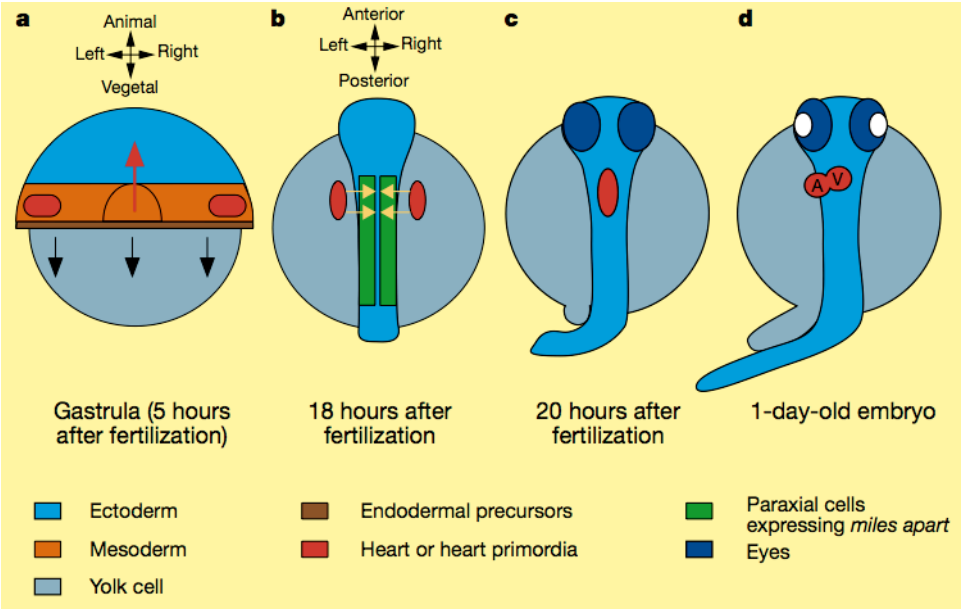

Figure 12-162. Post-gastrulation midline convergence of heart primordia.

Dorsal views of the zebrafish embryo at shield (a), 8-somite (b), 22-somite (c), and 24 hpf (d) stages. (a) The forming dorsal axis will extend (red arrow) towards the 'animal pole' (see directional indicator), while other cells of the embryo will cover the yolk cell (black arrows). The heart precursor cells (heart primordia) form bilaterally. (b) Green stripes of cells next to the midline that express *miles apart* mRNA are likely to be required for proper migration (yellow arrows) of the heart primordia and joining of the two bilateral groups of heart precursor cells (Kupperman et al., 2000). (c) By 20 hours after fertilization, a single medial heart tube has formed. (d) The heart starts to beat and circulation begins at 24 hours after fertilization; by 36 hours, looping movements have positioned the heart's atrium (A) to the left of the more centrally located ventricle (V). The figure was adapted from (Driever, 2000).

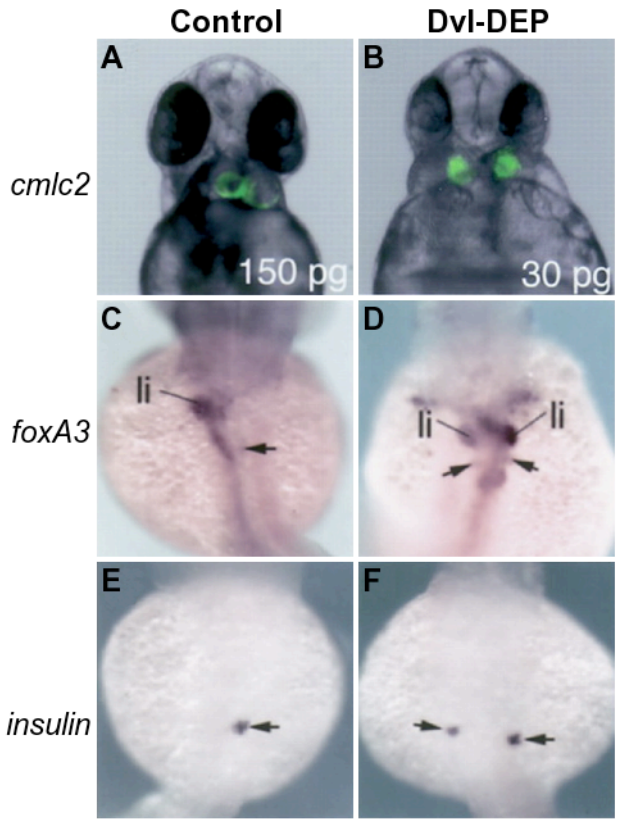

Figure 13-163. Wnt signaling regulates midline convergence of organ primordia without affecting their cell fate.

Dishevelled (Dvl), one of intracellular components of Wnt signalling pathway, plays a key positive role in transducing both canonical and noncanonical Wnt signals (Roberts et al., 2007). All the images are taken at 48 hpf. (A, C, E) Embryos are injected with mRNA encoding the negative control alkaline phosphatase (AP). (B, D, F) Dominant negative expression of a truncation mutation of Dvl (Dvl-DEP), which lacks the DEP domain (Axelrod et al., 1998; Tada and Smith, 2000; Wallingford et al., 2000) by injecting with mRNA of Dvl-DEP. (A-B) Ventral views, anterior to the top. Transgenic zebrafish embryos carrying cmlc2-GFP reporter (Huang et al., 2003) demonstrate the effects of Dvl-DEP on morphogenesis of the heart in zebrafish. Cardia bifida phenotype is observed in Dvl-DEP mRNA injected embryo (B). (C-F) These are dorsal view images orientated with the anterior to the top. Whole-mount in situ hybridization of *fox*A3 (C, D) or *insulin* (E, F). Antagonizing Wnt/Dvl signalling led to the formation of a Y-shaped gut tube (D, arrows), and the duplication of liver buds (li) and the duplication of pancreas buds (F, arrows). This figure was edited from (Matsui et al., 2005).

1.7 Approaches

Tracing & Labelling Cells

There are three techniques for tracing or labelling cells in a developing embryo to date. Firstly, WISH, or immunostaining, reflects the gene expression status of a cell in mRNA or protein level, and is the most straightforward method for labelling embryonic cells. The technique involves fixation of embryos at desired stages, which results in all the biological information detected from the cell as a snapshot in time. The second method of tracing, or labelling, embryonic cells is the direct introduction of detectable agents into living embryos (desired regions) at desired stages. Behaviour of the labelled/marked cells can be monitored in real-time during the development of the embryo. The information provided by this technique is more related to locations and to changes in the cells in a spatial manner, rather than the cellular status of the cells. Finally, the third technique is to trace or label cells by using transgene expression and/or transgenic systems. In this method, the quantity and location of the detectable agents (regarded as reporter gene products) are controlled by the selected promoter through genetic engineering of plasmids and introduction of the plasmids into embryos. Transcriptional or translational status and behaviour of the cells can be monitored during embryonic development in real-time.

These experiments include, firstly, construction of a plasmid. In this construct, β-*actin* promoter (zebrafish) driven *rfp* was floxed by loxP. The second reporter gene, GFP, was adjacent to a loxP at the 3'-end of RFP. Secondly, transgene expression was monitored following construct microinjection into zebrafish embryos. Ideally, the presence of Cre removes *rfp* from the construct and changes the reporter to GFP. The colour change of the fluorescent reporters can reflect the

biological status of the cells, when *cre* expression is driven by the promoter of the marker genes. The results of the experiments are detailed in Chapter 3 (§3).

Cre-loxP system

The Cre-loxP system was originally discovered from prokaryotes. Phage P1 encodes a recombinase called Cre and a short asymmetric DNA sequence called loxP. The composition of Cre and loxP is an efficient site-specific recombination system (Abremski et al., 1983; Hoess and Abremski, 1985; Sternberg and Hamilton, 1981; Van Duyne, 2001). Later the functional expression of the system in yeast was demonstrated (Sauer, 1987). The Cre-loxP system is now an important tool for conditional gene knock-out, genome modification, termination of transgenes, and cell lineage mapping in mice (Branda and Dymecki, 2004). The application of the Cre-loxP system in transgenic *Xenopus* (Ryffel et al., 2003) and zebrafish (Langenau et al., 2005; Pan et al., 2005) has however shown insufficient phenotypes (reporter gene expression) of the system, which possibly correlates with the quantity of Cre recombinase or concatamerization of the transgenes. The strategy to overcome this problem is to make a transgenic line, which has single copy, single insertion of the floxed reporter construct and transgenic lines, which have specific Cre transgene expression.

ITR

All the constructs used in this project were built within an ITR cassette (Fu et al., 1998). Inverted terminal repeat (ITR) was first isolated from the Adeno-associated virus which has a single-stranded DNA genome of approximately 4.7 kb (Srivastava

et al., 1983). Each ITR consists of 145 nucleotides and forms a palindromic hairpin (Samulski et al., 1989), and presence of a pair of ITRs in a plasmid significantly increases the efficiency and specificity of transgene expression in *Xenopus* embryos (Fu et al., 1998) and enhances the reporter gene expression level in zebrafish embryos (Hsiao et al., 2001; Huang et al., 2003). Ideally, the enhanced expression of reporter genes is useful when embryos are monitored under the microscope.

Wt1

Wilms tumor suppressor gene (*wt*1) is a zinc-finger transcription factor (Call et al., 1990; Gessler et al., 1990). The human *wt*1 gene is approximately 50 kb and has 10 exons, which generate 3-kb mRNA. Up to 24 different *wt*1 mRNA may result from a combination of alternative RNA splicing and alternative translational start sites (Mrowka and Schedl, 2000). The biology of Wt1 is complex since, in addition to its function as a tumour suppressor, Wt1 has multiple roles during development and maintenance of body functions (Gao et al., 2005; Wagner et al., 2003).

Although the pronephric ducts and tubules remain as bilaterally paired structures, cells at the anterior intermediate mesoderm coalesce and migrate to fuse at the midline and form glomeruli in zebrafish (Hong et al., 2005). This process is marked by *wt*1 expression (Drummond et al., 1998; Serluca and Fishman, 2001). Recently, two *wt*1 genes were found in zebrafish, which share similar sequences and expression patterns regarded as *wt*1a (referred to the earlier discovered *wt*1) and *wt*1b (Bollig et al., 2006). The marker for the nephrogenic mesenchyme in this thesis is *wt*1a. The results of monitoring the dynamic morphologic pattern of PGP during organogenesis in zebrafish using *wt*1 WISH, are detailed in §4.1.

Pinpointing Signaling Pathways for PGP Midline Convergence

Cell-cell communication in development

During organogenesis, a type of close range interaction between two or more cells or tissues (regarded as the inducers and the responders) of different biological history and properties is termed induction (Gilbert et al., 2000). The ability to respond to a specific inductive signal is called competence. The signals are transmitted between inducer and responders by direct physical contact between the cells, regarded as juxtacrine signalling, or by secretion of inductive molecules, regarded as paracrine factors (Saxen et al., 1976). The paracrine factors can be soluble molecules (Grobstein, 1956) or extracelluar matrix components (Slavkin et al., 1972). In juxtacrine interactions, proteins from the surface of inducing cells interact with receptor proteins of adjacent responding cells or signals are directly transmitted through gap junctions.

The Notch pathway is a well-known juxtacrine signal and is activated by ligands (Delta, Jagged, or Serrate) on an adjacent cell (Fiuza and Arias, 2007). The ligands for Notch signalling are also transmembrane proteins (Lissemore and Starmer, 1999). Gap junctions serve as direct communication channels between adjacent cells. Small molecules (such as cAMP) and ions can pass from one cell to another through the junction. The channels are composed of connexin proteins (Houghton, 2005). The importance of junctions in development has been demonstrated in the amphibian (Warner et al., 1984) and sea urchin (Yazaki et al., 1999).

The soluble paracrine factors can be categorized into five families; the FGF family, the Hedgehog family, the Wnt family, the TGF-β superfamily (Attisano and

Wrana, 2002) and others, based on the relevance of their amino acid structures. In vertebrates, the Fibroblast growth factor (FGF) family currently constitutes 22 member genes, which share 13-71% amino acid identity (Ornitz and Itoh, 2001). Between vertebrate species, amino acid sequences of FGFs are highly conserved. FGFs activate Fibroblast growth factor receptors (FGFRs), a subfamily of cell surface receptor tyrosine kinases (RTKs). Four genes are reported to encode the FGFR, but alternative RNA splicing can result in more than 100 possible protein sequences (Lappi, 1995). During embryonic development, FGF signalling plays diverse roles in regulating cell proliferation, migration and differentiation. (Bottcher and Niehrs, 2005).

The Transforming Growth Factor-β (TGF-β) superfamily includes the TGF-β family, the *activin* family, the Bone Morphogenetic Protein (BMP) family, and other proteins (Fig 173) (Hogan, 1996; Massague, 1998). The TGF-β family regulates a plethora of developmental processes, such as epithelial-mesenchymal transition which is a highly conserved and fundamental process during embryonic development (Ahmed and Nawshad, 2007; Thiery, 2003). One of critical roles that the BMP family plays is in the regulation of kidney development (Cain et al., 2008).

Wnt (***wingless***/i***nt***egrated) is the vertebrate Wingless homolgue (Berry, 2002). The Wnt signalling pathway is an ancient system that has been well conserved during evolution. It plays a crucial role in the embryonic development of all animal species (Klaus and Birchmeier, 2008). Previous work has shown that intracellular signalling of the Wnt pathway diversifies into several branches (Huelsken and Birchmeier, 2001), when Wnt signalling is transmitted through its receptor (Frizzled) to beta-catenin, which is often called the canonical pathway (Logan and Nusse,

2004). In contrast, noncanonical Wnt signalling does not involve beta-catenin in its cascade components (Veeman et al., 2003a; Veeman et al., 2003b).

Unlike the fly, which has a single *hedgehog* gene (Ingham and McMahon, 2001), three *hedgehog* genes have been identified in the mouse: *desert hedgehog* (*dhh*), indian hedgehog (*ihh*), and sonic hedgehog (*shh*) (Echelard et al., 1993). The Shh signalling is the most studied signalling among the three hedgehogs and mainly focuses on formation of the central nervous system and patterning neurons (Bertrand and Dahmane, 2006; Ericson et al., 1995; Placzek, 1995). Transmission of the Hedgehog signal is through interaction between the Shh receptor, Patched (Ptc), and another cell surface protein, Smoothened (Smo) (van den Brink, 2007). Furthermore, the signalling is also associated with patterning of somites, formation of limbs, and development of endodermal tissues (Francis-West and Hill, 2008; McDermott et al., 2005; Moore-Scott and Manley, 2005).

There are soluble paracrine factors that are not structurally related to the four families previously mentioned, but which also play important roles in the embryonic development. For example, the ligand, Epidermal Growth Factor (EGF) (Carev et al., 2008) and its receptor (EGFR) (Herbst, 2004) was reported to be expressed in the early embryo, suggesting that the EGF system is related to early embryo development (Cai et al., 2003; Heo and Han, 2006; Wei et al., 2001).

The extracellular matrix is composed of a variety of macromolecules that are secreted locally and assembled into a mesh, in close association with the surface of the cell producing them (Alberts, 2002). These macromolecules include collagen, proteoglycans, and specialized glycoprotein molecules, such as fibronectin and laminin. The extracellular matrix is a source of signals of cell survival, cell

differentiation, and cell migration (Zagris, 2001) through cell surface receptors, such as Integrin (Boudreau and Jones, 1999; Hayashi et al., 2007), and the Discoidin Domain Receptor (DDR) (Vogel et al., 2006).

After reviewing the vast number of signalling pathways that are essential for embryonic development, the central question arising in this research was, 'Which of these signalling pathways are important for PGP midline convergence but not heart primordial midline convergence during organogenesis in zebrafish embryos'? A clear picture emerged. The PGP are not tissues floating in the air during zebrafish embryonic development, indeed, they are tissues surrounded by other developing tissues (Fig 172). The PGP midline convergence must depend on PGP-adjacent tissues (somites and endodermal tissues). The hypothesis thus put forward is that the signalling pathways are essential for somite or endodermal tissue formation, and very probably also regulate PGP midline convergence.

Nodal signalling pathway and endodermal tissue development

In zebrafish *one-eyed pinhead* (*oep*) involved in Nodal-related TGF-β signalling is essential for the formation of all endodermal and several mesodermal tissues (Feldman et al., 2000; Feldman et al., 1998; Schier and Shen, 2000). *Oep* was originally identified during genetic mutagenesis in zebrafish embryos (Driever et al., 1996; Haffter et al., 1996; Schier et al., 1997). Oep is an EGF-related protein (EGF-CFC) consisting of an EGF-like motif at the N-terminal in addition to a cysteine-rich domain, CFC (Cripto, FRL-1 and Cryptic) at the C-terminal (Zhang et al., 1998). Functions of Oep, however, are Nodal-related. Oep acts as a cofactor of Nodal receptors (Activin receptors) in Nodal signalling (Gritsman et al., 1999; Shen and

Schier, 2000; Yeo and Whitman, 2001). Nodal signalling triggers a cascade of transcription factor expression to regulate formation of endodermal tissues in zebrafish (Bjornson et al., 2005), such as Gata5, and Bonnie and Clyde (Bon) (Kikuchi et al., 2000), which are required to maintain expression of a *sox* factor Casanova (Cas) (Aoki et al., 2002; Kikuchi et al., 2001). A simplified genetic control map for zebrafish endodermal tissue formation is shown in Fig 173. The zebrafish mutant, *oep* was selected for the study of Nodal signalling in pronephric-glomerular morphogenesis in zebrafish embryos. The results of these experiments are detailed in Chapter 4 (§4).

FGF signalling pathway and somitogenesis in zebrafish embryos

Inhibition of FGF signalling in zebrafish embryos using injection of a dominant negative FGFR (dnFGFR) RNA, down regulates *spt* and *ntl* expression and generates subsequent phenotypes lacking trunk and tail mesoderm (Griffin et al., 1995). Mutant analysis in zebrafish has demonstrated that Spt is required through regulation of the cell adhesion molecule, poaraxial protocadherin (PAPC), for the movement of somite progenitors and subsequent somitogenesis (Amacher and Kimmel, 1998; Ho and Kane, 1990; Kimmel et al., 1989; Weinberg et al., 1996; Yamamoto et al., 1998). These studies of zebrafish embryonic development, suggest that the T-box transcription factor, *spt* is a key mediator of FGF signalling in the formation of trunk mesoderm (Griffin et al., 1998), in addition to a supporting mediator *ntl* (Griffin et al., 1995). The minor effect contributed by *ntl* is subsequently mediated by another T-box gene, *tbx6* (Chapman and Papaioannou, 1998; Griffin et al., 1998). A simplified genetic interaction map for zebrafish somitogenesis is shown in Fig 174.

The zebrafish mutants, *spt* and *ntl* were selected for the study of the FGF signalling pathway in pronephric-glomerular morphogenesis in zebrafish embryos. The results are detailed in Chapter 5 (§5).

In summary, a combination of transgenic techniques and phenotype analysis in mutant embryos was planned to study the morphogenesis of pronephric-glomerulus in zebrafish with the main interest in the Nodal and FGF signalling pathways.

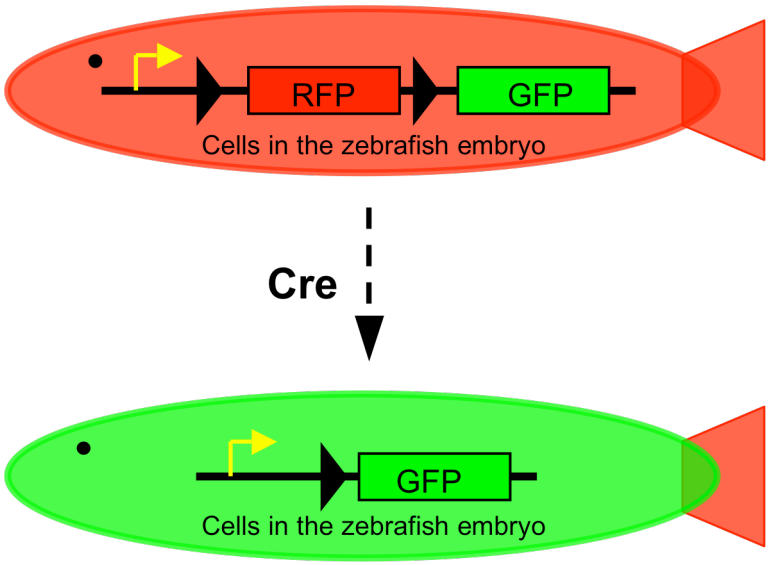

Figure 14-171. Diagram of the approach to tracing and labelling in developing zebrafish embryos.

In order to trace and label PGP in the developing zebrafish embryos in real-time, a Cre-loxP transgene expression system was designed. In this system, detectable agents to label/mark cells are gene products of fluorescence reporters (RFP & GFP). This system is designed to undergo colour change (RFP to GFP) when Cre first presents in the cells. A simplified DNA construct structure (black line) is shown on the top of this diagram. The RFP (red box) that is floxed by loxP (black triangles) is transcriptionally regulated by zebrafish β-*actin* promoter (yellow arrows) and the GFP (green boxes) is located to the 3' of RPF. Hence, every cell that contains this construct is labelled with red fluorescence in the fish embryos (top). When Cre is introduced into cells in the embryo, RFP is floxed out by Cre, then cells that receive the Cre change colour from red to green (bottom). If Cre is introduced into targeted cells by the promoter of the desired marker gene at early embryonic stages, the cell lineage can be reflected by the red to green colour change.

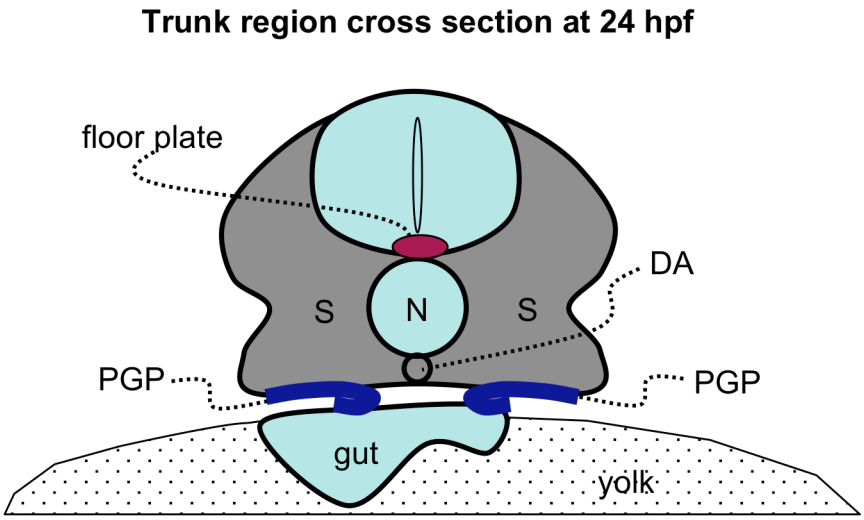

Figure 15-172. Diagram of a trunk region cross section of 24 hpf zebrafish embryo.
The pronephric-glomerular primordia (PGP) localize underneath the somite and above the gut at 24 hpf. The abbreviations in this diagram are: DA, dorsal aorta; N, notochord; S, somite. The diagram is based on (Drummond et al., 1998).

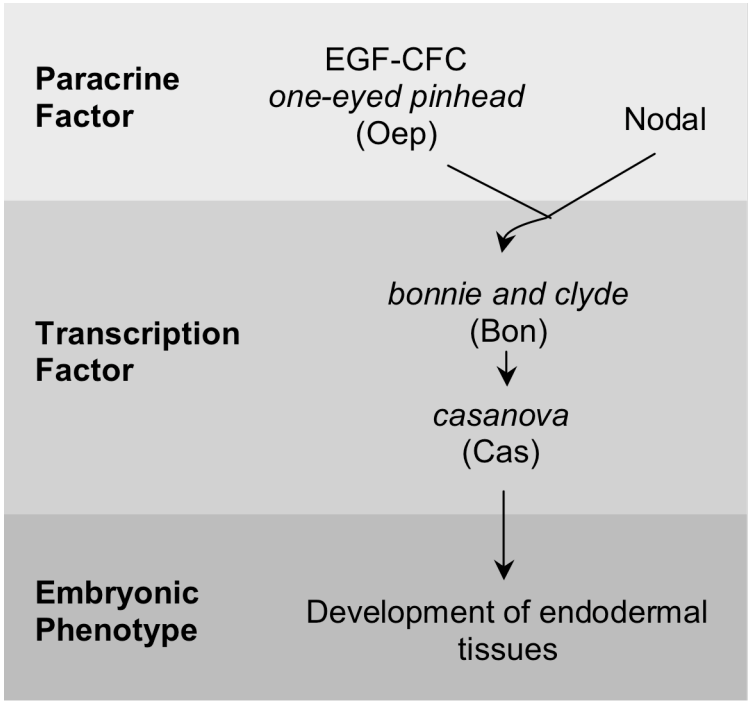

Figure 16-173. Genetic control of endodermal tissue formation by Nodal signalling.
This simplified diagram summarizes the genetic control of Nodal signalling in the formation of endodermal tissues. Nodal signalling triggers a transcriptional cascade including Gata5/Faust, and the homeodomain containing factors *bonnie and clyde* (Bon), which are required to maintain expression of the sox factor *casanova* (Cas), the key endodermal determinate in zebrafish. Although formerly regarded as signalling molecules that are distant relatives of Epidermal growth factor (EGF), recent findings indicate that EGF-CFC proteins act as cofactors for Nodal signalling. *One-eyed pinhead* (*oep*) is one of the zebrafish EGF-CFC genes. The Oep acts as a Nodal-receptor cofactor. Zygotic *oep* mutant (Z*oep*) embryos have attenuated Nodal signalling and lack endodermal tissue formation. This diagram is based on (Bjornson et al., 2005; Griffin and Kimelman, 2002; Shen and Schier, 2000).

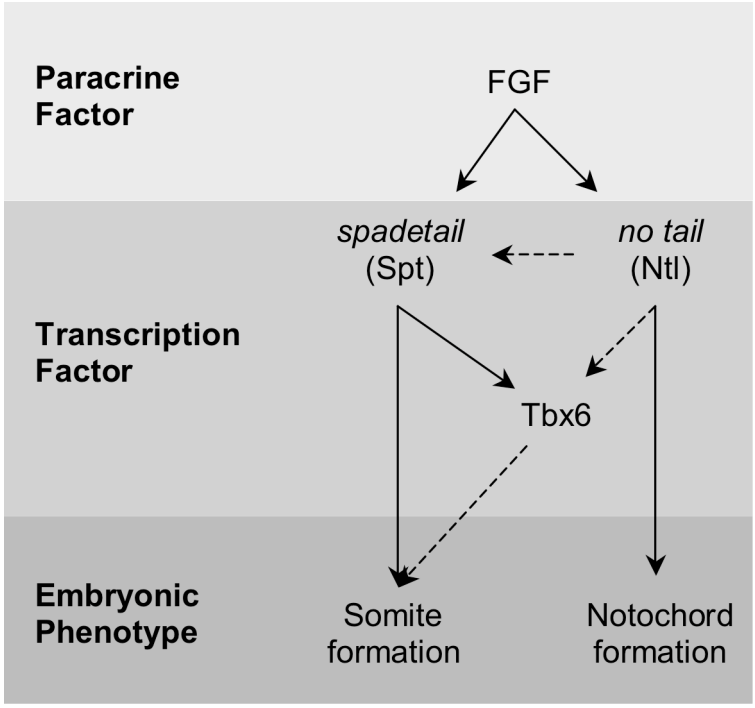

Figure 17-174. Genetic interaction map for FGF signalling in the somite formation.
This simplified genetic interaction map summarizes the regulatory relationship among *spt*, *ntl* and *tbx*6 in mesodermal tissue development. Spt and Ntl mediate FGF signalling in regulating somite formation and notochord formation respectively. Solid arrows indicate strong influences, whilst dashed arrows indicate weak influences. The control of somite development is based on (Chapman and Papaioannou, 1998; Griffin et al., 1998). The control of notochord development is edited from (Amacher and Kimmel, 1998; Halpern et al., 1997).

2. Materials & Methods

2.1 Zebrafish Strains & Maintenance

Strains

Zebrafish (*Danio rerio*) ENU mutants (Haffter et al., 1996; Haffter and Nusslein-Volhard, 1996; Mullins et al., 1994; Solnica-Krezel et al., 1994), spt^{b104} (Griffin et al., 1998), ntl^{tc41} (Odenthal et al., 1996b) and oep^{tz57} (Zhang et al., 1998) were selected for this study of pronephric-glomerular morphogenesis. These strains originated from a stock with a complex genetic background (Kimmel et al., 1989). Information on further genetic characterization is described in §2.6. Wild type fish were identified following genotyping for *oep* or *ntl* heterozygotes.

Maintenance

Embryos bred from mating *spt*, *ntl* or *oep* heterozygote and wild type were kindly provided by the Zebrafish Facility, MRC Centre for Developmental and Biomedical Genetics, University of Sheffield (http://cdbg.shef.ac.uk/facilities/zebrafish/). These embryos were raised in the Zebrafish Facility, Centre for Cardiovascular Science, QMRI, the University of Edinburgh. In this facility, the temperature and light cycles were restricted to the range 25°C to 30°C and 14 h-light/10 h-dark (light being from 9:30 am until 11:30 pm) respectively. Three sizes of fish tank were provided, 1-, 3-, and 10-litre. The capacity of a 10-litre tank is 50 adult fish. System water was at pH 7 without detectable chlorine, ammonia, or nitrate. Water temperature of 28.5°C was maintained by an indirect-water heating system (Fig 211). Air was pumped through hoses, which connected to an air stone within into individual tanks. Sufficient food (Table 212), enough space and good quality water (pH 7, no detectable chlorine,

ammonia, or nitrate) are essential for zebrafish to grow healthily. Providing enough hatched brine shrimps for adult zebrafish is important for sustainable collection of a good quantity of quality embryos (Westerfield, 1995).

When embryo collection was required, a pair of fish were mated in a 1-litre tank with a layer of marbles on the bottom (Fig 213) to protect the embryos from being eaten by their parents. Fish were mated during the night before collection of the embryos. Zebrafish lay eggs within two hours after dawn. Embryos were raised in blue egg water (Bretaud et al., 2004) or in system water with Aquarium Treatment Methylene Blue (Interpet Aquatic) in Petri dishes prior to 6 hpf. Adult fish for $spt^{b104/+}$, $ntl^{tc41/+}$ or $oep^{tz57/+}$ were obtained by PCR genotyping (§2.6). When two heterozygous carriers were crossed, on average 25% of the embryos produced were homozygous. Homozygous embryos were identified based on their distinct body shape (Fig 423, Fig513).

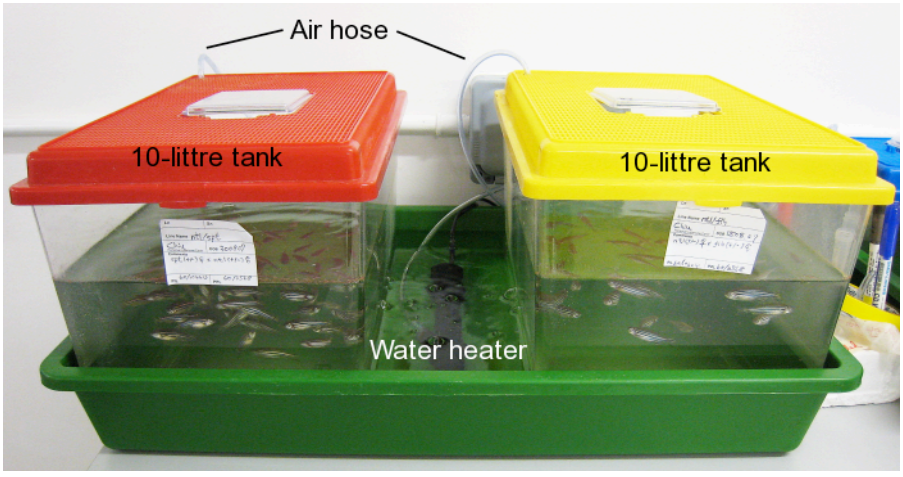

Figure 18-211. A tank system for zebrafish maintenance.

Table 1-212. Food for Zebrafish During Maintenance.

Days post fertilization	Complementary diet
5 to 14	ZM-000
15 to 21	ZM-001 & brine shrimp
22 to 28	ZM-001, -002 & brine shrimp
29 to 60	ZM-002, -003 & brine shrimp
61 upwards	ZM-003, -004, -flake & brine shrimp

In general, live food is better than packaged artificial substitutes. It is easier for zebrafish to digest and for keeping better water quality. Paramecia and brine shrimp are the best food for zebrafish, younger and older than 15 dpf respectively. In the zebrafish facility, ZM-000 is a high protein artificial substitute for Paramecia. Packaged artificial substitutes from ZM Ltd. (ZM) were used in addition to brine shrimp in the zerbrafish diet. Different sizes of the ZM artificial substitutes were utilised according to the developmental stage and size of the zebrafish. ZM-000, 001, 002, 003, and 004 are 30-50, 80-200,150-300, 300-500, and 500-800 microns particle size respectively. These substitutes contain 50 to 60% protein.

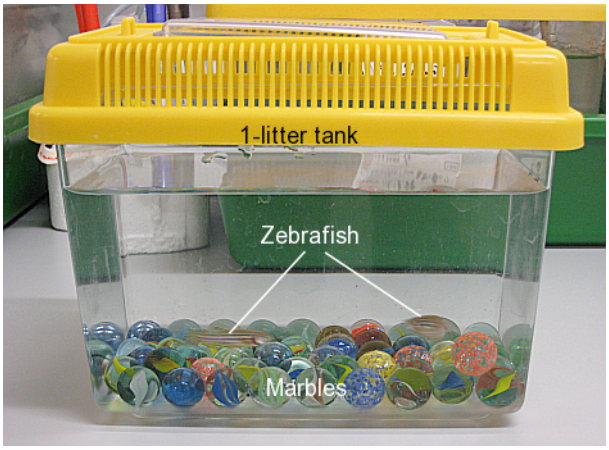

Figure 19-213. A marbled 1-litre tank.

2.2 Plasmid Engineering & Construction

Preparation of competent cells

E. coli strain, DH5α was used throughout this research. Two types of competent cell were prepared for the experiments. To prepare competent cells for transformation by calcium chloride, 40 μl glycerol stock of DH5α was cultured in 40 ml SOC medium (2% Bacto Tryptone, 0.5% Bacto Yeast Extract, 0.05% NaCl, 2.5 mM KCl, pH 7, with addition of sterile 1 M glucose to a final concentration of 20 mM before use) at 37°C for 1 hr then transferred to a shaker at 37°C and at 200 rpm for 3 hours until the OD_{600} reached 0.3. The DH5α broth was then transferred to a 2-liter flask with 500 ml LB medium (1% Bacto tryptone, 0.5% Bacto Yeast Extract, 1% NaCl, pH 7.5) and shaken at 200 rpm and 37°C for 3 hr until the OD_{600} reached 0.6. The DH5α broth was then centrifuged (Sorvall Instruments, RC5C, SS-34 rotor) at 4°C and at 5000 rpm for 10 min and washed once with ice-cold TB (250 mM KCl, 15 mM $CaCl_2$, 10 mM PIPES and 15 mM $MnCl_2$) followed by incubation on ice for 10 min. The DH5α was centrifuged again, re-suspended in 1 ml of ice cold TB with 70 μl DMSO and then incubated on ice for a further 10 min prior to producing 50 μl aliquots for storage at -80°C. The transformation efficiency of these competent cells was around 10^6 colonies per microgram DNA plasmid.

For electro-competent cells, the cultured DH5α was washed once with ice-cold 10% glycerol and incubated on ice for 10 min. It was then centrifuged at 4°C, 5000 rpm for 10 min and re-suspended in 1 ml ice-cold 10% glycerol and incubated on ice for 10 min prior to making 50 μl aliquots for storage at -80°C. The transformation

efficiency of these competent cells was approximately 10^8 colonies per microgram plasmid DNA.

When DH5α or plasmid-transformed DH5α was required for storage at -80°C, a colony was picked from the agar plate and cultured in LB, LB-ampicillin (50 mg/ml) or LB-kanamycin (50 mg/ml) at 37°C for 16 hr. The culture (200 μl) and 200 μl of 60% glycerol was mixed together in a 2 ml-microcentrifuge tube. The reagents used in the preparation of competent cells were sterile.

Agarose gel electrophoresis of DNA

For the gel, agarose (SeaKem LE Agarose) powder was mixed with electrophoresis buffer, 0.5X TAE (50X TAE: 2 M Tris base, 1M acetic acid, 50 mM EDTA) at the desired percentages, then heated in a microwave oven until completely melted. The gel solution was cooled in case of any possible evaporation of ethidium bromide (EtBr). EtBr (5 mg/ml) was added to the gel solution to achieve a final concentration of 100 ng/ml to facilitate visualization of DNA after electrophoresis. The solution was poured into a casting tray (HYBAID Electro-4) containing sample combs and allowed to solidify at room temperature. The gel was 0.6 cm thick with well capacity of up to 36 depending on the combs used. The tray was able to take two combs and still have decent distance for DNA fragments to separate at the same time. There were standard combs for 10, 20 or 30 μl loading capacity in each well.

The combs were removed prior to electrophoresis. The tray containing the gel was inserted horizontally into the electrophoresis chamber (HYBAID Electro-4) and just covered with 0.5X TAE. Samples containing DNA mixed with 1X DNA loading

dye [6X DNA loading dye: 18% glycerol, 0.03% bromophenol blue, 0.03% xylene cyanol FF, 10 mM Tris-HCl (pH 7.5), 50 mM EDTA (pH 8.0)] were then loaded into wells. The currents applied for electrophoresis were dependent on time and resolution. The slower the DNA migrates the better the resolution generated when all other factors were controlled. DNA migrates towards the positive electrode. Bromophenol blue and xylene cyanol FF indicate the migrations of 300 bp and 4 kb double strand DNA respectively.

To observe DNA, the gel was placed on an ultraviolet transilluminator (TL-33, UVP Ltd). Digital images of the results were taken with a Kodak EDAS 290 imaging system (EDAS 290 cabinet and DC290 camera adapted to 590DF filter) using Kodak 1D (vision 3.5.3 USB) software. The image could then be converted into the desired file format for processing in different software. Digital images of the results were taken shortly after electrophoresis because DNA diffused within the gel over time.

Isolating fragments of DNA from agarose gel

When a DNA fragment needed to be separated from others, the DNA sample was loaded in an agarose gel, which has suitable composition of agarose. The length of time of electrophoresis for a good separation of DNA fragments depends on percentage of the gel and voltage of the electrophoresis. In general, high percentage agarose gels (i.e. 4% gel) have higher resolution for small DNA fragment (i.e. 100 bp) and take more time. Low percentage gels (i.e. 0.8% gel) have higher resolution for big DNA fragment (i.e. 5 kb) and take less time. The separation results of the gels

were checked on an ultraviolet lightbox covered with cling film. If the separation was not good enough, the gel was returned to electrophoresis for a longer period.

The gel with the target DNA fragment was placed on an ultraviolet lightbox covered with cling film. The target DNA fragment was cut using a clean blade and placed into a labelled 1.5-ml microcentrifuge tube. Gels were exposed to ultraviolet for the minimum time and maximum wavelength. QIAEX II or QIAquick Gel Extraction Kit (QIAGEN) was used to extract DNA from the gels.

Ligation and transformation

Adjacent DNA fragments in either a cohesive-ended or blunt-ended configuration were ligated using T4 DNA Ligase (which catalyzes the joining of two strands of DNA between the 5′-phosphate and the 3′-hydroxyl groups). Some of the blunt-ended DNA fragment was generated by filling in 5′-protruding ends with dNTPs or generated from 3′-overhang by using the 3′ to 5′ exonuclease activity of DNA Polymerase I Large (Klenow) Fragment (Promega).

In some cases, the DNA mixture (up to 1/5 volume of ligation reaction) generated from the Klenow Fragment reaction was added directly into ligation reactions. The amount of DNA used for one ligation reaction varied from reaction to reaction. The reactions however always contained 1X reaction buffer and 2 units T4 DNA ligase (Promega) in a total volume of 10 or 20 μl. The reactions were left at 16°C for 16 hr. If transformation was conducted directly after the ligation reaction, the samples were kept at 4°C. When T4 DNA ligase was purchased, 10X reaction buffer (300 mM Tris-HCl, pH 7.8 at 25°C; 100 mM $MgCl_2$; 100 mM DTT; 10 mM

ATP) was included. The 10X reaction buffers were aliquoted into 0.5-ml microcentrifuge tubes containing 10 μl. (Cautions: DTT oxidation occurs naturally in solution and is accelerated by repeated freezing and thawing or excessive heating.)

For transformation by calcium chloride, competent cells were removed from the -80°C freezer and immediately placed on ice. The cells remained on ice for 6 min. When the frozen competent cells had completely melted, up to 5 μl (one tenth of the volume of the competent cells) ligation reaction was added to the competent cells and gently pipetted to ensure good mixing. The mixture of competent cells and DNA was left on ice for 20 min prior to heat shock at 42°C for 30 sec. The heat shocked mixture was placed on ice for 1min, 900 μl ice-cold LB medium was added and the mixture incubated in a shaker at 37°C for 40 min at 50 rpm. The LB culture was plated on plates that contain the appropriate antibiotic for selection. The plates were incubated normally at 37 °C for up to 16 hr and stored at 4°C for up to two weeks.

For transformation by electroporation, competent cells were taken from the freezer (-80°C) and immediately put on ice. These cells were left on ice for 6 min. When the frozen cells had completely thawed, up to 5 μl ligation reaction was added to the competent cells and the mixture of competent cells and DNA was pipetted into an ice-cold electroporation cuvette (2 mm, ECU102, Equibio Ltd.). The cuvette was then set in the electroporater EasyjecT Plus (Equibio Ltd.). After electroporation (Table 221) the cuvette was again placed on ice, 900 μl ice-cold LB medium added then incubated at 37°C in a shaker at 50 rpm speed for 40 min. Suitable amounts of the LB culture were plated onto a LB plate with suitable antibiotics for selection.

Usually plates were incubated at 37°C for up to 16 hr and stored at 4°C for up to two weeks.

Table 2-221. Settings of the Electroporator.

Applied volts	Field strength	Resistance	Capacitance
2300 V	5 kV/cm	201 Ω	25 μF

Instruction manual of ElectroTen-Blue electroporation competent cells (Stratagene) is a useful reference.

Extraction and enzyme digestion of plasmid DNA

Using rich-LB medium (1% Bacto tryptone, 2% Bacto Yeast Extract, 0.5% NaCl, pH 7.4) instead of LB, a colony picked from a plate took only 8 hr to reach 0.9 OD_{600} at 37°C, ready for plasmid DNA extraction. When extraction of DNA was required for further construction steps or for sequencing purposes, DNA was extracted by using QIAprep Spin Miniprep Kit (QIAGEN). When extraction of DNA was for screening for a target plasmid construct, simple-miniprep was used. Simple-miniprep was a method similar to the kit but without use of spin columns. Firstly, the same solution I, II and III as in QIAprep Spin Miniprep Kit was used, but in 100 μl, 200 μl and 150 μl quantities respectively, to the generate cell lysate. DNA was extracted from the lysate by ethanol precipitation. The DNA pellet was dissolved in 20 μl ddH_2O. Normally 10-μl reaction was prepared for enzyme digestion analysis, in which purified DNA, 1 μl, suitable enzyme and buffer were mixed. Five micro litre of the reaction were loaded for agarose gel electrophoresis.

Plasmid drawing software

Plasmid drawing software, XplasMap 0.96 was used to draw plasmid maps and store information for DNA fragments in the plasmid constructs. This free software was downloaded from Ian York's homepage (http://www.iayork.com/XPlasMap/). The software draws plasmid by simply inputting the information on plasmid, genes, and restriction enzymes one by one. It is suitable hence for drawing the map with critical information rather than the detailed restriction enzyme map. If detail restriction enzyme information is needed free software, ApE (Table 222) is a good choice.

Sequencing

A list of sequencing primers and sequenced plasmid used for this research is summarized in Table 222. When the sequence of a plasmid needed to be checked, the plasmid DNA was transformed into DH5α competent cells and extracted using QIAprep Spin Miniprep Kit (QIAGEN) after the DH5α cells cultured for 16 hr. A 10 μl aliquot of 50 ng/μl plasmid DNA solution in an 1.5 ml microcentrifuge tube was then posted to The Sequencing Service, University of Dundee (Table 222). Results of a sequencing reaction were composed of two types of files, one was a text file with 'seq' as its file extension and the other was a graphic file with 'ab1' as its file extension. Both types of files could be accessed using ApE (Table 222).

Table 3-222. Sequenced Plasmids and Their Sequencing Primers

pITR-bAcP-loxP-RFP-loxP-GFP-ITR Plasmid Construction	
pBSKHcRed	
T3	5'- ATT AAC CCT CAC TAA AGG GA
pCS2ITRX*	
SP6	5'-GAT TTA GGT GAC ACT ATA G
pITRE	
EGFP_S200	5'-GCA TCG CCC TCG CCC TCG
EGFP_S1002	5'-AGA CCC CAA CGA GAA GCG
*pH4HcRedN**	
Red_D100	5'-TGA CCG CCC ACC AGG ACA CC
pBSKCre_1 & _2	
T7	5'-GTA ATA CGA CTC ACT ATA GGG C
T3	5'-ATT AAC CCT CAC TAA AGG GA
pBSKloxInR & pBSKloxInG	
EGFP_S200	5'-GCATCGCCCTCGCCCTCG
pGEMF2R2 (Fig 333)	
T7	5'-GTA ATA CGA CTC ACT ATA GGG C
§4 & 5	
pGEM_ATP_S	
T7	5'-GTA ATA CGA CTC ACT ATA GGG C
pGEM_ISL_S, pGEM_MIB_S, pGEM_NEU_S, pGEM_SAN_S, pGEM_POD_S, pGEM_NE_S	
SP6	5'-GAT TTA GGT GAC ACT ATA G

Sequencing primers T7, T3 and SP6 were provided by The Sequencing Service, University of Dundee. (http://www.dnaseq.co.uk/home5.html). More information about designing a primer in Table 253. ApE (A Plasimd Editer) was developed by M. Wayne Davis, which can be download free from the web site of Jorgensen Laboratory, Department of Biology, University of Utah (http://www.biology.utah.edu/jorgensen/wayned/ape/). This software was recently updated to version 1.12 from version 1.10.4 for Mac OS 10.4.

2.3 pITR-bAcP-loxP-RFP-loxP-GFP-ITR Plasmid Construction

pITRE

The strategy for construction of pITRE is summarized in Fig 231. The XbaI restriction site located near ITR-5' was eliminated from pCS2-ITR (Table 231). XbaI partial digestion, filling in the XbaI digested site (to blunt end) and recircularization of the plasmid were used to generate pCS2-ITRX*. The GFP fragment was cut from pEGFP-N1 (Table 231) by XhoI and XbaI, and then was ligated with XhoI/XbaI pBSK (pBSKpapc, Table 231) to form pBSKE. The GFP fragment was again digested from pBSKE by XhoI and XbaI, and ligated with SalI/XbaI pCS2-ITRX* to form pITRE.

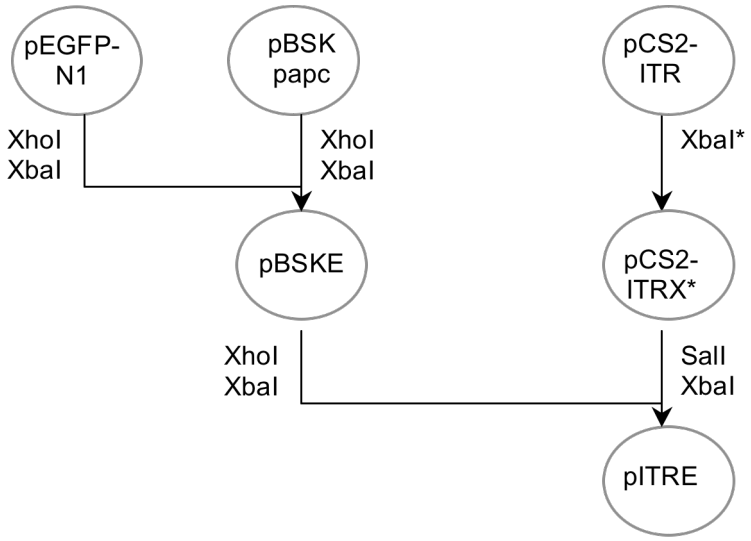

Figure 20-231. Scheme of construction of pITRE.

This chart shows the strategy for constructing pITRE. The circles represent plasmids with their names in the centres. The enzymes that are used to treat the plasmids are shown beside the lines. The arrows always begin from vectors and point to produced plasmids.

Table 4-231. Ingredient Plasmids for pITR-bAcP-loxP-RFP-loxP-GFP-ITR Construction.

Plasmid	Description
pL452	This plasmid provided loxP DNA fragment to pITRbAcRG, pITRbAcRsvG and pITRbAcRvsG constructions. Detailed sequence information for pL452 (Liu et al., 2003) could be found on Recombineering website (http://recombineering.ncifcrf.gov/default.asp). This plasmid was received from Mrs Nina Kotelevtseva, Molecular Physiology, Centre for Cardiovascular Science, University of Edinburgh.
pBSKpapc	This plasmid provided a pBluescript SK II (Stratagene) cloning vector for some intermediary clones. It was EcoRI digested full-length cDNA of zebrafish *papc* from λgt10 cDNA library in pBluescript SK II (Yamamoto et al., 1998). This plasmid was received from Prof E. M. De Robertis, Department of Biological Chemistry, University of California, Los Angeles.
pGEMmyodF	This plasmid provided a pGEM Easy (Promega) cloning vector for some intermediary clones. It was PCR product of full-length cDNA of myod in pGEM-T Easy but there was no reference for this plasmid. This plasmid was received from Dr Sari Pennings, Molecular Physiology Group, Centre for Cardiovascular Science, University of Edinburgh.
pBSKbAcP	This plasmid provided zebrafish β-actin promoter region (Higashijima et al., 1997) for pITRbAcRG, pITRbAcRsvG and pITRbAcRvsG constructions. In the Higashijima's paper pBSKbAcP was named βp-G-β3' plasmid and provided detailed information on the plasmid. Sequence information of zebrafish β-actin gene can be found in GeneBank with accession number zC255L18. The plasmid was received from Dr Shin-ichi Higashijima, Okazaki Institute for Integrative Bioscience, Japan.
pcH4HcRed	This plasmid provided *HcRed*1 (Clontech), red fluorescent reporter gene (*RFP*) with TRF2 3'UTR (Zhang et al., 2008) and poly(A)$_{83}$ (Gu et al., 1999)for pITRbAcRG, pITRbAcRsvG and pITRbAcRvsG constructions but there was no reference for this plasmid. This plasmid was received from Dr Sari Pennings, Molecular Physiology Group, Centre for Cardiovascular Science, University of Edinburgh.

pEGFP-N1	This plasmid provided EGFP (BD Biosciences Clontech), green fluorescent reporter gene (*GFP*) to pITRE and ultimately to pITRbAcRG, pITRbAcRsvG and pITRbAcRvsG constructions. The plasmid was a commercial product from BD Biosciences Clontech and had GenBank accession number U55762.
pCS2-ITR	This plasmid provided ITR (Fu et al., 1998) cassette vector to pITRE and ultimately to pITRbAcRG, pITRbAcRsvG and pITRbAcRvsG constructions. This plasmid was received from Prof Sylvia Evans, Department of Medicine, University of California, San Diego.

pITRbAcRG

The strategy for constructing pITRbAcRG is summarized in Fig 232. The DNA fragment containing loxP sequence was digested by StuI and EcoRI, extracted from pL452 (Table 231), ligated into EcoRV and EcoRI digested pBluscript II SK (pBSKpapc, Table 231) to form pBSKlox. The fragment containing part of the first *intron* and beginning few bases of *exon* 2 of β-*actin* was digested with NheI and NcoI from pBSKbAcP (Table 231), ligated into SpeI and NcoI cut pGEM vector to form pGEMIn. The pBSKloxInG and pBSKloxInR were generated by ligating EcoRI and XbaI digested pBSKlox, EcoRI and NcoI digested In with NcoI and XbaI treated *GFP* (from pITRE, Fig 231) or *HcRed* (from pcH4HcRed N* which comes from NotI digested and filled in pcH4HcRed) respectively. EGFP_S200 (Table 222) was used to sequence both plasmids to check that the reading frame of the reporter gene is correct. Then NheI and BstXI digested loxInG fragment was ligated into XbaI and BstXI digested pBSKloxInR to produce pBSKloxInRG. Using SalI and XbaI to cut loxInRG from pBSKloxInRG, it was then put into SalI and XbaI digested pITR

(from pITRE) to generate pITRloxInRG. The final step for this construct was to insert the SalI and NheI digested beta-actin promoter region into SalI and NheI treated pITRloxInRG to generate pITRbAcRG.

pITRbAcRsvG & pITRbAcRvsG

Fig 233 illustrates the strategy for constructing pITRbAcRsvG. Firstly, the DNA fragment, which consisted of SV40 pA and ITR (SVI) was cut with BamHI and PvuII from pCS2-ITR and then ligated into EcoRV and BamHI digested pBluescript II SK vector (pBSK) to form pBSKSVI. To eliminate the ITR sequence from pBSKSVI, partial digestion of SnaBI was combined with HindIII complete digestion. HindIII sticky ends on the remaining backbone were filled into blunt ends, followed by recircularization to generate pBSKSV. The SV40 pA fragment was digested by XhoI and SalI, and inserted into XhoI digested and alkaline phosphatase (CIP, Promega) treated pITRbAcRG to generate pITRbAcRsvG and pITRbAcRvsG (the XhoI-digested vector can receive both orientations of insert, if the SV40 pA direction is the same as β-*actin* promoter transcription, the plasmid has the label “sv”; the reverse, the label is “vs”).

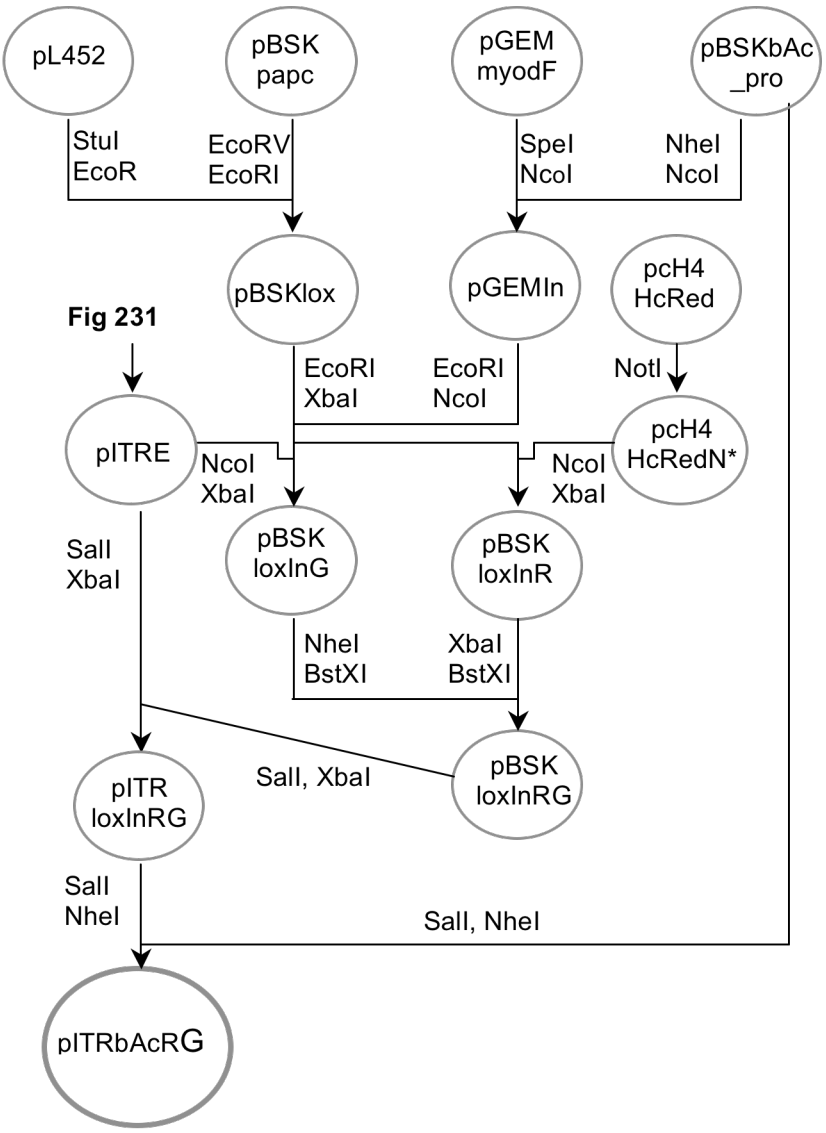

Figure 21-232. Scheme of pITRbAcRG construction.

This chart shows the strategy for constructing pITRbAcRG. The circles represent plasmids with their names in the centre. The enzymes that are used to treat the plasmids are shown beside the lines. The arrows always begin from a vector and point to a produced plasmid, except pBSKloxInR and pBSKloxInG which are generated by using pBSKlox as vectors and pGEMIn, pITRE or pGEMIn, pcH4HcRedN* providing insert DNA fragments respectively.

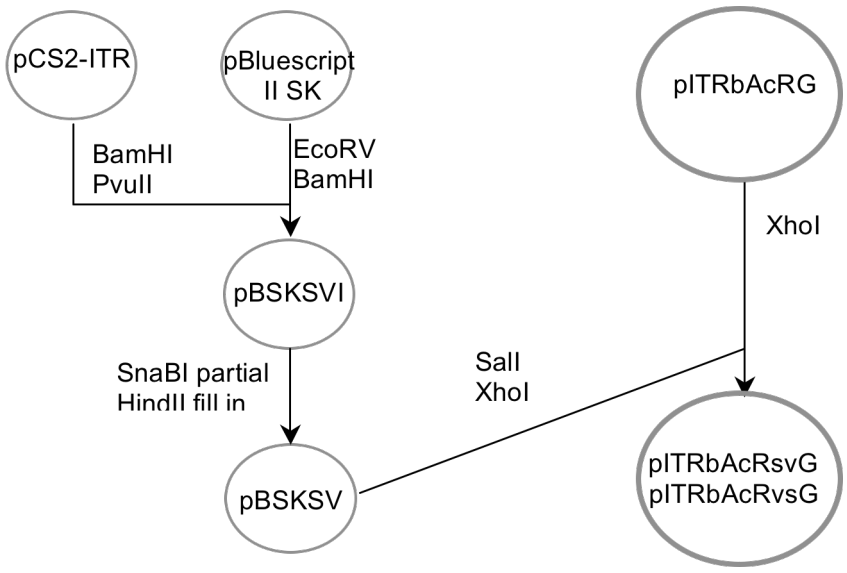

Figure 22-233. Scheme of pITRbAcRsvG and pITRbAcRvsG construction.

This chart shows the strategy for constructing pITRbAcRsvG and pITRbAcRIG (indicated with heavier lines). The circles represent plasmids with their names in the centre. The enzymes that are used to cleave the plasmids are shown beside the lines. The arrows always begin from a vector and point to a produced plasmid.

2.4 Microinjection of Zebrafish Embryos

Preparation of microinjection needles

The micropipettes used in the microinjection were generated by pulling glass capillaries, GC100TF-10 (Harvard Apparatus Ltd.) with the micropipette puller, PC-10 (NARISHIGE). Pulling and clip temperature were 69°C and 75.9°C respectively with light tension adjustment. The general outcome was needles of 0.0003 inches diameter and closed tip just after pulling. The needle tips were then ground to 0.0005 to 0.0008 inches diameter and sharp edge (Fig 241) by using Tip-grinder,

Kapillarschleifer (H. SAUR). In fact the outcome for micropipettes generated by PC-10 depends on the combination of settings of temperature and pulling force. The manufacturer's instruction for the PC-10 provides details.

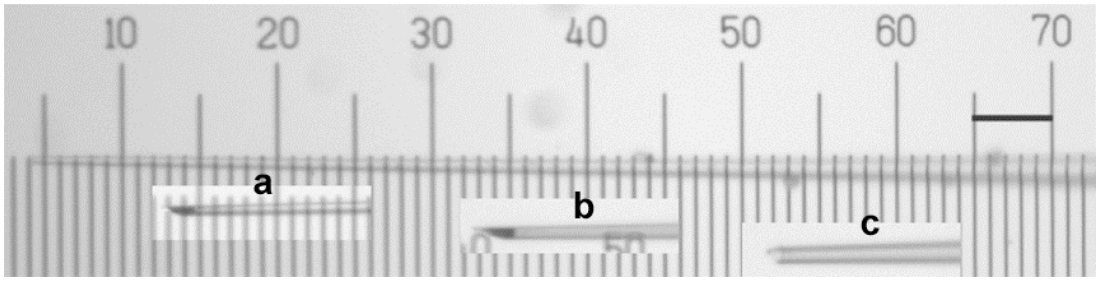

Figure 23-241. A Suitable Micropipette for Microinjection.
The illustration shows three different needles. The tip of the needles suitable for injection is 'b', whereas tip 'a' is too thin and tip 'c' is too wide for the microinjection of zebrafish embryos. The scale bar represents 0.005 inches.

Preparation of equipment for handling zebrafish embryos, Part II

Agarose gel trays for array of embryos for microinjection were prepared with 0.8% agarose (SeaKem LE Agarose) in ddH_2O. Firstly, 15 ml of melted agarose were poured into a 9-cm Petri dish, left to cool and solidify, then 10 ml of melted agarose was topped on the solid agarose to form a second layer. Prior to the second layer becoming solid a mould (Fig 242a) (for making three slits in the top layer of the gel) was placed into this layer. When the top gel became solid, the mould was carefully removed from the gel to generate an agarose gel tray with three slits (Fig 242c). The gel trays were stored at 4°C with a thin layer of ddH_2O and reused many times.

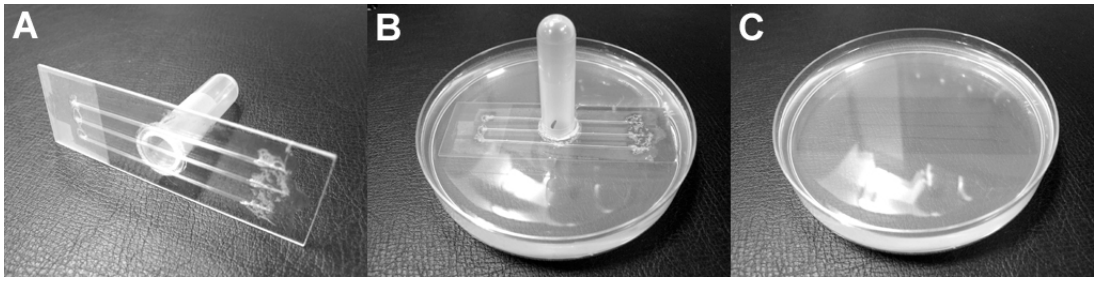

Figure 24-242. Making Agarose Gel Trays.

(A) The mould is generated by sticking a few pieces of double-sided sticky tape onto one side of a glass slide (Premium Microscope Slides, BDH), attaching three half-length glass capillaries, GC100TF-10, and glueing a handle onto the other side of the slide. The Shape of GC100TF-10 and the flexibility of agarose gel gave suitable space to hold chorion-shelled zebrafish embryos. (B) Capillary side of the slide is merged into melted agarose. (C) An agarose gel tray ready to use.

Microinjection

The plasmid DNAs of pITRbAcRG, pITRbAcRsvG and pITRbAcRvsG for microinjection were prepared by using QIAprep Spin Miniprep Kit (QIAGEN). Prior to microinjection, the DNA mixture was freshly prepared. The plasmid DNA concentration was diluted to 10 μg/ml in 250 mM KCl and 0.2% (v/v) phenol red with sterile distilled water (dH_2O) to a volume of 20 μl. A suitable micropipette was connected to the microinjector, IM 300 (NARISHIGE). The DNA solution was laid on a piece of Parafilm (Pechiney Plastic Packaging Company) and loaded into the micropipette from the tip of needle by adjusting injection pressure to slightly less than the pressure of the DNA solution. Around 50 zebrafish, 1- to 8-cell embryos were arrayed on an agarose gel tray and injected one by one. Injection pressure was 10 psi. Each injection took 0.01 sec. In order to maintain a good pressure balance between inside and outside the micopipette, the pressure balancer was increased little by little as the DNA solution deceased in volume when the number of embryo injections increased.

2.5 Analysis Of RNA Structure For Transgenes In Microinjected Embryos With RT-PCR

RNA extraction

Embryos (Table 251), which were non-injected or had fluorescent signal after microinjection of pITRbAcRG, pITRbAcRsvG or pITRbAcRvsG, were collected and incubated at 28°C until 5 dpf. Six to twelve 5-dpf embryos, that were of the non-injected wild type or had been injected with one of the three plasmids, were put into a 1.5-ml microcentrifuge tube with 100 μl Trizol reagent (Invitrogen) and homogenized using a glass pestle, Tissue Grind Micro (Fig 251, KONTES) or by MM301 mixer (Retsch). When MM301 was used to homogenize embryo samples, the embryos were put into a 2-ml microcentrifuge tube with a stainless steel grinding ball (EW-04185-63, Cole-Rarmer, 4 mm). Once all the tissue lysed properly, 100 μl more Trizol was added to the tube, then Trizol manufacture protocol was followed with 200 μl solution. The chloroform extracted aqueous phase was treated with 1 unit of DNase (RQ1, RNase Free, Promega) at 37°C for 30 min and the DNase was inactivated by incubation at 65°C for 10 min. Finally an RNA pellet was dissolved in 20 μl RNase-free water and stored at -20°C. Information about precautions for handling RNA can be found on the web site of Leeward Community College, University of Hawaii.
(http://abe.leeward.hawaii.edu/Protocols/General%20Guidelines%20for%20Working%20with%20RNA.htm)

Table 5-251. Embryos Collected for RNA Extraction.

Injected Plasmid	Non-injected	pITRbAcRG	pITRbAcRsvG	pITRbAcRvsG
Number of Embryos	10	12	6	11

Microinjection experiments of the three plasmids were done on different days, hence different plasmid injected embryos were from different zebrafish mating pairs.

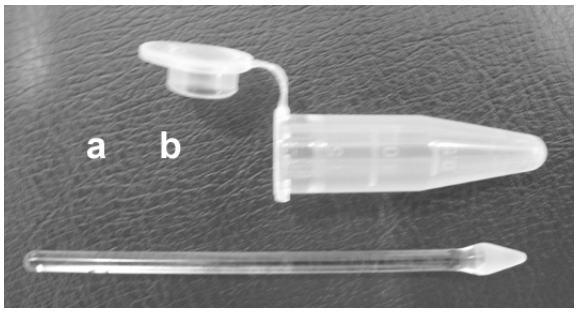

Figure 25-251. Tissue Grind Micro.
The Tissue Grind Micro is glass pestle (a). The pestle end mates with 0.5-ml and 1.5-ml (b) microcentrifuge tubes.

Reverse transcription (RT) reaction

RT reactions (Table 252) were set up using 500 ng total RNA, 500 ng Oligo$(dT)_{15}$ (Promega) or 100 ng random primers (Promega), 1 μl dNTP Mix (10 mM each of dATP, dCTP, dGTP and dTTP, Promega), 40 units RNase inhibitor (RNasin, Promega) and 160 units SuperScript^{TM} II or III reverse transcriptase (Invitrogen) in 0.2-ml PCR tubes. The temperature programme was: 65°C for 5 min, 4°C for 5 min, 42°C for 3 min for Oligo $(dT)_{15}$ primers or 25°C for 13 min for random primers, 42°C for 50 min, 70°C for 15 min, 37°C for 22 min, final step 95°C for 5min on a

PCR machine (TGradient, Biometra). Mixture I (Table 252) was heated to 65°C for 5 min to start the temperature programme on the PCR machine. The reaction tube was kept in the PCR machine until the temperature programme had finished. Mixture II (Table 252) was added to mixture I the end of 4°C. SuperScript II or III reverse transcriptase was added into the mixture after 3 min incubation at 42°C or 25°C. *E. coli* RNase H (1.6 units, Invitrogen) which was added after 2 min incubation at 37°C, was used to remove RNA complementary to the first strain cDNA after inactivation of reverse transcriptase and its activity was further inactivated at 95°C for 5 min. The template for PCR reaction was generated. Note: RNase H treatment is an optional step for PCR product size longer than 3 kb.

Table 6-252. RT Reactions

RNA from	WT	RG	RG	SV	SV	VS	VS
Mixture I	500 ng total RNA 500 ng Oligo(dT)$_{15}$ or 100 ng random primers 1 μl of 10 mM dNTP Mix DEPC treated distilled water to 12.2 μl						
Mixture II	4 μl of 5X First-Strand Buffer 2 μl of 0.1 M DTT 1 μl of RNasin (40 units/μl)						
Superscript™ II or III (units)	160	0	160	0	160	0	160

The dNTP mix was prepared by mixing together and diluting from100 mM dATP, dTTP, dCTP and dGTP. The DTT and 5X First-Strand Buffer (250 mM Tris-HCl, pH8.3 at room temperature; 375 mM KCl; 15 mM $MgCl_2$) came commercially with Superscript™ II or III as a package. WT, non-injected embryos; RG, pITRbAcRG injected embryos; SV, pITRbAcRsvG injected embryos; VS, pITRbAcRvsG injected embryos.

Polymerase chain reaction (PCR)

Six primer pairs: F1/R2, F2/R3a, F1/R3b, F2/R3b, F2/R4; and F1/R5 (Table 253) were used to analyze the structure of both mature and precursor mRNA. Every PCR reaction was conducted in a 20 μl reaction that consisted 500 nM of each forward and reverse primer, 1 mM $MgSO_4$, 250 μM of each dNTPs, 1 μl of cDNA from first-strand (RT) reaction and 1 unit of Taq DNA polymerase (ABgene) 1X PCR Buffer by PCR machine, TGradient (Biometra) with the thermal cycle programme: 94°C for 2 min; 94°C for 20 sec, 60°C for 1 min, and 72°C for 2 min for 30 cycles. The PCR Buffer was supplied with Taq DNA polymerase (ABgene) as 10X that consisted 200mM Tris-HCl (pH 8.4), 500 mM KCl. In general, 94°C is the denaturation temperature; 60°C and 72 °C are annealing and elongation temperatures respectively. The optimal annealing temperature and concentration of Mg^{2+} depend on the template and the primer pair. Both $MgSO_4$ and $MgCl_2$ are frequently used as Mg^{2+} reagents.

Agarose gel electrophoresis of DNA

The PCR products were analysed using 1.5% agarose gel electrophoresis. The photographs of the gel electrophoresis results were taken using a Kodak EDAS 290 imaging system (EDAS 290 cabinet and DC290 camera) with Kodak 1D software. More detailed information about agarose gel electrophoresis of DNA can be found in §2.2.

Table 7-253. Sequences of PCR Primers Used in §3

F1 (bAc_D100)	5'-CTAGTGCGGAATATCTGCTTG
F2 (Red_D100)	5'-TGACCGCCCACCAGGACACC
R2 (Red_D200)	5'-GTGTCCTGGTGGGCGGTC
R3a (EGFP_S200)	5'-GCATCGCCCTCGCCCTCG
R3b (EGFP_S100)	5'-CGCTTCTCGTTGGGGTCT
R4 (bAc_i_200)	5'-CGAATGAGCCGATGTTAGATTGATG
R5 (bAc_D200)	5'-GACGGGGTGCTCCTCTGGG

These primers were designed based on several principles. Firstly 300 bp to 1 kb PCR products can be generated in detection reactions. Secondly all the primers have Tm 60 °C or higher. Finally the secondary structures, for example hairpin, dimer and cross dimer of the primers are as little as possible. Primer sequences without any secondary structure or with less stable secondary structure are favourable. All the primers were analysed to check their secondary structures and Tm by NetPrimer, free primer analysis software, on Primer Soft International web site (http://www.premierbiosoft.com/netprimer/).

2.6 Genotyping For *Spt*, *Ntl* & *Oep* Mutant Alleles

Preparation of DNA for Genotyping (Appendix, A1)

Three month old zebrafish were anesthetized using 0.016% Tricaine (Ethyl 3-aminobenzoate, Sigma) in water from 0.4% Tricaine stock solution. A fin clip, 2 mm^2 in size, was put into 2 ml microcentrifuge tube containing 100 µl of extraction buffer (100mM NaCl, 0.5% N-lauroylsarcosine) and a stainless steel grinding ball (EW-04185-63, Cole-Rarmer, 4 mm). The fin clip was homogenized with MM301 mixer (Retsch) for 1 min at 30/s frequency. The microcentrifuge tube was transferred to boiling water and incubated for 15 min. After cooling for 3 min, 100 µl of 20 %

Chelex® (Bio-Red) in ddH_2O, which had been equilibrated for 12 h and then autoclaved, were added. The sample was mixed gently every 3 min while being incubated at room temperature for 15 min. The sample was placed back into boiling water for a further 15 min. The sample can be kept at room temperature for at least four weeks (Altschmied et al., 1997; Kawakami and Hopkins, 1996; Walsh et al., 1991).

Polymerase chain reaction (PCR)

The DNA-containing solutions, directly before PCR, were centrifuged for 10 min at 15000x g. Specific primer pairs (Table 261) were used to identify *spt*^{b104}, *ntl*^{tc41} and *oep*^{tz57} alleles. Each PCR reaction was conducted in a 20 μl sample consisting of 500 nM of each forward and reverse primer, 3 mM $MgSO_4$, 250 μM of each dNTPs, 1 μl of genomic DNA extraction supernatant and 1 unit of Taq DNA polymerase (ABgene) 1X PCR Buffer by PCR machine, TGradient (Biometra). The thermal cycle programme was 94°C for 2 min; 94°C for 20 sec, 62°C for 1 min, and 72°C for 30 sec to 2 min (depending on the size of the target product) for 30 cycles.

Agarose gel electrophoresis of DNA

The PCR products were analysed using 1% agarose gel electrophoresis. Photographs of the gel electrophoresis results were taken using a Kodak EDAS 290 imaging

system (EDAS 290 cabinet and DC290 camera) with Kodak 1D software. More detailed information about agarose gel electrophoresis of DNA can be found in §2.2.

Table 8-261. Sequences of PCR Primers Used in Genotyping

Spt	
sptF	5'-TTG ACC ACA ATC CCT TTG CCA A
sptb104F	5'-CCT TTA CTG CCG TCA CTG CCT ACC
sptb104R	5'-GCC TTC ACC TCC AGC TCT TTA CG
Ntl	
ntlF	5'-CG AAT GTT TCC CGT GCT CAG AG
ntltc41R	5'-GTG TAT CCT GGG TTC GTA TTT GTG CT
ntltc41wtR	5'-GTG TAT CCT GGG TTC GTA TTT GTG CA
Oep	
oepF	5'-CTG GGG CTC TAA GCG GCT GCT
oeptz57R	5'-CTC ACC CGA ACA GTT GAC TCG TCA C
oeptz57wtR	5'-CTC ACC CGA ACA GTT GAC TCG TCA T

2.7 Immunostaining & RNA Whole Mount *In Situ* Hybridization

Cloning plasmid of Probes For* In Situ *Hybridization

The primers (Table 271) were designed for amplification of approximately of 500 bp PCR products for each gene. Cloning vectors, pGEM-T Easy (Promega), had a 3'-terminal thymidine (3'-T) to both ends. These single 3'-T overhangs at the insertion site have better efficiency of ligation of a PCR product into the plasmids because of the prevention of recircularization of the vector. These single 3'-T overhangs also provide a compatible overhang for PCR products generated by polymerases that

often add a single deoxyadenosine, in a template-independent fashion, to the 3'-ends of the amplified fragments (e.g. Taq, AmpliTaq®). In the experiment, Taq DNA polymerase (ABgene) was used to amplify target DNA. PCR products for each gene were cloned into pGEM-T Easy. Orientation of the PCR product insertion was verified using various appropriate restriction enzymes. If anti-sense RNA was synthesized by T7 RNA polymerase, the plasmid was named by addition of '_A' (Table 271). If anti-sense RNA was synthesized by SP6 RNA polymerase, the plasmid was named by addition to '_S' (Table 271). In order to ensure specificity of the probes, sequence on the vector between SP6 promoter and DNA insertion was deleted by appropriate restriction enzymes digestion and recircularization of the plasmid ('_dS', Table 272).

Table 9-271. Sequences of Primers Used in Cloning Probes

pGEM_ATP_S	ATP_F atp2a1 WISH probe, NM_001007029 (1-23) ATGGAGAACGCACACACCAAGGA ATP_R atp2a1 WISH probe, NM_001007029 (650-628) CCAGCAGCGATGTTAGTGCCAGA
pGEM_NEU_A	NEU_F neurolin WISH probe, NM_131000 (614-634) GGGAATGTGTGGTGGAGAGCG NEU_R neurolin WISH probe, NM_131000 (1168-1143) TTAACACCTTGCCTGTAGGAGTGAGG
pGEM_SAN_A	SAN_F santa WISH probe, NM_199572 (925-948) CCATAGTCCCCATTTCAAAGGTCA SAN_R santa WISH probe, NM_199572 (1420-1397) GTGTGATTTGGTTACCCATACGCA

pGEM_ISL_S	ISL_F Islet2a WISH probe, NM_130970 (626-646) AGCAGTCGGAGAAAACCACGC ISL_R Islet2a WISH probe, NM_130970 (1148-1129) CACGTCTCCACGGGACTGGG
pGEM_MIB_A	MIB_F Mibp2 WISH probe, NM_198877 (202-226) CAAAATCACGTCGAGGATGAAGTTC MIB_R Mibp2 WISH probe, NM_198877 (919-900) AAACAACAGCGATGCAGCCG
pGEM_POD_A	POD_F podocin WISH probe, AY956356 (667-692) CGTCTCTGTGTGTTATTCCTCCTTCG POD_R podocin WISH probe, AY956356 (1147-1125) AGCAGGTCTGGTCAAACTGGCGA
pGEM_NE_A	NE_F nephrin WISH probe, NM_001040687 (240-263) GCGATACAGCATGACAGGAGACCA NE_R nephrin WISH probe, NM_001040687 (782-756) GCATACCACTTTGAGAAAGGAGCCG
pGEM_SPD_A	Spon1b_F Spondin 1b WISH probe, NM_131517 (1549-1568) AGGGGCGGAGGATGAGGCAG Spon1b_R Spondin 1b WISH probe, NM_131517 (2299-2279) TGGACCGTCTCAGGACAGGGC
pGEM_SHH_A	SHH_F Sonic hedgehog WISH probe, NM_131063 (146-168) CGTTATCAGTCGCACGTTTCCGC SHH_R Sonic hedgehog WISH probe, NM_131063 (1606-1580) TTCTCTTGCTTTATTTCCACACGAGGG
pGEM_CML_S	CML_F Cmlc2 WISH probe, AF425743 (1-25) TGAACATGGCTAGTAAGAAAGCCGC CML_R Cmlc2 WISH probe, AF425743 (587-561) GCTGCTGATGTGAATGTTGAACTGAAC
pGEM_FOX_A	FOX_F FoxA3 WISH probe, NM_131299 (891-912) CGGCTCTGATGGGGCTGAATCT FOX_R FoxA3 WISH probe, NM_131299 (1408-1381) CAACTGGCTGGTAAACACATTAGGATGC

Preparation Of Dig Labelled RNA Probes (Appendix, A2)

Dig labelled RNA probes were generated by *in vitro* transcription. DNA template was prepared by linearization of a plasmid with a restriction enzyme (Table 272) located at an appropriate length downstream of the promoter (Table 272). To avoid transcription of undesirable sequences, a restriction enzyme, which creates 5´-overhangs was used. A minimum of 2 μg of plasmid DNA was used in one labelling reaction. A small amount of the linearized DNA was loaded on an electrophoresis agarose gel, to ensure that the linearization was completed. The linearized DNA was treated with 1 μl of 10 mg/ml PK and incubated at 37°C for 30 min. After this step, the DNA sample was carefully stored in an RNAse free environment. The DNA was then purified by Phenol/Chlorofrom extraction and ethanol precipitation (one tenth sample volume of 3M NaOAc, pH 5.2; three times sample volume of ethanol; incubation at -70°C for 20 min). The purified DNA was dissolved in 14 μl of DEPC-treated ddH_2O. One micro litre of this was loaded on an electrophoresis agarose gel, to ensure that the purification and the amount of DNA were appropriate.

Labeling reaction

The 13 μl purified template DNA was kept on ice, 2μl of 10X NTP labelling mixture (Table 272), 2 μl of 10X transcription buffer, 1μl of 40 unit/μl RNase inhibitor (RNasin, Promega) and 1μl of RNA polymerase (Table 272) were added to the sample. The reaction was incubated at 37°C for 2 hr and inactivated by addition of 2 μl 0.2 M EDTA, pH 8. The labelled RNA was purified by adding 2.5 μl of 4M LiCl

and 75 µl of 100% EtOH to the sample and incubating at -20°C for 2 hr. After centrifugation at 4°C for 20 min the purified RNA probe was dissolved in 21 µl DEPC-treated ddH_2O. One µl of RNA probe was analyzed using 2% electrophoresis agarose gel to ensure the quality and quantity of the probe. Finally, the 20 µl RNA probe was suspended in 180 µl hybridization buffer (Appendix, A2) and store at -20°C.

Table 10-272. Labelling Mixture, Promoters and Enzymes for Synthesis of Anti-sense RNA probes

Plasmid	Promoter	Restriction enzyme	Labelling Mix
pBKSwt1_A	T7	StuI	DIG
pBSKmyod_A	T7	BamHI	Fluorescein
pGEM_ATP_dS	SP6	BglII	Fluorescein
pGEM_NEU_A	T7	BglII	Fluorescein
pGEM_SAN_A	T7	SpeI	Fluorescein
pGEM_ISL_dS	SP6	MluI	Fluorescein
pGEM_MIB_A	T7	XhoI	Fluorescein
pGEM_POD_A	T7	NheI	DIG
pGEM_NE_A	T7	XbaI	DIG
pGEM_SPD_A	T7	BamHI	Fluorescein
pGEM_SHH_A	T7	BglII	Fluorescein
pGEM_CML_dS	SP6	SpeI	Fluorescein
pGEM_FOX_A	T7	BamHI	Fluorescein

The Promoter column indicates corresponding RNA polymerase used in the RNA probe labelling reaction. Restriction enzymes employed for linearization of template plasmids are shown. Some of probes were labelled with digoxigenin-UTP (DIG) and the others were labelled with fluorescein-12-UTP (Fluorescein). Two colour whole mount *in situ* hybridizations were conducted using the appropriate mix of probes.

Whole Mount In Situ Hybridization

At the required stage of development, after dechorionation, embryos were fixed in 4% paraformaldehyde (PFA) at 4°C overnight. The embryos were dehydrated in 100% methanol and stored at -20°C at least 16 hr prior to whole mount *in situ* hybridization. Whole mount *in situ* hybridization was performed as described in Appendix, A3.

Whole Mount Immunostaining

Embryos were maintained in 0.003% PTU prior to the desired developmental stage (36 or 48 hpf) then fixed overnight at 4°C in 4% paraformaldehyde (PFA) in PBS, pH 7.4. Permeabilization was carried out by adding 2% Triton X-100 (overnight at 4°C). After four 5-min washing steps with PBST (1X PBS, 1% Tween 20), the embryos were blocked for 1 hr at 25°C in PBST with the blocking solution (1% BSA, 1% DMSO). A primary antibody (Table 273) was used at 1:400 in the blocking solution and incubated at 4°C overnight. After four 15-min washing steps with PBST (1X PBS, 1% Tween 20), the embryos were incubated overnight at 4°C with a secondary antibody (Table 273), 1:400 in blocking solution. Sometimes 2.5 mg/ml Alexa-fluor-488-phalloidin (Molecular Probes) and DAPI (1:400) were added to the solution. The embryos were washed four times, 15 min each time, with PBST. Finally the embryos were fixed in 4% PFA.

Table 11-273. List of the Fluorescent Dyes, Primary and Secondary Antibodies for the Experiment

Fluorescent Dyes		Supplier (Catalogue number)
DAPI		Sigma (D9564)
Alexa Fluor 488 phalloidin		Invitrogen (A12379)
Alexa Fluor 594 phalloidin		Invitrogen (A12381)
Primary antibodies	Host animal	Supplier (Catalogue number)
Anti-Tubulin	Mouse	Sigma (T6074)
Anti-Fibronectin	Rabbit	Sigma (F3648)
Anti-Invadolysin	Rabbit	Heck Laboratory
Secondary antibodies	Host animal	Supplier (Catalogue number)
Anti-mouse Alexa Fluor 488	Donkey	Invitrogen (A21202)
Anti-mouse Alexa Fluor 594	Donkey	Invitrogen (A21203)
Anti-rabbit Alexa Fluor 488	Donkey	Invitrogen (A21206)
Anti-rabbit Alexa Fluor 594	Donkey	Invitrogen (A21207)
Anti-mouse Fluorescein	Donkey	Jackson ImmunoResearch (71535)
Anti-rabbit Fluorescein	Donkey	Jackson ImmunoResearch (71452)

2.8 Cryosection

Embryos were removed from 4% PFA and rinsed with 1X PBS in 2ml-microcentrfuge tube five times, 5 min for each rinse. The embryos were soaked in 25% sucrose in 1X PBS at room temperature until the embryos sank to the bottom of the tube. The 25% sucrose was removed and 35% sucrose in 1X PBS was added until the embryos again sank to the bottom of the tube (the embryos can be stored in 35% sucrose at 4°C for up to one week). The cryostat (Bright, Model OTF) was set to -20°C. Inside the cryostat was the microtome (Bright, Microtome 5040). A 0.5 mm

thick layer of OCT (Raymond A Lamb) was applied to the centre of a chilled cryostage and either allowed to solidify slowly by sitting in the chamber of the cryostat or instantly by spraying the cyostage with Cryospray 134 (Bright). A further layer of OCT was applied on top of the solid layer of OCT. One of the embryos was carefully placed onto the OCT and embedded well into it. This layer of OCT was allowed to solidify slowly by sitting in the chamber of the cryostat. The cryostage was transferred to the cryostage holder. A section of thickness 15 μm was trimmed from the appropriate part of the embryo. Sections were firstly laid on the section stages then the series of sections were arrayed on a Superfrost Plus microscope slide (BDH) by allowing the cryosection to gently melt onto the slide. The sections were allowed to adhere to the slide overnight at room temperature prior to application of mounting medium (20 g/ml Mowiol, 50% glycerol) and a coverslip. The slide was left at room temperature overnight again prior to sealing of the edge of the coverslip with clear nail varnish.

2.9 Imaging

Microinjection of pITRbAcRG, pITRbAcRsvG and pITRbAcRvsG

The images of microinjected embryos were taken under a fluorescent microscope, M2FLIII (Leica), with a Leica DFC (300 FX) camera system. The filter sets used for RFP and GFP expression (Table 291) were Texas Red and GFP Plus (Table 292) respectively. When images were taken, a live embryo was placed onto a glass bottomed culture dish (FluoroDish™, 35mm, 10mm well, World Precision

Instrument) without any anaesthesia treatment. Embryos had however been incubated in 0.003% phenylthiourea (PTU) prior to 10 hpf until the desired developmental stage for image taking was reached. The PTU stock solution was 0.15%. If crystals of phenylthiourea appeared in the stock solution, the stock solution was incubated at 65°C to dissolve the crystals.

Whole mount in situ hybridization embryos

In addition to the LEICA M2 16F (Leica) and the Leica DFC (300 FX) camera system, Leica LED 1000 modular daylight illumination (ringlight) was used to take images. Embryos were embedded in 3% Methylcellulose (Table 293) in a glass bottomed culture dish (FluoroDish™, 35mm, 10mm well, World Precision Instrument).

Whole mount immunostained embryos

Fluorescent microscope M2FLIII (Leica) and filter sets (Table 292) and a Leica DFC (300 FX) camera system were used to take images. Fluorescent stain or conjugates applied in this research work were DAPI, Alexa Fluor 488 and Alexa Fluor 594 (Table 294). Embryos were embedded in a Mowiol mounting medium (20 g/ml Mowiol, 50% glycerol) in a glass bottomed culture dish (FluoroDish™, 35mm, 10mm well, World Precision Instrument).

Table 12-291. Living Colours Fluorescent Proteins (Clontech)

	Excitation maximum (nm)	Emission maximum (nm)
HcRed1	588	618
EGFP	489	508

Table 13-292. Leica MZ16 F & MZ16 FA Filter Sets (Leica)

	Exciter filter	Barrier filter
GFP Plus	480/40 nm	510 LP
Texas Red	560/40 nm	610 LP
UV	360/40 nm	420 LP

Table 14-293. Preparation of 3% Methylcellulose. (Sigma M-6385)

(1) Bring 194 ml ddH_2O to 90°C, remove from heat and add 6 g methylcellulose.
(2) Mix, then place in an ice bucker and stir slowly, covered with a plastic Petri dish, until the solution reach 10°C
(3) Seal with Parafilm and leave stirring over night in the cold room.
(4) Turn the stirring off on the following day and let the mixture 'ripen' for 3 days in the cold room.

More information of preparation of 3% Methylcellulose can be found in this web link 'http://www.liv.ac.uk/emunit/root/electron%20microscopy%20unit/research/Protocols/Recipes.pdf'

Table 15-294. Fluorescent stain or conjugates. (Molecular Probes)

	Excitation maximum (nm)	Emission maximum (nm)
DAPI	402	421
FITC/Fluorescein	468-509	504-541
Alexa Fluor 488	495	519
Alexa Fluor 594	590	617

3. Tracing Cell Lineage Using The Cre-LoxP System

In order to trace and label PGP in the developing zebrafish embryos in real-time, a Cre-loxP transgene gene expression system was designed. The Cre-loxP system was discovered in prokaryotes and the phage P1 encodes a recombinase called Cre, which acts at a short asymmetric pair of DNA sequence called loxP. The composition of Cre and loxP is an efficient site-specific recombination system (Abremski et al., 1983; Hoess and Abremski, 1985; Sternberg and Hamilton, 1981; Van Duyne, 2001) and has become an important tool for conditional gene knock out, genome modification, termination of transgenes, and cell lineage mapping (Branda and Dymecki, 2004). A pair of target sequence acting as a substrate for a recombinase is termed "floxed".

In this study I aimed to generate a Cre-loxP system, which enables a colour change to be observed (RFP to GFP) when Cre is first expressed in cells in the microinjected developing embryos. In this construct, β-*actin* promoter (zebrafish) driven *rfp* will be floxed and the second reporter gene, GFP, will be placed adjacent to a loxP site at the 3'-end of RFP. Transgene expression will be assessed following microinjection of the construct into zebrafish embryos.

3.1 pITR-bAcP-loxP-RFP-loxP-GFP-ITR Constructs

pITRE

The strategy for construction of pITRE is summarized in Fig 231. The square of flanking ITR (see pCS2-ITR, Table 231) in pITRE was verified by two sequencing reactions, EGFP_S200 and EGFP_S100 (Table 222). The plasmid was 4852 bp in

size, with a 500 bp DNA fragment between the ITR-5' (see pCS2-ITR, Table 231) and a multiple cloning site (MCS) and GFP followed by a reversed SV40 poly adenine (pA) signal and the ITR-3' (see pCS2-ITR, Table 231). A map of pITRE is shown in Fig 311. The process was lengthy for the construction of pITRbAcRG, pITRbAcRsvG and pITRbAcRvsG plasmids; pITRE was a plasmid prepared to provide ITR-cassette and GFP to the three final plasmids.

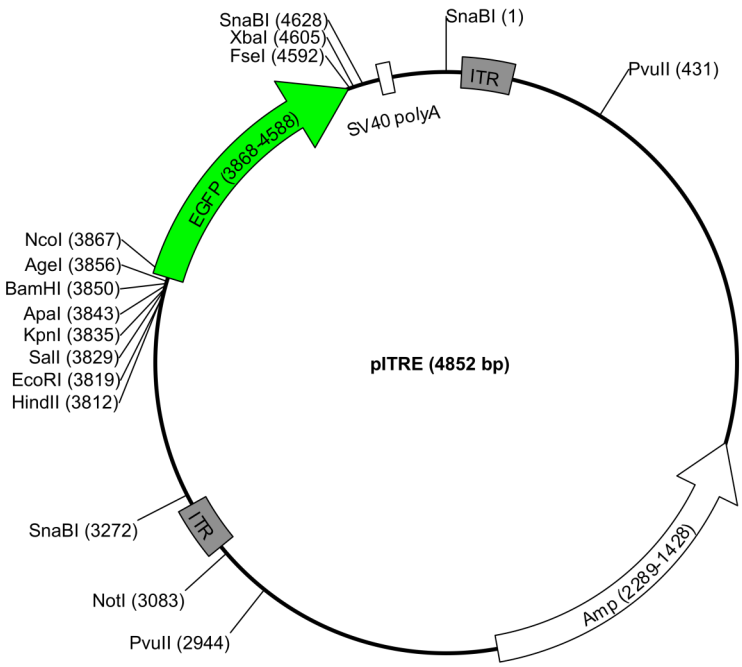

Figure 26-311. Restriction enzyme map & gene layout for pITRE.

The MCS between 3812 and 3867 is adjacent to the upstream of the EGFP. The arrow in EGFP indicates the direction of sense strand of GFP transcripts. This map was drawn using MacPlasmap (version 1.83), free software for Mac OS 7 to Mac OS 9. Further information on pITRE can be found in the Discussion (§6.1).

pITRbAcRG, pITRbAcRsvG & pITRbAcRvsG

Constructs pITRbAcRG and pITRbAcRsvG were generated for the purpose of Cre-mediated colour-exchange expression. Construct pITRbAcRvsG was produced as a control for reverse SV40 pA signal for pITRbAcRsvG. The three plasmids had several common features in their structures, for instance a 15 kb zebrafish β-*actin* upstream region (Higashijima et al., 1997), *exon*1 and first intron. Translation start site of β-actin in *exon* 2 was fused with RFP or GFP reporter genes. RFP cDNA was flanked by loxP. The structure of promoter-loxP-RFP-loxP-GFP was flanked by ITR-5' and ITR-3' (see pCS2-ITR, Table 231). The first plasmid pITRbAcRG (Fig 312) was 23 kb in size, had no SV40 polyA signal at the 5'-end of RFP but had the 3' untranslated region of the mouse TBP-related factor 2 (TRF2 3'UTR) and polyadenine (Yamagata et al., 2005). The SV40 pA signal (Weiss et al., 1991) was inserted into 3'-end of TRF2 3'UTR and polyadenine in plasmids pITRbAcRsvG (Fig 313A) and pITRbAcRvsG (Fig 313B) with conventional and inverse orientation respectively.

Predicted sequences for pITRbAcRG, pITRbAcRsvG and pITRbAcRvsG plasmids were produced by linking together sequences of a relevant part of pUC19 (GenBank accession number L09137), genomic DNA of beta-actin (GenBank accession number zC255L18), ITR, loxP, RFP cDNA and GFP cDNA according to their construction strategies (Fig 232 & 233).

When pITRbAcRG was generated, its DNA structure was verified by restriction enzyme mapping. A schematic diagram of the restriction enzyme analysis of pITRbAcRG is shown in Fig 314A. When the predicted sequence of pITRbAcRG was analyzed using ApE (Table 222) software, KpnI, NotI, XhoI, and NcoI were

found to have 3, 1, 1, and 4 digestion sites respectively. A digital image of the result of the enzyme digestion is shown in Fig 314B. The patterns of KpnI, NotI or XhoI digestion of pITRbAcRG on agarous gel were the same as the patterns from ApE analysis. NcoI digestion of pITRbAcRG did not however match the prediction, since one of the NcoI digestion sites, NcoI/18043, was not effective in pITRbAcRG.

Constructs pITRbAcRsvG and pITRbAcRvsG were generated by insertion of the XhoI/SalI SV40 pA fragment into XhoI-digested pITRbAcRG (Fig 233). When the SV40 pA signal insertion was orientated towards transcription (AAUAAA), pITRbAcRsvG (sv indicated this orientation) was produced. In contrast when the SV40 pA signal insertion was orientated against transcription (UUUAUU), pITRbAcRvsG was produced (vs indicated this orientation).

Restriction enzyme digestion was employed to verify the orientation of SV40 pA in pITRbAcRsvG and pITRbAcRvsG (Fig 315). A schematic diagram (Fig 315A) illustrates the method. Firstly BamHI-digestion identified the insertion of SV40 pA (280 bp) into pITRbAcRG. When there was an insertion into pITRbAcRG, either ‘sv’ or ‘vs’, BamHI digestion produced a 2170 bp fragment instead of an 1890 bp fragment. Clones, 2, 3, and 4 in Fig 315B are plasmids with SV40 pA insertion. Secondly BamHI/XhoI double digestion distinguished insertion of ‘sv’ from insertion of ‘vs’. When the insertion was ‘sv’, BamHI/XhoI digestion produced an 1170 bp BamHI-XhoI fragment and 1000 bp XhoI-BamHI fragment. Clones, 2 and 3 in Fig 315B are pITRbAcRsvG. When the insertion was ‘vs’, BamHI/XhoI digestion produced an 890 bp BamHI-XhoI fragment and a 1270 bp XhoI-BamHI fragment. Clone 4 in Fig 315B is pITRbAcRsvG. Structures of the clones in Fig315B were further verified by NheI/XhoI double digestion. When

pITRbAcRsvG and pITRbAcRvsG were double digested by NheI/XhoI, pITRbAcRsvG produced an 1880 bp NheI-XhoI fragment and pITRbAcRvsG produced a 2150 bp NheI-XhoI fragment.

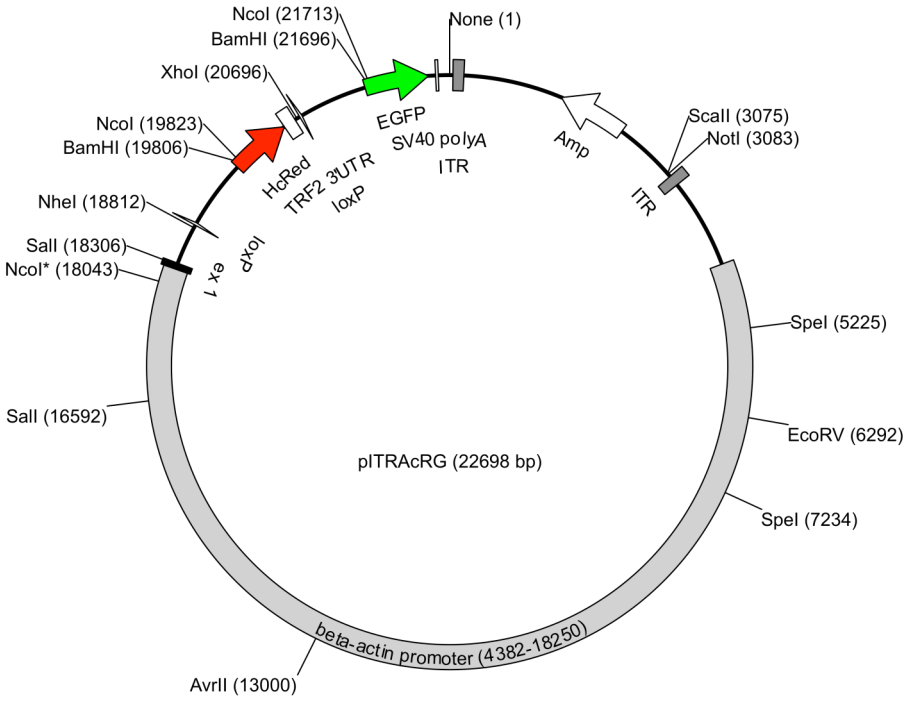

Figure 27-312. Restriction enzyme map & gene layout for pITRbAcRG.

Numbers given beside enzyme cutting sites are nucleotide positions. Numbers in brackets indicate the number of restriction enzyme sites. The first nucleotide is counted from the 5'-end of ITR-3'. The reason 5'-end of ITR-3' was assigned as the starting nucleotide, was because sequence of pITRbAcRsvG and pITRbAcRvsG could be obtained by editing the sequence of pITRbAcRG more easily. The arrow in beta-actin promoter indicates the direction of transcription for this plasmid. The map was produced using MacPlasmap (v1.83). NcoI* is a digestion site that was not effective in this plasmid.

A

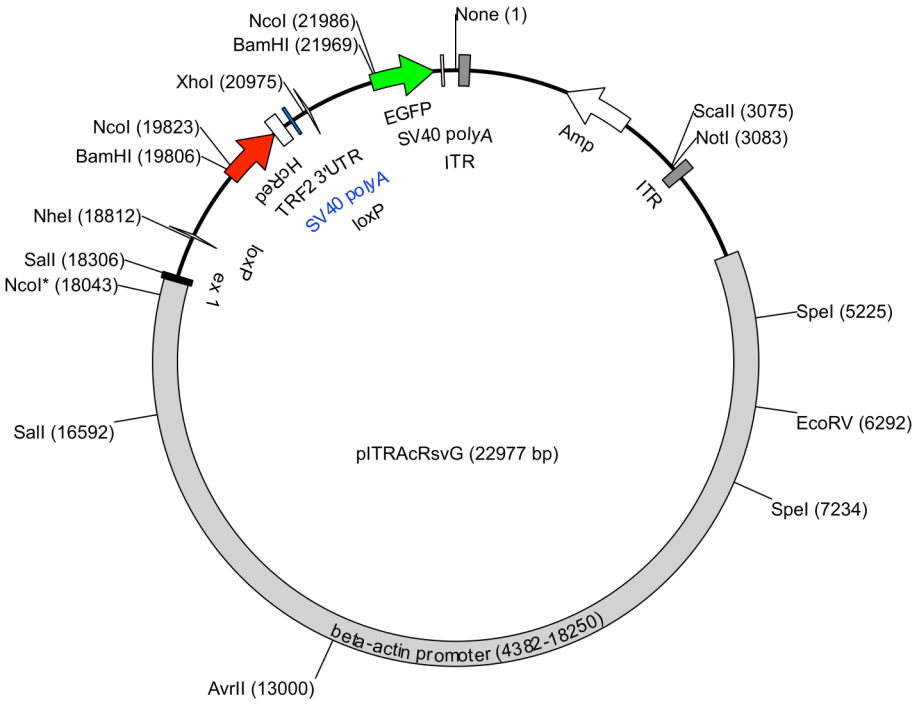

B

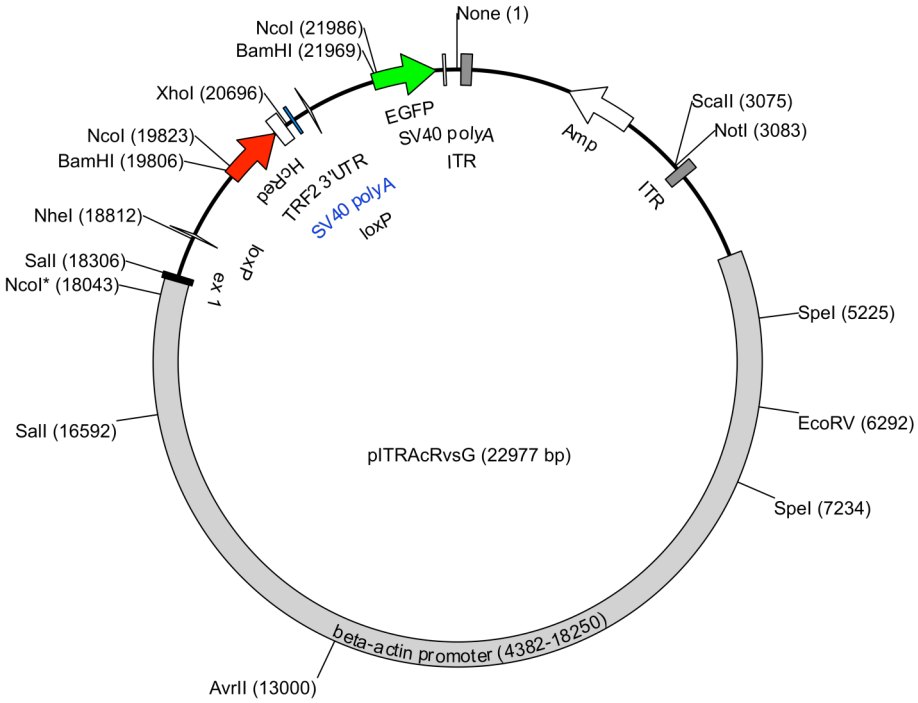

Figure 28-313. Restriction enzyme map & gene layout for plTRbAcRsvG and plTRbAcRvsG.
Further information on the map can be found in Fig 312.

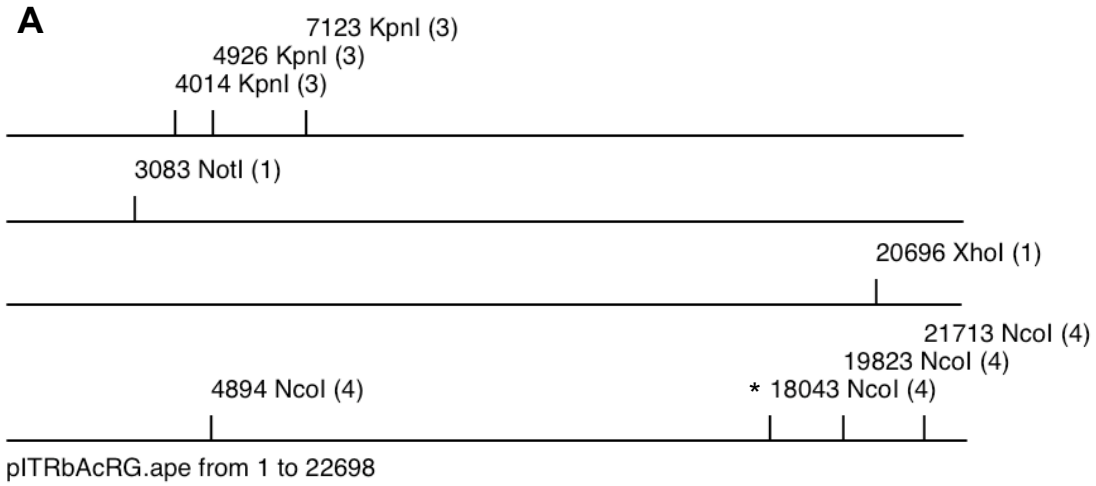

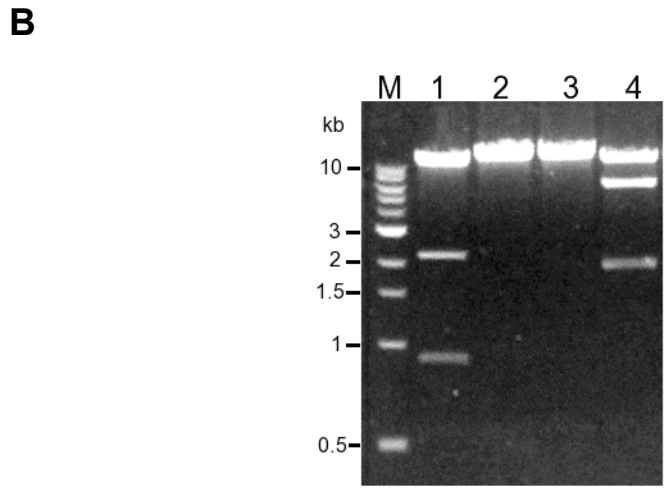

Figure 29-314. Examination of the structure of pITRbAcRG.

(A) Linear form of pITRbAcRG with predicted enzyme digestion sites. The graph was produced using ApE. Each horizontal line represents a linearized pITRbAcRG from nucleotide position 1 to 22698. KpnI was predicted to have three cutting sites in pITRbAcRG at nucleotide position 4014, 4926, and 7123. NotI and XhoI were predicted to have only one digestion site in pITRbAcRG at positions 3083 and 20696 respectively. NcoI was predicted to have 4 cutting sites in pITRbAcRG at 4894, 18043, 19823 and 21713. (B) Enzyme digestion of pITRbAcRG on agarose gel. M, 1 kb Ladder (NEB); 1, KpnI digestion; 2, NotI digestion; 3, XhoI digestion; 4, NcoI digestion; *, ineffective NcoI site.

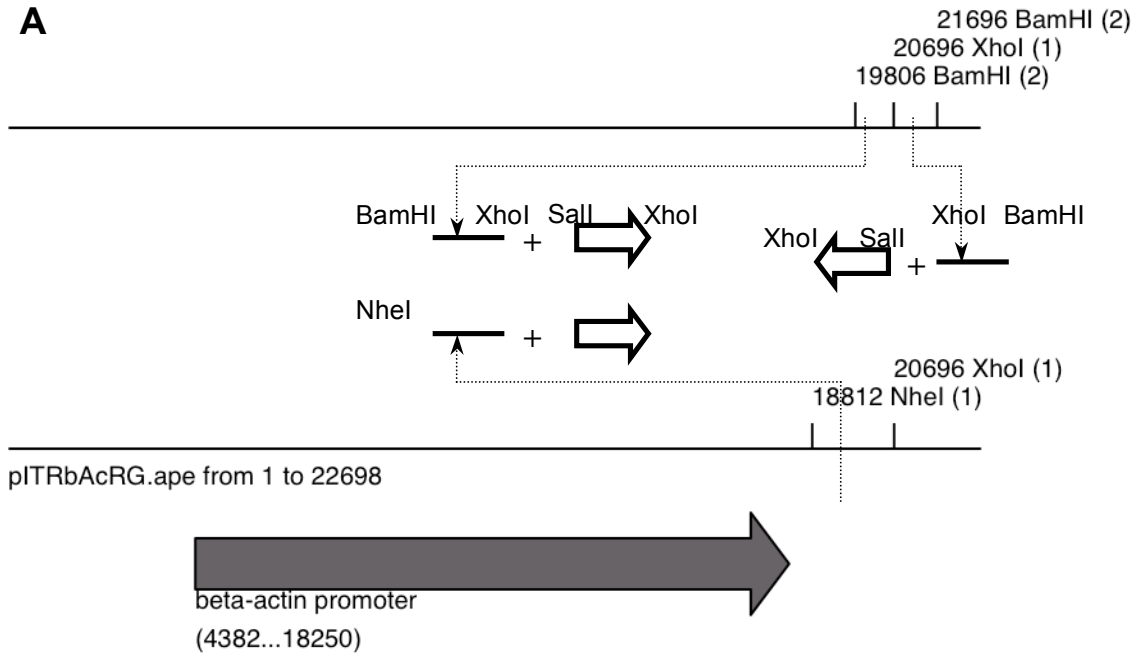

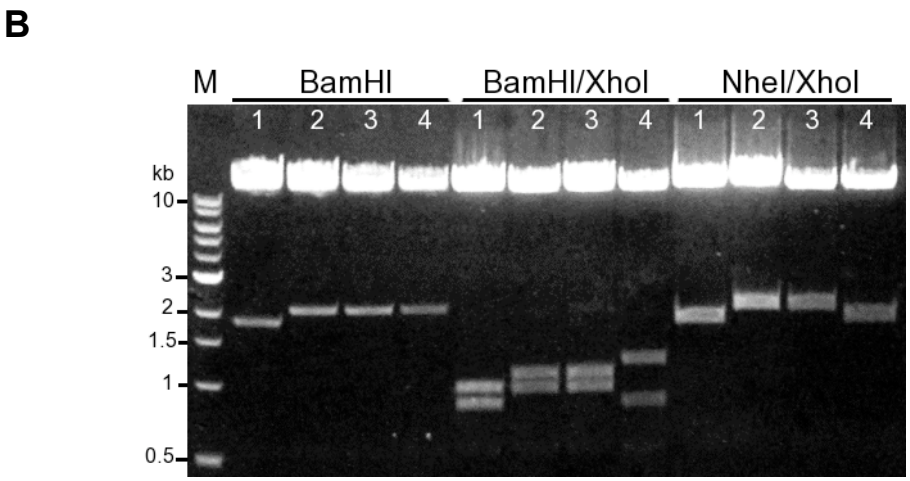

Figure 30-315. Verification of the insertion and orientation of SV40 pA.

(A) A schematic diagram of BamHI/XhoI double digestion and NheI/XhoI double digestion of pITRbAcRG with insertion of SV40 pA. SV40 pA is represented by an arrow-box. Head of the arrow-box is XhoI digested. Tail of the arrow-box is SalI digested. When XhoI digestion is ligated (+) with SalI digestion, neither XhoI nor SalI can cut the site of ligation again. (B) Examination of plasmid clones, 1, 2, 3, and 4 with BamHI, BamHI/XhoI or NheI/XhoI digestion. M, 1 kb Ladder (NEB); 1, pITRbAcRG; 2, pITRbAcRsvG; 3, pITRbAcRsvG; 4, pITRbAcRvsG.

3.2 Unexpected RFP &GFP Co-Expression In Microinjected Embryos in The Absence Of Cre Recombinase

The schematic outline of the linear structure of pITRbAcRG and its deduced mRNA structure are shown in Fig 321. Utilization of the transcription start site of β-*actin* was designed into pITRbAcRG. Transcripts from this plasmid consisted of β-*actin* exon 1, 5'-partial exon 2, RFP, 3'-half of first intron of β-*actin*, 5'-partial exon 2 and GFP. The translations from these transcripts were expected to be restricted to RFP in the absence of Cre recombinase in microinjected embryos.

Plasmid, pITRbAcRG, was microinjected into zebrafish embryos in circular form. The microinjection outcome is given in Table 321. In total 147 embryos were injected with pITRbAcRG however only 58 survived beyond 24 hpf. The numbers of reporter gene expression embryos were counted at 24 hpf. Every reporter gene expressing-embryo appeared to co-express of RFP and GFP. Overall the injections gave a survival rate of 40% at 24 hpf. In these surviving embryos there was a 50% expression rate. Mortality for a microinjection experiment can be attributed to either the bad quality of embryos or to the mechanical destruction due to injection.

RFP expression was observed in all types of tissue. The expression patterns of RFP in 32 embryos were mosaic. The embryos however expressed not only RFP but also GFP in the absence of Cre. The GFP expression pattern was similar to that of RFP without the effect from Cre recombinase. Images of two microinjected embryos are shown in Fig 322. Two images of each embryo were taken, under red and green filter systems respectively. Comparison of RFP and GFP images suggested that two reporters co-expressed in most of the reporter gene positive cells but at different intensities. Some reporter positive cells had brighter images in green fluorescence

(Fig 322A), whereas some were stronger in red (Fig 322A). Some had only red colour (Fig 322A), whilst others had only green colour (Fig 322A). Overall, the unexpected GFP expression was stronger than RFP expression but not restricted to certain tissues. This poses the question as to whether there was anything wrong with the design or the construction of pITRbAcRG, which resulted in the unexpected GFP expression.

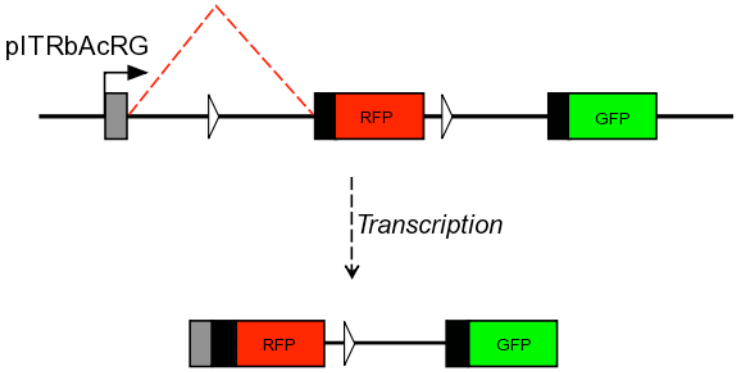

Figure 31-321. Schematic diagram of Deduced mRNA structure for pITRbAcRG in microinjected embryos.

Linear form of pITRbAcRG structure is shown in the upper drawing and its deduced mRNA structure is shown at the bottom of the figure. β-*actin* exon 1 represented as grey boxes; loxP sequence as triangles; 5'-partial exon 2 of β-*actin* as black boxes; RFP cDNA as red boxes; GFP cDNA as green boxes; intron and vector shown as black lines. The structures are not to scale.

Table 16-321. Microinjection of pITRbAcRG

Concentration of DNA in injection solution: 10 μg/ml

Injected embryos	Surviving embryos	None	RFP only	GFP only	RFP+GFP
97	23 (24%)	12	0	0	11
50	35 (70%)	14	0	0	21

Numbers in this table indicate the number of embryos in the experiment. The RFP only and GFP only columns show numbers of embryos expressing only RFP or GFP. RFP+GFP indicates co-expression of RFP and GFP. In the None column: no reporter gene expression observed.

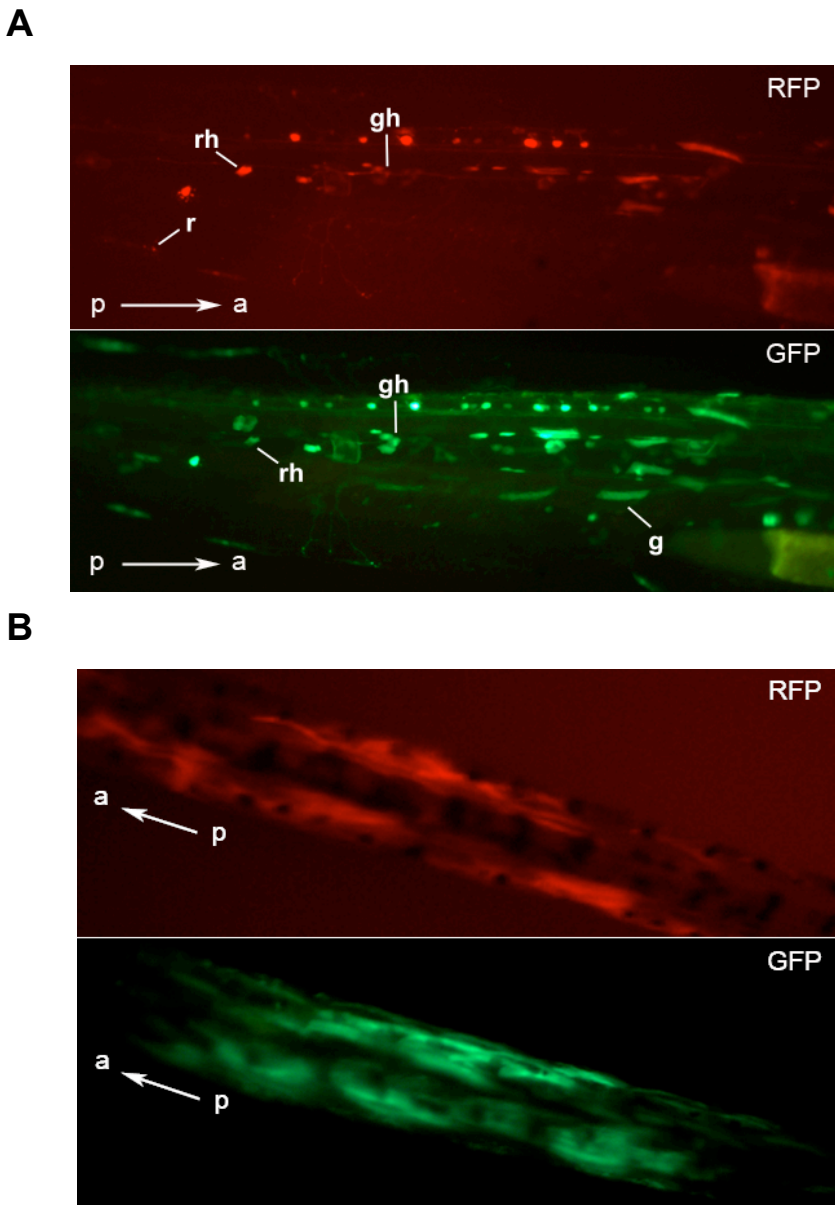

Figure 32-322. Images of pITRbAcRG microinjected embryos in the trunk region.
(A) Lateral view of a 36 hpf embryo, anterior to the right. (B) Dorsal view of a 6 dpf embryo, anterior to the upper left corner. RFP: image taken under red fluorescence filter system; GFP: image taken under green fluorescence filter system; rh: stronger RFP expression; gh: stronger GFP expression; r: RFP expression only; g: GFP expression only; a: anterior; p: posterior.

3.3 Indiscriminate Alternative Splicing

Alternative RNA splicing explains co-expression of RFP & GFP

In order to investigate the causes of the unexpected expression of GFP, RT-PCR was used to examine the transcript structure from pITRbAcRG in microinjected embryos. Schematic graphics of the primer design for this experiment are shown in Fig 331A.

Total RNA extracted from non-injection embryos (W in Fig 331B) and from pITRbAcRG-injection embryos but without reverse transcriptase in their RT reaction (N in Fig 331B), was used as negative controls. Pairing F1 and R2 in the PCR reaction generated a 400 bp DNA fragment (Fig 331B), which was the RNA splicing product of β-*actin* exon 1 and exon 2- fusion RFP as predicted. This splicing gave rise to red fluorescence, which was observed under the microscope. PCR product from F1 and R3b was a 730 bp DNA fragment (Fig 331B), which was exactly the same size as the RNA splicing product of β-*actin* exon 1 and exon 2- fusion GFP. In other words, the half duplicated intron and partial exon 2 of β-*actin,* that fused with GFP cDNA induced an alternative splicing which led to green fluorescence expression.

PCR product from F2 and R3a was a fragment of 550 bp (Fig 331B). This product was much smaller than the predicted 1700 bp. It is thus designated by a question mark in the figure. The question is resolved by the following experimental results.

An Ectopic Splicing Donor Site in pITRbAcRG

Pre-mRNA structures for pITRbAcRG in zebrafish embryos were analyzed using RT-PCR in which the first-strand cDNA was synthesized with random (hexamer) primers (Fig 332). Oligo (dT) primers were also used in a RT reaction as a control for mature RNA or RNA with a polyadenine tail. The primers used in this analysis are illustrated in Fig 332A. F2 and R4 primers targeted the sequence of RFP and the half duplicated intron.

DNA was not amplified in the no-RT control (N, Fig 332), nor in the polyA tail mRNA control (T, Fig 332) by the F2R4 PCR reaction. A faint DNA signal appeared at a low annealing temperature (58°C) PCR reaction from the first-strand cDNA synthesized with random (hexamer) primers. A stronger band was generated when the temperature was increased to 62°C (Fig 332B). F2R3a PCR however produced the unknown 550 bp bands with both types of first-strand cDNA, random (hexamer) and oligo (dT). These results suggest that the pre-mRNA structure was normal from pITRbAcRG and of predicted length even though the RNA became shorter in mature RNA.

The unknown product from the F2R3 (Fig 331B) PCR reaction was cloned into pGEM-T Easy vector and sequenced (pGEMF2R3, Table 222). Alignment of the sequence of F2R3a PCR product with pITRbAcRG revealed an ectopic splicing donor site at the 3'-end of RFP cDNA (black arrow head in Fig 333A). Finally, a clear picture of mRNA structures of pITRbAcRG in zebrafish embryos was revealed. There were three exons in this construct, exon 1 of β-actin, RFP and GFP. Red fluorescence expression was generated by RNA splicing, which produced mRNA consisting of all three exons (Fig 333B). Green fluorescence expression was

generated by an alternative splicing which produced mRNA consisting of exon 1 of β-actin and GFP (Fig 333B).

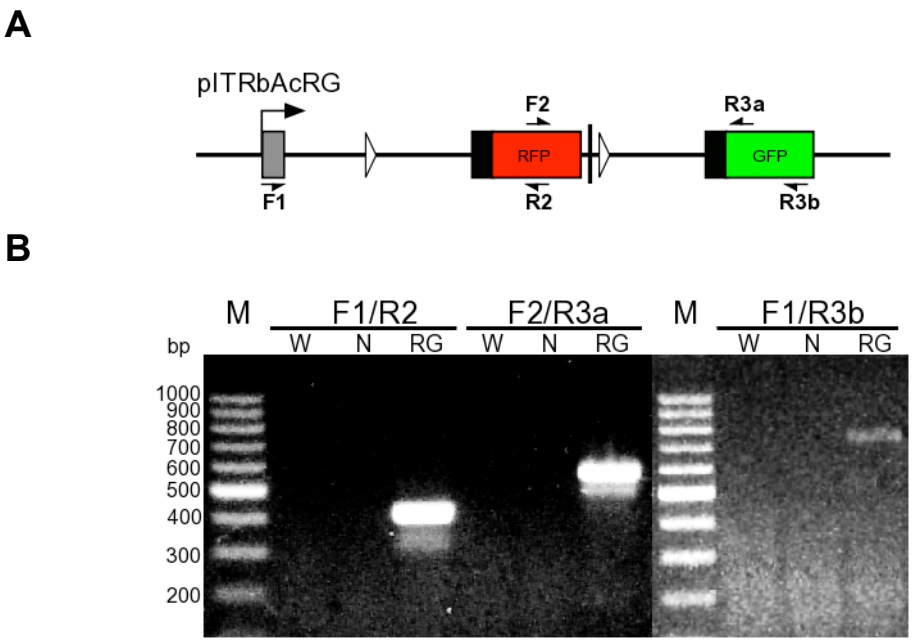

Figure 33-331. mRNA structure for pITRbAcRG in microinjected embryos.

(A) Primer designs. Five primers were designed to analyze the structure of mRNA for pITRbAcRG in microinjected embryos. F1 was a forward primer in the exon 1 of β-*actin*. F2 & R2 were forward and reverse primers respectively, both located in the middle of RFP cDNA. R3a & R3b were reverse primers, the former located at 5'-end of GFP cDNA; the latter located at 3'-end of GFP cDNA. More detail of the pITRbAcRG structure is described in Fig 3.2.2. (B) RT-PCR results. F1R2 reactions analyzed the mRNA structure of β-*actin* exon 1 and exon 2-fusion RFP. F1R3b reactions amplified a fragment of 730 bp, a result of alternative splicing of β-*actin* exon 1 and exon 2-fusion GFP. F2R3a reactions produced an unknown PCR product. M: 100 bp ladder (Promega) with major sizes labelled. W: RT template extracted from non-injection embryos. N: RT template extracted from pITRbAcRG-injection embryos but without reverse transcriptase in its RT reaction. RG: RT template extracted following pITRbAcRG-injection.

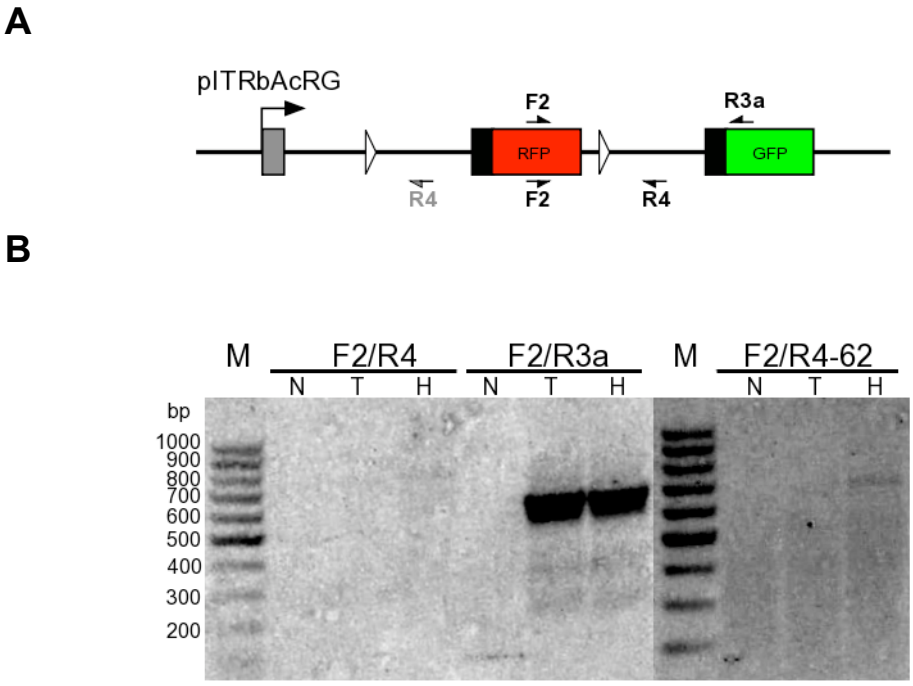

Figure 34-332. Pre-mRNA structure for pITRbAcRG in microinjected embryos.

(A) Primer designs. Two primers were designed to analyze the structure of pre-mRNA for pITRbAcRG in microinjected embryos. R4 was a reverse primer, located in the middle of β-*actin* first intron, paired with F2 for analysis of pre-mRNA structure between RFP and GFP. F2 & R3a were control primers from previous experimental results (Fig 3.3.1). More detail of the pITRbAcRG structure is described in Fig 3.2.2. (B) RT-PCR results. F2R4 reactions amplified DNA between RFP cDNA and the half duplicated intron as a 750 bp fragment. Results from different PCR conditions are shown on the gel photos. F2R4-62 reactions were conducted at 62°C elongation temperature at PCR in place of 58°C for F2R4 reactions. N: a negative control, in which total RNA extracted from pITRbAcRG-injection embryos but without reverse transcriptase in its RT reaction with Random Hexamer. T: PCR templates from Oligo $(dT)_{15}$ primed RT reaction. H: PCR templates from Random Hexamer primed RT reaction.

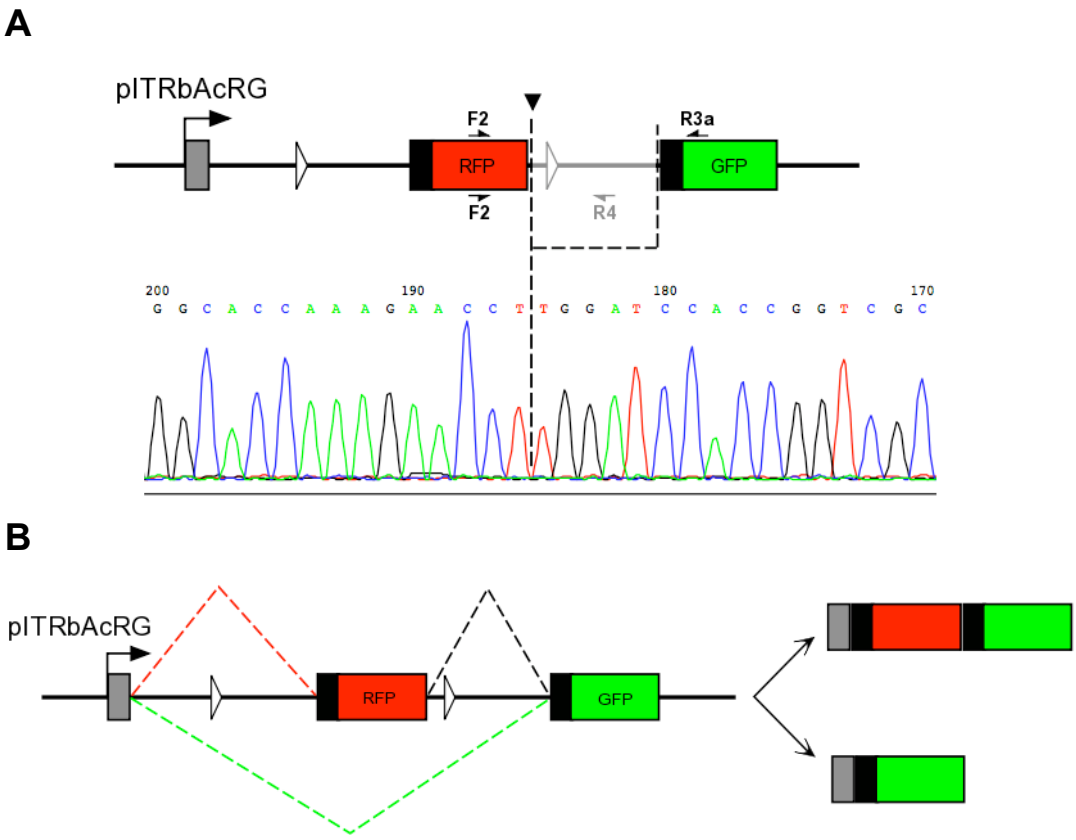

Figure 35-333 An ectopic splicing donor site.

(A) Sequence of F2R3a PCR products. Partial sequencing plot is shown beneath the diagram of pITRbAcRG structure. An ectopic splicing donor site in pITRbAcRG, (black arrow head) was discovered by alignment of the sequences between F2R3a PCR Products and pITRbAcRG. The size of F2R3a is thus much smaller than predicted, the sequence between RFP and GFP was spliced out during transcription process. (B) pITRbAcRG is a construct with three exons. This construct produced two types of final mRNA products; one consisted of three exons, which contributed to red fluorescence expression and the other consisted of two exons, which gave rise to green fluorescence expression. More detail of the pITRbAcRG structure is described in Fig 322.

3.4 Splicing Over SV40 PolyA Signal

The Cre-loxP cell lineage tracing system cannot work properly if GFP expresses prior to engagement of Cre, hence the SV40 pA signal was used to tackle the problem. An SV40 polyA signal was inserted at the 3'-end of RFP cDNA in pITRbAcRG (Fig 341). The polyA signal did not stop transcription of GFP. Co-expression of RFP and GFP was still observed in pITRbAcRsvG-microinjected embryos (Fig 342). Expression patterns of FRP and GFP were similar to the patterns that were observed in pITRbAcRG-microinjection embryos (Fig 322), mosaic and dominating in green fluorescence.

The mRNA structures for pITRbAcRsvG in embryos were analyzed by RT-PCR (Fig 343). The alternative splicing between β-actin exon 1 and GFP occurred in pITRbAcRsvG-microinjection embryos, the same as in pITRbAcRG-microinjection embryos. The ectopic splice donor site was retained in pITRbAcRsvG. RT-PCR products of F1R2, F2R3a and F1R3b for pITRbAcRsvG were 400 bp, 550 bp and 730 bp. They are exactly the same sizes as PCR products from the RT-PCR for pITRbAcRG (Fig 343).

Furthermore pre-mRNA structures for pITRbAcRsvG were also analyzed by RT-PCR. Interestingly, F2 and R4 primers were unable to amplify any DNA fragment from pITRbAcRsvG-injection embryos whereas a 750 bp and a 1030 bp DNA fragment were amplified from pITRbAcRG- and pITRbAcRvsG-injection embryos respectively. In addition, the PCR results for β-actin reactions indicated that the RT reactions were viable. In summary, there was cleavage at SV40 polyA site but the cleavage did not stop the transcription of GFP nor alter the splicing of GFP.

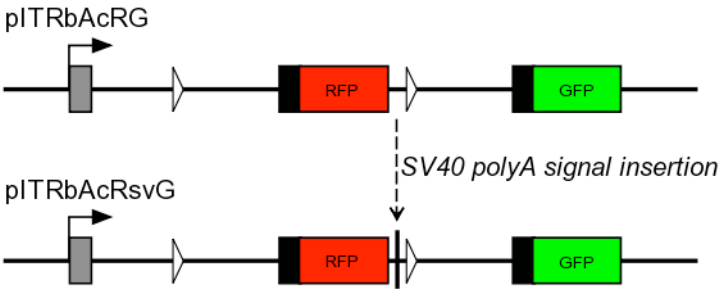

Figure 36-341 Structure of pITRbAcRsvG construct.

An SV40 polyA signal was inserted at the 3'-end of RFP cDNA in pITRbAcRG. The purpose of insertion SV 40 polyA signal was to prevent the expression of green fluorescence. β-*actin* exon 1 shown as grey boxes; loxP sequence shown as triangles; 5'-partial exon 2 of β-*actin* shown as black boxes; RFP cDNA shown as red boxes; GFP cDNA shown as green boxes; intron and vecor shown as black lines. The structures were not drawn to scale.

A

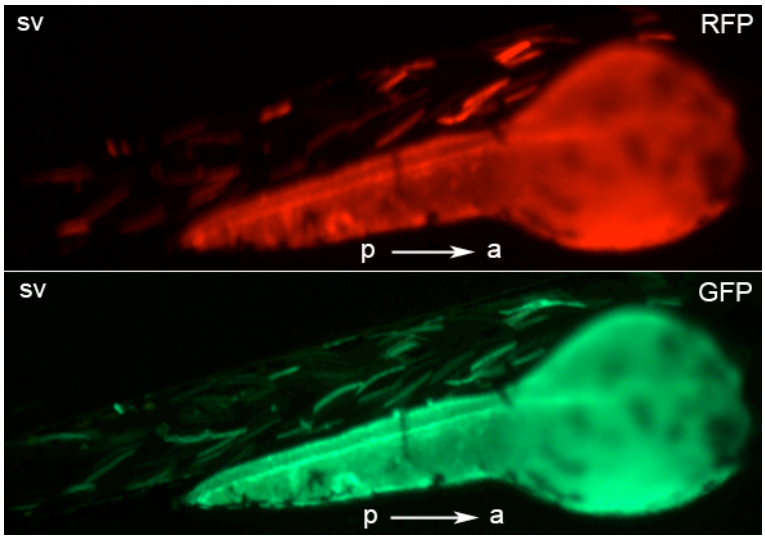

B

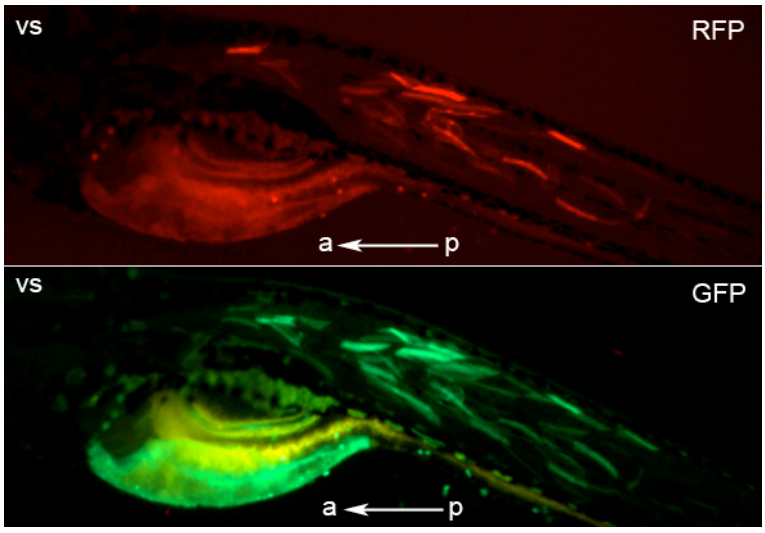

Figure 37-342 Images from pITRbAcRsvRG- & pITRbAcRvsG-injection embryos.

The insertion of SV 40 polyA signal did not prevent the expression of GFP, no matter the orientation of insertion of SV40 polyA signal. Expression patterns of RFP and GFP in these embryos were similar to those in pITRbAcRG-injection embryos (Fig 3.2.2). (A) Ventral-lateral view of a 3 dpf embryo, anterior to the right. (B) Dorsal-lateral view of a 6 dpf embryo, anterior to the left. RFP: image taken under red fluorescence filter system; GFP: image taken under green fluorescence filter system; sv: embryos microinjected with pITRbAcRsvG; vs: embryos microinjected with pITRbAcRvsG.

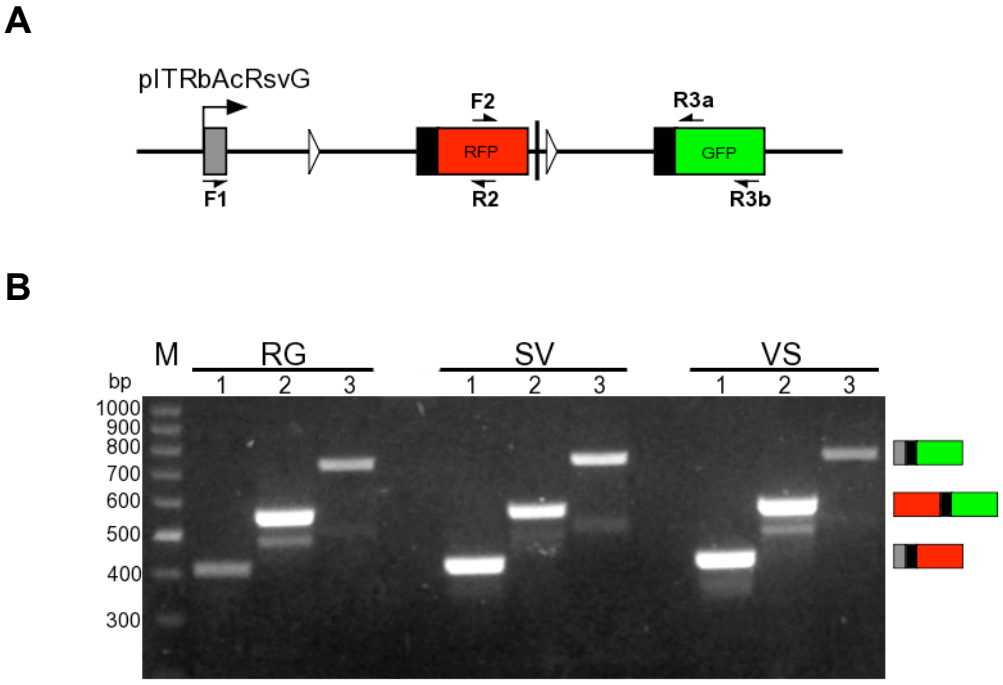

Figure 38-343 Insertion of SV40 polyA signal did not affect RNA splicing structure.

(A) Relative primer locations in pITRbAcRsvG. (B) Gel image of RT-PCR results. RNA splicing structures were exactly the same between the three constructs in microinjection embryos. RG: total RNA was extract from pITRbAcRG-injection embryos; SV: total RNA was extract from pITRbAcRsvG-injection embryos; VS: total RNA was extract from pITRbAcRvsG-injection embryos; M: 100 bp Ladder (Promega); 1: F1 & R2 primer paired PCR reactions; 2: F2 & R3a primer paired PCR reaction; 3: F1 & R3b primer paired reaction. See Fig 3.4.1 for more information on plasmid structures.

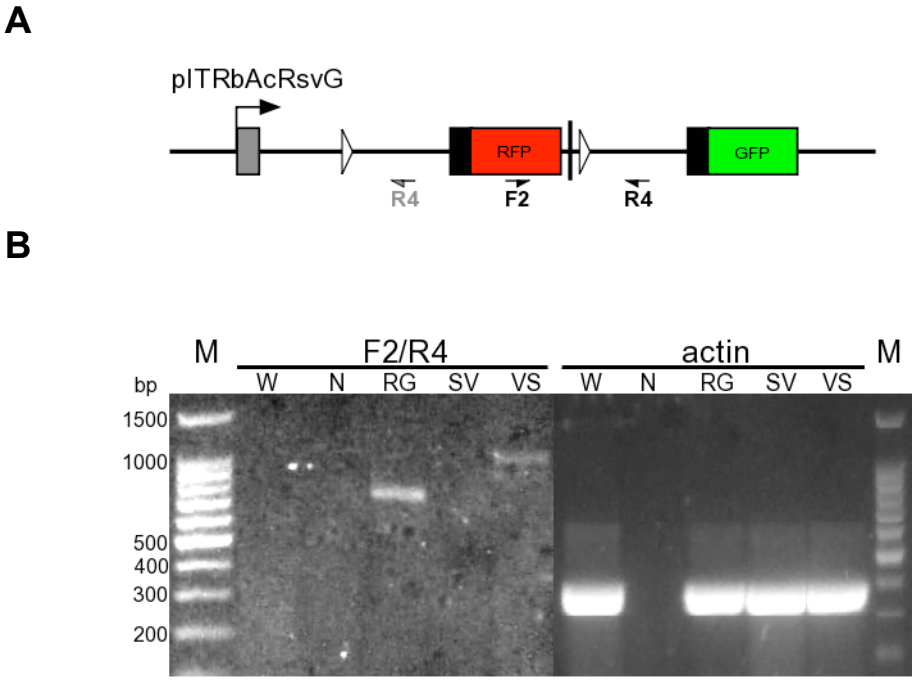

Figure 39-344 Splicing over SV 40 polyA signal.

(A) Primer locations on pITRbAcRsvG. (B) RT-PCR results for F2R4 and β-actin exon 1 to 3 reactions. In this experiment, all the first-strand cDNA was generated by random (hexamer) primer RT reactions. Cleavage at SV40 polyA site was detected in pITRbAcRsvG-injected embryos, but not in pITRbAcRG nor in pITRbAcRvsG. F2R4: PCR reaction conducted with F2 and R4 primers; actin: PCR reaction conducted with specific primers for β-actin exon 1 and 3; M: 100 bp Ladder (Promega); W: total RNA extracted from non-injection embryos; N: no-RT control; RG: total RNA extracted from pITRbAcRG-injection embryos; SV: total RNA extracted from pITRbAcRsvG-injection embryos; VS: total RNA extracted from pITRbAcRvsG-injection embryos.

3.5 Conclusion

To trace cell lineage in zebrafish embryos, plasmid pITRbAcRG consisting of ITR sequence, β-*actin* promoter, loxP-floxed RFP reporter gene and the GFP reporter gene was constructed. GFP co-expressed with RFP in pITRbAcRG-microinjected embryos in the absence of Cre recombinase (Fig 322) due to indiscriminate alternative splicing of the red and green reporter genes (Fig 331 to Fig 333).

To eliminate the indiscriminate alternative splicing, plasmids pITRbAcRsvG and pITRbAcRvsG were constructed. In these plasmids, SV40 pA signal was added to the 3'-end of RFP in a right (pITRbAcRsvG) and reverse (pITRbAcRvsG) orientation. The pITRbAcRsvG-injected and pITRbAcRvsG-injected embryos display the same phenotypes as pITRbAcRG-injected embryos. The SV40 pA cleavage did not affect the alternative splicing of the RFP and GFP genes (Fig 341 to Fig 344), hence GFP and RFP are still co-expressed in the pITRbAcRsvG-injected embryos.

The Cre-loxP system for tracing cell lineage was not established, because the expression of GPF from pITRbAcRG and pITRbAcRsvG was not controllable in the microinjected embryos. The structure of pITRbAcRG needs significant rearrangement to solve this problem, which is created by the alternative splicing. Several potential solutions to the problem are discussed in §6.1.

Different approaches, WISH and IM, have been used to investigate midline convergence of PGP in zebrafish embryos. The results of the analysis of mutant embryos are detailed in §4, 5 and discussed in §6.2, §6.3.

4. Nodal Signalling Is Essential For PGP Midline Convergence

Zebrafish mutant, *oep*, was selected for the investigation of the effects of Nodal signalling in pronephric-glomerular morphogenesis in zebrafish embryos. In zebrafish *one-eyed pinhead* (*oep*), which is involved in Nodal-related TGF-β signalling, is essential for the formation of all endodermal and several mesodermal tissues (Feldman et al., 2000; Feldman et al., 1998; Schier and Shen, 2000). *Oep* was originally identified during genetic mutagenesis in zebrafish embryos (Driever et al., 1996; Haffter et al., 1996; Schier et al., 1997). Oep is an EGF-related protein (EGF-CFC) consisting of an EGF-like motif at the N-terminal in addition to a cysteine-rich domain, and CFC (Cripto, FRL-1 and Cryptic) at the C-terminal (Zhang et al., 1998). Functions of Oep are, however, Nodal-related. Oep acts as a cofactor of Nodal receptors (Activin receptors) in Nodal signalling (Gritsman et al., 1999; Shen and Schier, 2000; Yeo and Whitman, 2001). Nodal signalling triggers a cascade of transcription factor expression to regulate formation of endodermal tissues in zebrafish (Bjornson et al., 2005), such as Gata5, and Bonnie and Clyde (Bon) (Kikuchi et al., 2000), which are required to maintain expression of a *sox* factor Casanova (Cas) (Aoki et al., 2002; Kikuchi et al., 2001).

In this chapter I will investigate PGP midline convergence phenotypes in $oep^{-/-}$ embryos.

4.1 *Wt1* Expression In Wild-Type Embryos

To examine the timing of the specification of anterior intermediate mesoderm and the dynamic pattern of pronephric-glomerular precursor cells during zebrafish

embryonic development, *wt1* WISH was performed. In some cases, double WISH of *wt1* and *myoD* was used.

The expression of wt1 mainly occurs in several phases during early embryonic development in zebrafish. In the first phase, during 10 to11 hpf (bud to 3-somite stages), the *wt1* transcript is first detected by WISH (Fig 411) and is regarded as the specification of the anterior intermediate mesoderm. The specification of the anterior intermediate mesoderm starts at a location approximately 150 μm directly lateral to the adaxial cells on either side of central axis, at the bud stage, with small bilateral patches of cells (Fig 411C). The observation of this *wt1* transcript, first detected at bud stage, is slightly earlier than the stage described in a previous study (Serluca and Fishman, 2001). *Wt1*-expressing cells increase in both quantity and quality during the bud and 3-somite stages (Fig 411). *Wt1* probe blue staining extends in both the anterior and posterior directions and forms long bilateral stripes at the 3-somite approximately 40 μm wide and 100 μm long (Fig 411F).

From the 3- to 6-somite stages, the anterior intermediate mesoderm exhibits typical convergence and extension cell movement, in which the tissue narrows in shape and extends in length (Fig 412). Meanwhile, the bilateral stripes become closer and closer to each other (Fig 418). The *myoD* expression in the lateral projecting bands (somites) from the adaxial cells becomes visible from the 5-somite stage (Fig 412C). The developmental stage of zebrafish embryos can thus be precisely indicated by *myoD* WISH from this stage. At the 6-somite stage, the pair of stripes of *wt1*-expressing cells is long (approximately 200 μm) and narrow (approximately 20 μm). The posterior end of the *wt1*-expressing stripes extends almost to reach the of fifth-somite (Fig 412C, D). Convergence and extension movement of *wt1*-expressing cells

is not observed after the 7-somite stage. Instead of narrowing and extension, the stripes of *wt1*-expressing cells become shorter and wider during the 7- to 8-somite stages. Furthermore, the posterior end of the *wt1*-expressing stripes shortens towards the level of the third-somite (Fig 412E, F).

At 15 hpf (12-somite stage), the pronephric-glomerular precursor cells construct an elongated triangular shape and continue to bilaterally adjust to the third somites bilaterally at this stage (Fig 413A). The somite morphology is further differentiated. The somites become shorter and shorter forming block-shaped structures with intensive *myoD* expression from the long lateral projecting bands with faint *myoD* expression at the earlier stages (Fig 412). This morphological change in the somites is accompanied by a distance change between the bilateral patches of *wt1*-expressing cells. The distance between the bilateral patches of *wt1*-expressing cells decreases continuously after 10 hpf (bud stage) (Fig 418). By 24 hpf, the morphology of the anterior intermediate mesoderm has changed dramatically. The dynamic patterns, constructed by the *wt1*-expressing cells during 14-24 hpf, show that pronephric-glomerular precursor cells coalesce towards the posterior end at the third-somite level from the wide spread anterior end and form round shape tissues (PGP) with a more morphologically definable edge at 24 hpf (Fig 413, Fig 414). From 16 hpf, the cells at third-somite level invade the main embryo structure between the somites and gut (Fig 172). By 22 hpf, only those cells at third-somite level show intensive *wt1* expression. At 24 hpf these cells construct more definable round shaped tissue and locate completely inside the main embryo structure (Fig 413). At this stage most of the somites are formed and the level of *myoD* expression drops sharply through the trunk.

During 24-48 hpf, the two PGP migrate toward each other, fuse in the midline, and differentiate into pronephric glomerulus (PG) (Drummond et al., 1998). Similar conclusions were drawn from Fig 415 and 416. There were, however, three new observations. Firstly the PGP midline migration is mediated by growth of tissue extensions in the direction of subsequent migration at 32 hpf (Fig 416, Fig 417). At 36 hpf, the bilateral PGP has more contact along the central axis and the *wt1*-expressing cells form a bow shaped structure. By 48 hpf, the bow shaped structure becomes a circular PG along the central axis (Fig 415, Fig 416).

The distance between the two patches of *wt1*-expressing cells (PGP) is quantified by measuring the direct-line distance from 2-dimentional images of *wt1* WISH embryos from 10-48 hpf (Fig 418). The PGP midline convergence can be modelled using a cubic function:

$$y = -0.0176x^3 + 1.8271x^2 - 61.932x + 717.16,\ R^2 = 0.9497\ (x \geq 10)$$

Based on this model, the developmental stage at which the distance between PGP is zero (pixel) is 48.9 hpf. Calculation of the speeds of PGP midline convergence ($y' = -0.0528x^2 + 3.6542x - 61.932$) demonstrates that between 29.7 and 39.5 hpf the PGP migrate in a reverse direction (separating). The highest speed of PGP midline convergence is approximately 33.3 μm/hr at 10 hpf.

The mathematical model can also be used to determine the developmental stage (x) of a wild-type embryo given its PGP distance (y) between 10 and 48.9 hpf, or, to determine the developmental stage (x) of mutant embryos when PGP midline converge is independent of the mutated genes. Furthermore, a new insight into the mechanisms of general and tissue specific midline convergence can be obtained,

when heart primordia and endoderm midline convergence are also quantified using the same approach.

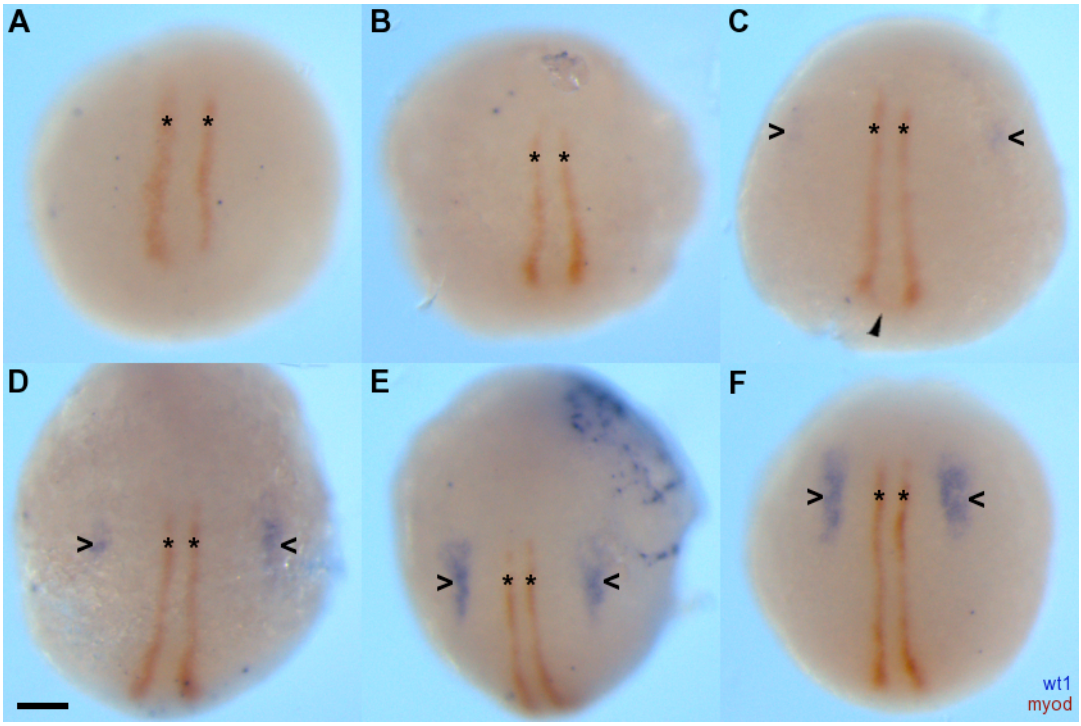

Figure 40-411. Specification of anterior intermediate mesoderm in zebrafish embryos.
Wt1 and *myoD* double WISH in 8-11 hpf zebrafish embryos (A-F), were stained blue and brown respectively. All images are the dorsal view with anterior to the top. MyoD is one of the popular developmental stage markers in zebrafish. *MyoD*-expressing cells at 80% to 90% epiboly (A, B) are located in a pair of longitudinal rows, which lie on either side of the prospective notochord, and are regarded as adaxial cells (asterisks). At bud stage (C), cells in the tail-bud express *myoD* (arrowhead). Prior to the formation of somites the distance between the two rows of *myoD*-expressing cells is narrower anteriorly than posteriorly. *Wt1* transcript was first detected by WISH at this stage (open arrowheads); the two faint blue patches of cells represent the beginning of the specification of anterior intermediate mesoderm. The embryos in D, E and F are 1-, 2-, and 3-somite embryos respectively. The *myoD* expression in the lateral projecting bands from the longitudinal rows is not yet visible, even though the anterior adaxial cells have started segmentation. Wt1 probe blue staining becomes more intensive during the 1- to 3-somite stages. The anterior intermediate mesoderm specification extends in both anterior and posterior directions. The blue bilateral patches of cells become approximately 40 μm wide and 100 μm long stripes (open arrowheads). The asterisks in A-C indicate the prospective third-somite adaxial cells. The asterisks in F indicate the third-somite adaxial. The series of somite formation is from the anterior to posterior hence the most anterior somite pair is named 1st-somite. The scale bar in D indicates 100 μm; all panels are at the same magnification.

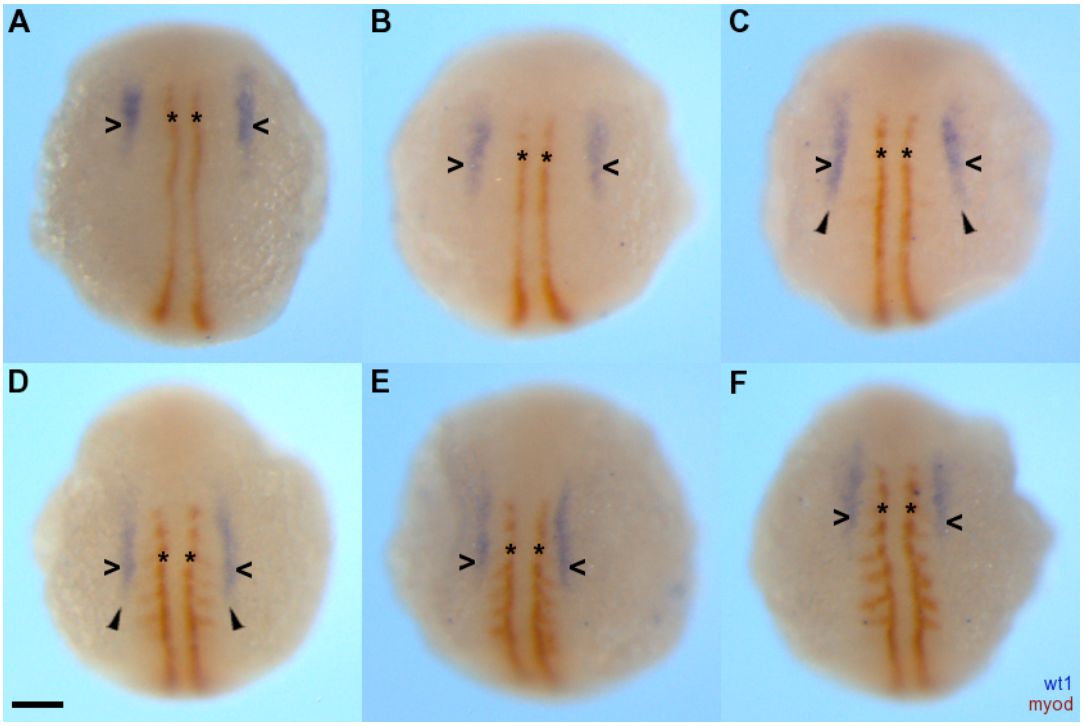

Figure 41-412. Convergence and extension of pronephric-glomerular precursor cells during 3- to 6-somite stages.

Wt1 and *myoD* double WISH in 11-13 hpf zebrafish embryos (A-F), *wt1* and *myoD* RNA probes were stained blue and brown respectively. All images are dorsal view with anterior to the top. From 3- to 6-somite stages (A-D), the pair of stripes of anterior intermediate mesoderm exhibits typical convergence and extension cell movement, in which the tissue narrows in shape and extends in length (open arrowheads). The two stripes of anterior intermediate mesoderm are getting closer and closer. The *myoD* expression in the lateral projecting bands from the adaxial cells is visible from the 5-somite stage (C). The developmental stage of zebrafish embryos can thus be precisely indicated by *myoD* WISH from this stage. At the 6-somite stage (D), the pair of stripes of *wt1*-expressing cells becomes long (approximately 200 μm) and narrow (approximately 20 μm). The posterior end of the *wt1*-expressing stripes extends almost to reach the level of the 5th-somite (C, D, solid arrowheads). Convergence and extension movement of *wt1*-expressing cells is not observed after the 7-somite stage (E). Instead of narrowing and extension, the stripes of *wt1*-expressing cells shorten and widen during the 7- to 8-somite stages (E, F). The posterior end of the *wt1*-expressing stripes shortens towards the level of 3rd-somite (E, F, open arrowheads). The asterisks in A-F indicate the 3rd-somite adaxial cells. The series of somite formation is from the anterior to posterior hence the most anterior somite pair is named 1st-somite. The scale bar in D indicates 100 μm; all panels are at the same magnification.

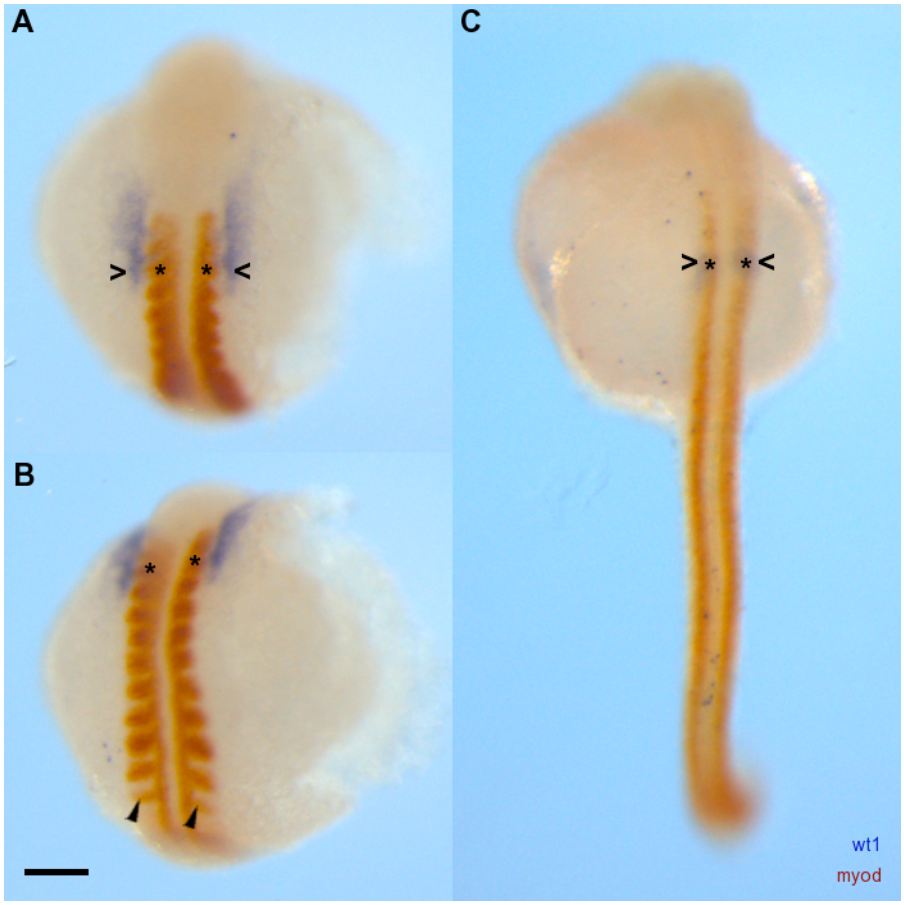

Figure 42-413. Coalescence of pronephric-glomerular precursor cells during 14-24 hpf, part 1/2. *Wt1* and *myoD* double WISH in 15 hpf (A, B) and 24 hpf (C) zebrafish embryos, *wt1* and *myoD* RNA probes were stained blue and brown respectively. All images are dorsal view with anterior to the top. At 15 hpf (A, B), the anterior somites are block shaped and contain a wedge-shaped zone of intensive *myoD* expressio, which fills the posterior half of the block. *MyoD* expression, in the forming posterior somites, is fainter and similar to a stripe in shape (B, solid arrowheads). The pattern of *wt1* expression becomes wing-shaped pattern (open arrowheads) along lateral edge of 1st- to 4th-somites at 14 hpf from narrow-long stripe (Fig 412). The pair of 3rd-somite is seemingly the axillas of 'the wings' (asterisks). The length of a formed somite is laterally shorter than at the 8-somite stage. This change pulls the two wings (*wt1* expression cells) closer to each other. At 24 hpf (C), most of the somites are formed and the level of *myoD* expression drops markedly along the trunk (brown). The *wt1*-expressing cells become two round tissues regarded as pronephric-glomerular primodia (PGP) that locate between the ventral side of the somites and the dorsal side of the gut (open arrowhead, see also Fig 172). The asterisks in A-C indicate 3rd-somite. The series of somite formation is from anterior to posterior hence the furthest anterior somite pair is named 1st-somite. The scale bar in B indicates 100 μm; all panels are at the same magnification.

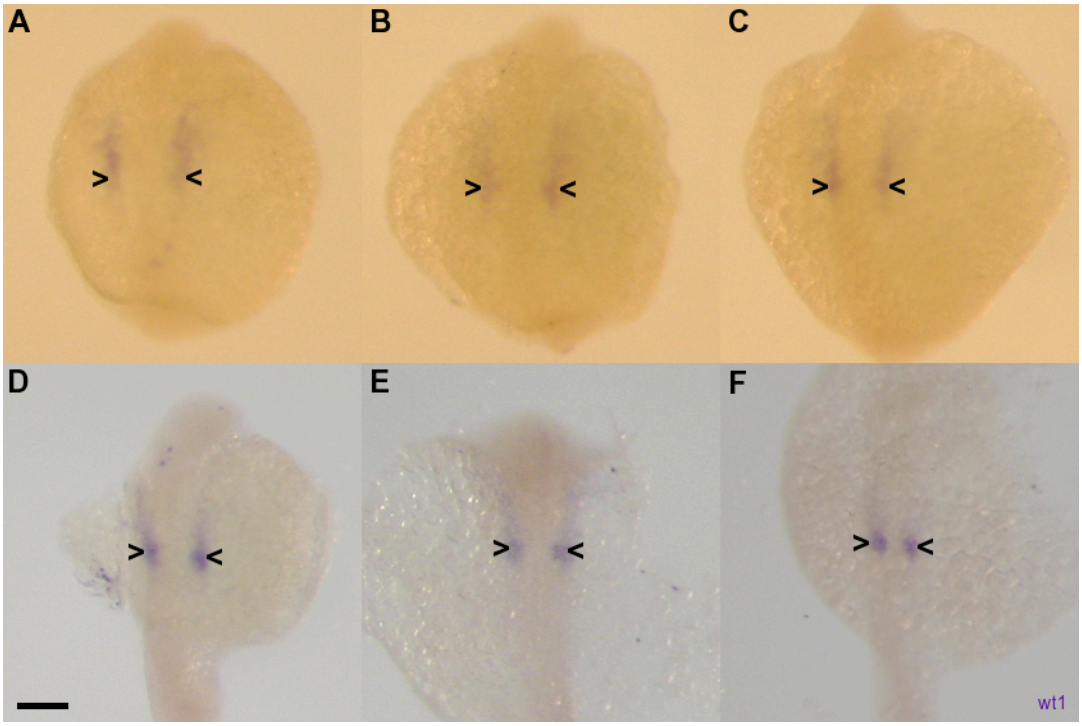

Figure 43-414. Coalescence of pronephric-glomerular precursor cells during 14-24 hpf, part 2/2. *Wt1* WISH in 14-24 hpf zebrafish embryos at 2-hour intervals (A-F), *wt1* probe was stained indigo. All images are dorsal view with anterior to the top. The dynamic patterns constructed by the *wt1*-expressing cells during 14-24 hpf show that pronephric-glomerular precursor cells coalesce towards the posterior end at the 3rd-somite level (open arrowheads) from the wide spread anterior end (A-F) and form circular tissues (PGP) with more morphologically definable edge at 24 hpf (F). (B) The wing-shaped *wt1* expression pattern becomes comet-shaped pattern with head next to the 3rd-somite (open arrowheads). (C) The comet-shaped intermediate mesoderm starts to invade the main embryo structure between the somites and gut. (D-F) The 'comet head' becomes more and more intensive with *wt1* expression (open arrowheads). *Wt1* expression in the 'comet tail' goes from blurry to ghostly. At 24 hpf (F) the *wt1* expressing cells construct more definable round shaped tissue with ghostly tail and locate completely inside the main embryo structure (open arrowhead). The scale bar in D indicates 100 μm; all panels are at the same magnification.

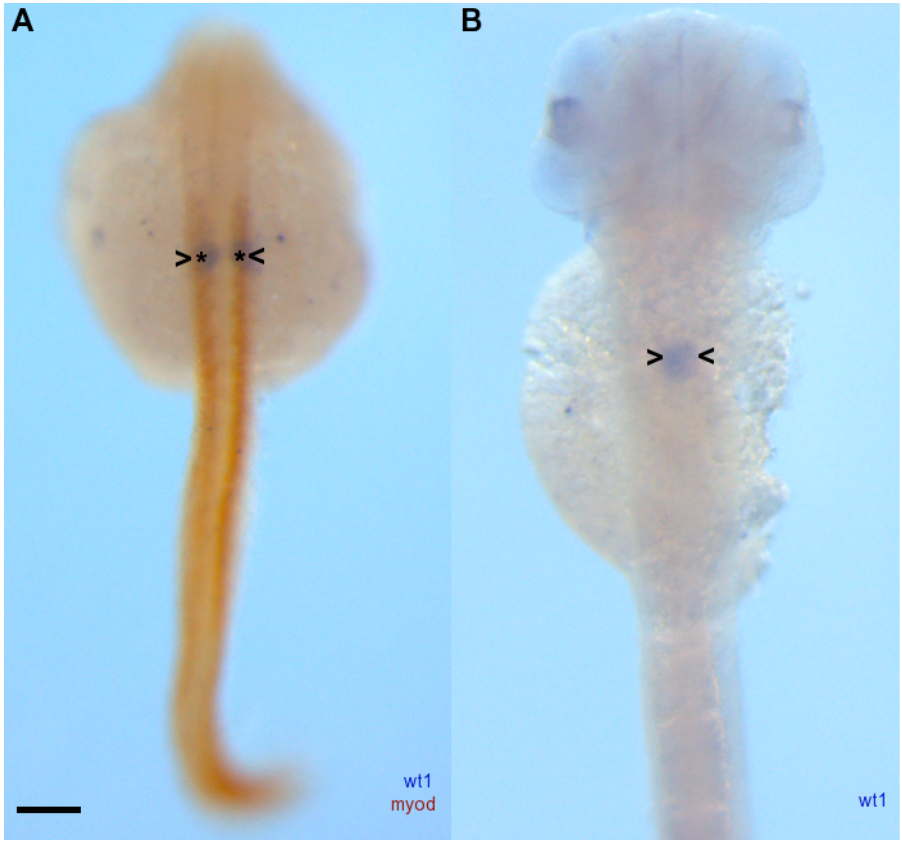

Figure 44-415. PGP midline convergence during 24-48 hpf, part 1/2.

Wt1 and *myoD* double WISH in 24 hpf (A) zebrafish embryos, *wt1* and *myoD* RNA probes were stained blue and brown respectively. In 48 hpf embryos (B), *wt1* probes were stained blue. All images are dorsal view with anterior to the top. At 24 hpf (A), the two PGP are distant to each other and locate bilaterally of the central axis (open arrowheads) to the ventral side of the somites (asterisks). At 48 hpf (B), the PGP fuse along the central axis (open arrowheads). The scale bar in B indicates 100 μm; all panels are at the same magnification.

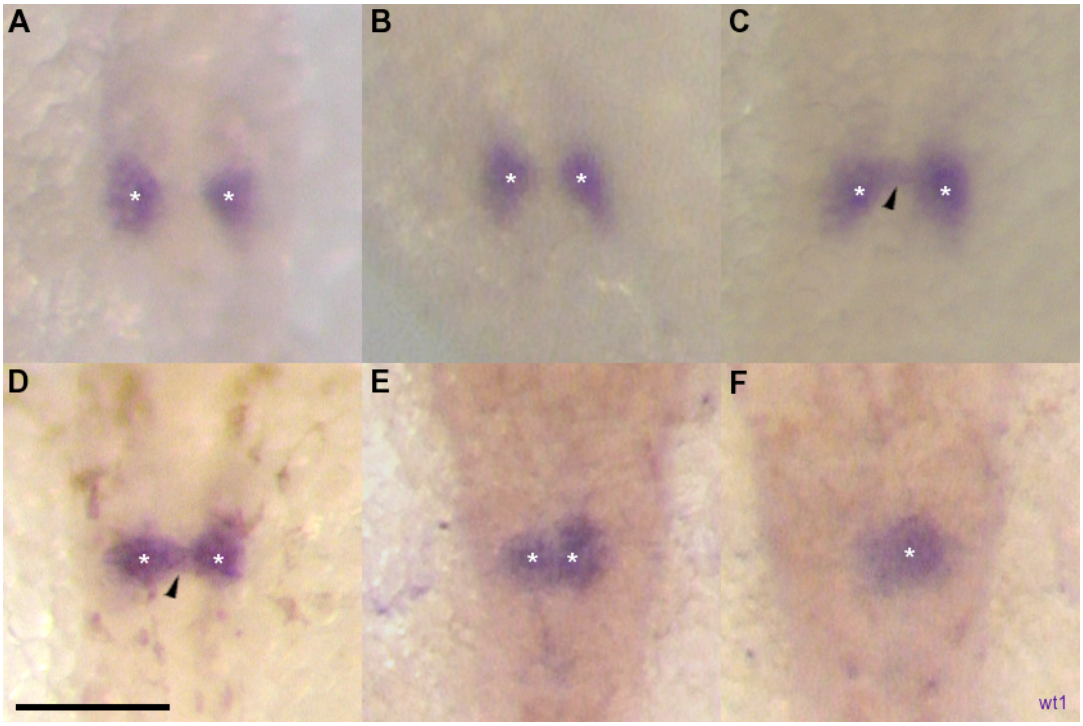

Figure 45-416. PGP midline convergence during 24-48 hpf, part 2/2.

Wt1 WISH in 24-36 hpf zebrafish embryos at 4-hour intervals (A-D) and in 36-48 hpf embryos at 6-hour intervals (D-F), *wt1* probe was stained indigo. All images are dorsal view with anterior to the top. (A-C) This series of WISH reveals changing mechanism of PGP midline convergence before and after 28 hpf (B). The PGP with ghostly tail (asterisks) indicates that PGP midline convergence consists movement of both PGP and its tail, prior to 28 hpf. (C) At 32 hpf, a small group of *wt1*-expressing cells that construct a narrow bridge (arrowhead) in-between the two PGP. Other parts of the PGP including the ghostly tail remain at the same location as 28 hpf. (D-E) During 36-48 hpf, the ghostly tail is not observed. The two PGP change morphology and pull each other together then fuse together at 48 hpf (F). The scale bar in D indicates 100 μm; all panels are at the same magnification.

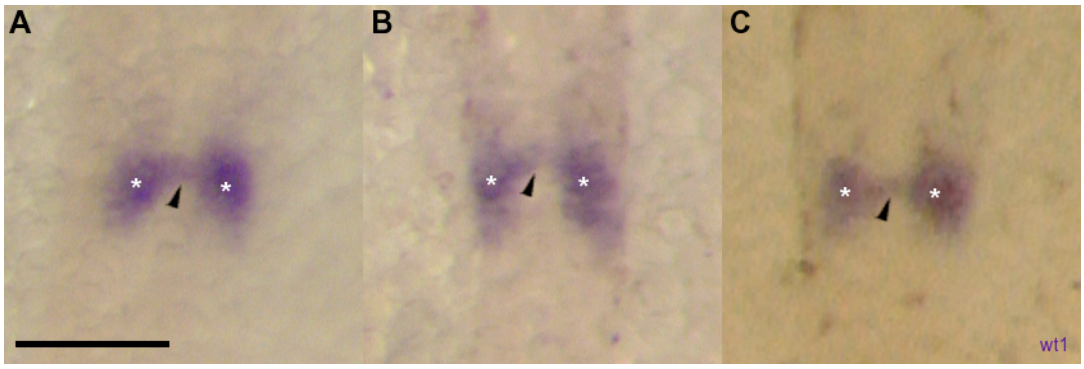

Figure 46-417. PGP midline convergence is initiated by growth of tissue extensions.
Wt1 WISH in 32 hpf zebrafish embryos (A-C), *wt1* probes were stained indigo. All images are dorsal view with anterior to the top. Long extension tissue (arrowhead) in the direction of subsequent migration was observed, at approximately 32 hpf in zebrafish embryos. The asterisks indicate the PGP. The scale bar in D indicates 100 μm; all panels are at the same magnification.

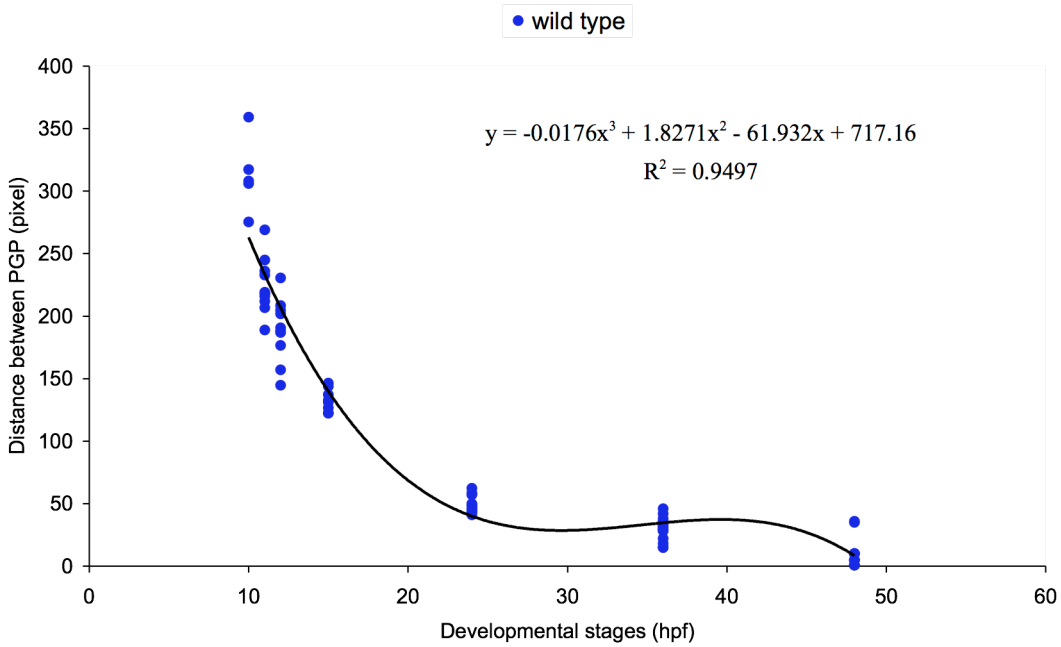

Figure 47-418. Quantification of PGP midline convergence during 10 to 48 hpf in wild type zebrafish embryos.

The distance between PGP (y-axis) was measured using the straight-line distance from a 2-dimentional digital image of a *wt1*-WISH embryo at a selected developmental stage (x-axis). The magnification of the images is 91 pixels every 100 μm. The scatter plot stage illustrates the results, which were collected at 7 developmental stages, namely 10 (n=5), 11(n=11), 12 (n=10), 15 (n=8), 24 (n=16), 36 (n=16) and 48 (n=14) hpf. The mathematical relationship between Distance Between PGP an developmental stage can be described by a cubic function, $y = -0.0176x^3 + 1.8271x^2 - 61.932x + 717.16$, R2 = 0.9497, with R-squared value of 0.9497. The closer R^2 is to 1.00, the better the fit of the mathematical model (Excel, Microsoft).

4.2 Mutant Allele Specific Genotyping For *Oep* Heterozygotes

Polymerase chain reaction (PCR) was used to identify *oep* heterozygotes. Firstly, a method, which allows extracting DNA rapidly from zebrafish fin clips, was developed (§2.6). Three primers were designed. Specific reverse primers, oeptz57R and oeptz57wtR can recognize oep^{tz57} and wild type allele respectively because of the difference in the last 3'-end base of their sequence. Both primer pairs, oepF-oeptz57R and oepF-oeptz57wtR, can generate 977 bp products in PCR reactions. The optimal PCR conditions for oepF-oeptz57R and oepF-oeptz57wtR reactions are 1.5 mM Mg^{2+}, annealing at 64°C for **1 min**, and repeating 30 cycles (Fig 421, Fig 422). In total 40 fish were detected for oep^{tz57} allele. Twenty-one $oep^{tz57+/-}$ were identified, namely 14 female and 7 male fish.

A quarter of the embryos collected from crossing *oep* heterozygotes appeared to have two typical *oep* homozygotes phenotypes (Fig 423). Firstly, during early eye morphogenesis in zebrafish, midline neuroepithelial tissue moves into the eye field displacing the eye field cells to the left and right optic primordium forming the protuberance of rostral hypothalamus (Kennedy et al., 2004; Kudoh and Dawid, 2001; Schmitt and Dowling, 1994). No separation of eye field occurs in *Zoep* embryos, only one optic primordium is observed at 16 hpf. The midline neuroepithelial tissue is neither differentiated nor distinguishable from the optic primordium (Fig 423D). Secondly, after 16 hpf, yolk begins to extend and appears kidney bean shaped from the lateral view (Kimmel et al., 1995). *Zoep* embryos have defects in yolk extension (Fig 423C) and the yolk appears like a ball instead of a kidney bean shape at 16 hpf.

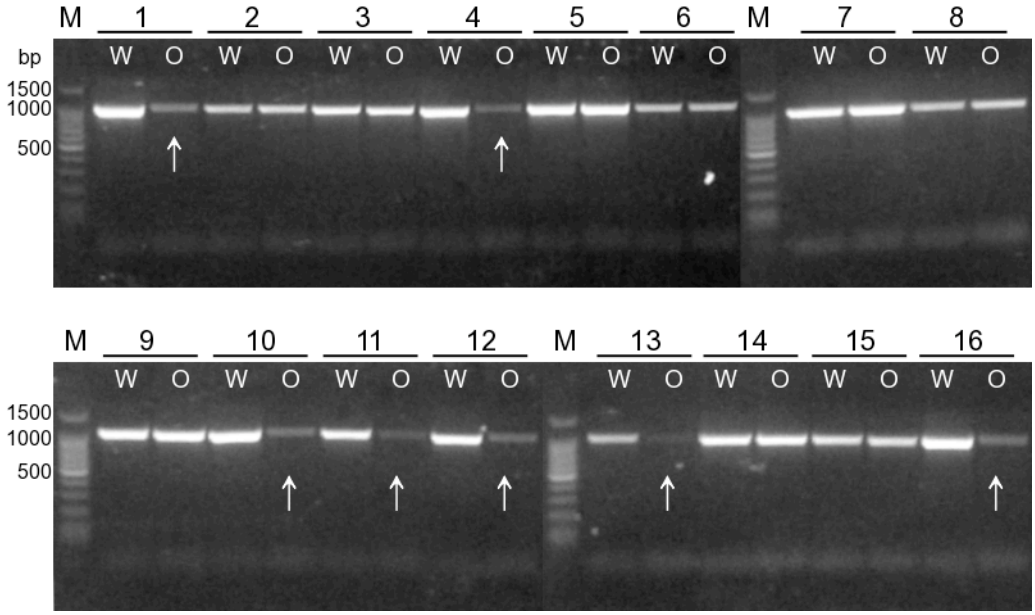

Figure 48-421. Optimization of PCR conditions for *oep*$^{tz57/+}$ genotyping, part 1/2.

This PCR result image was taken from four electrophoresis agarose gels (1.2% agarose, 140 V, 30 min). Each gel had its own marker. The DNA markers (M) were Promega 100 bp Ladder (1500, 1000, 900, 800, 700, 600, **500**, 400, 300, 200, 100 bp). Sixteen 3- to 4-month old zebrafish had their caudal (tail) fin clips removed (1-16) and these fin clips were processed for *oep*^{tz57} allele (O) and wild type allele (W) PCR reactions (Mg^{2+} conc. = 1.5 mM, Anealing condition = 64°C for **1 min**, Cycles = 30). Despite all the reaction results appearing positive, *oep*^{tz57} allele (O) PCR reactions for fish 1, 4, 10, 11, 12, 13 and 16 had notably fewer PCR products than the wild type allele (W) PCR reactions (arrows). The reactions in Fig 422 were performed under more stringent PCR conditions (Annealing condition = 64°C for **30 sec**).

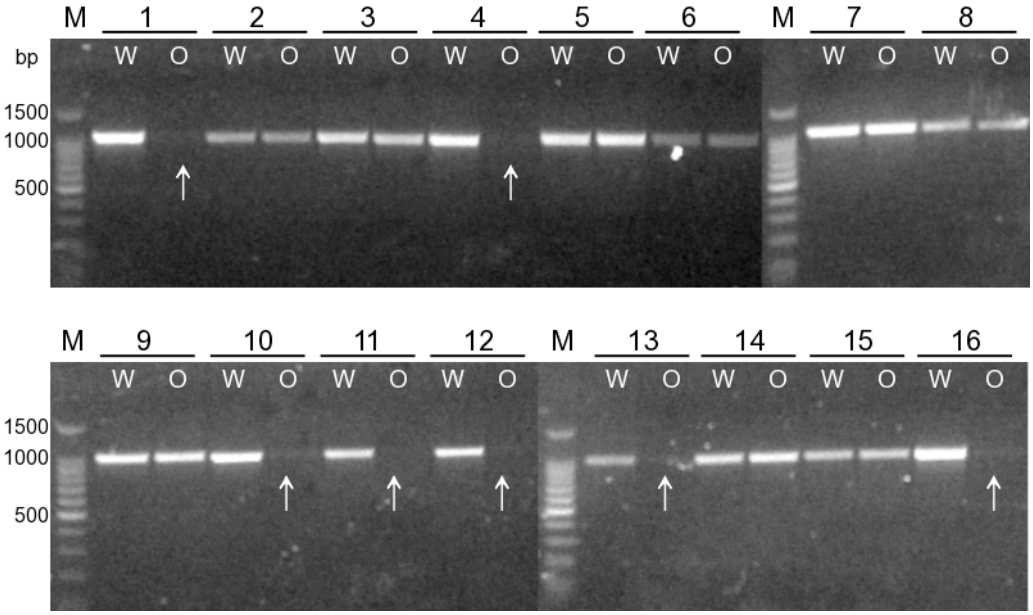

Figure 49-422. Optimization of PCR conditions for *oep*$^{tz57/+}$ genotyping, part 2/2.

The PCR result image was taken from four electrophoresis agarose gels (1.2% agarose, 140 V, 40 min). Each gel had its own marker. The DNA markers (M) were Promega 100 bp Ladder (1500, 1000, 900, 800, 700, 600, **500**, 400, 300, 200, 100 bp). The fin clips samples were the same as in Fig 4.2.1 (1-16). The PCR conditions for these reactions were 'Mg^{2+} conc. = 1.5 mM, Annealing condition = 64°C for **30 sec**, Cycles = 30'. Under these conditions, reactions for fish 1, 4, 10, 11, 12, 13 and 16 had no PCR products (arrows), which indicated these fish were wild types. In other words, *oep*$^{tz57/+}$ (2, 3, 5, 6, 7, 8, 9, 14 and 15) was identified when both *oep*^{tz57} (O) and wild type allele (W) PCR reactions had positive results.

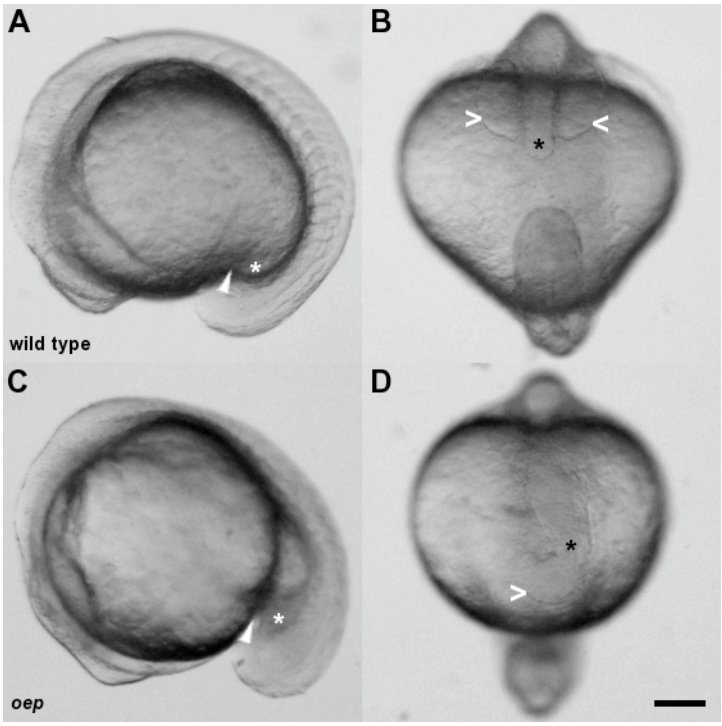

Figure 50-423. Zoep$^{-/-}$ phenotype at 16 hpf.

Bright field phase contrast images were taken (ateral view) for the wild type (A) and Z*oep*$^{-/-}$ (C) embryos, anterior to the right and dorsal view for wild type (B) and for Z*oep*$^{-/-}$ (D) embryos anterior to the top. A quarter of the embryos collected from crossing *oep*$^{+/-}$ appear to have typical Z*oep*$^{-/-}$ phenotype(C, D). At 16 hpf, wild type embryos begin yolk extension (A, white asterisk & arrow head) and to look like a kidney-bean from the lateral view. Z*oep*$^{-/-}$ embryos have defects in yolk extension (C, white asterisk & arrow head) and the yolk appears like a ball at this stage instead of like a kidney-bean. In wild type embryos, midline neuroepithelial tissue (prospective hyothalamus) moves into the eye field displacing the eye field cells to the left and right optic primordium (open arrowheads) and forming the protuberance of rostral hypothalamus (black asterisk). No separation of eye field occurs in Z*oep* embryos, only one optic primordium is observed (D, open arrowhead). The midline neuroepithelial tissue (black asterisk) is neither located in the midline nor differentiated or distinguishable from the optic primordium. The scale bar in D indicates 100 μm; all panels are at the same magnification.

4.3 Maternal Oep Partially Rescues MZoep Phenotypes

Severe patterning defects in embryos lacking maternal and zygotic Oep activity (MZ*oep*) were described in a previous study (Gritsman et al., 1999). The *oep* gene is expressed both maternally and zygotically (Zhang et al., 1998). Null allele *oep* female zebrafish were generated by *oep* mRNA rescue. MZ*oep* embryos were generated by crossing $oep^{-/-}$ females to $oep^{-/-}$ or $oep^{-/+}$ male fish (Gritsman et al., 1999). MZ*oep* embryos display phenotypes including cyclopic eye, lack of the notochord, and trunk somites. In fact the only endomesodermal tissue detected in MZ*oep* embryos are tail somites (Gritsman et al., 1999).

To study the rescue effect of maternal Oep, RNA WISH of *muscle-specific beta 1 integrin biding protein 2* (*mibp2*), and *ATPase,* Ca^{2+} *transporting cardiac muscle, fast twitch 1* (*atp2a1*) was carried out to examine the morphogenesis of lenses and, trunk somites respectively in the embryos lacking zygotic *oep* activity only ($Zoep^{-/-}$). Partial *mibp2* (718 bp) and *atp2a1* (650 bp) cDNA were cloned respectively into pGEM-T Easy (Promega) vectors for the preparation of probes. $Zoep^{-/-}$ embryos were generated by crossing $oep^{-/+}$ male and female fish, then collecting the embryos displaying abnormality in yolk extension and eye field separation (Fig 423). Presumably, $Zoep^{-/-}$ embryos carry normal maternal Oep.

The WISH results demonstrate that maternal Oep rescues some eye and mesodermal tissue development, such as somite morphogenesis during zebrafish embryonic development (Fig 431, Fig 432). The *mibp2* expression is a marker for the lenses in adult zebrafish (Vihtelic et al., 2005). *Mibp2* expressed strongly in the lenses in both the wild type and $Zoep^{-/-}$ embryos. Approximately 64% (n = 28/44) of $Zoep^{-/-}$ embryos display two-eye development and share a border, each eye having a

lens in the centre (Fig 431). In addition, 36% (n = 16/44) *Zoep*$^{-/-}$ embryos develop cyclopic eye similar to MZ*oep* (Gritsman et al., 1999). At 36 hpf, eyes develop on both sides of the body axis and are separated by rostral hypothalamus and telencephalon (Kennedy et al., 2004) in wide type embryos. In another words, MZ*oep* eye phenotypes were partially rescued by maternal Oep in 64% of *Zoep*$^{-/-}$ embryos.

Atp2a1 gene encoding for SERCA1 is exclusively expressed in somites from 15 hpf (Hirata et al., 2004). *Atp2a1* RNA WISH was performed to examine the development of somites in *Zoep*$^{-/-}$ at 36 hpf. *Atp2a1* is intensively expressed in the trunk somites in wild type embryos, which demonstrates the highly organized structure of these somites (Fig 432A). In half (n = 5 out of 11) Zoep$^{-/-}$ embryos, morphogenesis of the somites is no different from the wild type embryos (Fig 432C). In the other half (n = 6/11), *atp2a1* expresses normally but the somites are, however, relatively loose in structure (Fig 432B).

Fig 432 also demonstrates that PGP specification, but not most of the PGP midline convergence, proceeds normally. The RNA WISH of *wt1* also shows some PGP phenotypes are rescued by maternal Oep (open arrowhead). Most Zoep$^{-/-}$ embryos are normal in PGP specification but become defective during PGP midline convergence. Normal PGP morphogenesis is also observed in a few Zoep embryos. A more detailed analysis of PGP morphogenesis in Zeop$^{-/-}$ embryos is described in the following sections.

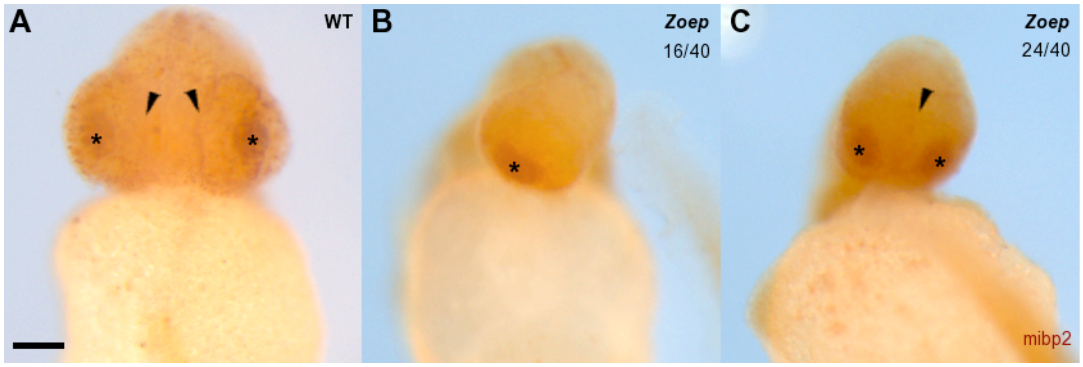

Figure 51-431. Maternal Oep partially rescues eye phenotypes.

Mibp2 RNA WISH was performed to examine the development of the lenses in zebrafish embryos, which lack zygotic Oep activity (*Zoep*$^{-/-}$) at 36 hpf (B, C). The *mibp2* probe was stained brown. All images were taken from the ventral view and anterior to the top. The eyes in wild type (WT) embryos (A) at this stage have a lens (asterisks) located in the centre, which are developed and separated by rostral hypothalamus and telencephalon (between arrowheads). Sixteen of the 40 *Zoep*$^{-/-}$ embryos have the cyclopic eye phenotype (B), in which an embryo only develops one eye, as M*Zoep*. Twenty-four of the 40 *Zoep*$^{-/-}$ embryos developing two eyes share a borderline (C, arrowhead) without rostral hypothalamus and telencephalon in between. The results (C) suggest maternal Oep activity partially rescues the cyclopic eye phenotype in Zoep$^{-/-}$. The scale bar in A indicates 100 μm; all panels are at the same magnification.

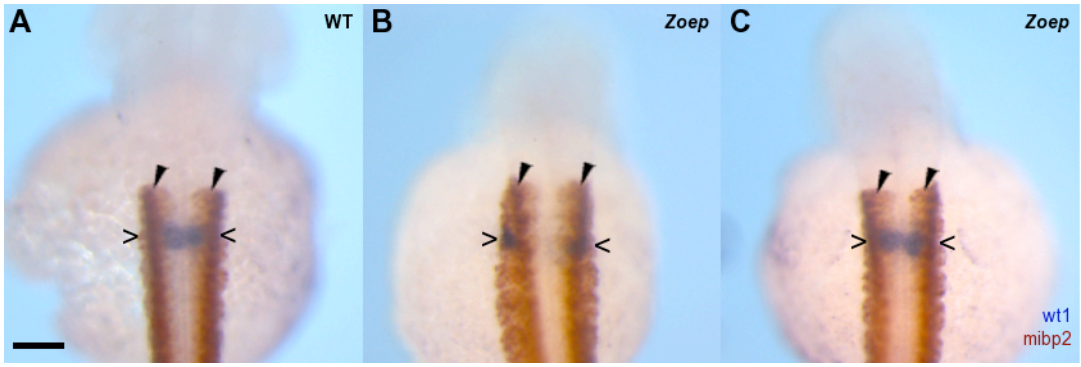

Figure 52-432. Development of trunk somites was rescued by maternal Oep.

Atp2a1 RNA WISH was performed to examine the development of somites in zebrafish embryos, which lack zygotic Oep activity (*Zoep*) at 36 hpf (B, C). The *atp2a1* probe was stained brown. All images are in dorsal view and anterior to the top. (A) *Atp2a1* is intensively expressed in the trunk somites in wild type (WT) embryos. Structure of the somites is highly organized (arrowheads). (B) Despite the slightly rambling structure of the somites, *atp2a1* expresses normally in the somites in several *Zoep*$^{-/-}$ embryos (n = 5 out of 11). (C) *Atp2a1* expression pattern in several *Zoep*$^{-/-}$ embryos (n = 6 out of 11) is indistinguishable from WT embryos. (A-C) Most *Zoep*$^{-/-}$ embryos are normal in PGP specification but defective in PGP midline convergence (open arrowheads). More detailed analysis of *wt1* WISH in *Zoep*$^{-/-}$ embryos is discussed in the following sections. The scale bar in A indicates 100 μm; all panels are at the same magnification.

4.4 Nodal Signalling Is Essential For PGP Midline Convergence

To examine whether Nodal signalling is involved in regulation of PGP midline convergence, analysis of phenotypes in *Zoep* embryos was conducted using WISH. Oep is an important cofactor in *nodal* signalling. The effects of zygotic Oep are discussed in this chapter.

The pattern of distribution of the *wt1* expressing cells during pronephric glomerular morphogenesis is not affected by mutated *oep* allele. At 15 hpf, *Zoep*$^{-/-}$ embryos exhibit curvy neck (Fig 441). The expression patterns of *myoD* and *wt1* in *Zoep*$^{-/-}$ were the same as in wild type emvryos (Fig 441). The phenotypes of intermediate mesoderm and somites in *Zoep*$^{-/-}$ embryos are almost the same as WT embryos, except in some (n = 2 out 0f 3) the distribution of somites is wider than in WT at this stage. At 24 hpf, the pattern of distribution of the *wt1* expressing cells is transformed successfully from blurred *wt1* expression to a defined rounded shape (PGP) (n = 8 out of 8) (Fig 441). This observation suggests mechanism of intermediate mesoderm specification and coalescence is independent of the effect of zygotic Oep.

Unlike WT embryos, in most *Zoep*$^{-/-}$ embryos (n = 7 out of 8), PGP remains bilaterally at the sides of the somites at this stage (Fig 411). The PGP distance values are similar to the PGP values of the WT embryos at 15 hpf. At 48 hpf, in *Zoep* embryos, the two PGP are separated from each other (n = 35 out of 36) and most have a PGP distance equivalent to that 15 hpf (n = 26 out of 36). This means that in these embryos the mechanism of PGP midline convergence is affected by mutation of *oep* as early as 15 hpf.

Muscle-specific beta 1 integrin binding protein 2 (*mibp2*) is a marker gene for a broad range of tissues at 36 hpf. In this experiment, *mibp2* was used as a marker for the musculature system and pectoral fin. At 36 hpf, WISH of *wt1* and *mibp2* demonstrates differential PGP migration phenotypes in *Zoep* embryos (Fig 442). At this stage, the two PGP well incorporate themselves into the main embryo stripe and are adjacent to each other at the central axis in WT embryos. In some *Zoep*$^{-/-}$ embryos (n = 3 out of 9), the PGP migration mechanism is damaged at an early stage (15 hpf), hence either one, or both, of the PGP are unable to incorporate into the structure of embryo stripe remaining outside. For some *Zoep*$^{-/-}$ embryos (n = 4 out of 9), the PGP migration mechanism is damaged at a later stage (24 hpf), when the two PGP are located in the main embryo structure but separate from each other. In contrast to the differential phenotypes of PGP midline convergence, the pectoral fin phenotype is constant in that the pectoral fin is budded at a more distant location along the central axis than in the wild type. PGP is thus independent of the mechanism of the pectoral fin formation.

PGP distance in *Zoep*$^{-/-}$ embryos at 15 (n = 3), 24 (n = 8), 36 (n = 34), and 48 (n = 34) hpf was quantified using the same methods as for wild type embryos. The results are presented in the scatter plot in Fig 443. PGP distance for 36 and 48 hpf is widely distributed between 30 and 200 pix. This distribution pattern suggests the effect of the mutated *oep*^{tz57} alleles on PGP midline convergence can be at any developmental stage between 12-36 hpf. The distribution pattern of the PGP distance for 24 hpf suggests a different conclusion, that 15 hpf is an important stage for PGP midline convergence. PGP midline convergence is impaired in most *Zoep*$^{-/-}$ embryos (n = 7 out of 8) at approximately 15 hpf.

For these embryos, the PGP midline convergence is damaged at the early developmental stage (15 hpf), which raises the questions about maturation and differentiation of the proneohric glomerulus. Nephrin and Podocin are key proteins required to maintain the filtration barrier of the foot process of podocytes (Nilius et al., 2007). In zebrafish, these two genes, *nephrosis 1, congenital, finish type (nephrin)-like* (*nph*/*nphs1l*) and *nephrosis 2, idiopathic, steroid-resistant (podocin)* (*pod*/*nphs2*), first express exclusively at 24 hpf in PGP (Kramer-Zucker et al., 2005). The differentiation status of PGP was examined by using WISH of *nph* and *pod* to study mRNA expression of these two genes. Partial *nph* (543) and *pod* (481 bp) cDNA were cloned into pGEM-T Easy (Promega) vectors for the preparation of probes.

The results shown in Fig 444 demonstrate PGP differentiation is not affected by defective PGP midline convergence. *Nph* and *pod* express normally in *Zoep*$^{-/-}$ embryos at 36 hpf, despite PGP midline convergence damaged at 15 hpf. In other words, the mechanism, which controls PGP differentiation, is independent of the mechanism, which regulates PGP midline convergence after 15 hpf. In summary maternal Oep rescues most PGP specification and differentiation mechanisms but not the midline migration mechanism.

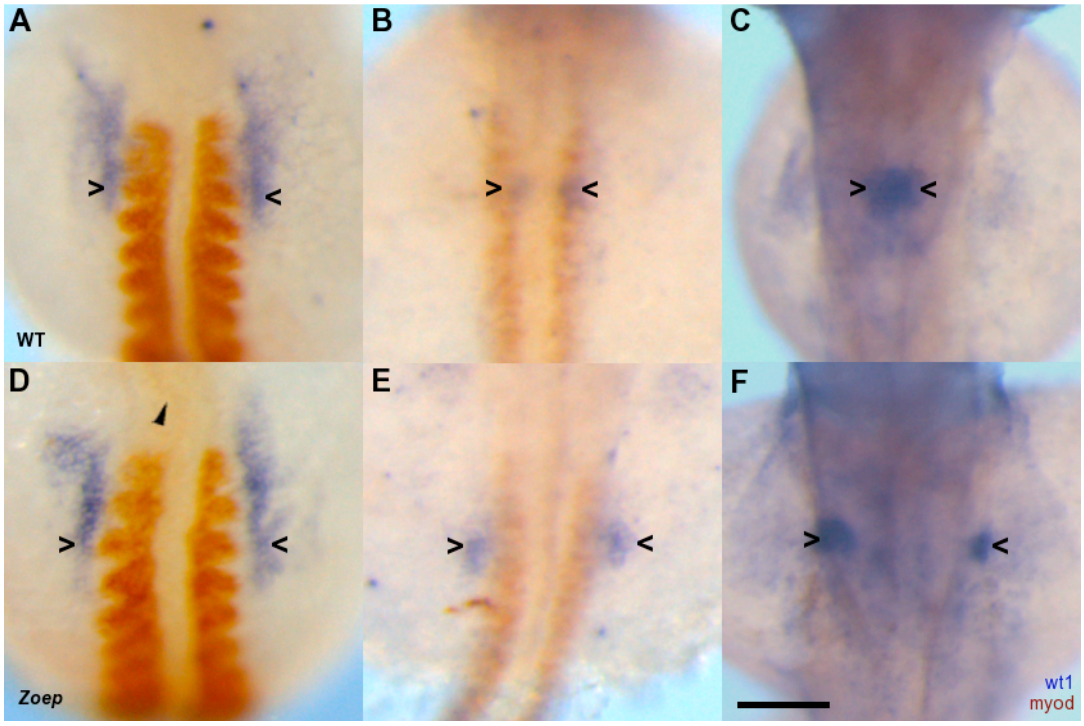

Figure 53-441. Morphogenesis of the pronephric glomerulus in *Zoep*$^{-/-}$ from 15 to 48 hpf.
Wt1 and *myoD* double WISH at 15 (A, D), 24 (B, C), and 48 (C, F) hpf. Zebrafish embryos were stained blue and brown respectively. The pattern of *wt1* expression in *Zoep*$^{-/-}$ embryos (D-F) was compared with that in wild type (WT) embryos (A-C) at the analogue stages. All images are dorsal view and anterior to the top. (D) The *Zoep*$^{-/-}$ embryos display twist neck (arrowhead). The pattern of *wt1* expression (open arrowhead) in *Zoep*$^{-/-}$ is similar to that in WT embryos. (E) The bilateral PGP does not invade the main embryo stripe successfully (open arrowheads). (F) PGP midline convergence is seriously defective in *Zoep*$^{-/-}$ embryos, even though *wt1* expression is normal. The scale bar in F indicates 100 μm; all panels are at the same magnification.

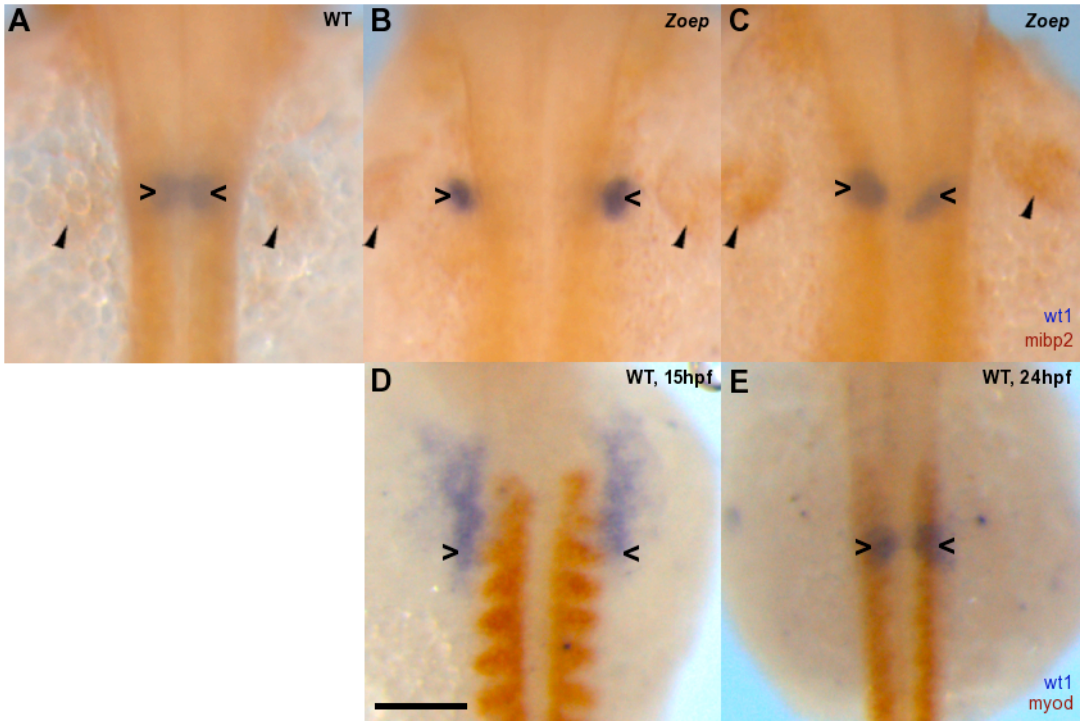

Figure 54-442. Varied severity of PGP midline convergence phenotype in *Zoep*$^{-/-}$ embryos.
Wt1 and *mibp2* double WISH at 36 hpf zebrafish embryos (A-C) were stained blue and brown respectively. All images are dorsal view with anterior to the top. *Wt1* gene expression pattern displays varied severity of PGP midline convergence phenotype in *Zoep*$^{-/-}$ embryos. This diversity of PGP phenotype is not correlated with the phenotype of fin bud formation. (A) At this stage, the bilateral PGP lie right next to each other along the midline (open arrowheads). (B) The bilateral PGP lie on the outside of the main embryo stripe. The distance between the bilateral PGP remain at 15 hpf (D). (C) The two PGP are in the main embryo stripe and keeping distance from each other (open arrowheads). The distance between the bilateral PGP remain at 24 hpf (E). (A-C) In *Zoep*$^{-/-}$ embryos, the pectoral fin develops in a more distant location to the midline than in WT. The scale bar in D indicates 100 μm; all panels are at the same magnification.

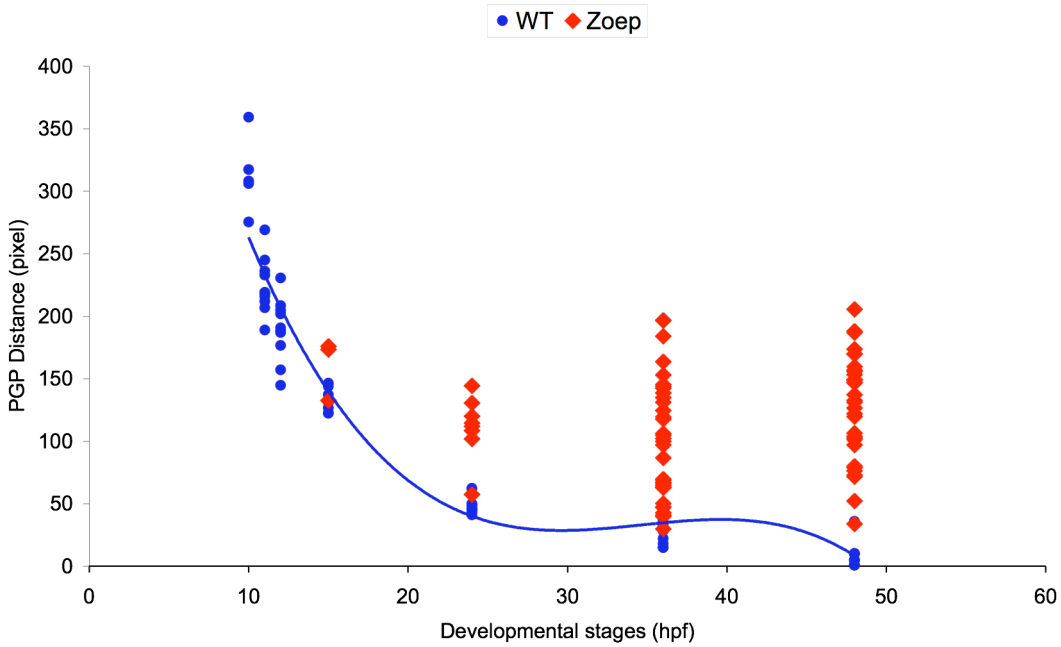

Figure 55-443. Quantification of PGP midline convergence during 15 to 48 hpf in *Zoep*$^{-/-}$ embryos.

The straight-line distance between PGP (y-axis) was measured from 2-dimentional digital images of *wt1*-WISH embryos at selected developmental stages (x-axis). The magnification of the images is 91 pixels for every 100 μm. This scatter plot illustrates the results for *Zoep*$^{-/-}$ (red diamonds). Data of the measurement of PGP distance was collected at 4 developmental stages namely 15 (n = 3), 24 (n = 8), 36 (n = 34) and 48 (n = 34) hpf (every red diamond represents a measurement from an embryo). The detailed information on PGP distance for wild type embryos (WT, blue circles) is described in §4.1 and Fig 418. The Unpaired Student's t-Test was applied to compare the PGP distance between wild-type and *oep*$^{-/-}$ embryos at 15, 24, 36 and 48 hpf. The statistical test results support the claim that PGP phonotype is abnormal in *oep*$^{-/-}$ embryos. The P values from the test are 0.0017, < 0.001, < 0.001 and < 0.001 for 15, 24, 36 and 48 hpf respectively.

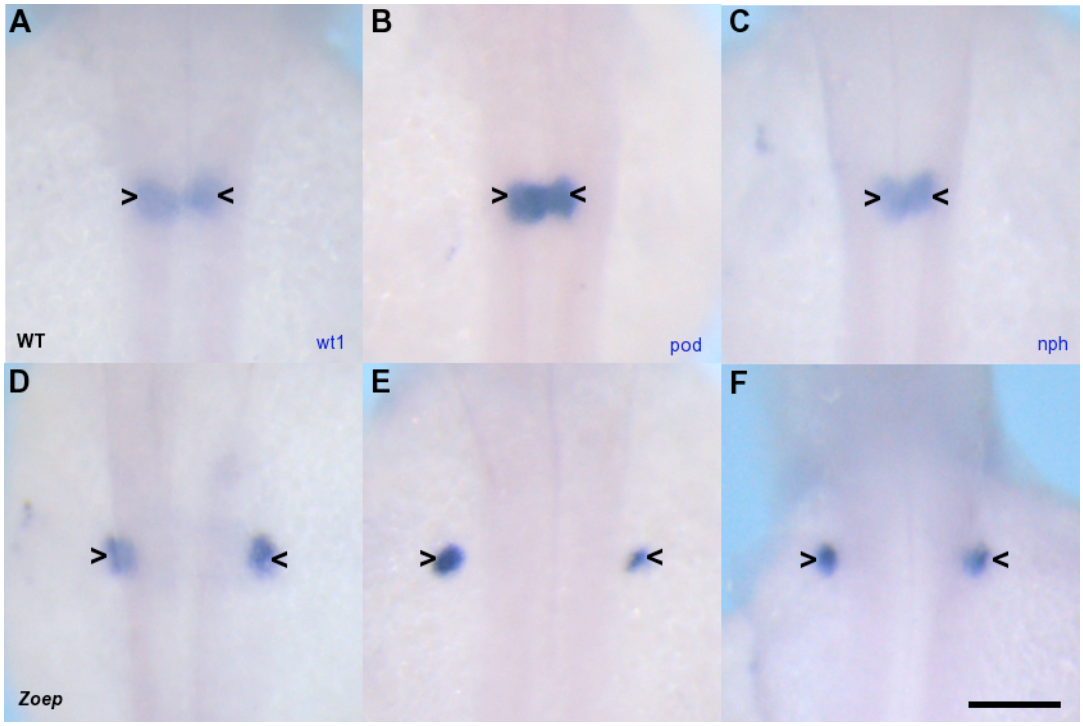

Figure 56-444. Mechanisms for pronephric glomerulus differentiation are independent of the mechanisms for PGP midline convergence.

Gene expression, of *podocin* (*pod*) and of *nephrin* (*nph*), was used to detect the differentiation status of PGP. *Wt1* (A, D, arrowheads), *pod* (B, E, arrowheads), and *nph* (C, F, arrowheads) WISH at 36 hpf in wild type (A-C) and *Zoep*$^{-/-}$ (D-F) embryos. All images are dorsal view and anterior to the top. Even though the PGP convergence impaired during early stages (E, F) in *Zoep*$^{-/-}$ embryos, the expression of *pod* (E) and of nph (F) appears to be normal. The scale bar in F indicates 100 μm; all panels are at the same magnification.

4.5 Comparing The Differential Phenotypes Between PGP And Surrounding Tissue in *Zoep*$^{-/-}$

PGP midline convergence is a post-gastrulation process in the zebrafish embryonic development. From 10 hpf, specification of intermediate mesoderm continues 48 hpf when a fused pronephric glomerulus forms. The *Zoep*$^{-/-}$ embryo is a perfect model to study more detailed mechanisms of Nodal signalling in tissue/organ morphogenesis because of the differential rescue effects of maternal Oep in *Zoep*$^{-/-}$ embryos. Nodal signalling has a broad effect in most mesoderm and endoderm derived tissue development (Gritsman et al., 1999). Comparing different phenotypes of different tissues in *Zoep*$^{-/-}$, subdivision of Nodal signalling pathways can be determined.

To investigate whether PGP midline convergence is associated with the development of the surrounding tissues, double WISH of *wt1* was carried out using each of the following genes; *cardiac myosin light chain 2* (*cmlc2*), *sonic hedgehog a* (*shha*), *spondin 1b* (*spon1b*), and *islet2a* (*isl2a*). Partial *cmlc2* (588 bp), *shha* (1461 bp), *spon1b* (751 bp), and *isl2a* (523 bp) cDNA were cloned into pGEM-T Easy (Promega) vectors for the preparation of probes.

Cmlc2 gene is used as a marker for heart morphogenesis. Primordia fuse together along the central axis by 24 hpf (Huang et al., 2003). At 36 hpf, heart tube morphology can be observed using WISH of *cmlc2*. In *Zoep* embryos, both one- (n = 6 out of 9) and two-heart tube (cardiac bifida) (n = 3 out of 9) phenotypes were observed (Fig 451). Importantly, these heart midline convergence phenotypes are not synchronized with PGP midline convergence phenotypes. The hypothesis of this research is correct. There are factors that are involved in the PGP midline convergence but not essential for cardiac midline convergence. The *Zoep*$^{-/-}$ embryos,

which display normal heart primordium midline convergence, contain the normal *wnt/Dvl/RhoA* pathway but defective PGP midline convergence mechanism.

Shh expresses in both notochord and floor plate at early developmental stages and more specifically in floor plate at later stages (Krauss et al., 1993; Schafer et al., 2005). A previous study suggests that *shh* signalling pathway is essential for PGP midline convergence (Majumdar and Drummond, 2000). Firstly, double WISH at 28 hpf was performed. *Shh* expression is normal in the trunk region, regarded as notochord in *Zoep*$^{-/-}$, compared to WT (Fig 452). In most of these embryos (n = 5 out of 6), PGP distance remains the at a stage equivalent to 15 hpf in WT. The defect in PGP midline migration prior to 28 hpf is hence not an effect of *shh* signalling in *Zoep*. At 36 hpf, the expression of *shh* in the trunk region, regarded as floor plate, is sharply reduced in *Zoep*$^{-/-}$ (n = 10). In summary, PGP midline convergence is not linked to notochord formation, but may be associated with floor plate development.

Spon1b is another floor plate marker that also expresses in the pancreatic bud (Kim et al., 2005; Schafer et al., 2005). Double WISH of *wt1* and *Spon1b* were used to examine *Zoep*$^{-/-}$ embryos at 36 (n = 26) and 48 (n =25) hpf. None of floor plate phenotype was rescued by maternal Oep in these embryos (Fig 453). *Spon1b* expression was completely absent in all the *Zoep*$^{-/-}$ embryos, even though PGP midline convergence was damaged at later stages (18 hpf) in some embryos (n = 8 out of 51). The process of PGP midline migration during 10 to 18 hpf is independent of floor plate development. On the other hand, pancreatic budding shows strong correlation with PGP midline convergence (Fig 453). Zebrafish pancreatic primodia first appear in two bilateral rows of cells adjacent to the midline at 14 hpf (Biemar et al., 2001). By 18 hpf the rows of cells approach each other and fuse to form a single

field of *pdx-1* expressing cells (Biemar et al., 2001). At 36 hpf, posterior pancreatic buds can be identified by *spon1b* WISH in the midline in WT embryos (Fig 453A). During the early stage (by 18 hpf), PGP collocates with ectopic pancreatic budding (Fig 453B, C). After 18 hpf, endoderm convergence is independent of PGP midline convergence (Fig 453). The PGP midline convergence process is divided into two stages, prior to 18 hpf and after 18 hpf. PGP midline convergence is dependent on the endoderm convergence process prior to 18 hpf. After 18 hpf, PGP midline migration needs other factors, which are in addition to endoderm convergence and regulated by *nodal* signalling.

Finally, the connection between PGP midline convergence and formation of primary sensory and motor neurons was examined using double WISH of *wt1* and *isl2a* at 36 hpf. The *isl* family is expressed in the primary sensory neurons and the onset of the primary motor neurons (Segawa et al., 2001). The *isl2a* expression pattern shows no difference between WT and *Zoep*$^{-/-}$ embryos especially in the trunk region (Fig 454, Fig 455). The differential PGP midline convergence phenotype in *Zoep*$^{-/-}$ appears not to be associated with the formation of primary sensory neurons and the primary motor neurons. In WT embryos, the two long rows of neurons are divided by the floor plate and lie bilaterally. These rows of neurons sit side by side relative to each other in *Zoep*$^{-/-}$ (Fig 454, Fig 455), because the floor plate failed to differentiate (Fig 453). PGP midline convergence is not associated with the formation of primary sensory neurons, the primary motor neurons or floor plate.

The *isl2a* WISH results demonstrate an additional conclusion, which is consistent with the results of *spon1b* WISH. The differential PGP midline convergence phenotype in *Zoep*$^{-/-}$ is connected with the formation of swim bladder

primordium or anterior pancreas (Fig 454, Fig 455). For *Zoep*$^{-/-}$ embryos in which PGP midline convergence is damaged at early stages, the specification of swim bladder primordium is defective too (Fig 454, Fig 455). When the PGP phenotype is rescued, the endoderm phenotype is also rescued.

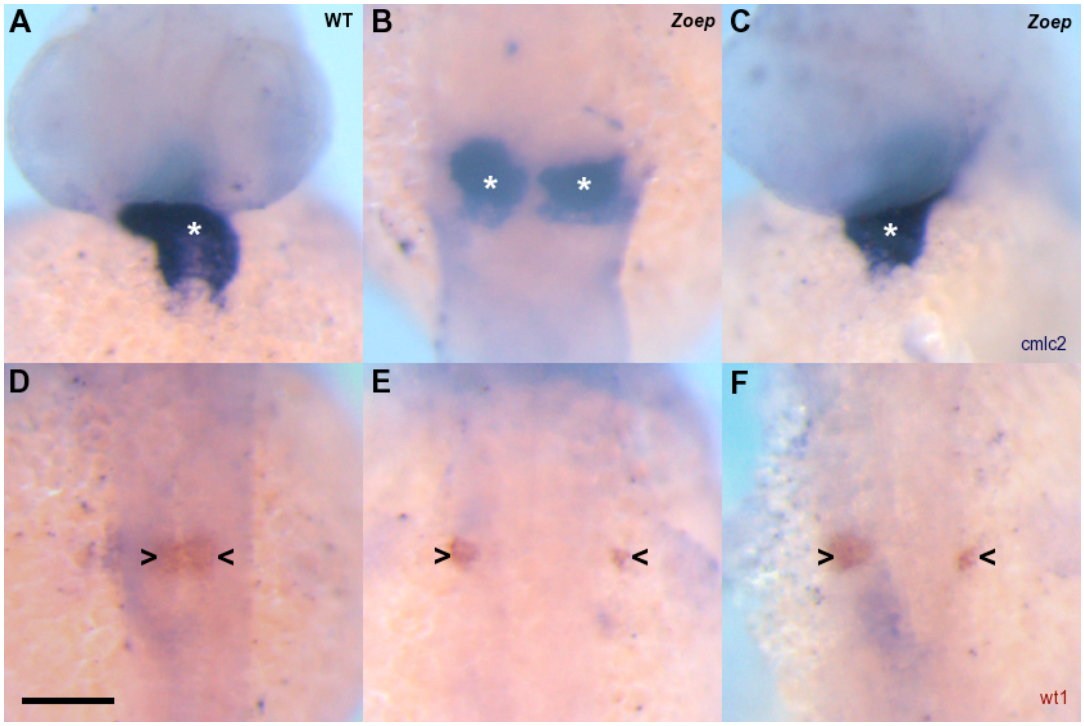

Figure 57-451. Cardiac bifida phenotype is not synchronized with PGP midline convergence phenotype.

The heart phenotype was detected by WISH of *cardiac myosin light chain 2* (*cmlc2*) (A-C, asterisks) at 36 hpf. *Cmlc2* probe was stained blue. The PGP phenotype was represented using WISH of *wt1* (D-F, open arrowheads) at 36 hpf. The *wt1* probe was stained red. Images A, C are ventral view with anterior to the top. Image B is dorsal view with anterior to the bottom. Images D-F are dorsal view with anterior to the top. A & D; B & E; C & F images are taken from same embryos. The scale bar in D indicates 100 μm; all panels are at the same magnification.

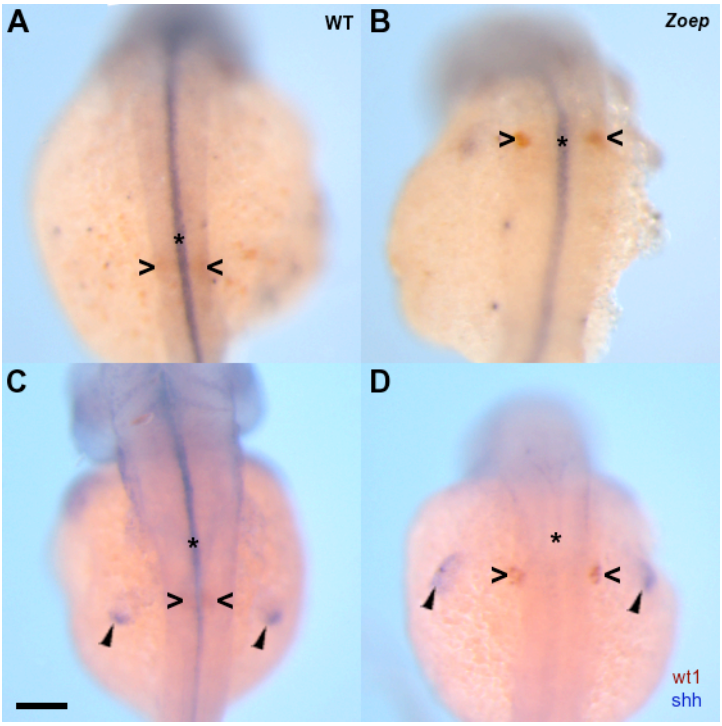

Figure 58-452. *Shh* expression appears normal in the trunk region by 28 hpf in *Zoep*$^{-/-}$ embryos. *Wt1* and *shh* double WISH in 30 (A, B) and 36 (C, D) hpf zebrafish embryos, *wt1* and *shh* RNA probes were stained brown and blue respectively. (A) *Shh* expresses in the notochord and floor plate at 30 hpf in wild type (WT) embryos (asterisk). (B) The expression pattern of *shh* in the trunk region (asterisk) in *Zoep*$^{-/-}$ is similar to WT, despite PGP midline migration deficiency (open arrowheads). (C) *Shh* expresses in the floor plate at 36 hpf in WT embryos (asterisk). (D) In *Zoep*$^{-/-}$, the expression of *shh* is absence in the floor plate (asterisk) but normal in the pectoral fin (arrowheads). All images were taken from the dorsal view with anterior to the top. The scale bar in C indicates 100 μm; all panels are at the same magnification.

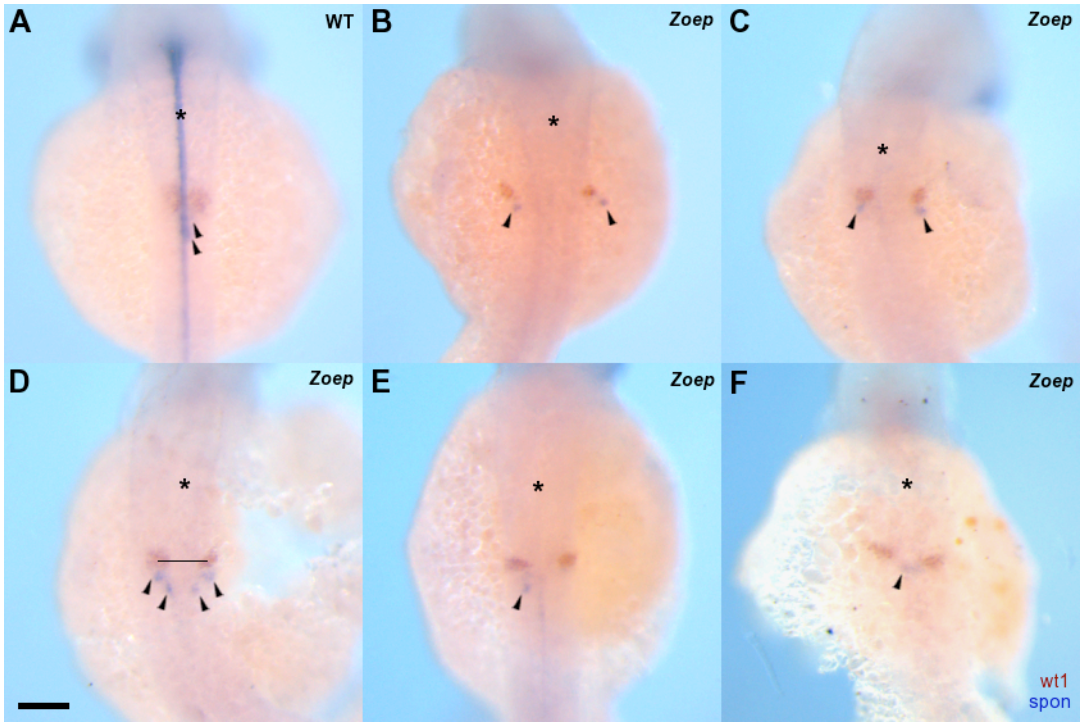

Figure 59-453. *Spon* expression pattern in *Zoep*$^{-/-}$ embryos.

Wt1 and *spondin 1b* (*spon*) double WISH in 36 (A-E) and 48 (F) hpf zebrafish embryos, *wt1* and *spon* RNA probes were stained brown and blue respectively. (A) *Spon* expresses in the floor plate (asterisk) and pancreatic buds (arrowhead) in wild type (WT) embryos. (B-F) The floor plate formation is defective (asterisk) in *Zoep*$^{-/-}$, this result is consistent with the *shh* WISH results (Fig 4.5.2). (B, C) Differential severity of the PGP midline convergence phenotype is accompanied by varied severity of the ectopic-pancreatic budding (arrowheads). (D-F) When the PGP distance is shorter than 95 [(38 pix/40 pix) x 100] μm (D, straight-line), pancreatic budding phenotypes (arrowheads) are independent from PGP midline convergence phenotypes (brown). All images were taken from the dorsal view with anterior to the top. The scale bar (40 pix) in D indicates 100 μm; all panels are at the same magnification.

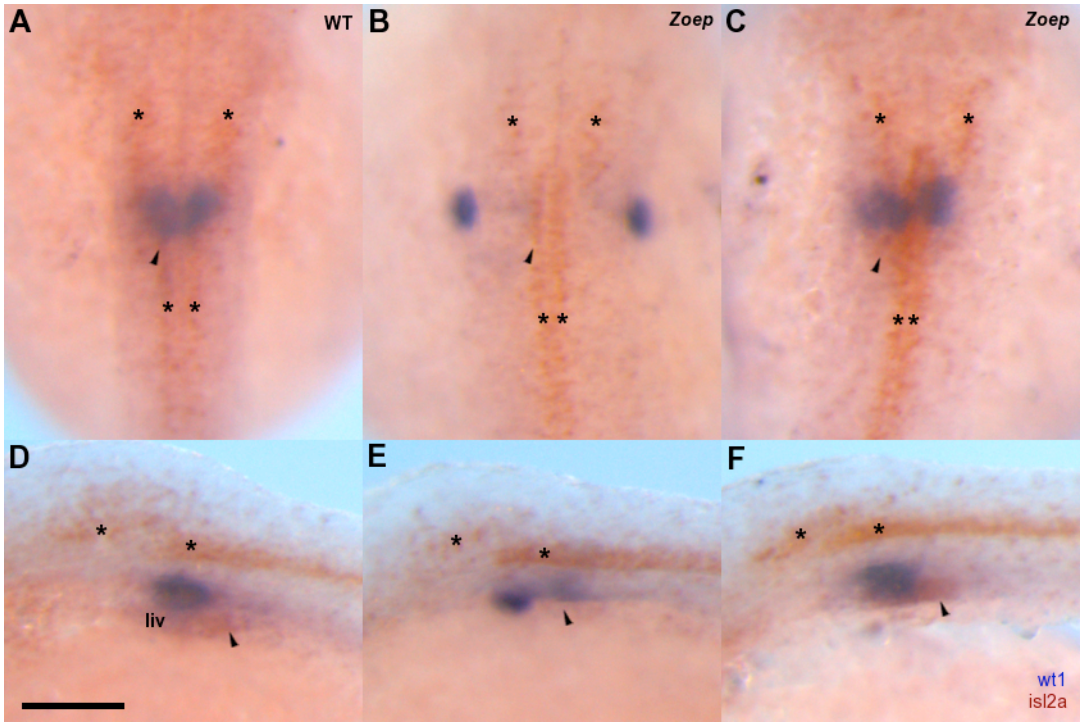

Figure 60-454. *Isl2a* expression pattern in *Zoep*$^{-/-}$ embryos, part 1/2.

Wt1 and *islet2a* (*isl2a*) double WISH in 36 hpf zebrafish embryos (A-F), *wt1* and *isl2a* RNA probes were stained blue and brown respectively. Images A-C were taken from the dorsal view and anterior to the top. Images D-F were taken from the lateral view with anterior to the left. (A, D) *Isl2a* expresses intensively in primary motoneurons (asterisks) and swim bladder primordium (arrowhead) at 36 hpf in wild type (WT) embryos. Low-level isl2a expression in the liver (liv) was observed (D). The bilateral lines of primary motoneurons are at a short distance from each other because the floor plate is in-between (A, asterisks). (B, E) Severely damaged PGP midline convergence is accompanied by normal primary motoneuron development and absence of the swim bladder primordium (arrowhead). (C, F) Normal PGP midline convergence is accompanied by normal isl2a expression in the swim bladder (arrow head). (B, C) The bilateral lines of primary motoneurons are next to each other without floor plate in-between (asterisks). The results are consistent with the results in Fig 4.5.3 and Fig 4.5.4. The floor plate is not differentiated in *Zoep*$^{-/-}$ embryos. The varied phenotypes of PGP convergence are not correlated with the floor plate phenotypes prior to 36 hpf.. The scale bar (80 pix) in D indicates 100 μm; all panels are at the same magnification.

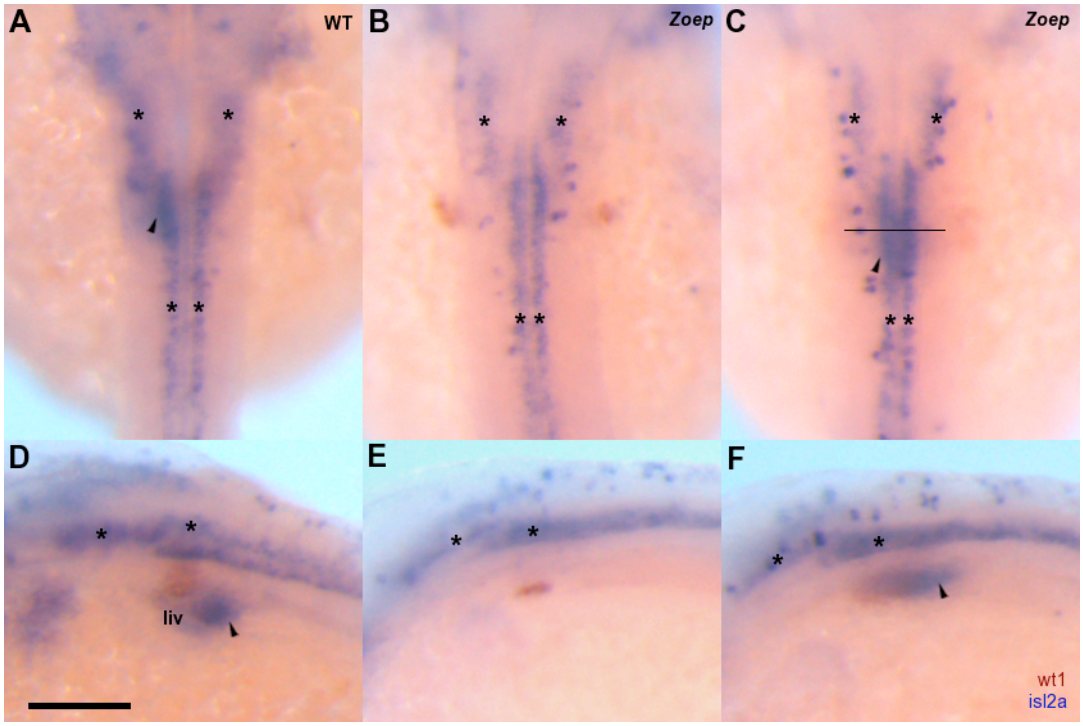

Figure 61-455. *Isl2a* expression pattern in *Zoep*$^{-/-}$ embryos, part 2/2.

This figure shows the same information as Fig 4.5.4 and emphasizes the staining of the swim bladder (arrowheads). *Wt1* and *islet2a* (*isl2a*) double WISH in 36 hpf zebrafish embryos (A-F), *wt1* and *isl2a* RNA probes were stained brown and blue respectively. Images A-C were taken from the dorsal view with anterior to the top. Images D-F were taken from lateral view with anterior to the left. In the *Zoep* embryo shown in C, F, PGP distance (straight-line) is approximately 97.5 [(78 pix/ 80 pix) x 100] μm when *isl2a* expressed normally in the swim bladder (arrowhead). The scale bar (80 pix) in D indicates 100 μm; all panels are at the same magnification.

4.6 Conclusion

According to the dynamic pattern of *wt1* expressing cells, the morphogenesis of the pronephric glomerulus is divided into three stages, or processes, specification (10-12 hpf), coalescence (12-24 hpf) and fusion (24-48 hpf) (Fig 461). PGP midline migration processes continuously through out the entire three stages (10-48 hpf) in a developing embryo. A cubic equation with an R-squared value of 0.9497, shown below, was generated by quantification of PGP distance and Excel (Microsoft) to model the PGP migration process (y = PGP distance; x = developmental stage, hpf, $10 \leq x \leq 50$):

$$y = -0.0176x^3 + 1.8271x^2 - 61.932x + 717.16.$$

When a certain developmental stage is given (x), a value of PGP distance is deduced (y). Given a value for the PGP distance the associated developmental stage can be calculated. In the case of the analysis of the PGP phenotypes in *Zoep*$^{-/-}$ embryos, this formula suggests the stage that process of PGP midline convergence is affected by giving a value for the PGP distance.

Zoep$^{-/-}$ embryos display differential phenotypes in many aspects, for example PGP midline migration, heart primordium midline migration and eye differentiation, which are due to maternal Oep rescue effects. PGP midline convergence affected by *oep* mutant alleles can be as early as 12 hpf (n = 3 out of 34) (Fig 443). Mechanisms of specification and coalescence of the anterior intermediate mesoderm are independent of the effects of *oep* mutant alleles. They appear to be three important times in the entire process of PGP midline migration, 15 (n = 60 out of 112), 18 (n = 40 out of 112), 36 (n = 12 out of 112) hpf, which suggests that PGP midline convergence is processed by different mechanisms at the three different stages. In

addition, the mechanism of PGP midline convergence by 18 hpf is closely associated with the differentiation of the pancreas and swim bladder.

Finally, Nodal signalling is essential for the midline migration of both PGP and heart primordia (Fig 462). The phenotypes of PGP and heart midline convergence are not synchronized, suggesting nodal signalling modulates PGP and heart midline convergence is mediated by additional factors.

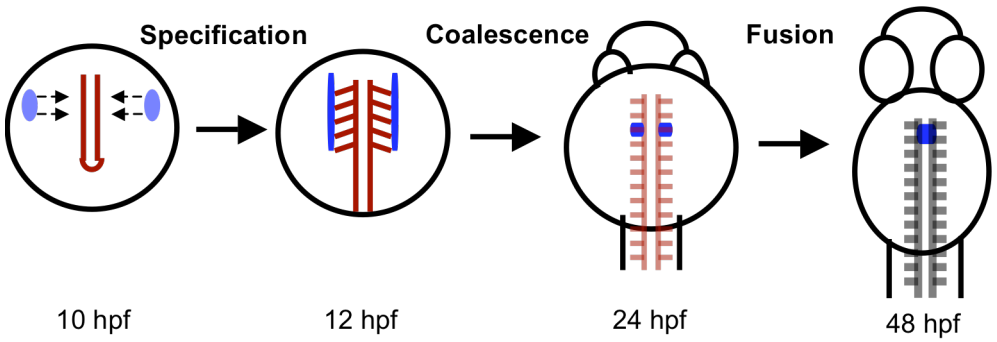

Figure 62-461. PGP midline convergence during 10-48 hpf.
Dorsal views of the zebrafish embryo with anterior to the top, at 10, 12, 24 and 48 hpf. The blue represents the expressing cells. Brown and grey represent somites (and adaxial cells). According to the dynamic pattern of *wt1* expressing cells, the morphogenesis of the pronephric glomerulus is divided into three stages, or processes, specification (10-12 hpf), coalescence (12-24 hpf) and fusion (24-48 hpf). The bilateral patches of *wt1* expressing cells continuously move towards each other from 10 hpf till fused along the central axis at 48hpf. Convergence is, hence, a long process during zebrafish embryonic development. The graphic is not to scale.

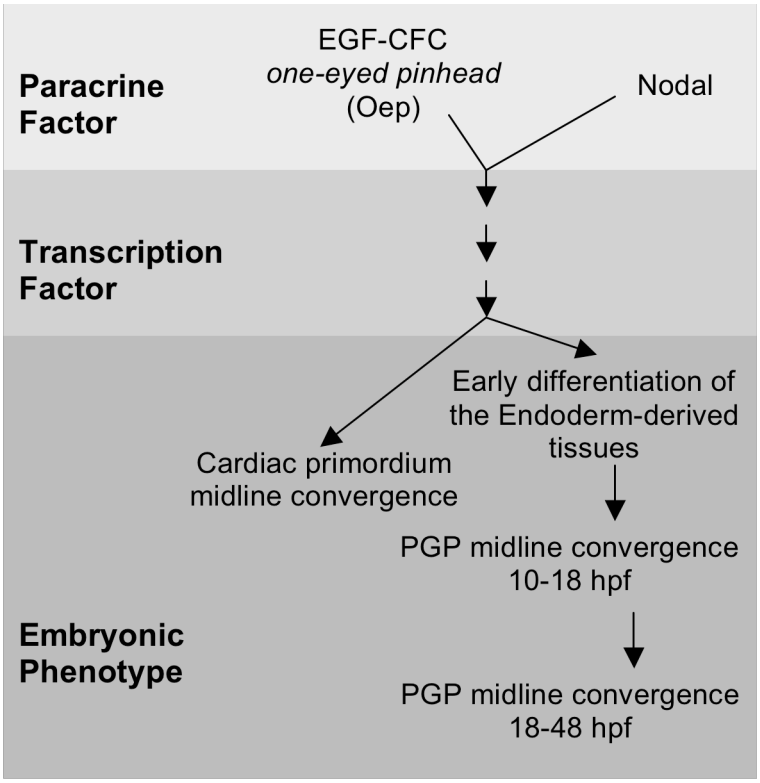

Figure 63-462. Genetic control of PGP midline convergence by Nodal signalling.

This simplified diagram summarizes the genetic control of Nodal signalling in the PGP midline convergence. Nodal signalling triggers a transcriptional cascade including Gata5/Faust, and the homeodomain containing factors *bonnie and clyde* (Bon), which are required to maintain expression of the sox factor *casanova* (Cas), the key endodermal determinate in zebrafish (Reiter et al., 2001). Paracrine factors of Nodal and its cofactors (Oep) are in the top column. These transcription factors are represented using arrows in the middle column. Prior to 18 hpf, PGP midline convergence associate with early differentiation of the endoderm-derived tissues. After 18 hpf, PGP midline convergence is not closely associated with the development of endoderm-derived tissues. A previous study suggests myocardial morphogenesis is independent of further differentiation of endoderm (Trinh and Stainier, 2004). Bon and Cas have been shown essential for cardiac primordium midline migration (Griffin and Kimelman, 2002).

5. Spt/Tbx16 Is Essential For PGP Midline Convergence

The zebrafish mutants, *spt* and *ntl* were selected for the study of the FGF signalling pathway in pronephric-glomerular morphogenesis in zebrafish embryos. Inhibition of FGF signalling in zebrafish embryos using injection of a dominant negative FGFR (dnFGFR) RNA, down regulates *spt* and *ntl* expression and generates subsequent phenotypes lacking trunk and tail mesoderm (Griffin et al., 1995). Mutant analysis in zebrafish has demonstrated that Spt is required through regulation of the cell adhesion molecule, poaraxial protocadherin (PAPC), for the movement of somite progenitors and subsequent somitogenesis (Amacher and Kimmel, 1998; Ho and Kane, 1990; Kimmel et al., 1989; Weinberg et al., 1996; Yamamoto et al., 1998). These studies of zebrafish embryonic development suggest that the T-box transcription factor, *spt,* is a key mediator in FGF signalling in the formation of trunk mesoderm (Griffin et al., 1998) in addition to the supporting mediator *ntl* (Griffin et al., 1995). The minor effect contributed by *ntl* is subsequently mediated by another T-box gene, *tbx6* (Chapman and Papaioannou, 1998; Griffin et al., 1998).

In this chapter I will investigate PGP midline convergence phenotypes in $spt^{-/-}$ and $ntl^{-/-}$ embryos.

5.1 Mutant Allele Specific Genotyping For *Ntl* and *Spt* Heterozygotes

The two T-box genes, *ntl* and *spt,* are important FGF signalling mediators in regulating the development of the tissues in the trunk and tail region in zebrafish (Amacher et al., 2002). The PGP midline convergence was studied using WISH and IM to analyse $ntl^{-/-}$ and $spt^{-/-}$ embryos.

Polymerase chain reaction (PCR) was used to identify *ntl*^{tc41} and *spt*^{b104} mutant alleles as described in §4.1. Three primers were designed for detecting *ntl*^{tc41}, including two specific reverse primers, ntltc41R and ntltc41wtR, which can recognize *ntl*^{tc41} and wild type allele respectively, because of the difference in the 3'end-most base of their sequences. Both primer pairs, ntlF-ntltc41R and ntlF-ntltc41wtR, can generate 457 bp products in PCR reactions. The optimal PCR condition for these primers is 2 mM Mg^{2+}, annealing at 64°C for 1 min and repeating 30 cycles (Fig 511). In total 52 fish fin-clips were taken. Eighteen *ntl* heterozygotes were identified, including 4 fish with polymorphism alleles.

The *spt*^{b104} mutant allele is a 0.9 kb deletion mutation. *Spt*^{b104} and WT alleles can be distinguished by comparison of the size of PCR products. Three primers were designed for detecting the *spt*^{b104} allele; forward primers sptF and sptb104F and a reverse primer sptb104F. Primer pair sptF-sptb104R amplifies 1.9 and 1.0 kb fragments for WT and *spt*^{b104} alleles respectively. This pair of primers produced cleaner PCR results than sptb104F-sptb104R under the PCR condition: 2 mM Mg^{2+}, annealing at 62°C for 1 min and repeating 30 cycles (Fig 512). In total 63 fish fin clips were taken. Twelve *spt* heterozygotes were identified.

A quarter of the embryos collected from crossing *ntl* heterozygotes *or spt* heterozygotes have typical *ntl*$^{-/-}$ or *spt*$^{-/-}$ phenotypes (Fig 513). At 24 hpf, *ntl*$^{-/-}$ embryos displayed severe defects in tail development but normal head region phenotype. The segmentation of somites appeared to be normal but the development of subdivision of somites was disrupted in *ntl*$^{-/-}$ embryos (Stickney et al., 2000). Head region morphology appeared normal in the *spt*$^{-/-}$ embryos, however, there was an extreme deficiency of somites in the trunk and tail (Fig 513). The spade tail

phenotype in the *spt*$^{-/-}$ embryos was due to trunk somatic precursors that failed to migrate during gastrulation (Amacher et al., 2002).

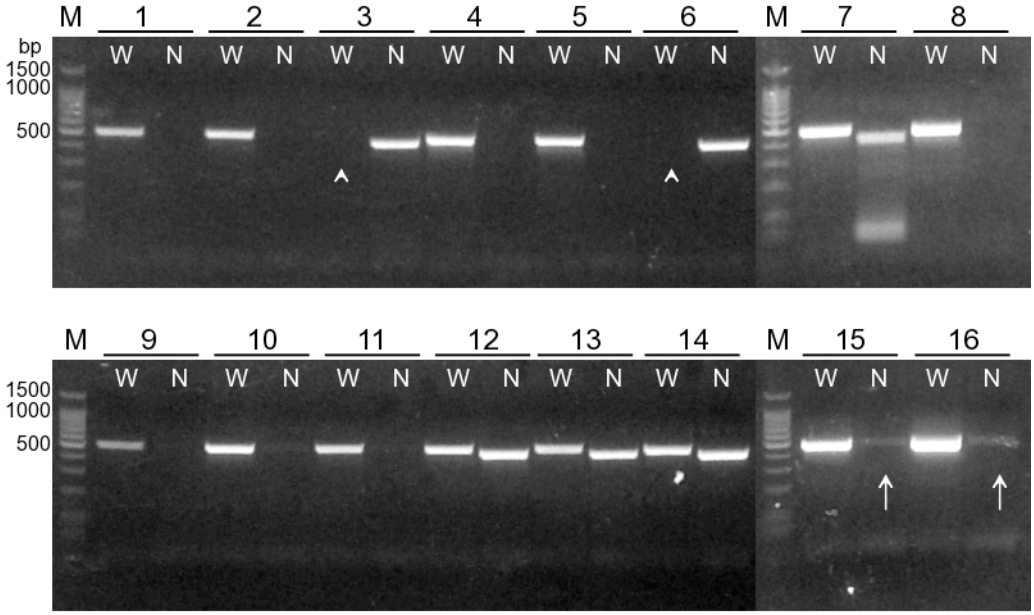

Figure 64-511. Optimization of PCR condition for *ntl*^{tc41} genotyping.

This PCR result image combines four electrophoresis agarose gels (1.2% agarose, 140 V, 30 min). Each gel had its own marker. The DNA markers (M) were Promega 100 bp Ladder (1500, 1000, 900, 800, 700, 600, **500**, 400, 300, 200, 100 bp). Sixteen 3- to 4-month old zebrafish had caudal (tail) fin clips taken (1-14) and these fin clips were processed for *ntl* allele (N) and wild type allele (W) PCR reactions (Mg^{2+} conc. = 2 mM, Annealing condition = **64**°C for 1 min, Cycles = 30). (15, 16) In these fish, the PCR condition was not recommended, because in this condition (Mg^{2+} conc. = 2 mM, Annealing condition = **62**°C for 1 min, Cycles = 30) the *ntl* allele reaction produced false positive results (arrow). (3, 6) These two fish had polymorphism allele in *ntl*^{tc41} loci (arrowhead).

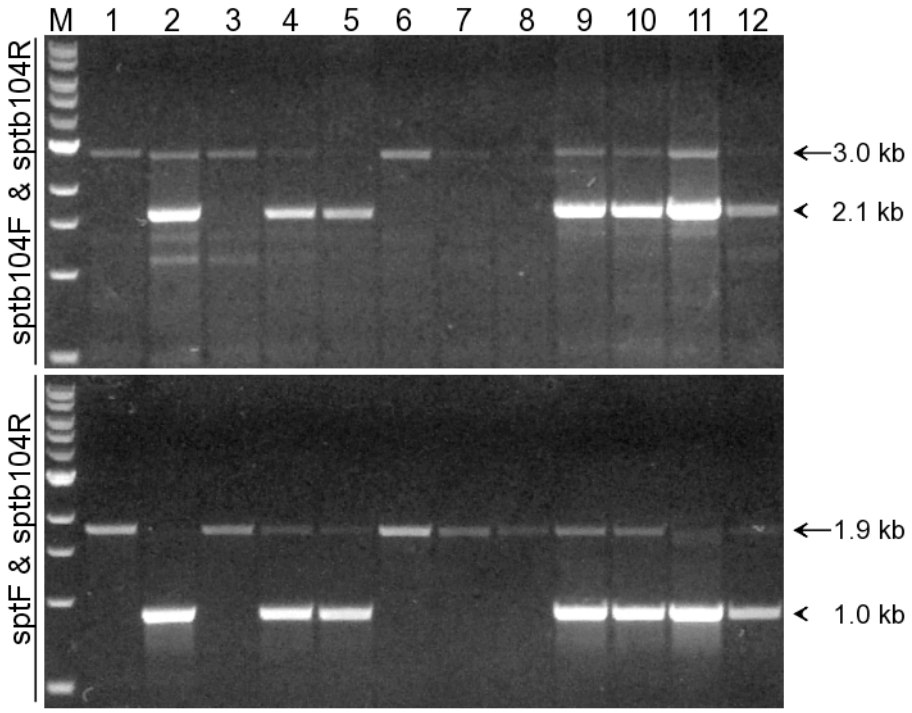

Figure 65-512. Optimization of PCR condition for *spt*^{b104} genotyping.

Two sets of primers, sptb104F-stb104R and sptF-sptb104R, were examined for suitable PCR condition for *spt*^{b104} allele genotyping. The first set of primers, sptb104F-stb104R, amplified 3.0 and 2.1 kb fragments for wild type and *spt*^{b104} allele respectively (top image). The second set of primers, sptF-sptb104R, amplified 1.9 and 1.0 kb fragments for wild type and *spt*^{b104} allele respectively (bottom image). Twelve 3- to 4-month old zebrafish had caudal (tail) fin clips taken (1-12) and these fin clips were processed for PCR reactions with the two sets of primers under the condition of (Mg^{2+} conc. = 2 mM, Annealing condition = 64°C for 1 min, Cycles = 30). The DNA marker in the upper gel was Promega 1kb Ladder (10, 8, 6, 5, 4, **3**, 2.5, 2, 1.5, and 1 kb). The DNA marker (M) for the lower gel was NEB 1kb Ladder (10, 8, 6, 5, 4, **3**, 2, 1.5, 1, and 0.5 kp). The primer set, sptF-sptb104R, in the lower gel produced favourable results.

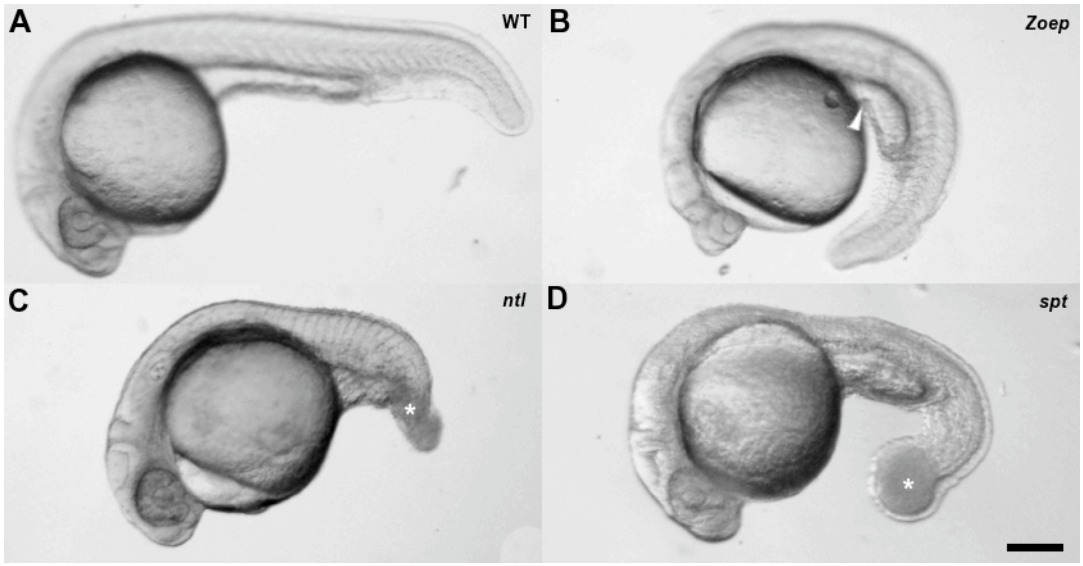

Figure 66-513. *Ntl*$^{-/-}$, and *spt*$^{-/-}$ phenotypes at 24 hpf.

Bright field phase contrast images were taken in lateral view of wild type (A), *Zoep*$^{-/-}$ (B), *ntl*$^{-/-}$ (C), and *spt*$^{-/-}$ (D) embryos at 24 hpf, dorsal view with the anterior to the left. A quarter of the embryos collected from crossing mutant heterozygotes appeared to have typical *Zoep*^{tz57}, *ntl*^{tc41}, and *spt*^{b104} homozygotes phenotypes respectively. (B) Besides having one eye, the extension of yolk (arrowhead) was defective in *Zoep*$^{-/-}$ embryos. (C) In *ntl*$^{-/-}$ embryos, the tail failed to develop (asterisk) and the segmentation of somites was not defined by notochord structure. (D) There was no segmentation of somites in *spt*$^{-/-}$ embryos. The spadetail (asterisk) distinguishes *spt* embryos from WT. The scale bar in D indicates 200 μm; all panels are at the same magnification.

5.2 Spt/Tbx16 Is Essential For PGP Midline Convergence

To examine the effects of FGF signalling on PGP midline convergence, the phenotypes of *ntl* and *spt* embryos were analysed using WISH. Both Ntl and Spt/Tbx16 are T-box transcription factors and are regarded as mediators of FGF signalling in the development of mesoderm-derived tissues in the trunk and tail (§1.7).

The *wt1* expression pattern in $ntl^{-/-}$ embryos is almost the same as the expression pattern in WT embryos at 13, 24, and 48 hpf (Fig 521). The PGP distance in some $ntl^{-/-}$ embryos was quantified and the results were compared with WT (Fig 522). At 15 (n = 5), and 24 (n = 4) hpf, there was no significant difference in PGP distance between $ntl^{-/-}$ and WT embryos. At 13 hpf (8-somite stage), the pronephric-glomerular precursor cells construct bilateral long stripes adjacent to the first-fifth somites (Fig 521A, D). By 24 hpf, the morphology of the anterior intermediate mesoderm has changed dramatically as these cells construct a more definable round shape tissue and locate completely inside the main embryo structure (Fig 521B, E). At 48 hpf, the two PGP fuse along the central axis to form the pronephric glomerulus (Fig 521C, F). There is, however, a small difference in PGP distance between *ntl* and WT embryos at 48 hpf (Fig 522). The 48-hpf -PGP distance in $ntl^{-/-}$ (n = 28) is closer to the distance at 36 hpf in WT. This indicates that prior to 36 hpf PGP midline convergence is not affected by mutation of *ntl* gene. Ntl might, however, associate with the end process of PGP convergence during 36 to 49 hpf.

WISH results from the analysis of *spt*/*tbx16* mutants provide a very different picture from $ntl^{-/-}$. At 15 hpf, *myoD* expression is severely deficient. These $spt^{-/-}$ embryos lack normal trunk somites. Clumps of *myoD* expressing cells are found in

the location of adaxial cells in WT embryos (Fig 523A, D). *Wt1*-expressing cells are adjacent to these *myoD*-expressing cells hence the PGP distance is much shorter in *spt*$^{-/-}$ than in WT embryos. Notably, there are fewer *wt1*-expressing cells in *spt*$^{-/-}$ than in WT embryos. The specification of intermediate mesoderm is partially affected by mutation of *spt*$^{-/-}$. At 24 hpf, the pattern of distribution of the *wt1*-expressing cells is successfully transformed from a blurred wing-shaped pattern to compact patches (PGP) successfully in *spt*$^{-/-}$ embryos (Fig 523B, E). The area of the PGP in *spt*$^{-/-}$ is smaller than in WT. The shape of the PGP in *spt*$^{-/-}$ embryos is irregular as opposed to the round-shape in WT. The PGP seem trapped at the bilateral edge of the main embryo stripe, which does not undergo further midline convergence as in WT embryos.

A collection of quantified PGP distances from embryos at 15 (n = 5), 24 (n = 5), and 48 (n = 19) hpf are presented in Fig 524 along with the data from WT embryos. As shown in Fig 523, the PGP distance at 15 hpf in *spt*$^{-/-}$ embryos is shorter than in WT, due to missing somite formation. The PGP distance at 24, and 48 hpf in *spt*$^{-/-}$ embryos is slightly longer than in WT embryos and similar to that at 15 hpf in *spt*$^{-/-}$. This observation suggests mechanisms of PGP midline migration are completely blocked in *spt*$^{-/-}$.

Unlike in *Zoep*$^{-/-}$, PGP midline convergence phenotypes in *ntl*$^{-/-}$ and *spt*$^{-/-}$ embryos are more unified (Fig 525). Comparing the PGP distance between WT, *Zoep*$^{-/-}$, *ntl*$^{-/-}$, and *spt*$^{-/-}$ at 48 hpf, data measured from 34 *Zoep*$^{-/-}$ embryos is widely distributed between 31 and 207 pix; data measured from *ntl*$^{-/-}$ embryos is distributed between 1 and 53 pix (n = 26/28); data measured from 19 *spt*$^{-/-}$ embryos is distributed between 67 and 95 pix.

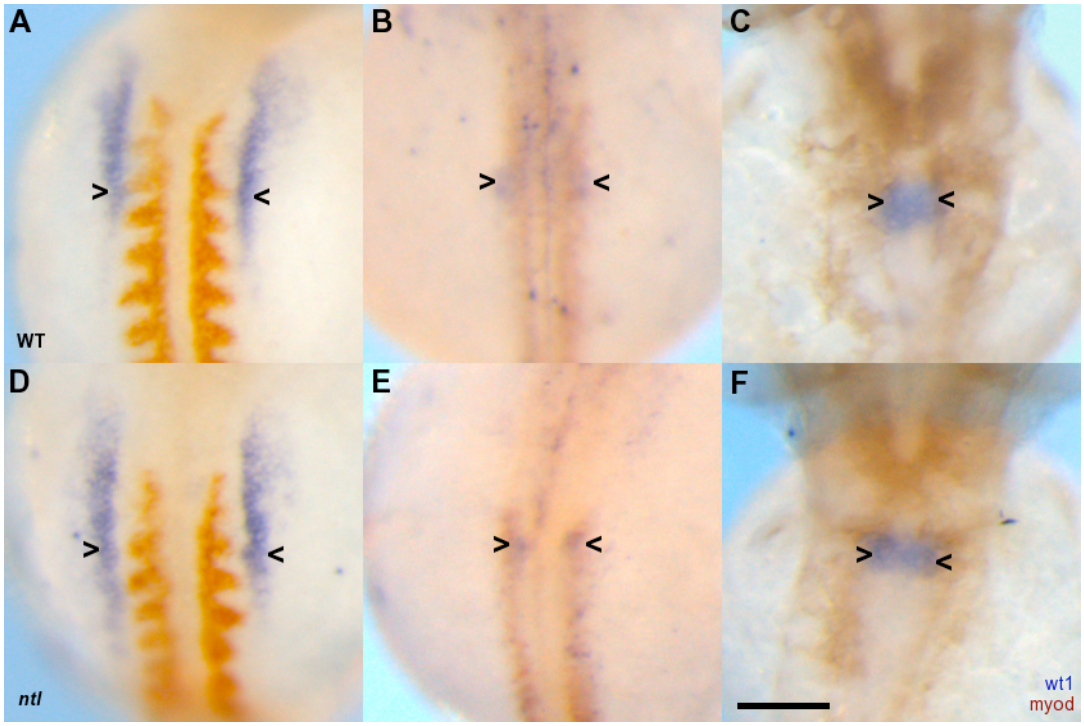

Figure 67-521. Morphogenesis of the pronephric glomerulus in *ntl*$^{-/-}$ from 13 to 48 hpf.
Wt1 and *myoD* double WISH at 13 (A, D), 24 (B, C), and 48 (C, F) hpf zebrafish embryos, were stained blue and brown respectively. *Wt1* gene expression pattern in *ntl*$^{-/-}$ embryos (D-F) is compared with wild type (WT) embryos (A-C) at their analogous stages. The expression pattern of *wt1* in *ntl*$^{-/-}$ embryos is almost indistinguishable from WT (open arrowheads). All images are dorsal view with anterior to the top. The scale bar in F indicates 100 μm; all panels are at the same magnification.

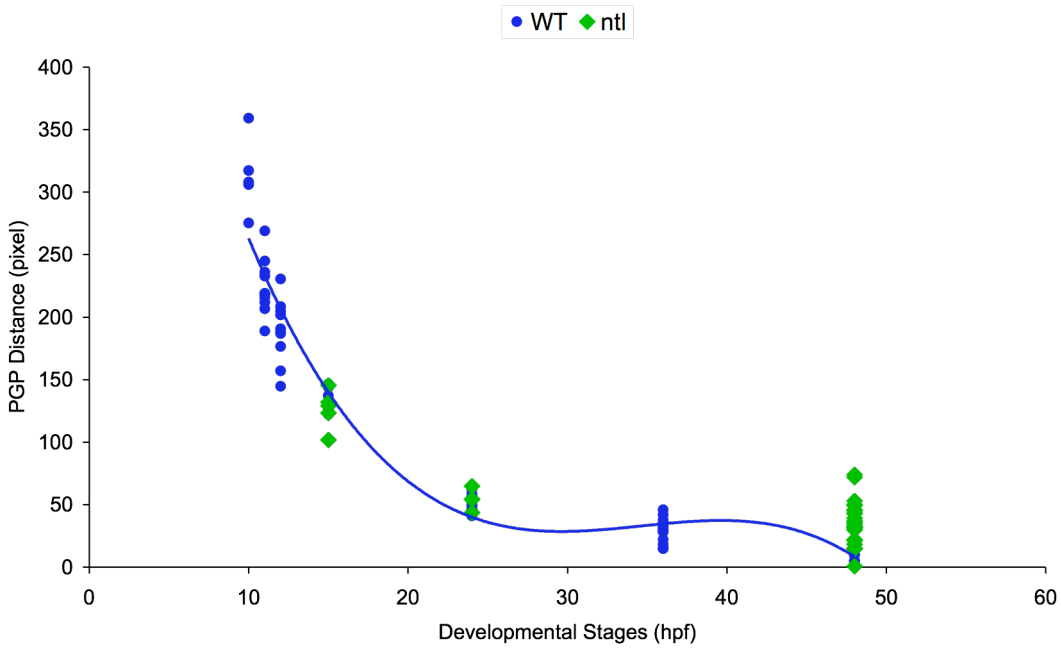

Figure 68-522. Quantification of PGP midline convergence during 15 to 48 hpf in *ntl*$^{-/-}$ embryos. The distance between PGP (y-axis) was measured using the straight-line distance from a 2-dimentional digital image of a *wt1*-WISH embryo at a desired developmental stage (x-axis). This scatter plot demonstrates a collection of results form *ntl* embryos at 15 (n=5), 24 (n=4), and 48 (n=28) hpf (each green diamonds represent a measurement from an embryo). Detailed information on PGP distance for wild type embryos (WT, blue circles) is described in §4.1 and Fig 418. The magnification of the images is 91 pixels for every 100 μm. The Unpaired Student's t-Test was applied to compare the PGP distance between wild-type and *ntl*$^{-/-}$ embryos at 15, 24 and 48 hpf. The test results suggest PGP abnormality is stage dependent. There is no difference between wild-type and *ntl*$^{-/-}$ embryos in PGP phenotype at 15 and 24 hpf but there is a significant difference at 48 hpf. The P values from the test are 0.368, 0.191, and < 0.001 for 15, 24 and 48 hpf respectively.

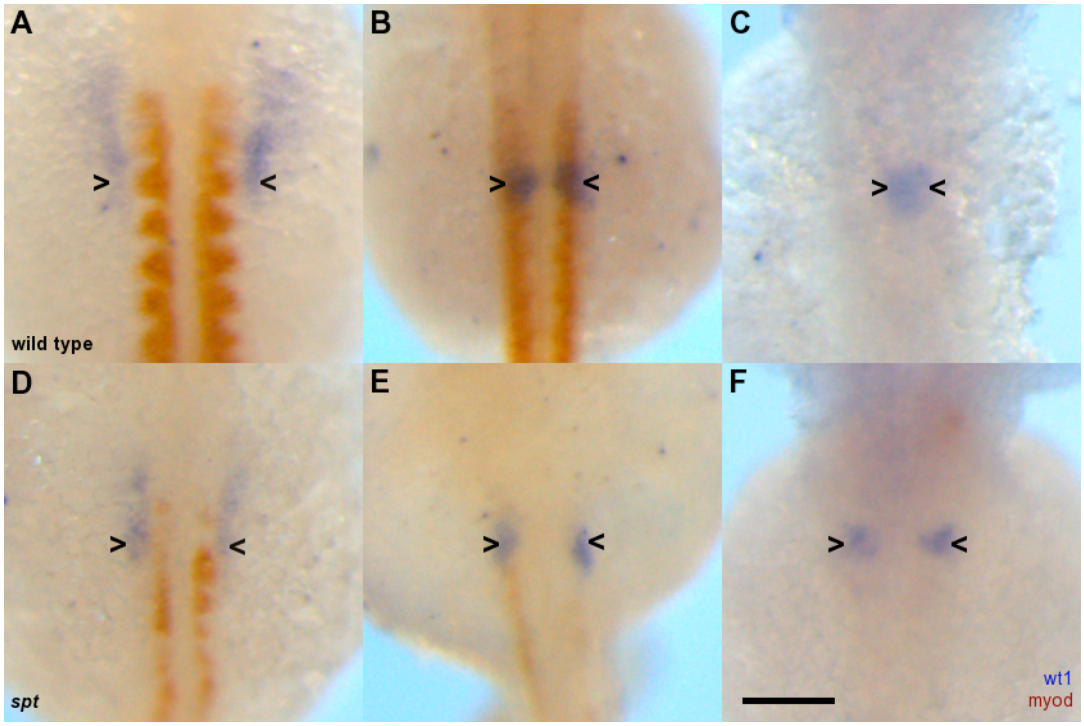

Figure 69-523 Morphogenesis of the pronephric glomerulus in *spt*$^{-/-}$ from 13 to 48 hpf.
Wt1 and *myoD* double WISH at 15 (A, D), 24 (B, C), and 48 (C, F) hpf zebrafish embryos, were stained blue and brown respectively. *Wt1* gene expression pattern in *spt*$^{-/-}$ embryos (D-F) is compared with WT embryos (A-C) at their analogous stages. (A, D) *MyoD* expression is dramatically reduced in *spt*$^{-/-}$ embryos (brown). *Wt1* expressing cells directly adjust to adaxial cells in *spt*$^{-/-}$ embryos, unlike WT in which *wt1* expressing cells are next to somites. Without somite between, the PGP distance is much shorter in *spt*$^{-/-}$ at 15 hpf. In addition, *wt1* expressing cells occupy a much smaller area in *spt*$^{-/-}$ than in WT (open arrowheads). (B, E) By 24 hpf, the *wt1* expressing cells coalesce to form compact PGP. This mechanism is not affected by the mutation of *spt*^{b104} alleles. The shape of PGP, however, is relatively irregular and smaller than in WT (open arrowhead). (C, F) PGP midline convergence is defective in *spt*$^{-/-}$ embryos, and the PGP fails to fuse along the central axis (open arrowheads) at 48 hpf. All images are dorsal view with anterior to the top. The scale bar in F indicates 100 μm; all panels are at the same magnification.

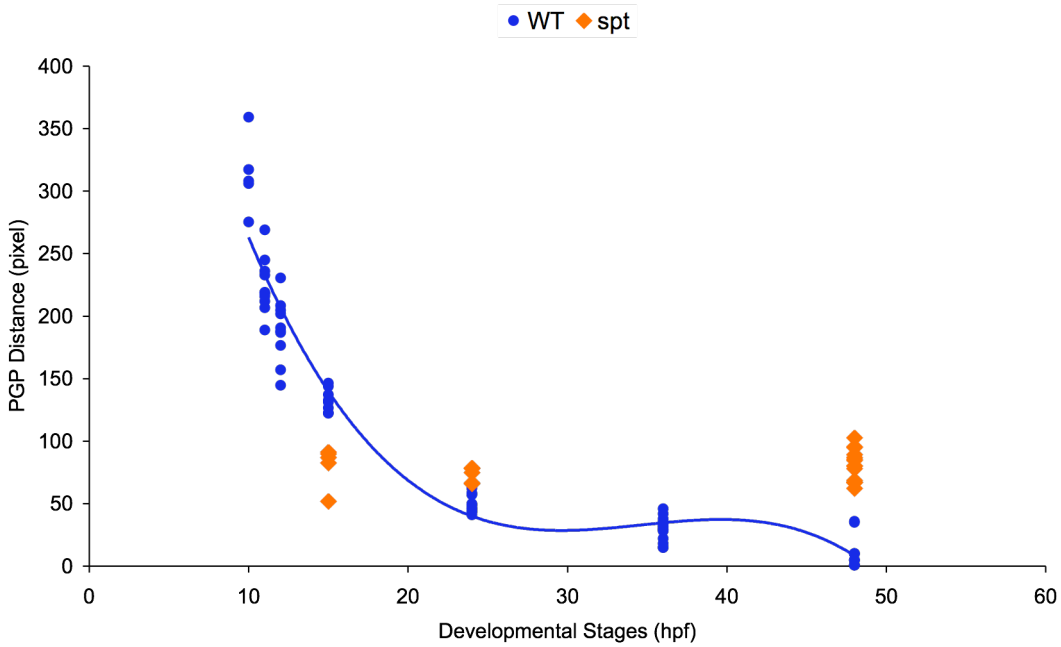

Figure 70-524. Quantification of PGP midline convergence during 15 to 48 hpf in *spt*$^{-/-}$ embryos. The distance between PGP (y-axis) was measured using the straight-line distance from a 2-dimentional digital image of a *wt1*-WISH embryo at a desired developmental stage (x-axis). This scatter plot illustrates a collection of results form *spt*$^{-/-}$ embryos at 15 (n = 5), 24 (n = 5), and 48 (n = 19) hpf (each orange diamond represents a measurement from an embryo). Detailed information on PGP distance for wild type embryos (WT, blue circles) is described in §4.1 and Fig 418. The magnification of the images is 91 pixels for every 100 μm. The Unpaired Student's t-Test was applied to compare the PGP distance between wild-type and *spt*$^{-/-}$ embryos at 15, 24 and 48 hpf. The statistical test results suggest the PGP phonotype is abnormal in *spt*$^{-/-}$ embryos. All the P value for 15, 24 and 48 hpf are < 0.001.

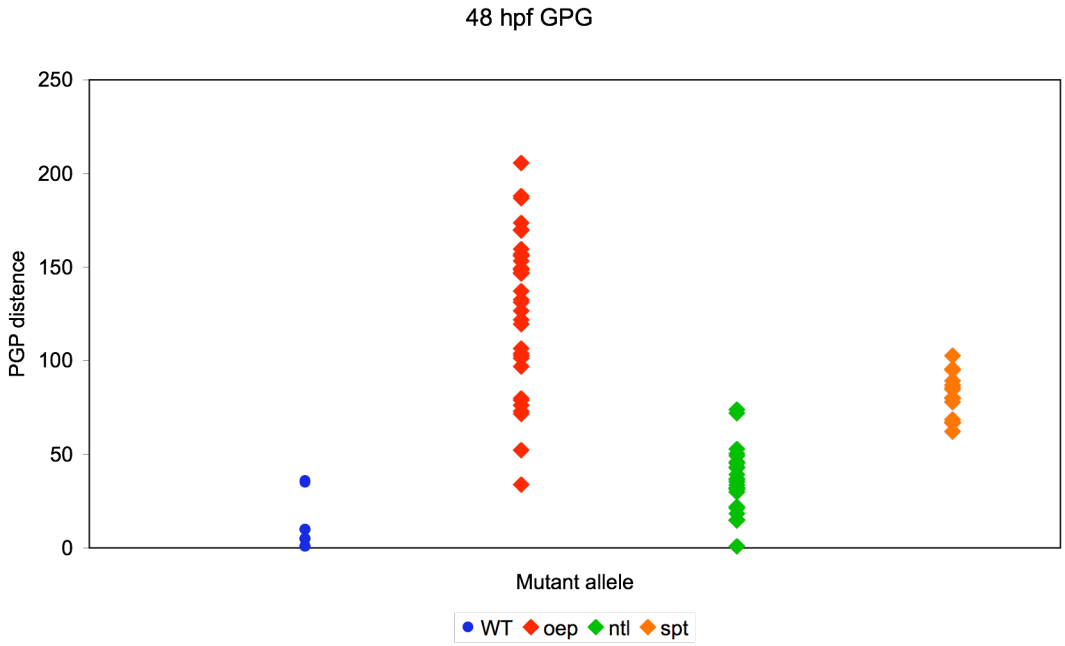

Figure 71-525. Comparison of PGP midline convergence at 48 hpf between mutant embryos.
The distance between PGP (y-axis) was measured using the straight-line distance from a 2-dimentional digital image of a *wt1*-WISH embryo at a desired developmental stage (x-axis). Data measured from WT (n = 14), *Zoep*$^{-/-}$ (n = 34), *ntl*$^{-/-}$ (n = 28), and *spt*$^{-/-}$ (n = 19) embryos are displayed in blue circle, red diamond, green diamond, and orange diamond respectively. The magnification of the images is 91 pixels for every 100 μm.

5.3 Is Notochord Or Floor Plate Required For PGP Midline Convergence?

A previous study indicated that midline signals, i.e. Shh, are required for proper glomerular morphogenesis (Majumdar and Drummond, 2000). The reason that Shh is recognized as a midline signal is because *shh* expresses along the midline axis tissues, in notochord and floor plate (Halpern et al., 1997; Krauss et al., 1993). To verify that the midline signal, in floor plate or notochord, is actually required for PGP midline migration, *ntl*$^{-/-}$ embyos were processed for WISH of *spon1b* and INV4597 immunostaining. The results shown in Fig 521 demonstrate PGP midline convergence is relatively normal by 36 hpf in *ntl*$^{-/-}$ embryos. However, differentiated notochord is absent in *ntl*$^{-/-}$ embryos (Fig 531) (Halpern et al., 1997; Odenthal et al., 1996a). In brief, differentiated notochord is not required for PGP midline migration.

Furthermore, blocked expression of *spon1b* and *shh* in the floor plate indicates the abnormity of floor plate formation in *Zoep*$^{-/-}$ embryos (Fig 453, Fig 454). This floor plate phenotype is not, however, synchronized with the varied phenotype of PGP midline convergence, thus suggesting that PGP midline convergence is not associated with the formation of floor plate.

Finally, *spon1b* expression is normal in the floor plate in *ntl*$^{-/-}$ embryos (Fig 532), hence floor plate development is normal in *ntl*$^{-/-}$ embryos. It thus appears PGP midline convergence requires Shh midline signal from either floor plate or notochord.

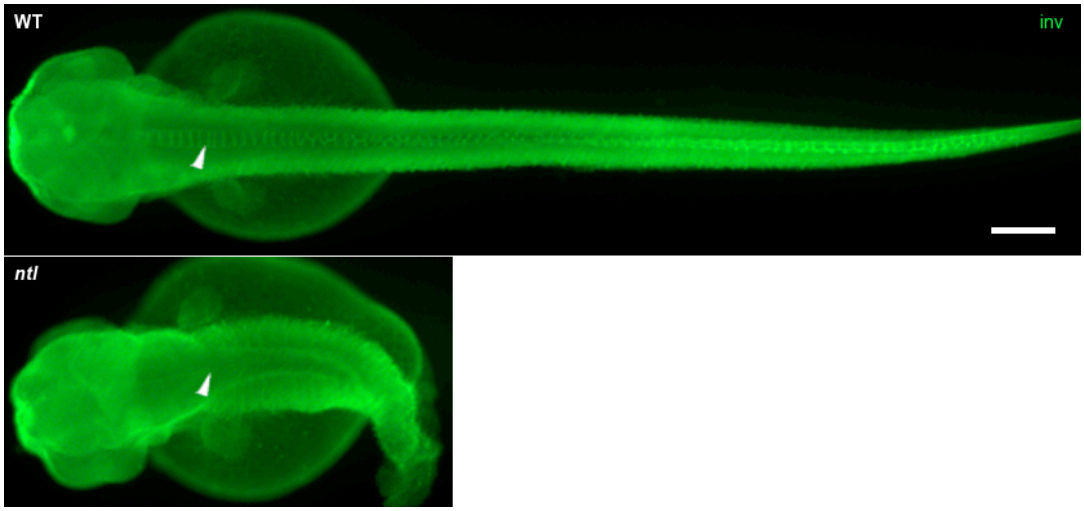

Figure 72-531 Notochord differentiation is not essential for PGP midline convergence.
To demonstrate notochord differentiation is not essential for midline convergence, *ntl*$^{-/-}$ and wild type (WT) embryos at 48 hpf were processed for INV4597 immunostaining (*inv*). The images are dorsal view with the anterior to the left. The Inv antibody labels against notochord along the central axis (arrowhead) in WT embryos. In *ntl*$^{-/-}$ embryos, there was no notochord structure (arrowhead) observed after INV4597 immunostaining. The scale bar indicates 100 μm; all panels are at the same magnification.

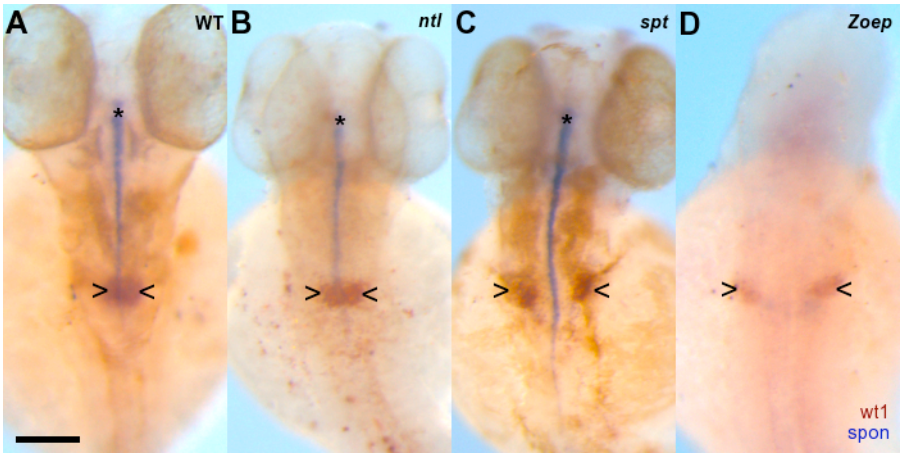

Figure 73-532. Floor plate formation in *ntl*$^{-/-}$, and *spt*$^{-/-}$ embryos.

Wt1 and *spon1b* double WISH in 48 hpf embryos, *wt1* and *spon1b* RNA probes were stained brown and blue respectively. (A) Floor plate marker gene, *spon1b*, expresses intensively in the floor plate (asterisk) in wild type (WT) embryos. (B) *Spon1b* is slightly down regulated (asterisk) in *ntl*$^{-/-}$ embryos in which PGP midline convergence (open arrowheads) is almost the same as in WT embryos. (C) Floor plate formation (asterisk) is not effected by mutated *spt*$^{-/-}$ alleles, but PGP midline migration is blocked in *spt*. (D) In *Zoep*$^{-/-}$ embryos, *spon1b* expression is completely abolished in floor plate. (A-D) All images are dorsal view with anterior to the top. The scale bar in A indicates 100 μm; all panels are at the same magnification.

5.4 Extracellular Matrix Might Play A Key Rule In PGP Midline Convergence

Spt/Tbx16 is required for PGP midline convergence, which is described in §5.2. In this section, whether Spt/Tbx16 is an essential factor for midline convergence for both PGP and cardiac primordium, or for PGP specifically, is considered. To investigate cardiac phenotypes, *spt*$^{-/-}$ and WT embryos were processed for double WISH of *cmlc2* and *wt1*. The results are shown in Fig 541. Cardiac primordium midline convergence is not affected by the mutation of *spt* gene. It is evident that *spt/tbx16* is one of the essential genetic factors specifically for PGP midline convergence but not for cardiac midline convergence.

In a previous study, analysis of *spt* expression by WISH revealed that *spt* was expressed in the segmental plate during 1- and 4-somite stages (Yamamoto et al., 1998). No expression was detected in the PGP (Thisse et al., 2001). It suggested that mutation of the transcription factor indirectly affects PGP midline convergence. To investigate further the possible mediators for the *spt* genetic effects on PGP midline convergence, other phenotypes in *spt*$^{-/-}$ embryos were studied. Results of fibronectin immunostaining and phalloidin staining demonstrate extracellular matrix organization is seriously damaged in *spt*$^{-/-}$ embryos (Fig 542). In wild type embryos, phalloidin stained F-actin exhibits two long spiky stripes located adjacent to the dorsal and ventral sides of the notochord. In *spt* embryos, small clumps of F-actin locate randomly around the notochord. Anti-Fibronectin antibody was stained with green fluorescence conjugated secondary antibody. Fibronectin expression appears reduced in *spt*$^{-/-}$ embryos. Further study is required to verify whether, or not, the

effects of mutation of *spt* on PGP midline convergence is mediated by somite formation and/or extracellular matrix or by other different mediators.

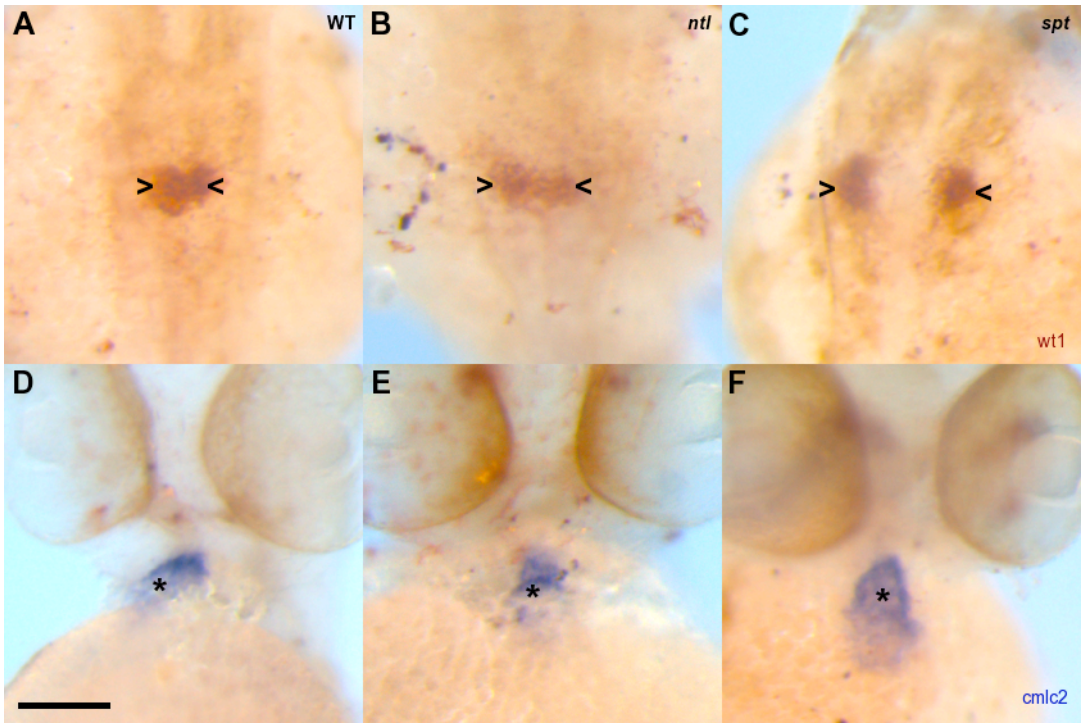

Figure 74-541. Heart primordium midline convergence in *ntl*$^{-/-}$ and *spt*$^{-/-}$ embryos.
Wt1 and *cmlc2* double WISH in 48 hpf embryos, *wt1* and *cmlc2* RNA probes were stained brown and blue respectively. (A, D) PGP (open arrowheads) and heart (asterisk) phenotypes in wild type (WT) embryos. (B, E) In *ntl*$^{-/-}$ embryos, PGP midline convergence is not 100 % complete (open arrowheads) but heart primordium midline migration progresses normally to form a heart tube (asterisk). (C, F) *Spt*$^{-/-}$ embryos normal heart tube (asterisk) developed but defective PGP midline convergence (open arrowheads). (A-C) Dorsal view with anterior to the top. (D-F) Ventral view with anterior to the top. The scale bar in D indicates 100 μm; all panels are at the same magnification.

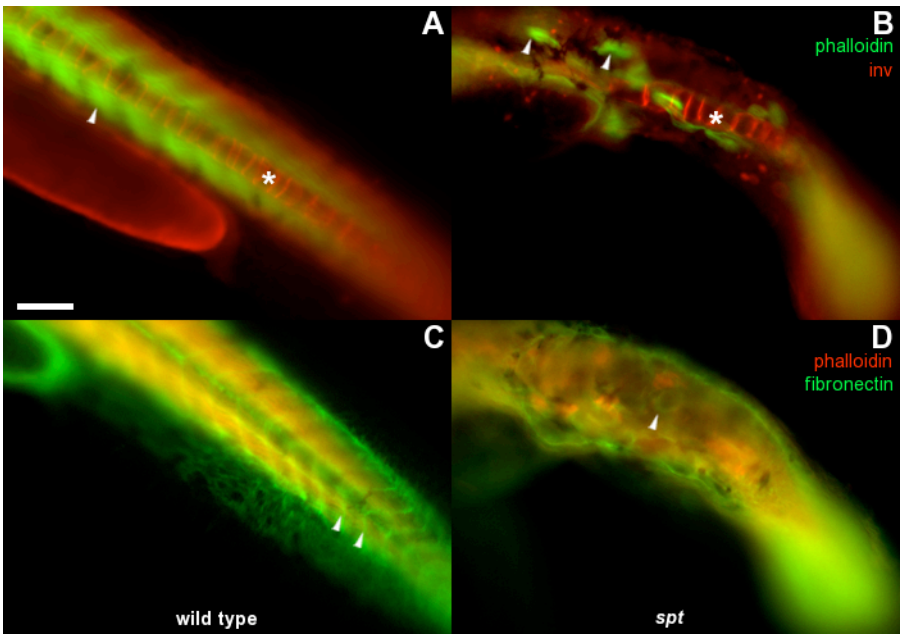

Figure 75-542 Extra cellular matrix deposit might be a key factor in the PGP midline convergence mechanism.

To investigate whether other phenotypes in *spt*$^{-/-}$ associated with PGP midline convergence, *spt*$^{-/-}$ (B, D) and wild type (A, C) embryos at 36 hpf were processed by phalloidin staining of F-actin (A-D) and immunostaining of fibronectin (C, D). The images are left-lateral view of lower trunk and tail with the anterior to the upper left. (A) In wild type embryos, phalloidin stained F-actin (green, arrowhead) exhibits two long spiky stripes located adjacent to dorsal and ventral sides of notochord (asterisk). (B) In *spt*$^{-/-}$ embryos, small clumps of F-actin (arrowheads) locate randomly around notochord. (C, D) Anti-Fibronectin antibody stained with green fluorescence-conjugated secondary antibody. Fibronectin expression appears reduced (green, arrowheads) in *spt*$^{-/-}$ embryos. The regular structure of somites surrounded by Fibronectin is not observed in *spt*$^{-/-}$ embryos (arrowhead). The scale bar in A indicates 100 μm; all panels are at the same magnification.

5.5 Conclusion

The T-box gene, *ntl* is not required for PGP midline convergence by 36 hpf (Fig 531, Fig 532). Whether *ntl* is involved in the convergence between 36 and 48 hpf, requires further investigation. Another t-box gene, *spt* is essential for PGP midline convergence after early stages (Fig 533, Fig 534). Extracellular matrix structure could play a key role in mediating the effect of *spt* mutation.

In conclusion, PGP midline convergence proceeds from 10 hpf (specification of intermediate mesoderm) to 48 hpf (fused pronephric glomerulus) in zebrafish embryos. Prior to 18 hpf, PGP midline convergence is closely correlated with the midline convergence of mesoderm, but not at later stages in *Zoep*$^{-/-}$. *Spt* is essential for PGP but not for cardiac primordium midline convergence. Data from this research suggests there is no single universal mechanism, which controls all the midline migration of organ primordia. Tissue-specific and developmental stage-specific factors are also required for this process.

6. Discussion

6.1 Genetic Engineering: From DNA Fragment To Embryonic Phenotype

Cre-mediated Recombination in Injected Zebrafish Embryos

Plasmid pITRE (Fig 311) was used to provide vector and ITR cassette for pITRbAcRG. This had a 500 bp nonessential sequence between ITR-5' and the MCS, which was derived from pCS2-ITR (Table 231). The original plasmid also contained a reverse SV40 pA signal at the 5'-end of ITR-3'. None of these features are thought to affect reporter gene expression hence pITRbAcRG inherits these features from its structure.

In a previous study, the Cre-loxP recombination system was examined in a stable transgenic zebrafish line (Pan et al., 2005). The excision of the floxed GFP could be controlled by microinjection of Cre RNA into the embryos of floxed reporter gene transgenic zebrafish. The downstream RFP reporter failed to express after excision of floxed GFP due to the frame shift of the RFP codon. Another study shows that CMV promoter drives the ubiquitous expression of the floxed d2RED2 reporter gene (Fig 611) without Cre and then changes to second reporter gene expression when the plasmid is co-injected with Cre-RNA into zebrafish embryos (Langenau et al., 2005).

As described in Chapter 3, when pITRbAcRG was engineered, half the first intron of β-*actin* and RFP cDNA was floxed to avoid frame shift. The results of the pITRbAcRG-injected embyos, however, raise another issue. The duplicated intron in the structure of pITRbAcRG (Fig 321) induces indiscriminate alternative splicing (Fig 331 to Fig 333). Consequently the second reporter gene, GFP, is expressed

without the presence of Cre recombinase (Fig 322). Duplication of introns thus has to be eliminated from pITRbAcRG to improve the construct for future research.

Due to time constraints, the method used to analyze the RNA structure in Chapter 3 was RT-PCR. Other molecular techniques such as northern blot, in situ hybridization, and ribonuclease protection assay (RPA) are also common approaches that allow the study of mRNA expression. Each method has different advantages and disadvantages depending on the purpose of the experiments. The purposes of the experiments in §3.3 and §3.4 were firstly to explain the reasons for the failure of the reporter construct by examining the reporter gene mRNA structure and also to explain the reasons for the insufficient transcription termination by examining the reporter gene pre-mRNA in the microinjected embryos. Both RT-PCR and RPA were suitable techniques for these experimental purposes. The RT-PCR technique was used and several primer sets were prepared. After generation of the first-strand cDNA, the PCR results were produced within few hours. Performing RPA is more complex than RT-PCR. First of all arrangement of radioactive experiments and plasmids of probe templates are required. From synthesis of probe, hybridization, post hybridization processing, to detection, an assay takes more than a week to complete (Huang et al., 1999). The RPA sensitivity is 10^5 copies in a complex total RNA sample, which is not as sensitive as RT-PCR, which can detect 50-100 copies (Rottman, 2002). Thus means RPA requires much more total RNA extracts than RT-PCR. The main advantage that RPA has over RT-PCR is reliability. There are no amplification steps involved in RPA and therefore few false positive signals can be generated in the assay. Given more time RPA could be a good alternative approach to verify the hypothesis.

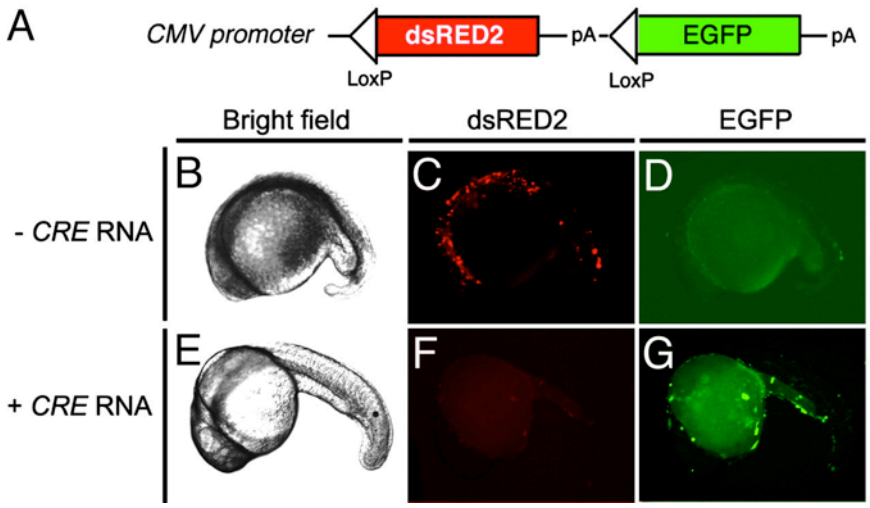

Figure 76-611. Cre-mediated recombination in transiently injected embryos.
(A) Diagram of the CMV-loxP-dsRED2-loxP-EGFP construct. (B-G) One-cell-stage embryos were injected with the CMV-loxP-dsRED2-loxP-EGFP vector in the absence of Cre RNA (- Cre RNA) (B-D) or with Cre RNA (+ Cre RNA, 25 ng/μl) (E-G). Shown are bright-field (B and E), red fluorescence (dsRED2) (C and F), and green fluorescence (EGFP) images (D and G) of embryos at 26 h postfertilization. Anterior is to the left with dorsal to the top. This figure was adapted from (Langenau et al., 2005).

Polyadenine signals, in fact, may not be critical to the regulation of expression of the second reporter gene, because it is rare to have bi- or polycistronic gene expression in eukaryotes (Gray and Wickens, 1998). Arguably, a bi-cistronic mRNA, containing two ORFs, has been reported in *Drosophila* (Brogna and Ashburner, 1997). It is not clear whether translation of the downstream ORF involves re-initiation or internal initiation (Brogna and Ashburner, 1997). Internal initiation, referred to as cap-independent initiation, is mediated by a sequence structure within the 5'UTR known as an internal ribosome entry site (IRES) and was first discovered in picornaviruses (Jackson and Kaminski, 1995).

The mRNA Assembly Line

Transcription of protein-encoding genes by RNA polymerase II (Pol II) is the primary step in gene expression (Hahn, 2004). Prior to a gene transcript being ready to be exported to the cytoplasm, it has to undergo three major processes to produce translatable mRNA. These processes are usually capping, splicing out of introns and generation of a 3' polyadenine tail. There is an emerging consensus that pre-mRNA processing occurs co-transcriptionally (Proudfoot et al., 2002). Factors that promote capping, RNA splicing and RNA export can be recruited to elongating Pol II (Bentley, 2002). At the end of a gene, the pre-mRNA is cleaved at the polyA site and a polyadenine tail is added to the exposed 3' end. Termination, namely the release of Pol II from DNA template, occurs from 100 bp to several kb downstream of the polyA site (Ashfield et al., 1991; Dye and Proudfoot, 2001; Hagenbuchle et al., 1984; Tantravahi et al., 1993).

In the case of microinjection of pITRbAcRsvG into zebrafish embryos, the GFP transgene at 1 kb downstream of the SV40 pA site still undergoes splicing (Fig 343), even though cleavage at the SV40 pA site was demonstrated (Fig 344). An Exon Tethering Model (Fig 612) suggests that for some genes a continuous intron transcript is not required for RNA splicing (Dye et al., 2006). Transcribed exons are tethered to the elongating Pol II. In this way splicing is unaffected by cleavage of the growing pre-mRNA, in other words release of mature mRNA (polyadenylated mRNA) from transcription machinery is not immediate after cleavage and polyadenylation. The preparation for the release of mature mRNA is carried out on elongating transcription machinery and could depend on the mechanism of release of Pol II from the DNA template. Arguably the multiple transcript cleavage model for

Pol II transcription termination (Fig 613) might not be the case for the SV40 pA signal dependent termination.

SV40 pA Signal

A functional polyA signal is characterized by cis-acting RNA sequence including the conserved AAUAAA hexamer, located 10-30 nt upstream of the cleavage site (polyA site), and a highly variable downstream GU- or U-rich element (Hu et al., 2005; Weiss et al., 1991). The SV40 pA signal was shown to be efficient for RNA cleavage both *in vivo* (McDevitt et al., 1986) and *in vitro* (Gilmartin et al., 1988). The spacing between the AAUAAA and downstream GU- or U-rich element is critical for efficient cleavage, since insertion of a spacer sequence abolished the cleavage (Gil and Proudfoot, 1987; Heath et al., 1990). Insertion of 36 nucleotides of spacer sequence between the AAUAAA site and the downstream element markedly reduced cleavage activity *in vitro* (Weiss et al., 1991). Interestingly, when an 850 bp fragment of the SV40 early region was used as the ployA signal in a retrovirus expression system, expression of the *env* gene was abolished. The *env* expression was rescued by shortening the SV40 early region to 140 bp (Yamagata et al., 2005).

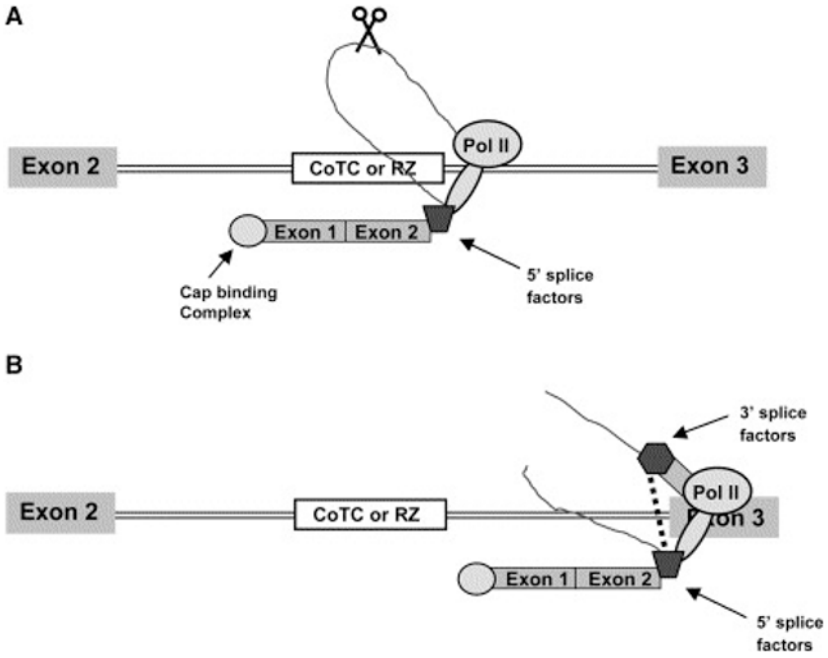

Figure 77-612. Exon tethering model.

(A) Tethering of pre-mRNA to RNA Pol II. In the diagram (not to scale), the black line indicates the intron 2 DNA template. The curved line represents the nascent transcript. Grey boxes, with black outline, represent tethered exons. The rhombus represents splice factors associated with the intron 2 splice donor site. The scissors represent CoTC or RZ cleavage of the nascent intron transcript. Association of CBC with splice factors and the transcription complex (Görnemann et al., 2005) is not shown for illustrative reasons.(B) Cotranscriptional splicing. The black hexagon represents splice factors associated with the intron 2 splice acceptor site. The thick dashed line represents interaction between 5′ and 3′ splice factors. This figure was adapted from (Dye et al., 2006).

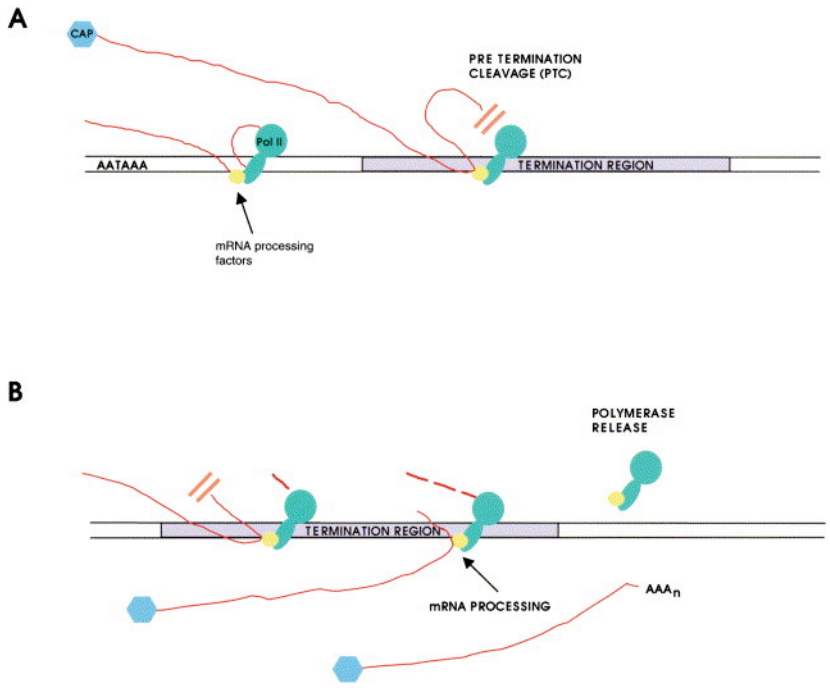

Figure 78-613. A Two step model for Pol II transcription termination.
(A) Step 1: pretermination cleavage. In the diagram, the parallel black lines indicate the DNA template and AATAAA denotes the polyA signal. The red lines indicate the nascent RNA transcript and the blue hexagon attached to the transcript represents the mRNA cap structure. The thick parallel orange bars represent pretermination cleavage of the nascent transcript.(B) Step 2: polymerase release. In this diagram, the thick broken line represents reiteratively cleaved transcripts. AAAn denotes the polyA tail. This figure was adapted from (Dye and Proudfoot, 2001).

PolyA-dependent Transcription Termination

The mechanism of Pol II termination is poorly understood. This is because the site of Pol II release from the DNA template is often distinct from the polyA site and at various positions downstream of the polyA site (Ashfield et al., 1991; Dye and Proudfoot, 2001; Hagenbuchle et al., 1984; Tantravahi et al., 1993). Cleavage at the polyA site has long been thought to be essential for transcription termination

(Proudfoot et al., 2002; Yonaha and Proudfoot, 2000). Transcription termination, that does not require cleavage at the polyA site, has been shown in Xenopus oocytes (Osheim et al., 1999), in HeLa cell extracts (Tran et al., 2001) or in yeast (Sadowski et al., 2003). A study, in which the polyA signal was inactivated at increasing times post-extrusion, demonstrates that interconnection between the polyA site and the Pol II complex is not temporarily restricted to the time of polyA site extrusion, but is prolonged and, perhaps, random (Kim and Martinson, 2003).

Not only polyA signals but also downstream terminator sequences are crucial to Pol II transcription termination (Gromak et al., 2006). An element, C2-MAZ site, which binds the transcription factor MAZ in vitro, is thought to pause Pol II and promote termination of the human C2 complement gene (Ashfield et al., 1994). Another sequence, co-transcriptional cleavage site (CoTC) position 800 bp downstream of the polyA site, was identified as being essential for transcriptional termination of the human beta-globin gene (Dye and Proudfoot, 1999). In summary, termination depends on the polyA site in the nascent transcript. Downstream elements and numerous proteins involved in cleavage and polyadenylation also appear to participate in termination (Zhang et al., 2005).

Multiple Copies of a Gene in Genomes and Indiscriminate Alternative Splicing

Copy number variation of DNA segments, ranging in size from kilobases to megabases, has been discovered (Iafrate et al., 2004; Redon et al., 2006; Sebat et al., 2004; Sharp et al., 2005; Tuzun et al., 2005). This is one type of genetic variation in the human genome termed copy number variations (CNVs). In fact, CNVs are also

found in other mammals (Graubert et al., 2007). The biological consequences of CNVs are largely undefined. In some cases CNVs cause gene dosage effects, which are implicated in phenotypic variation (Buckland, 2003; Nguyen et al., 2006), whilst in other cases CNVs are associated with cancer and disease (Aitman et al., 2006; Cappuzzo et al., 2005; Lonn et al., 1992). The study in this chapter provided evidence that a duplicate intron causes indiscriminate alternative splicing. The results suggest indiscriminate alternative splicing may be a consequence of multiple copies of a gene tandem arrayed in a genome (Fig 614).

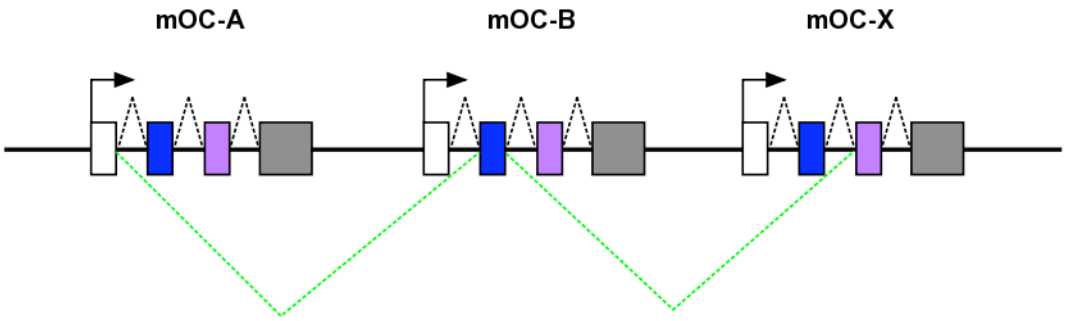

Figure 79-614. An indiscriminate alternative splicing model for CNVs.

Bone-specific osteocalcin gene (OC) is used as an example of multiple copies of a gene in a genome. OC has 4 exons and 3 introns (Celeste et al., 1986; Lian et al., 1989). Three copies of tandem arrayed OC have been shown in mouse genome (Rahman et al., 1993). The solid line represents a 19 kb region of mouse genome. The black dashed lines above the structure indicate RNA splicing. The green dash-lines indicate examples of indiscriminate alternative splicing predicted by the model. The white, blue, purple and grey boxes represent exons 1 to 4 respectively. The first to third copies of OC are represented by mOC-A, mOC-B and mOC-X respectively. The diagram is not to scale.

6.2 Mechanisms Behind The Morphogenesis Of Pronephric Glomerulus

The Specification of Wt1 Expressing Cells

*Wt*1 expressing cells were first observed at 10 hpf (Fig 411) in WT embryos, which indicates the specification of anterior intermediate mesoderm. During the first hour (10 to11 hpf), more and more *wt*1 expressing cells were observed. Two potential mechanisms for the specification are proposed. Firstly, transcription of *wt*1is activated in a small number of proliferating mesoderm cells. When the *wt*1 expressing cells reach a certain level, they undergo extension and convergence movement during 11 to 12 hpf (Fig 412). Secondly, a certain area of mesoderm differentiates into *wt1* expressing cells during 10 to 11 hpf, and than undergoes extension and convergence movement during 11 to 12 hpf.

In $spt^{-/-}$ embryos, the anterior intermediate mesoderm is further differentiated from the mesoderm but the number of *wt1* expressing cells formed is much lower than in WT (approximately 1/2) at 15 hpf (Fig 523). The $spt^{-/-}$ autonomously affects only the paraxial mesoderm, not other mesodermal cells (Ho and Kane, 1990). The paraxial mesoderm cells removed from $spt^{-/-}$ embryos are aggregated in the tail and fail to form somites in WT embryos (Ho and Kane, 1990). *Spt* and other unknown factors have a synergistic effect on the number of *wt1* expressing cells but not on the activation of *wt*1 gene.

Previous research shows that *wt1* expressing cells are not formed in $Zoep^{-/-}$ and $spt^{-/-}$ double mutant embryos (Weidinger et al., 2002). Fig 432 suggests that maternal Oep rescues the specification of intermediate mesoderm. In other words mutation in *spt/tbx16* blocks the maternal Oep (MOep) effects. In the mechanism for the specification of intermediate mesoderm, *spt* is a target gene for MOep. Results

nevertheless suggest strong correlation between the formation of paraxial and intermediate mesoderm. The specification of intermediate mesoderm appears normal whereas the differentiation of paraxial mesoderm is blocked in double mutants of *Zoep*$^{-/-}$ and *ntl*$^{-/-}$ (Schier et al., 1997; Weidinger et al., 2002). The mechanism for the specification of intermediate mesoderm is not dependent on paraxial mesoderm. Interplay between FGF, Nodal signalling and T-box transcription factors (Griffin and Kimelman, 2002; Griffin and Kimelman, 2003; Mizoguchi et al., 2006; Reiter et al., 2001) in the mechanism for the specification of intermediate and paraxial mesoderm is summarized in Fig 621.

*Wt*1a gene might be involved in the mechanism for the specification of anterior intermediate mesoderm. The morpholino inhibition of *wt*1b does not interfere with the formation of the pronephric glomerulus. Inactivation of *wt*1a, however, leads to the absence of podocytes (Perner et al., 2007).

The Coalescence of Wt1 Expressing Cells

In all vertebrates, the heart develops from the bilateral population of cells in the anterior lateral plate mesoderm (McFadden and Olson, 2002). The myocardial precursors appear to move in a coordinated manner towards the midline and fuse to form the myocardial layer of the heart tube in zebrafish. The myocardial precursors form polarized epithelia during somitogenesis, hence they migrate as a coherent population. In addition *fibronectin* regulates this epithelial organization during myocardial migration (Trinh and Stainier, 2004).

The dynamic pattern of pronephric-glomerular precursors, that is represented by *wt*1 expressing cells, suggests that during 11 to 15 hpf the movement of the pronephric-glomerular precursors is not coordinated but leads the morphological changes from the narrow stripe to the elongated triangular shape (Fig 412, Fig 413). It appears that the pronephric-glomerular precursors do not undergo epithelial movement.

In mammals, during nephron formation, the ureteric bud invades the metanephric mesenchyme and induces differentiation. Mesenchymal cells condense to form aggregates. The condensed mesenchyme undergoes a mesenchymal-to epithelial transformation and forms the epithelial structure. The epithelial structure differentiates further into the tubules and Bowman's capsule (Rivera and Haber, 2005). The coalescence of *wt1* expressing cells (Fig 413, Fig 414) might be a combination of the mesenchymal cell condensation and mesenchymal to epithelial transformation. *Mediator of RNA polymerase II transcription*, subunit 12 homolog (*med*12), is required for the coalescence of anterior intermediate mesoderm (Hong et al., 2005).

The Cubic Formula for PGP Midline Convergence

The Cubic formula, y = -0.0176x3 + 1.8271x2 - 61.932x + 717.16, generated from quantification of PGP midline convergence, gives two turning time points, 29.7 and 39.5 hpf, during the PGP convergence process (Fig 418). Between 29.7 and 39.5 hpf the PGP distance is increased. This mathematical description between 29.7 and 29.5 hpf does not, in fact, match the impression from the *wt*1 WISH images in which the

PGP gets closer during the morphogenesis. Increase in the PGP distance thus reflects a change of mechanism, interruption in the PGP midline convergence or reflects growth of the embryo. This can be clarified by normalizing the measurement using parameters of growth in the body size. There are no standard parameters, which accurately indicate the growth in size of zebrafish embryos, because massive cell relocation and morphological change of embryos (e.g. Fig 411 to Fig 413) occur during early developmental stages (prior to 24 hpf). By 24 hpf, the development of the somite is more mature in term of morphology. The somite increases in tissue mass and size during early development. This means that the left and right outer edges of a pair of somites move apart from each other as the embryo growth. Measurement of the width wideness of the bilateral somite in *atp2a1* WISH embryos (Fig 432) is thus a possible parameter to normalize PGP migration measurement. Another possible parameter is the distance between the two lenses of the embryos. Distance between these two lenses gradually increases during development (e.g Fig 432).

These approaches raise two questions. Is it theoretically correct to normalize PGP distance measurement only after 24 hpf? Should the measurement be normalized by a standard value according to developmental stage or by a parameter obtained from the same embryo? Rationalization of these issues is suggested as follows.

The value ($Y_{measured}$) of PGP distance taken from WISH images consist of the real PGP distance (Y_{real}) that represents the PGP migration and a value (Y_{growth}) which reflects the growth in size of the embryos:

$$Y_{measured} = Y_{real} + Y_{growth}.$$

The value actually required is Y_{real}.

$Y_{real} = Y_{measured} - Y_{growth}$.

It can be assumed prior to 24 hpf $Y_{growth} = 0$, since PGP is still located outside the main embryo. It is thus reasonable to amend PGP distance measurement only after 24 hpf. There is no simple direct method to measure Y_{growth}. The measurement, can however be generated indirectly. First of all producing a formula (Y_{growth}) for growth, width of somite or distance between lenses is y and developmental stage is x. The initial width of somite or distance between lenses is a. Y_{growth} is defined as y-a:

$Y_{growth} = y - a$. [Where $y = f(x)$ and $a = y_{24\ hpf} = f(24)$.]

Since a formula for Y_{growth} is necessary to correct the PGP measurement, it could be normalized by a standard value according to developmental stage rather than by a measurement obtained from the same embryo.

During 11 to 28 hpf, the midline converged *wt1* expressing cells exhibit a type of coordinated movement of the mesenchymal cells (Fig 412 to Fig 416). The WISH of *wt1* shows that the PGPs extend a narrow tissue toward each other prior to further convergence at 32 hpf (Fig 416, Fig 417). After 28 hpf, the *wt1* expressing cells exhibit the movement of an epithelial sheet. From 36 hpf, the PGPs undergo the fusion of the two epithelial sheets (Fig 416).

The quantified PGP distances for *Zoep*$^{-/-}$ embryos distribute over a wide area at 36 and 48 hpf (Fig 443) in the scatter plot. This indicates the rescue effect of maternal Oep on PGP midline convergence has a variable period of duration. The variation might be Oep dose dependent, because *Zoep*$^{-/-}$ embryos develop normally when enough *oep* mRNA is injected to the embryos (Zhang et al., 1998). In addition, *oep* is expressed in ventral mesoderm during 10 to 24 hpf (Thisse et al., 2001; Zhang

et al., 1998). Activin receptors (*acvr*) show ubiquitous expression prior to 24 hpf in zebrafish (Albertson et al., 2005; Bauer et al., 2001; Yelick et al., 1998). It is highly possible that Nodal signal regulates PGP midline convergence directly through the TGFβ super family receptors.

The T-box transcription factor *ntl*, or a differentiated notochord, is not required for PGP midline convergence prior to 36 hpf. There is no significant difference in PGP distance between WT and $ntl^{-/-}$ embryos at 15 or 24 hpf (Fig 522). At 48 hpf, the PGP still sit side by side but do not fuse together (n = 24 in 28). *Ntl* could play an important role in the fusion of the PGP.

The PGP midline convergence is completely blocked in $spt^{-/-}$ (*tbx*16) embryos. There is no difference in PGP distance at 15, 24 and 48 hpf in $spt^{-/-}$ embryos (Fig 524). The T-box transcription factor *spt* is essential for the PGP midline convergence. The PGP midline convergence is completely blocked in $spt^{-/-}$ (*tbx*16) embryos. There is no difference in PGP distance at 15, 24 and 48 hpf in $spt^{-/-}$ embryos (Fig 524). This result suggests the T-box transcription factor *spt* is essential for the PGP midline convergence. *Spt/tbx16* gene does not express in *wt*1 expressing cells during embryonic development, hence the role that Spt plays in PGP midline convergence does not have a direct effect on migration.

In general there are two types of mechanisms, active and passive migration. Active migration means that the migration mechanism consumes energy from the tissue itself. In passive migration, movement of tissue is due to the force from the surrounding tissues. An example of this type of tissue movement is gut looping (Horne-Badovinac et al., 2003). PGP midline migration most likely undergoes active migration since an embryo that displays gut looping phenotype and normal PGP

migration is observed (data not shown). Both mechanisms, however, needs cell surface molecules to connect and interact with the tissue's environment in order to change location.

One known cell surface molecule, Protocadherin 8 (*pcdh*8/*papc*) has been shown to be a down stream target of *spt* and is involved in morphogenesis of mesoderm (Yamamoto et al., 1998). Protocadherins are transmembrane glycoproteins belonging to the *cadherin* superfamily. *Pcdh* mediates cell movement by cell-cell contact dependent interaction in human astrocytoma cells (Nakao et al., 2008) or by regulating C-cadherin adhesion activity during the early development of *Xenopus laevis* embryos (Chen and Gumbiner, 2006). Spt is critical for extracelluar matrix organization in zebrafish embryos (Fig 534). Whether PGP midline convergence is promoted by cell-cell contact or cell-extracellular matrix interaction (Takada et al., 2007) remains to be clarified. One possible role Spt plays is that it regulates cell surface molecule gene expressions in the surrounding tissues of PGP/intermediate mesoderm. It is also possible that Spt regulates the full differentiation of PGP during gastrulation. A partially differentiated PGP looses important cell surface molecules for migration.

Signalling Pathways in the Regulation of PGP Midline Convergence

Both *oep* and *spt/tbx16* genes have been demonstrated to be required for PGP midline convergence from an early stage (Fig 443, Fig 524). Ntl is important for the fusion of the PGP after 36 hpf (Fig 522). What is the relationship between *oep* and *spt/tbx16* genes in the regulation of PGP midline convergence?

Matrix metalloproteinase-2 (MMP-2) activity and *island beat* (*isl*), *valentine* (*vtn*), and silent heart (*sih*) are required for fusion of the PGP (Serluca et al., 2002). *Floating head* (*flh*), *sonic hedgehog* (*shh*) and *GLI-Kruppel family member GLI2a* (*gli2a*) are essential for the PGP midline convergence (Majumdar and Drummond, 2000). Retinoic acid signalling and Cadherin-6 also appear to be involved in the regulation of PGP midline convergence (Kubota et al., 2007; Wingert et al., 2007). The way in which these signalling pathways and genes work together to regulate the PGP midline convergence remains to be answered.

Zebrafish embryos develop outside the mother and are transparent thus allowing easy visualization of internal tissues. In addition, hundred of eggs are produced every mating pair. These characteristics of zebrafish allow mutagenesis and screening strategies on a large scale (Rubinstein, 2003). Combining single-locus random mutagenesis with the transgenic technique, novel genes regulating PGP midline convergence can be screened with high-throughput. The strategy is to produce a transgenic fish, in which PGP is specifically labeled by fluorescent protein (e.g. EGFP) during 48 to 72 hpf. After the green-PGP transgenic line is generated, males from the line mutagenized with ethylnitrosourea (ENU) are mated with wild-type females (Haffter et al., 1996; Haffter and Nusslein-Volhard, 1996). In the F1 progeny, each individual is heterozygous for a different mutagenized genome. F2 can be raised from F1 x F1 or from F1 x wild-type fish. Embryos collected from F2 x F2, can then be screened under the fluorescent microscope for PGP phenotypes during 48 to 72 hpf. The final step is to identify which gene is mutated in the embryos that exhibit PGP phenotypes.

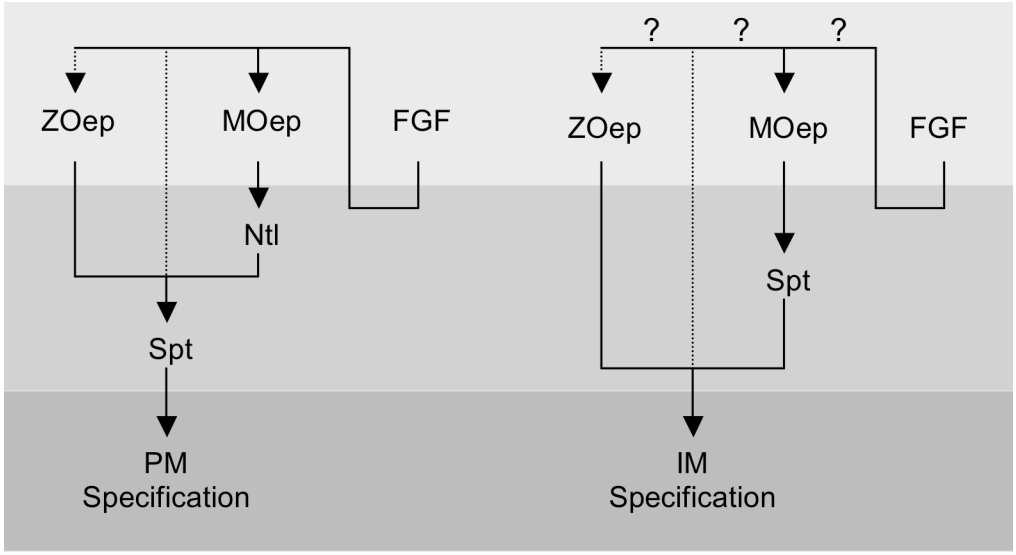

Figure 80-621. Specification of paraxial and intermediate mesoderm.

This simplified diagram summarizes the genetic interaction between Nodal and FGF signalling in the paraxial and intermediate mesoderm specification. The ZOep (zygotic Oep), MOep (meteral Oep) and FGF in the upper panel are paracrine factors. The Spt and Ntl in the medle panel represent transcription factors. In the bottom panel the paraxial mesoderm (PM) and intermediate mesoderm (IM) specification are embryonic phenotypes. In the specification of PM, Spt plays an essential role. *Spt*$^{-/-}$ embryos display server defect in PM specification (Yamamoto et al., 1998). MOep is unable to rescue PM phenotype in *Zoep*$^{-/-}$, *ntl*$^{-/-}$ double mutants (Griffin and Kimelman, 2003). In *ace*/*fgf8*$^{-/-}$ embryos or embryos express a dominate-negative FGF receptor (dnFGFG), *spt* and *ntl* expression is down regulated from the mid- and early-gastrula (Griffin et al., 1995; Griffin et al., 1998). Luck of MOep does not affect PM specification (Gritsman et al., 1999). An synergistic activity of Nodal and FGF pathways in IM specification (Mathieu et al., 2004). In the specification of IM, MOep is unable to rescue IM phenotype in *Zoep*$^{-/-}$, *spt*$^{-/-}$ double mutants (Weidinger et al., 2002). It is speculated Nodal and FGF pathways also active in an synergistic manner in the IM specification.

6.3 Can A Zebrafish Line Which Develops Bilateral Kidneys Be Obtained By Genetic Engineering?

Developing 'One Kidney' or 'Two Kidneys' Is Not Vital

From the literature review in §1.1 it is known that humans can survive even with a fused kidney, i.e. horseshoe kidney (Fig 113), which is a category of renal anomalies. The medaka fish has similar body size and habitat to the zebrafish (Furutani-Seiki and Wittbrodt, 2004) but develops bilateral kidneys (Fig 111). A previous study, in which rhodamine dextran was injected into the circulation of zebrafish embryos, demonstrated that functional pronephric glomeruli can be generated even in ectopic lateral locations (Majumdar and Drummond, 2000). The results of WISH shown in Fig 444 are consistent with this study. The mechanisms of PGP differentiation are independent of the mechanisms of PGP migration. It is, hence, assumed that bilateral kidney 'abnormality' is not fatal in zebrafish. If the mechanism of PGP midline convergence could be manipulated genetically, and without harming the functions of other organs, lines of zebrafish developing functional bilateral kidneys could be obtained.

Prior to discussion of potential approaches to producing two-kidney zebrafish, one point needs to be noted. Diversity of kidney morphology is huge among vertebrate. In the literature,types of kidney are categorized into aglomerular kidney, glomerular kidney (Beyenbach, 2004), head/cranial kidney, trunk/caudal kidney (Balfour, 1882; Prodocimo and Freire, 2003), pronephros, mesonephros, and metanephros. Further information is given in the Introduction (Fig 111, Fig 631). This huge diversity also increases the complications in the study of kidney evolution (Balfour, 1875; Marshall and Smith, 1930; Vize and Smith, 2004). This thesis thus

concentrates on the morphogenesis of the pronephric glomerulus and focuses on the mechanism for PGP midline convergence. Additionally, two further categories of kidney type have been included, namely fused and bilateral kidneys.

The pronephros (head kidney) and mesonephros (trunk kidney) coexist in adult zebrafish (Fig 111 & Fig 631). The fused head kidney lies at the anterior end of the swim bladder. The continuation of the kidney along the dorsal abdominal cavity wall towards the tail forms two small bands bilaterally separated from each other. The two bands unite together and form a fused trunk kidney (Fig 631) above the middle of the swim bladder. The head kidney is more active in hematopoiesis and the trunk kidney is more active in excretion (Danilova and Steiner, 2002; Davidson and Zon, 2004). Other research demonstrates that T cells aggregate in both part of the kidney (head and trunk) and suggests the kidney may play a dual role as a primary and secondary lymphoid organ (Danilova et al., 2004). It remains unclear as to weather the head kidney retains a function in excretion.

Unlike in zebrafish, in adult medaka pronephros and mesonephros are formed within a structure where they are indistinguishable from each other lay at the anterior end of the swimming bladder (Fig 631). The kidneys develop bilaterally, separated from each other by the whole of the vertebral column (Fig 631). Glomeruli are distributed throughout the entire length of the kidney including the cylindric caudal parts of the kidney (Fedorova et al., 2008)(Fig 111).

Comparing the morphology of pronephros of the zebrafish and medaka during early development. Parallel and distinctive morphogenesis is shown in Fig 632. At 22 hpf, the PGP coalescence almost ends, *wt1* expressing cells form compact patches projecting low level *wt1* expression toward the head in zebrafish. By 36 hpf, the low-

level *wt1* expression is no longer observed. The two PGPs migrate further towards each other and lie side by side along the midline (Fig 632). At corresponding stages in the medaka (2 days 6 h & 3 days 23 h), a similar *wt1* expression pattern is observed (Fig 632). The main *wt1* expression patches of cells project low-level *wt1* expression, however, in a wider spread of directions. The PGP midline convergence process appears very similar for both zebrafish and medaka during these early stages. Interestingly, during development the medaka embryos take a longer time to achieve the *wt1* expression than zebrafish (Fig 632). This could be due to the different habitat, in the laboratory, of these fish (Iwamatsu, 2004; Kimmel et al., 1995).

After 36 hpf in zebrafish (3 days 23 h in medaka), the major difference in the pronephros morphogenesis between zebrafish and medaka starts to appear. The distance between the PGP continues to decrease in zebrafish, until 49 hpf (Fig 418) the PGP form a fused glomerulus (Fig 632). By contrast, the convergence appears to stop in the medaka embryos and the two PGPs are separated by the dorsal aorta, an example is shown in Fig 632 (Fedorova et al., 2008). Consequently, PGP fuse or remain separate a pair bilateral pronephric respectively in zebrafish and medaka (Fig 632).

This comparison suggests that zebrafish with the bilateral head kidney may be generated by interruption of PGP midline convergence by 36 hpf. The following question is then what potential approaches can be used to interrupt PGP midline convergence. In this final section of discussion two methods are now suggested: (1) removal of the specific factors, which are essential for PGP midline convergence alone and (2) manipulation of key factors specifically in PGP midline convergence without disrupting the other functions of these factors.

Removal of Specific Essential Factors

Despite *Zoep*$^{-/-}$ (Fig 443) and *spt*$^{-/-}$ (Fig 524) exhibiting interrupted PGP midline convergence, the PGP phenotype also accompanies other phenotypes. A number of zebrafish mutants have been described with ectopic PGP differentiation (Kubota et al., 2007; Majumdar and Drummond, 2000; Serluca et al., 2002; Wingert et al., 2007), all have the same problem, as in *Zoep*$^{-/-}$ and *spt*$^{-/-}$ embryos, of multiple tissue phenotypes. In addition, most of the phenotypes are fatal.

The main conclusion of this thesis is there is no single universal mechanism, which controls all the midline convergence of organ primordia. Factors, which depend on tissues and development stages, are also required. If the specific essential factors in PGP midline convergence are identified, then the process can be manipulated by elimination of the specific factors at the relevant critical stages. Further research is necessary to clarify whether conditions essential for PGP midline convergence but not other tissue morphogenesis, exist.

Manipulation of Key Factors Specifically in PGP Midline Convergence

Further research is necessary to determine whether PGP midline convergence relies on interaction between PGP and extracellular matrix. Should the results be positive, which molecules on the PGP surface mediate the interaction? Upon identification of these molecules, they would become the target for the interruption of the PGP migration process.

How could gene expression be manipulated in targeted cell types at a desired developmental stage? Ablation of gene expression is an important approach to the

dissection of genetic mechanism in a model organism (Editorial, 2000). Until recently, several techniques have been used to regulate gene expression in zebrafish, for example RNAi (Li et al., 2000; Oates et al., 2000; Wargelius et al., 1999), morpholinos (Nasevicius and Ekker, 2000), and small molecules (Esengil et al., 2007). These techniques are not however sophisticated enough in terms of specificity of cell types or gene. Other methods that incorporate transgenic techniques (Kawakami, 2005; Kwan et al., 2007), such as Tetracyclin inducible system (Huang et al., 2005), and Cre-loxP system (Guo et al., 2005; Langenau et al., 2005), are often time-consuming.

A method, targeting mutagenesis in zebrafish (Doyon et al., 2008; Meng et al., 2008; Woods and Schier, 2008) and allowing direct genetic manipulation at a specific locus, was developed recently. In this technique, mRNA of zinc-finger endoneucleases (ZFNs) is introduced into zebrafish embryos to induce insertion, or deletion, mutation at targeted loci. ZFNs consist of a zinc-finger (ZF) domain and a cleavage domain. The ZF domain provides the DNA-binding specificity, which can be engineered to recognize a wide variety of target sequence (Carroll et al., 2006; Hurt et al., 2003; Liu et al., 2002; Pabo et al., 2001; Wright et al., 2006). The cleavage domain is derived from *Fok*I endonuclease (Kim et al., 1996; Porteus and Carroll, 2005). The ZFN mediated cleavage can lead to mutations when DNA breaks are repaired by nonhomologous end joining pathways (Beumer et al., 2006; Bibikova et al., 2002). ZFN or a combination of different techniques might therefore become the major technology for genetic manipulation in zebrafish. It is anticipated, in the future not only zebrafish lines that develop bilateral kidneys but also medaka lines that develop fused kidneys could be obtained by genetic engineering.

Timing of Zygotic Gene Activation

Embryonic development proceeds through a series of events well ordered in space and time. The Xenopus embryo undergoes rapid and synchronous cell cycles followed by asynchronous divisions at early development. This change in cell cleavage has been called the midblastula transition (MBT). An early study of Xenopus embryos shows that at the MBT the blastomeres become transcriptionally active for the first time (Newport and Kirschner, 1982a). Namely the transition occurs in the absence of zygotic transcription and is therefore dependent on the gene products accumulated in the oocyte during oogenesis (Stitzel and Seydoux, 2007). Genes synthesized and stored in the oocytes, and having important roles during embryonic development, are called maternal-effect genes (Minami et al., 2007). The transition from maternal to zygotic developmental control is termed maternal-zygotic transition, MZT. MZT occurs during the late 1-cell/early 2-cell stages in the mouse, which was demonstrated by applying a RNA synthesis inhibitor, α-amanitin, (Golbus et al., 1973; Warner and Versteegh, 1974) to mouse embryos at the1-cell and 2-cell stages. The 1-cell embryos divided normally to the 2-cell stage but no 2-cell stage embryos developed to the 4-cell stage. Cleavage of 1-cell to 2-cell embryos does not depend on newly synthesized zygotic gene products, whereas 2-cell embryos need zygotic gene expressions to proceed to the 4-cell stage (Moore, 1975; Schultz, 1993).

Zebrafish MZT is similar to *Xenopus* embryonic development, and overlaps with MBT. The excess repressor model has been implicated in the molecular mechanism of MZT. In this model, the cytoplasmic-nuclear ratio and the titration of a transcriptional repressor by the exponentially increasing amount of genomic DNA

determine the timing of MZT (Schier, 2007). Competition between the chromatin and transcription complex assembly is thought to be important in the zygotic gene activation (Kikyo and Wolffe, 2000; Prioleau et al., 1994). The onset of zygotic gene activation is due to abortion of transcriptional repressors.

Oep is a maternal-effect gene and is expressed both maternally and zygotically (Zhang et al., 1998). Severe patterning defects including cyclopic eye, lack of the notochord, and trunk somites in embryos lacking maternal and zygotic Oep activity (MZ*oep*) were described in a previous study (Gritsman et al., 1999). The embryos lacking maternal Oep activity (M*oep*), however, developed normally. Maternal Oep is not required during regular zebrafish development but can partially compensate for the loss of zygotic Oep (Fig 431 &432). The direct molecular evidence for this maternal rescue effect is elusive. It is envisaged that a probe, or an antibody, is capable of distinguishing between maternal and zygotic *oep* gene products. It can thus be used to provide evidence that maternal *oep* gene products are not degraded prior to zygotic *oep* activation.

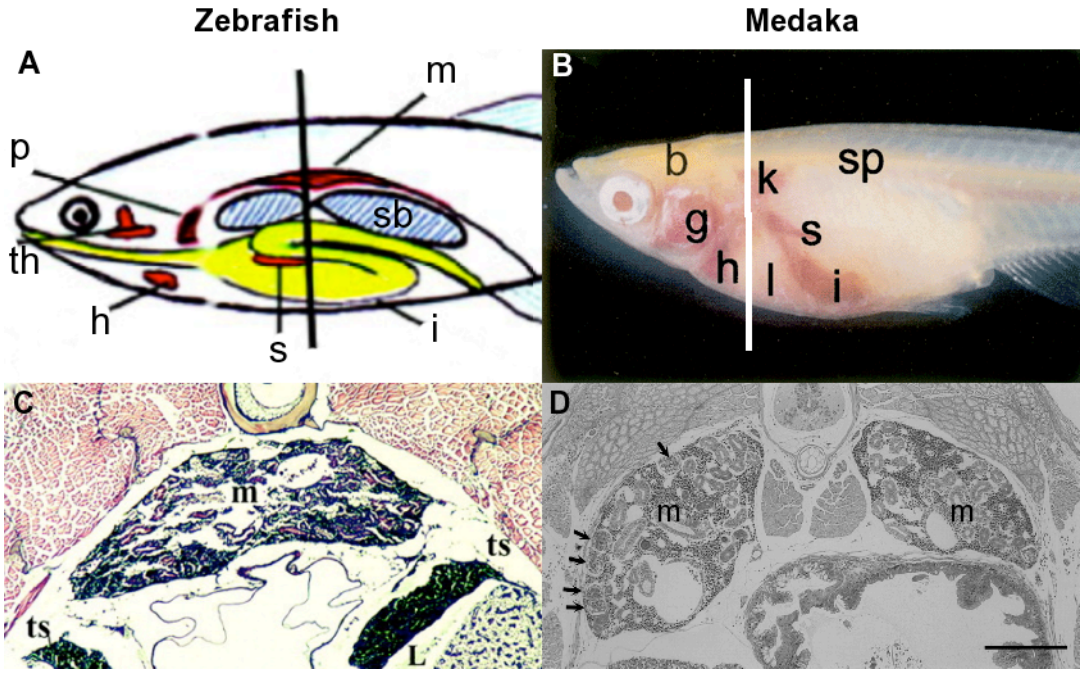

Figure 81-631. Mesonephros in zebrafish and medaka.

(A) Diagram illustrating the position of some of the internal organs of adult zebrafish. The vertical line indicates the position of the section shown in C. (B) Lateral view of an adult see-through medaka illustrates the position of some of the internal organs. The vertical line indicates the position of the section shown in D. (C) Transverse paraffin section, hematoxylin/eosin stain. The mesonephros (m) is fused and contains renal tubules and some hematopoietic tissue. (D) Cross-section of mesonephros in 20-day-old fry. The mesonephros (m) is bilateral and contains mesonephric glomeruli (arrows). The abbreviations for the internal organs are: b, brain; g, gill; h, heart; i, intestine; k, kidney; l or L, liver; m, mesonephros; p, pronephros; s, spleen; sb, swim bladder; sp, spinal cord; th, thymus; ts, testes. A and C were edited from (Danilova and Steiner, 2002). B and D were edited from (Mochizuki et al., 2005). The images are not to scale.

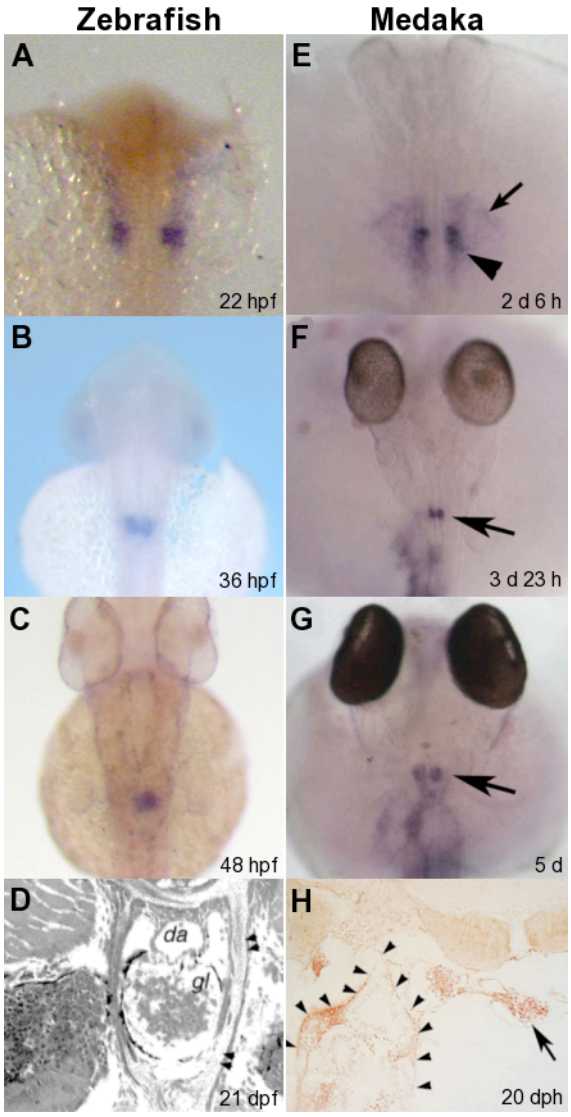

Figure 82-632. *Wt1* expression in pronephros in zebrafish and medaka.

(A-C) *Wt1* expression in the PGP in zebrafish embryos at 22, 36, and 48 hpf. (D) Transverse histological section through a 3-week-old zebrafish, shows the fused pronephric glomerulus (gl) is surrounded by bone and cartilaginous tissue (double arrows; da. dorsal aorta). (E-G) *Wt1* expression in the PGP in medaka embryos at stage 25-26, 31, and 35. (E) Arrowhead and arrow indicate the PGP and the faint signal in nephrocoel cells. (F) Arrow indicates the PGP. (F) Arrow indicates the pronephric glomerulus. (H) Transverse histological section through a medaka at 20 day-post-hatching (dph) shows the two separated pronephric glomeruli (arrow). Arrowheads indicate the intrarenal tissue of the pronephric sinus. D was adapted from (Majumdar and Drummond, 2000). E-H were adapted from (Fedorova et al., 2008). The stages of embryonic development in medak refer to (Iwamatsu, 2004). The images are not to scale.

6.4 Future Research

The understanding of the process underlying the ability of complex organisms to assemble themselves from single cells is one of the most fundamental goals in developmental biology. By using WISH and analysing phenotypes of the mutant embryos, the complexity surrounding PGP midline convergence and the importance of timing were demonstrated. Is there really a 'key' signal or a 'key' gene in the regulation of this dynamic and complicated network of molecules, cells, and tissues? Are there simple laws governing the tissue morphogenesis?

What are the forces shaping the embryonic morphology during the development of zebrafish (Keller et al., 2008; Krieg et al., 2008)? Do the forces change during the morphogenesis? How do the cells know which stage they are at during the development? Can we manipulate gene expression in the same way as zebrafish embryos? Can we manipulate cell behaviour like the zebrafish embryos? Can we grow functional zebrafish kidneys *in vitro* from the PGP? Future research will attempt to answer these questions and find the solutions.

Appendix (Laboratory Protocol)

A1. Mutant Allele-Specific Genotyping

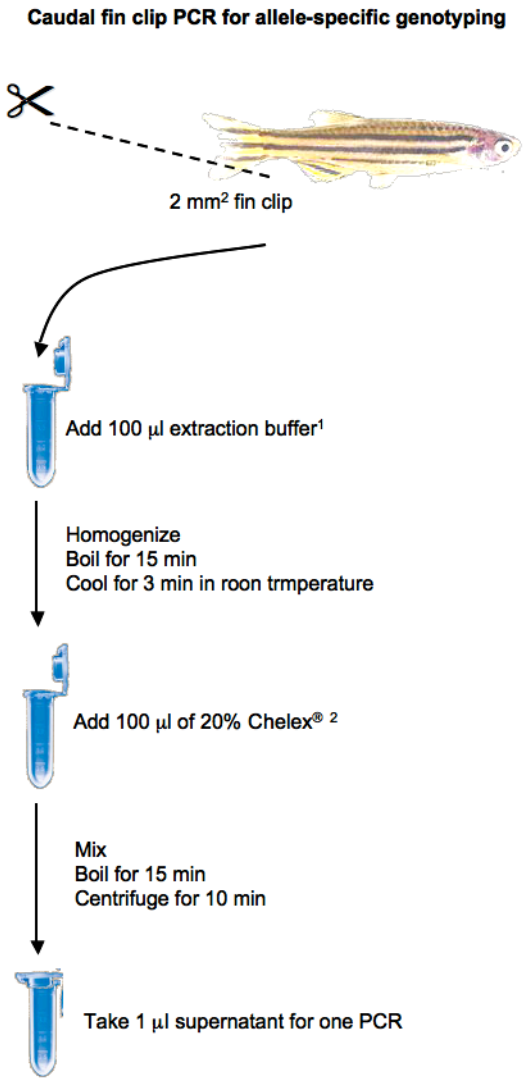

[1] extraction buffer (freshly prepared)

100 mM NaCl, 0.5% N-lauroylsarcosine

[2] 20% Chelex

Add 20 g Chelex into a beaker that contains 100 ml ddH_2O.

Stir the Chelex gently at room temperature for at least 12 h.

Aliquot the equilibrated Chelex into 2-ml microcentrifuge tubes.

Store the tubes at room temperature.

A2. RNA Labelling Reaction

Making the most of the RNA labelling reaction

DIG- or Fluorescein-labelled single-stranded RNA probes of defined length are generated by *in vitro* transcription. DIG- or Fluorescein-11-UTP is incorporated by SP6, T7 and T3 RNA polymerase at approximately every 20-25th nucleotide of the transcript. The amount of synthesized labelled RNA depends on the amount, size (site of linearization) and purity of the template DNA. Under standard conditions approximately 10 µg of full length DIG or FLU-labelled RNA will be transcribed from 1 µg template DNA.

Preparation of DNA template

Linearize minimum 2 µg of plasmid DNA with a suitable restriction enzyme and run a gel to make sure the DNA is digested completely.

Add 1 µl of 10 mg/ml PK and incubate the samples at 37°C for 30 min.

Phenol/Chlorofrom extraction.

EtOH precipitation (RNase free).

Dissolve the DNA in 14 µl of DEPC-treated H_2O and use 1 µl to analyze the quality and quantity on a 1% agarose gel.

Labelling reaction

Add the following to the 13 µl purified template DNA on ice:

10 x NTP labeling mixture (DIG or FLU)	2µl
10 x Transcription buffer	2µl
RNase inhibitor	1µl
RNA polymerase (T7, SP6 or T3)	1µl

Mix gently.

Incubate for 2 h at 37°C.

Stop the reaction by adding 2 µl 0.2 M EDTA [pH 8].

Add 2.5 µl 4M LiCl and 75 µl 100% EtOH.

Centrifuge at maximum centrifugation speed at 4°C for 20 min.

Dissolve the pellet in 21 µl DEPC-treated ddH_2O.

Analyze 1 µl of the transcript by 2% agarose gel electrophoresis in 0.5 x TAE buffer.

Suspend the 20 µl RNA probe in 180 µl hybridization buffer (see A3).

Store at -20°C.

A3. Whole Mount *In Situ* Hybridization On Zebrafish Embryos

The tips for a successful ISH:

1. Keep everything RNase Free before post-hybridization wash.
2. Synthesise of good quality RNA probes (see A2).
4. Make sure probes are able to access to the target.
5. Make suitable hybridization buffer.
6. Shake gently.
7. Wash properly post-hybridization.

Day 0

Preparation of reagents and equipment.

Preparation of RNA-probes (see A2).

Preparation of zebrafish embryos (see A4).

Day 1

Re-hydration of zebrafish embryos (in 2 ml tubes)

Note: Re-hydration is directly related to the access of hybridization buffer and probes into the embryos. Embryos stored longer in methanol might need longer re-hydration treatment.

Wash the embryos with 1 ml 75% methanol/25% PBST for 10 min at RT (short spin at 2000 rpm).

Wash the embryos with 1 ml 50% methanol/50% PBST for 20 min at RT (short spin at 2000 rpm).

Wash the embryos with 1 ml 25% methanol/75% PBST for 30 min at RT (short spin at 2000 rpm).

Wash 5 x 5 min with 1 ml PBST at 30°C. (short spin at 2000 rpm).

Permeabilization (10 μg/ml Protease K in PBST)

Note: Permeablization is a crucial step for successful WISH. If over-digested embryos will fall apart during subsequent steps, but if insufficiently digested, probes will not access the target. Unfortunately there is no standard protocol for permeablization, because the procedure is embryo quality and stage dependent. So trial and error, experience and good luck is required.

Treat 10 hpf embryos with Protease K at 30°C for 0 min.

Treat 11 hpf embryos with Protease K at 30°C for 1 min.

Treat 12 hpf embryos with Protease K at 30°C for 2 min.

Treat 24 hpf embryos with Protease K at 30°C for 15 min.

Treat 48 hpf embryos with Protease K at 30°C for 30 min.

Fix in 4 % PFA for 20 min at RT.

Rinse 5 x 5 min in PBST at RT.

Hybridization

Prehybridize the embryos for 4 h at 65°C in 1 ml hybridization buffer.

Add 100 ng labelled RNA probe (see A2) in a 500 µl hybridization buffer and incubate at 65°C for 5 min.

Change buffer from prebybridization buffer to hybridization buffer (mixed with probes).

Hybridize overnight (16 h) at 65°C.

Day 2

Post-hybridization wash

Wash 20 min in 1 ml 2 x SSC at 65°C.

Wash 20 min in 1 ml 2 x SSC at 65°C.

Wash 20 min in 1 ml 0.2 x SSC/0.1% Treen-20 at 65°C.

Wash 20 min in 1 ml 0.1 x SSC/0.1% Treen-20 at 65°C.

Wash 20 min in 1 ml 0.1 x SSC/0.1% Treen-20 at 65°C.

Wash 5 min in 1 ml 66% 0.2 x SSC/33% PBST at RT.

Wash 5 min in 1 ml 33% 0.2 x SSC/66% PBST at RT.

Wash 5 min in 1 ml PBST at RT.

Detection I: Incubation with anti-Dig-AP antibody

Incubate embryos in 1 ml blocking solution for 1 h at 30°C.

Dilute Anti-DIG-AP antibody in 1 ml blocking solution; 1:10000.

Incubate embryos in the antibody dilution for 2 h with shaking at 30°C.

Wash 4 x 15 min in PBST (may leave in the last PBST wash at 4°C overnight or proceed directly to the next step.)

Day 3

Detection I: Colouration

Note: Develop the colour at room temperature for one hour and then check the colour development under microscope. If the colour does not appear intense enough, check the sample at 30 min intervals until suitable colour intensity and then stop the reaction.

Wash 4 x 5 min in 1 ml colouration buffer.

Mix 2.7 µl NBT with 1 ml colouration buffer then add 2.1 µl BCIP.

Stop reaction by washing embryos 5 min in 1 ml ddH_2O at RT.

Incubate embryos in 500 µl of 0.1 M Glycine, pH 2.2 for 10 min.

Wash 4 x 5 min in 1 ml PBST at RT.

Detection II: Incubation with anti-Flu-AP antibody

Incubate embryos in 1 ml blocking solution 1 h at 30°C.

Dilute Anti-FLU-AP antibody in 1 ml blocking solution; 1:10000.

Incubate embryos in the antibody dilution for 2 h with shaking at 30°C.

Wash 4 x 15 min in PBST (may leave in the last PBST wash at 4°C overnight or proceed directly to the next step.)

Detection II: Colouration

Wash 4 x 5 min in 1 ml colouration buffer.

Mix 4 µl INT Red with 1 ml colouration buffer then add 3.2 µl BCIP.

Stop reaction by washing embryos 5 min in 1 ml ddH_2O at RT.

Incubate embryos in 500 µl of 0.1 M Glycine, pH 2.2 for 10 min.

Wash 4 x 5 min in 1 ml PBST at RT.

Store stained embryos in 4% paraformaldehyde.

Reagents and Equipment

Equipment

Note: RNase free working environment

(1) Glassware can be baked at 300°C for four hours.

(2) Plasticware, tubes can be DEPC-treated (0.05 to 0.1%) overnight then autoclaved and baked to dry or 3% H_2O_2-treated at RT for 15 min then rinse with DEPC treated water and baked to dry.

(3) Sealed factory packages are presumed RNase Free.

(4) RNaseZap, Ambion or equivalent can be used to eliminate RNase by wiping over surfaces.

0.5, 1.5 and 2 ml RNase Free tubes.

Hybridization oven for 2 ml tubes and 30°C and 65°C.

Pipetmans: 1000 µl, 200 µl, 20 µl and 2 µl.

Tips: 1000 µl, 200 µl, 20 µl and 10 µl.

Reagents

Note: Treating Solutions with DEPC to Remove RNase

(1) DEPC is a suspected carcinogen: Take appropriate precautions when handling; e.g., always wear gloves and handle under an approved fume hood.

(2) DEPC reacts with histidine residues of proteins and will inactivate RNases so needs to be

removed by heat treatment before the solution is used (DEPC breaks down to CO2 and ethanol). Add DEPC to solutions at a concentration of 0.05 - 0.1% (add 0.5 - 1 ml DEPC per litre); stir or shake into solution, incubate for 12 hours; autoclave at least 45 minutes.

(3) Compounds containing primary amine groups, such as Tris (2-Amino-2-hydroxymethyl-1,3-propanediol), will also react with DEPC, and thus should be added only after DEPC treatment is complete.

(4) Distilled and deionized water (ddH_2O) is generally already RNase-free, and so does not need to be treated.

10 x PBS (RT)

64 g NaCl

1.6 g KCl

9.2g Na_2HPO_4-$7H_2O$

1.6 g KH_2PO_4

ddH2O to 800 ml, DEPC treatment.

20% Tween-20 (from new factory package, RT) in DEPC treated ddH_2O.

PBST (RNase Free)

1 x PBS

0.1% Tween-20

10 mg/ml Protease K (-20°C)

Dissolve 10 mg proteinase K in 0.5 ml 10 mM Hepes-NaOH, pH 7.5, 1 mM CaCl2.

Self-digest 15 minutes at 37°C.

Add 0.5 ml 50% glycerol.

Divide into 100 µl aliquots.

Store at -20°C.

4% Paraformaldehyde (PFA) in PBS, warm up to 65°C to dissolve, store at 4°C.

20 x SSC (200 ml)

160 ddH_2O

35 g NaCl

Adjust pH to 7.0 with HCl.

Adjust volume to 200 ml and treat with DEPC.

50 mg/ml Heparin in DEPC treated ddH_2O

50 mg/ml Yeast total RNA in DEPC treated ddH_2O

Weigh out 0.5 gm total Yeast RNA.

Heat about 10 ml ddH2O in a microwave oven to biol.

Add Yeast RNA to the heated water.

Stir to dissolve.

Once dissolved, bring to 10 ml with ddH2O.

Centrifuge out and discard the undissolved material.

Aliquot 1 ml in 1 ml tubes, store at -20°C.

1M Citric acid (80 ml, DEPC treatment)

Hybridization Buffer (pH 6.0)	For 50 ml
50% formamide	25 ml formamide
10% Dextran sulfate	5 g dextran sulphate
0.5 mM EDTA	50 μl of 0.5 M EDTA
5 x SSC	12.5 ml 20 x SSC
50 μg/ml heparin	50 μl of 50 mg/ml heparin
1 mg/ml yeast total RNA	1 ml of 50 mg/ml yeast total RNA
0.1% Tween-20	250 μl of 20% Tween-20
0.092M citric acid	460 μl of 1M citric acid

store at 4°C

Note: the main parameters that influence hybridization, melting point of probes to the target ($\mathbf{T_m}$)

(1) Temperature.

(2) pH 6.5-7.5 are frequently used. Higher pH can be used to produce more stringent hybridization.

(3) Concentration of monovalent cations (Na^+).

(4) Remove divalent cations with EDTA.

(5) Probe length.

(6) Probe concentration.

(7) Presence of organic solvents: formamide, dextran sulphate, increase in probe concentration and higher hybridization rates.

100 mg/ml BSA in DEPC treated ddH_2O

Blocking Reagent	For 10 ml
2% goat serum	200 µl goat serum
2 mg/ml BSA	200 µl 100 mg/ml BSA
In PBST	

1M Tris-HCl, pH9.5 in DEPC treated ddH_2O

1M $MgCl_2$ in ddH_2O

5M NaCl in ddH_2O

Colouration Buffer (freshly prepared)	For 20 ml
100 mM Tris-HCl, pH9.5	2 ml of 1M
50 mM MgCl2	1 ml of 1M
100 mM NaCl	400 µl of 5M
0.1% Tween-20	100 µl of 20%
ddH_2O	to 20 ml

100% Methanol

50 mg/ml Nitro Blue Tetrazolium (NBT), store at -20°C

50 mg of NBT in 0.7 ml N,N dimethylformamide and 0.3 ml ddH_2O.

50 mg/ml 5-Bromo-4-Choloro-3-Indoyl Phosphate (BCIP), store at -20°C

50 mg of BCIP in 1 ml N,N dimethylformamide.

50 mg/ml Iodonitrotetrazolium cloride (INT Red), store at -20°C

50 mg of INT Red in 1 ml N,N dimethylformamide.

0.1 M Glycine

Add 0.75 g Glycine to 60 ml ddH_2O, adjust pH to 2.2 by using HCl.

Top the solution to 100 ml with ddH_2O and autoclave.

A4. Preparation of zebrafish embryos for WISH

Making Unpigmented Embryos with PTU (see Option in Fixation)

Make up a 0.15% stock of PTU (6-propylthiouracil, Sigma), which needs to be warmed to 65°C for a while before it dissolved.

Dilute the PTU down to 0.003% with blue water (see Chapter 2.1).

Incubate embryos in the 0.003% PTU.

Collect embryos at desired stages.

Dechorionation

Enzymatic method (not always working)

Add 2 ml ddH_2O in every well of a 24 well culture plate.

Add 20 μl of 100 mg/ml Pronase in one of the well with 2 ml ddH_2O.

Resuspend the collected embryos in to the Pronase well and incubate at RT for 20 min.

Wash away chorion debris with ddH_2O.

100 mg/ml Pronase in DEPC treated ddH_2O, store at -20°C

Mechanical method

Tear the chorion in ddH_2O in a 9-cm Petri dish on black colour bench with #5 tweezers one embryo by one embryo.

Fixation

Fix the embryos in 1 ml 4% PFA overnight (16 h) at 4°C.

(**Option**: Remove of pigment, incubate embryos in 0.8% KOH/0.9% H_2O_2 for 15 min, then rinse twice in PBST and re-fix in 4% PFA for 20 min.)

Wash embryos in 1 ml 100% methanol for 10 min.

Transfer embryos into 1 ml 100% methanol and store them at -20°C until use.

30% H_2O_2

20% KOH in ddH_2O

References

Abremski, K., Hoess, R., and Sternberg, N. (1983). Studies on the properties of P1 site-specific recombination: evidence for topologically unlinked products following recombination. *Cell* **32,** 1301-11.

Abu-Issa, R., and Kirby, M. L. (2008). Patterning of the heart field in the chick. *Dev Biol* **319,** 223-33.

Ahmed, S., and Nawshad, A. (2007). Complexity in interpretation of embryonic epithelial-mesenchymal transition in response to transforming growth factor-beta signaling. *Cells Tissues Organs* **185,** 131-45.

Aiello, V. D., and Xavier-Neto, J. (2006). Full intrauterine development is compatible with cardia bifida in humans. *Pediatr Cardiol* **27,** 393-4.

Aitman, T. J., Dong, R., Vyse, T. J., Norsworthy, P. J., Johnson, M. D., Smith, J., Mangion, J., Roberton-Lowe, C., Marshall, A. J., Petretto, E., Hodges, M. D., Bhangal, G., Patel, S. G., Sheehan-Rooney, K., Duda, M., Cook, P. R., Evans, D. J., Domin, J., Flint, J., Boyle, J. J., Pusey, C. D., and Cook, H. T. (2006). Copy number polymorphism in Fcgr3 predisposes to glomerulonephritis in rats and humans. *Nature* **439,** 851-5.

Alberts, B. (2002). "Molecular biology of the cell." Garland Science, New York.

Albertson, R. C., Payne-Ferreira, T. L., Postlethwait, J., and Yelick, P. C. (2005). Zebrafish acvr2a and acvr2b exhibit distinct roles in craniofacial development. *Dev Dyn* **233,** 1405-18.

Alexander, J., Stainier, D. Y., and Yelon, D. (1998). Screening mosaic F1 females for mutations affecting zebrafish heart induction and patterning. *Dev Genet* **22,** 288-99.

Altschmied, J., Hornung, U., Schlupp, I., Gadau, J., Kolb, R., and Schartl, M. (1997). Isolation of DNA suitable for PCR for field and laboratory work. *Biotechniques* **23,** 228-9.

Amacher, S. L., Draper, B. W., Summers, B. R., and Kimmel, C. B. (2002). The zebrafish T-box genes no tail and spadetail are required for development of trunk and tail mesoderm and medial floor plate. *Development* **129,** 3311-23.

Amacher, S. L., and Kimmel, C. B. (1998). Promoting notochord fate and repressing muscle development in zebrafish axial mesoderm. *Development* **125,** 1397-406.

Amsterdam, A., Nissen, R. M., Sun, Z., Swindell, E. C., Farrington, S., and Hopkins, N. (2004). Identification of 315 genes essential for early zebrafish development. *Proc Natl Acad Sci U S A* **101,** 12792-7.

Aoki, T. O., David, N. B., Minchiotti, G., Saint-Etienne, L., Dickmeis, T., Persico, G. M., Strahle, U., Mourrain, P., and Rosa, F. M. (2002). Molecular integration of casanova in the Nodal signalling pathway controlling endoderm formation. *Development* **129,** 275-86.

Armstrong, J. F., Pritchard-Jones, K., Bickmore, W. A., Hastie, N. D., and Bard, J. B. (1993). The expression of the Wilms' tumour gene, WT1, in the developing mammalian embryo. *Mech Dev* **40,** 85-97.

Ashfield, R., Enriquez-Harris, P., and Proudfoot, N. J. (1991). Transcriptional termination between the closely linked human complement genes C2 and factor B: common termination factor for C2 and c-myc? *Embo J* **10,** 4197-207.

Ashfield, R., Patel, A. J., Bossone, S. A., Brown, H., Campbell, R. D., Marcu, K. B., and Proudfoot, N. J. (1994). MAZ-dependent termination between closely spaced human complement genes. *Embo J* **13,** 5656-67.

Attisano, L., and Wrana, J. L. (2002). Signal transduction by the TGF-beta superfamily. *Science* **296,** 1646-7.

Axelrod, J. D., Miller, J. R., Shulman, J. M., Moon, R. T., and Perrimon, N. (1998). Differential recruitment of Dishevelled provides signaling specificity in the planar cell polarity and Wingless signaling pathways. *Genes Dev* **12,** 2610-22.

Balfour, F. M. (1875). On the Origin and History of the Urinogenital Organs of Vertebrates. *J Anat Physiol* **10,** 17-48.

Balfour, F. M. (1882). Memoirs: On the Nature of the Organ in Adult TELEosteans and Ganoids, which is usually regarded as the Head-Kidney or Pronephros. *Quarterly Journal of Microscopical Science* **s2-22,** 12-16.

Barak, H., Rosenfelder, L., Schultheiss, T. M., and Reshef, R. (2005). Cell fate specification along the anterior-posterior axis of the intermediate mesoderm. *Dev Dyn* **232,** 901-14.

Bard, J. B., Gordon, A., Sharp, L., and Sellers, W. I. (2001). Early nephron formation in the developing mouse kidney. *J Anat* **199,** 385-92.

Barnes, G. L., Alexander, P. G., Hsu, C. W., Mariani, B. D., and Tuan, R. S. (1997). Cloning and characterization of chicken Paraxis: a regulator of paraxial mesoderm development and somite formation. *Dev Biol* **189,** 95-111.

Bauer, H., Lele, Z., Rauch, G. J., Geisler, R., and Hammerschmidt, M. (2001). The type I serine/threonine kinase receptor Alk8/Lost-a-fin is required for Bmp2b/7 signal transduction during dorsoventral patterning of the zebrafish embryo. *Development* **128,** 849-58.

Bentley, D. (2002). The mRNA assembly line: transcription and processing machines in the same factory. *Curr Opin Cell Biol* **14,** 336-42.

Berry, C. (2002). Flies in the colon. *Qjm* **95,** 487-8.

Bertrand, N., and Dahmane, N. (2006). Sonic hedgehog signaling in forebrain development and its interactions with pathways that modify its effects. *Trends Cell Biol* **16,** 597-605.

Beumer, K., Bhattacharyya, G., Bibikova, M., Trautman, J. K., and Carroll, D. (2006). Efficient gene targeting in Drosophila with zinc-finger nucleases. *Genetics* **172,** 2391-403.

Beyenbach, K. W. (2004). Kidneys sans glomeruli. *Am J Physiol Renal Physiol* **286,** F811-27.

Bibikova, M., Golic, M., Golic, K. G., and Carroll, D. (2002). Targeted chromosomal cleavage and mutagenesis in Drosophila using zinc-finger nucleases. *Genetics* **161,** 1169-75.

Biemar, F., Argenton, F., Schmidtke, R., Epperlein, S., Peers, B., and Driever, W. (2001). Pancreas development in zebrafish: early dispersed appearance of endocrine hormone expressing cells and their convergence to form the definitive islet. *Dev Biol* **230,** 189-203.

Bjornson, C. R., Griffin, K. J., Farr, G. H., 3rd, Terashima, A., Himeda, C., Kikuchi, Y., and Kimelman, D. (2005). Eomesodermin is a localized maternal

determinant required for endoderm induction in zebrafish. *Dev Cell* **9,** 523-33.

Bollig, F., Mehringer, R., Perner, B., Hartung, C., Schafer, M., Schartl, M., Volff, J. N., Winkler, C., and Englert, C. (2006). Identification and comparative expression analysis of a second wt1 gene in zebrafish. *Dev Dyn* **235,** 554-61.

Bottcher, R. T., and Niehrs, C. (2005). Fibroblast growth factor signaling during early vertebrate development. *Endocr Rev* **26,** 63-77.

Bouchard, M., Souabni, A., Mandler, M., Neubuser, A., and Busslinger, M. (2002). Nephric lineage specification by Pax2 and Pax8. *Genes Dev* **16,** 2958-70.

Boudreau, N. J., and Jones, P. L. (1999). Extracellular matrix and integrin signalling: the shape of things to come. *Biochem J* **339 (Pt 3),** 481-8.

Branda, C. S., and Dymecki, S. M. (2004). Talking about a revolution: The impact of site-specific recombinases on genetic analyses in mice. *Dev Cell* **6,** 7-28.

Bretaud, S., Lee, S., and Guo, S. (2004). Sensitivity of zebrafish to environmental toxins implicated in Parkinson's disease. *Neurotoxicol Teratol* **26,** 857-64.

Brogna, S., and Ashburner, M. (1997). The Adh-related gene of Drosophila melanogaster is expressed as a functional dicistronic messenger RNA: multigenic transcription in higher organisms. *Embo J* **16,** 2023-31.

Buckland, P. R. (2003). Polymorphically duplicated genes: their relevance to phenotypic variation in humans. *Ann Med* **35,** 308-15.

Cai, L., Zhang, J., and Duan, E. (2003). Dynamic distribution of epidermal growth factor during mouse embryo peri-implantation. *Cytokine* **23,** 170-8.

Cain, J. E., Hartwig, S., Bertram, J. F., and Rosenblum, N. D. (2008). Bone morphogenetic protein signaling in the developing kidney: present and future. *Differentiation*.

Calderwood, W. L. (1891). The head kidney of teleostean fishes. *Journal of the Marine Biological Association of the United Kingdom* **2,** 43-46.

Call, K. M., Glaser, T., Ito, C. Y., Buckler, A. J., Pelletier, J., Haber, D. A., Rose, E. A., Kral, A., Yeger, H., Lewis, W. H., and et al. (1990). Isolation and characterization of a zinc finger polypeptide gene at the human chromosome 11 Wilms' tumor locus. *Cell* **60,** 509-20.

Cappuzzo, F., Hirsch, F. R., Rossi, E., Bartolini, S., Ceresoli, G. L., Bemis, L., Haney, J., Witta, S., Danenberg, K., Domenichini, I., Ludovini, V., Magrini, E., Gregorc, V., Doglioni, C., Sidoni, A., Tonato, M., Franklin, W. A., Crino, L., Bunn, P. A., Jr., and Varella-Garcia, M. (2005). Epidermal growth factor receptor gene and protein and gefitinib sensitivity in non-small-cell lung cancer. *J Natl Cancer Inst* **97,** 643-55.

Carev, D., Saraga, M., and Saraga-Babic, M. (2008). Expression of intermediate filaments, EGF and TGF-alpha in early human kidney development. *J Mol Histol* **39,** 227-35.

Carmany-Rampey, A., and Schier, A. F. (2001). Single-cell internalization during zebrafish gastrulation. *Curr Biol* **11,** 1261-5.

Carroll, D., Morton, J. J., Beumer, K. J., and Segal, D. J. (2006). Design, construction and in vitro testing of zinc finger nucleases. *Nat Protoc* **1,** 1329-41.

Celeste, A. J., Rosen, V., Buecker, J. L., Kriz, R., Wang, E. A., and Wozney, J. M. (1986). Isolation of the human gene for bone gla protein utilizing mouse and rat cDNA clones. *Embo J* **5,** 1885-90.

Chapman, D. L., and Papaioannou, V. E. (1998). Three neural tubes in mouse embryos with mutations in the T-box gene Tbx6. *Nature* **391,** 695-7.

Chen, J. N., Haffter, P., Odenthal, J., Vogelsang, E., Brand, M., van Eeden, F. J., Furutani-Seiki, M., Granato, M., Hammerschmidt, M., Heisenberg, C. P., Jiang, Y. J., Kane, D. A., Kelsh, R. N., Mullins, M. C., and Nusslein-Volhard, C. (1996). Mutations affecting the cardiovascular system and other internal organs in zebrafish. *Development* **123,** 293-302.

Chen, S., and Kimelman, D. (2000). The role of the yolk syncytial layer in germ layer patterning in zebrafish. *Development* **127,** 4681-9.

Chen, X., and Gumbiner, B. M. (2006). Paraxial protocadherin mediates cell sorting and tissue morphogenesis by regulating C-cadherin adhesion activity. *J Cell Biol* **174,** 301-13.

Cheng, J. C., Miller, A. L., and Webb, S. E. (2004). Organization and function of microfilaments during late epiboly in zebrafish embryos. *Dev Dyn* **231,** 313-23.

Chu, C. Y., Cheng, C. H., Chen, G. D., Chen, Y. C., Hung, C. C., Huang, K. Y., and Huang, C. J. (2007). The zebrafish erythropoietin: functional identification and biochemical characterization. *FEBS Lett* **581,** 4265-71.

Compernolle, V., Brusselmans, K., Franco, D., Moorman, A., Dewerchin, M., Collen, D., and Carmeliet, P. (2003). Cardia bifida, defective heart development and abnormal neural crest migration in embryos lacking hypoxia-inducible factor-1alpha. *Cardiovasc Res* **60,** 569-79.

Cooke, J. (1975). Control of somite number during morphogenesis of a vertebrate, Xenopus laevis. *Nature* **254,** 196-9.

D'Amico, L. A., and Cooper, M. S. (2001). Morphogenetic domains in the yolk syncytial layer of axiating zebrafish embryos. *Dev Dyn* **222,** 611-24.

Danilova, N., Hohman, V. S., Sacher, F., Ota, T., Willett, C. E., and Steiner, L. A. (2004). T cells and the thymus in developing zebrafish. *Dev Comp Immunol* **28,** 755-67.

Danilova, N., and Steiner, L. A. (2002). B cells develop in the zebrafish pancreas. *Proc Natl Acad Sci U S A* **99,** 13711-6.

Davidson, A. J., and Zon, L. I. (2004). The 'definitive' (and 'primitive') guide to zebrafish hematopoiesis. *Oncogene* **23,** 7233-46.

Denkers, N., Garcia-Villalba, P., Rodesch, C. K., Nielson, K. R., and Mauch, T. J. (2004). FISHing for chick genes: Triple-label whole-mount fluorescence in situ hybridization detects simultaneous and overlapping gene expression in avian embryos. *Dev Dyn* **229,** 651-7.

Dequeant, M. L., and Pourquie, O. (2008). Segmental patterning of the vertebrate embryonic axis. *Nat Rev Genet* **9,** 370-82.

Diogo, R., and Abdala, V. (2007). Comparative anatomy, homologies and evolution of the pectoral muscles of bony fish and tetrapods: a new insight. *J Morphol* **268,** 504-17.

Doyon, Y., McCammon, J. M., Miller, J. C., Faraji, F., Ngo, C., Katibah, G. E., Amora, R., Hocking, T. D., Zhang, L., Rebar, E. J., Gregory, P. D., Urnov, F.

D., and Amacher, S. L. (2008). Heritable targeted gene disruption in zebrafish using designed zinc-finger nucleases. *Nat Biotechnol* **26,** 702-8.

Dressler, G. R. (2006). The cellular basis of kidney development. *Annu Rev Cell Dev Biol* **22,** 509-29.

Driever, W. (2000). Developmental biology. Bringing two hearts together. *Nature* **406,** 141-2.

Driever, W., Solnica-Krezel, L., Schier, A. F., Neuhauss, S. C., Malicki, J., Stemple, D. L., Stainier, D. Y., Zwartkruis, F., Abdelilah, S., Rangini, Z., Belak, J., and Boggs, C. (1996). A genetic screen for mutations affecting embryogenesis in zebrafish. *Development* **123,** 37-46.

Drummond, I. A. (2005). Kidney development and disease in the zebrafish. *J Am Soc Nephrol* **16,** 299-304.

Drummond, I. A., Majumdar, A., Hentschel, H., Elger, M., Solnica-Krezel, L., Schier, A. F., Neuhauss, S. C., Stemple, D. L., Zwartkruis, F., Rangini, Z., Driever, W., and Fishman, M. C. (1998). Early development of the zebrafish pronephros and analysis of mutations affecting pronephric function. *Development* **125,** 4655-67.

Dudley, A. T., Lyons, K. M., and Robertson, E. J. (1995). A requirement for bone morphogenetic protein-7 during development of the mammalian kidney and eye. *Genes Dev* **9,** 2795-807.

Dye, M. J., Gromak, N., and Proudfoot, N. J. (2006). Exon tethering in transcription by RNA polymerase II. *Mol Cell* **21,** 849-59.

Dye, M. J., and Proudfoot, N. J. (1999). Terminal exon definition occurs cotranscriptionally and promotes termination of RNA polymerase II. *Mol Cell* **3,** 371-8.

Dye, M. J., and Proudfoot, N. J. (2001). Multiple transcript cleavage precedes polymerase release in termination by RNA polymerase II. *Cell* **105,** 669-81.

Echelard, Y., Epstein, D. J., St-Jacques, B., Shen, L., Mohler, J., McMahon, J. A., and McMahon, A. P. (1993). Sonic hedgehog, a member of a family of putative signaling molecules, is implicated in the regulation of CNS polarity. *Cell* **75,** 1417-30.

Editorial. (2000). Targeting zebrafish. *Nat Genet* **26,** 129-130.

Egerer, G., Taugner, R., and Tiedemann, K. (1984). Renin immunohistochemistry in the mesonephros and metanephros of the pig embryo. *Histochemistry* **81,** 385-90.

Ericson, J., Muhr, J., Placzek, M., Lints, T., Jessell, T. M., and Edlund, T. (1995). Sonic hedgehog induces the differentiation of ventral forebrain neurons: a common signal for ventral patterning within the neural tube. *Cell* **81,** 747-56.

Esengil, H., Chang, V., Mich, J. K., and Chen, J. K. (2007). Small-molecule regulation of zebrafish gene expression. *Nat Chem Biol* **3,** 154-5.

Fedorova, S., Miyamoto, R., Harada, T., Isogai, S., Hashimoto, H., Ozato, K., and Wakamatsu, Y. (2008). Renal glomerulogenesis in medaka fish, Oryzias latipes. *Dev Dyn* **237,** 2342-52.

Feldman, B., Dougan, S. T., Schier, A. F., and Talbot, W. S. (2000). Nodal-related signals establish mesendodermal fate and trunk neural identity in zebrafish. *Curr Biol* **10,** 531-4.

Feldman, B., Gates, M. A., Egan, E. S., Dougan, S. T., Rennebeck, G., Sirotkin, H. I., Schier, A. F., and Talbot, W. S. (1998). Zebrafish organizer development and germ-layer formation require nodal-related signals. *Nature* **395,** 181-5.

Fishelson, L. (1996). Ontogenesis and functional metamorphosis of the head-kidney in bottomspawner and mouthbrooder cichlid fishes (Cichlidae, Teleostei). *Journal of Morphology* **229,** 1-21.

Fiuza, U. M., and Arias, A. M. (2007). Cell and molecular biology of Notch. *J Endocrinol* **194,** 459-74.

Fondell, J. D., Ge, H., and Roeder, R. G. (1996). Ligand induction of a transcriptionally active thyroid hormone receptor coactivator complex. *Proc Natl Acad Sci U S A* **93,** 8329-33.

Francis-West, P., and Hill, R. (2008). Uncoupling the role of sonic hedgehog in limb development: growth and specification. *Sci Signal* **1,** pe34.

Fu, Y., Wang, Y., and Evans, S. M. (1998). Viral sequences enable efficient and tissue-specific expression of transgenes in Xenopus. *Nat Biotechnol* **16,** 253-7.

Funayama, N., Sato, Y., Matsumoto, K., Ogura, T., and Takahashi, Y. (1999). Coelom formation: binary decision of the lateral plate mesoderm is controlled by the ectoderm. *Development* **126,** 4129-38.

Furutani-Seiki, M., and Wittbrodt, J. (2004). Medaka and zebrafish, an evolutionary twin study. *Mech Dev* **121,** 629-37.

Gao, X., Chen, X., Taglienti, M., Rumballe, B., Little, M. H., and Kreidberg, J. A. (2005). Angioblast-mesenchyme induction of early kidney development is mediated by Wt1 and Vegfa. *Development* **132,** 5437-49.

Garcia-Martinez, V., Alvarez, I. S., and Schoenwolf, G. C. (1993). Locations of the ectodermal and nonectodermal subdivisions of the epiblast at stages 3 and 4 of avian gastrulation and neurulation. *J Exp Zool* **267,** 431-46.

Gessler, M., Poustka, A., Cavenee, W., Neve, R. L., Orkin, S. H., and Bruns, G. A. (1990). Homozygous deletion in Wilms tumours of a zinc-finger gene identified by chromosome jumping. *Nature* **343,** 774-8.

Gil, A., and Proudfoot, N. J. (1987). Position-dependent sequence elements downstream of AAUAAA are required for efficient rabbit beta-globin mRNA 3' end formation. *Cell* **49,** 399-406.

Gilbert, S. F., Tyler, M. S., and Kozlowski, R. N. (2000). Developmental biology, pp. xviii, 749p. Sinauer, Sunderland, Mass.

Gilmartin, G. M., McDevitt, M. A., and Nevins, J. R. (1988). Multiple factors are required for specific RNA cleavage at a poly(A) addition site. *Genes Dev* **2,** 578-87.

Glickman, N. S., Kimmel, C. B., Jones, M. A., and Adams, R. J. (2003). Shaping the zebrafish notochord. *Development* **130,** 873-87.

Golbus, M. S., Calarco, P. G., and Epstein, C. J. (1973). The effects of inhibitors of RNA synthesis (alpha-amanitin and actinomycin D) on preimplantation mouse embryogenesis. *J Exp Zool* **186,** 207-16.

Gore, A. V., Maegawa, S., Cheong, A., Gilligan, P. C., Weinberg, E. S., and Sampath, K. (2005). The zebrafish dorsal axis is apparent at the four-cell stage. *Nature* **438,** 1030-5.

Graubert, T. A., Cahan, P., Edwin, D., Selzer, R. R., Richmond, T. A., Eis, P. S., Shannon, W. D., Li, X., McLeod, H. L., Cheverud, J. M., and Ley, T. J. (2007). A high-resolution map of segmental DNA copy number variation in the mouse genome. *PLoS Genet* **3,** e3.

Gray, N. K., and Wickens, M. (1998). Control of translation initiation in animals. *Annu Rev Cell Dev Biol* **14,** 399-458.

Griffin, K., Patient, R., and Holder, N. (1995). Analysis of FGF function in normal and no tail zebrafish embryos reveals separate mechanisms for formation of the trunk and the tail. *Development* **121,** 2983-94.

Griffin, K. J., Amacher, S. L., Kimmel, C. B., and Kimelman, D. (1998). Molecular identification of spadetail: regulation of zebrafish trunk and tail mesoderm formation by T-box genes. *Development* **125,** 3379-88.

Griffin, K. J., and Kimelman, D. (2002). One-Eyed Pinhead and Spadetail are essential for heart and somite formation. *Nat Cell Biol* **4,** 821-5.

Griffin, K. J., and Kimelman, D. (2003). Interplay between FGF, one-eyed pinhead, and T-box transcription factors during zebrafish posterior development. *Dev Biol* **264,** 456-66.

Gritsman, K., Zhang, J., Cheng, S., Heckscher, E., Talbot, W. S., and Schier, A. F. (1999). The EGF-CFC protein one-eyed pinhead is essential for nodal signaling. *Cell* **97,** 121-32.

Grobstein, C. (1956). Trans-filter induction of tubules in mouse metanephrogenic mesenchyme. *Exp Cell Res* **10,** 424-40.

Gromak, N., West, S., and Proudfoot, N. J. (2006). Pause sites promote transcriptional termination of mammalian RNA polymerase II. *Mol Cell Biol* **26,** 3986-96.

Gu, H., Das Gupta, J., and Schoenberg, D. R. (1999). The poly(A)-limiting element is a conserved cis-acting sequence that regulates poly(A) tail length on nuclear pre-mRNAs. *Proc Natl Acad Sci U S A* **96,** 8943-8.

Guo, Z. M., Xu, K., Yue, Y., Huang, B., Deng, X. Y., Zhong, N. Q., Hong, X., Chen, X. G., and Xiao, D. (2005). Temporal control of Cre recombinase-mediated in vitro DNA recombination by Tet-on gene expression system. *Acta Biochim Biophys Sin (Shanghai)* **37,** 133-8.

Guyton, A. C., and Hall, J. E. (1996). "Textbook of medical physiology." W.B. Saunders, Philadelphia, Pa. ; London.

Haffter, P., Granato, M., Brand, M., Mullins, M. C., Hammerschmidt, M., Kane, D. A., Odenthal, J., van Eeden, F. J., Jiang, Y. J., Heisenberg, C. P., Kelsh, R. N., Furutani-Seiki, M., Vogelsang, E., Beuchle, D., Schach, U., Fabian, C., and Nusslein-Volhard, C. (1996). The identification of genes with unique and essential functions in the development of the zebrafish, Danio rerio. *Development* **123,** 1-36.

Haffter, P., and Nusslein-Volhard, C. (1996). Large scale genetics in a small vertebrate, the zebrafish. *Int J Dev Biol* **40,** 221-7.

Hagenbuchle, O., Wellauer, P. K., Cribbs, D. L., and Schibler, U. (1984). Termination of transcription in the mouse alpha-amylase gene Amy-2a occurs at multiple sites downstream of the polyadenylation site. *Cell* **38,** 737-44.

Hahn, S. (2004). Structure and mechanism of the RNA polymerase II transcription machinery. *Nat Struct Mol Biol* **11,** 394-403.

Hall, C., Flores, M. V., Storm, T., Crosier, K., and Crosier, P. (2007). The zebrafish lysozyme C promoter drives myeloid-specific expression in transgenic fish. *BMC Dev Biol* **7,** 42.

Halpern, M. E., Hatta, K., Amacher, S. L., Talbot, W. S., Yan, Y. L., Thisse, B., Thisse, C., Postlethwait, J. H., and Kimmel, C. B. (1997). Genetic interactions in zebrafish midline development. *Dev Biol* **187,** 154-70.

Hastie, N. D. (1994). The genetics of Wilms' tumor--a case of disrupted development. *Annu Rev Genet* **28,** 523-58.

Hatada, Y., and Stern, C. D. (1994). A fate map of the epiblast of the early chick embryo. *Development* **120,** 2879-89.

Hayashi, Y., Furue, M. K., Okamoto, T., Ohnuma, K., Myoishi, Y., Fukuhara, Y., Abe, T., Sato, J. D., Hata, R., and Asashima, M. (2007). Integrins regulate mouse embryonic stem cell self-renewal. *Stem Cells* **25,** 3005-15.

Heasman, J. (2006). Patterning the early Xenopus embryo. *Development* **133,** 1205-17.

Heath, C. V., Denome, R. M., and Cole, C. N. (1990). Spatial constraints on polyadenylation signal function. *J Biol Chem* **265,** 9098-104.

Heisenberg, C. P., and Tada, M. (2002). Zebrafish gastrulation movements: bridging cell and developmental biology. *Semin Cell Dev Biol* **13,** 471-9.

Heisenberg, C. P., Tada, M., Rauch, G. J., Saude, L., Concha, M. L., Geisler, R., Stemple, D. L., Smith, J. C., and Wilson, S. W. (2000). Silberblick/Wnt11 mediates convergent extension movements during zebrafish gastrulation. *Nature* **405,** 76-81.

Helde, K. A., Wilson, E. T., Cretekos, C. J., and Grunwald, D. J. (1994). Contribution of early cells to the fate map of the zebrafish gastrula. *Science* **265,** 517-20.

Heo, J. S., and Han, H. J. (2006). PKC and MAPKs pathways mediate EGF-induced stimulation of 2-deoxyglucose uptake in mouse embryonic stem cells. *Cell Physiol Biochem* **17,** 145-58.

Herbst, R. S. (2004). Review of epidermal growth factor receptor biology. *Int J Radiat Oncol Biol Phys* **59,** 21-6.

Higashijima, S., Okamoto, H., Ueno, N., Hotta, Y., and Eguchi, G. (1997). High-frequency generation of transgenic zebrafish which reliably express GFP in whole muscles or the whole body by using promoters of zebrafish origin. *Dev Biol* **192,** 289-99.

Hirata, H., Saint-Amant, L., Waterbury, J., Cui, W., Zhou, W., Li, Q., Goldman, D., Granato, M., and Kuwada, J. Y. (2004). accordion, a zebrafish behavioral mutant, has a muscle relaxation defect due to a mutation in the ATPase Ca2+ pump SERCA1. *Development* **131,** 5457-68.

Ho, R. K., and Kane, D. A. (1990). Cell-autonomous action of zebrafish spt-1 mutation in specific mesodermal precursors. *Nature* **348,** 728-30.

Hoess, R. H., and Abremski, K. (1985). Mechanism of strand cleavage and exchange in the Cre-lox site-specific recombination system. *J Mol Biol* **181,** 351-62.

Hogan, B. L. (1996). Bone morphogenetic proteins: multifunctional regulators of vertebrate development. *Genes Dev* **10,** 1580-94.

Hong, S. K., Haldin, C. E., Lawson, N. D., Weinstein, B. M., Dawid, I. B., and Hukriede, N. A. (2005). The zebrafish kohtalo/trap230 gene is required for the development of the brain, neural crest, and pronephric kidney. *Proc Natl Acad Sci U S A* **102,** 18473-8.

Horne-Badovinac, S., Rebagliati, M., and Stainier, D. Y. (2003). A cellular framework for gut-looping morphogenesis in zebrafish. *Science* **302,** 662-5.

Hoshijima, K., and Hirose, S. (2007). Expression of endocrine genes in zebrafish larvae in response to environmental salinity. *J Endocrinol* **193,** 481-91.

Houart, C., Westerfield, M., and Wilson, S. W. (1998). A small population of anterior cells patterns the forebrain during zebrafish gastrulation. *Nature* **391,** 788-92.

Houghton, F. D. (2005). Role of gap junctions during early embryo development. *Reproduction* **129,** 129-35.

Hoyme, H. E., Higginbottom, M. C., and Jones, K. L. (1981). Vascular etiology of disruptive structural defects in monozygotic twins. *Pediatrics* **67,** 288-91.

Hsiao, C. D., Hsieh, F. J., and Tsai, H. J. (2001). Enhanced expression and stable transmission of transgenes flanked by inverted terminal repeats from adeno-associated virus in zebrafish. *Dev Dyn* **220,** 323-36.

Hsu, H. J., Lin, G., and Chung, B. C. (2003). Parallel early development of zebrafish interrenal glands and pronephros: differential control by wt1 and ff1b. *Development* **130,** 2107-16.

Hu, J., Lutz, C. S., Wilusz, J., and Tian, B. (2005). Bioinformatic identification of candidate cis-regulatory elements involved in human mRNA polyadenylation. *Rna* **11,** 1485-93.

Huang, C. J., Jou, T. S., Ho, Y. L., Lee, W. H., Jeng, Y. T., Hsieh, F. J., and Tsai, H. J. (2005). Conditional expression of a myocardium-specific transgene in zebrafish transgenic lines. *Dev Dyn* **233,** 1294-303.

Huang, C. J., Lin, J. Y., and Tsai, H. J. (1999). Two distinct c-ski cDNAs of fish, tilapia (Oreochromis aurea). *Mol Reprod Dev* **54,** 223-31.

Huang, C. J., Tu, C. T., Hsiao, C. D., Hsieh, F. J., and Tsai, H. J. (2003). Germ-line transmission of a myocardium-specific GFP transgene reveals critical regulatory elements in the cardiac myosin light chain 2 promoter of zebrafish. *Dev Dyn* **228,** 30-40.

Huelsken, J., and Birchmeier, W. (2001). New aspects of Wnt signaling pathways in higher vertebrates. *Curr Opin Genet Dev* **11,** 547-53.

Hurt, J. A., Thibodeau, S. A., Hirsh, A. S., Pabo, C. O., and Joung, J. K. (2003). Highly specific zinc finger proteins obtained by directed domain shuffling and cell-based selection. *Proc Natl Acad Sci U S A* **100,** 12271-6.

Iafrate, A. J., Feuk, L., Rivera, M. N., Listewnik, M. L., Donahoe, P. K., Qi, Y., Scherer, S. W., and Lee, C. (2004). Detection of large-scale variation in the human genome. *Nat Genet* **36,** 949-51.

Iimura, T., Yang, X., Weijer, C. J., and Pourquie, O. (2007). Dual mode of paraxial mesoderm formation during chick gastrulation. *Proc Natl Acad Sci U S A* **104,** 2744-9.

Ingham, P. W., and McMahon, A. P. (2001). Hedgehog signaling in animal development: paradigms and principles. *Genes Dev* **15,** 3059-87.

Iwamatsu, T. (2004). Stages of normal development in the medaka Oryzias latipes. *Mech Dev* **121,** 605-18.

Jackson, R. J., and Kaminski, A. (1995). Internal initiation of translation in eukaryotes: the picornavirus paradigm and beyond. *Rna* **1,** 985-1000.

James, R. G., Kamei, C. N., Wang, Q., Jiang, R., and Schultheiss, T. M. (2006). Odd-skipped related 1 is required for development of the metanephric kidney and regulates formation and differentiation of kidney precursor cells. *Development* **133,** 2995-3004.

James, R. G., and Schultheiss, T. M. (2003). Patterning of the avian intermediate mesoderm by lateral plate and axial tissues. *Dev Biol* **253,** 109-24.

James, R. G., and Schultheiss, T. M. (2005). Bmp signaling promotes intermediate mesoderm gene expression in a dose-dependent, cell-autonomous and translation-dependent manner. *Dev Biol* **288,** 113-25.

Kalra, D., Broomhall, J., and Williams, J. (1985). Horseshoe kidney in one of identical twin girls. *J Urol* **134,** 113.

Kane, D. A., and Kimmel, C. B. (1993). The zebrafish midblastula transition. *Development* **119,** 447-56.

Kanka, J. (2003). Gene expression and chromatin structure in the pre-implantation embryo. *Theriogenology* **59,** 3-19.

Kawakami, K. (2005). Transposon tools and methods in zebrafish. *Dev Dyn* **234,** 244-54.

Kawakami, K., and Hopkins, N. (1996). Rapid identification of transgenic zebrafish. *Trends Genet* **12,** 9-10.

Keller, P. J., Schmidt, A. D., Wittbrodt, J., and Stelzer, E. H. (2008). Reconstruction of Zebrafish Early Embryonic Development by Scanned Light Sheet Microscopy. *Science*.

Keller, R., Davidson, L., Edlund, A., Elul, T., Ezin, M., Shook, D., and Skoglund, P. (2000). Mechanisms of convergence and extension by cell intercalation. *Philos Trans R Soc Lond B Biol Sci* **355,** 897-922.

Kennedy, B. N., Stearns, G. W., Smyth, V. A., Ramamurthy, V., van Eeden, F., Ankoudinova, I., Raible, D., Hurley, J. B., and Brockerhoff, S. E. (2004). Zebrafish rx3 and mab21l2 are required during eye morphogenesis. *Dev Biol* **270,** 336-49.

Kiecker, C., and Niehrs, C. (2001). The role of prechordal mesendoderm in neural patterning. *Curr Opin Neurobiol* **11,** 27-33.

Kikuchi, Y., Agathon, A., Alexander, J., Thisse, C., Waldron, S., Yelon, D., Thisse, B., and Stainier, D. Y. (2001). casanova encodes a novel Sox-related protein necessary and sufficient for early endoderm formation in zebrafish. *Genes Dev* **15,** 1493-505.

Kikuchi, Y., Trinh, L. A., Reiter, J. F., Alexander, J., Yelon, D., and Stainier, D. Y. (2000). The zebrafish bonnie and clyde gene encodes a Mix family homeodomain protein that regulates the generation of endodermal precursors. *Genes Dev* **14,** 1279-89.

Kikyo, N., and Wolffe, A. P. (2000). Reprogramming nuclei: insights from cloning, nuclear transfer and heterokaryons. *J Cell Sci* **113 (Pt 1),** 11-20.

Kim, H. J., Schleiffarth, J. R., Jessurun, J., Sumanas, S., Petryk, A., Lin, S., and Ekker, S. C. (2005). Wnt5 signaling in vertebrate pancreas development. *BMC Biol* **3,** 23.

Kim, S. J., and Martinson, H. G. (2003). Poly(A)-dependent transcription termination: continued communication of the poly(A) signal with the polymerase is required long after extrusion in vivo. *J Biol Chem* **278,** 41691-701.

Kim, Y. G., Cha, J., and Chandrasegaran, S. (1996). Hybrid restriction enzymes: zinc finger fusions to Fok I cleavage domain. *Proc Natl Acad Sci U S A* **93,** 1156-60.

Kimmel, C. B., Ballard, W. W., Kimmel, S. R., Ullmann, B., and Schilling, T. F. (1995). Stages of embryonic development of the zebrafish. *Dev Dyn* **203,** 253-310.

Kimmel, C. B., Kane, D. A., Walker, C., Warga, R. M., and Rothman, M. B. (1989). A mutation that changes cell movement and cell fate in the zebrafish embryo. *Nature* **337,** 358-62.

Kimmel, C. B., and Law, R. D. (1985a). Cell lineage of zebrafish blastomeres. I. Cleavage pattern and cytoplasmic bridges between cells. *Dev Biol* **108,** 78-85.

Kimmel, C. B., and Law, R. D. (1985b). Cell lineage of zebrafish blastomeres. II. Formation of the yolk syncytial layer. *Dev Biol* **108,** 86-93.

Kimmel, C. B., and Warga, R. M. (1987). Indeterminate cell lineage of the zebrafish embryo. *Dev Biol* **124,** 269-80.

Kimmel, C. B., Warga, R. M., and Schilling, T. F. (1990). Origin and organization of the zebrafish fate map. *Development* **108,** 581-94.

Klaus, A., and Birchmeier, W. (2008). Wnt signalling and its impact on development and cancer. *Nat Rev Cancer* **8,** 387-98.

Koshida, S., Shinya, M., Mizuno, T., Kuroiwa, A., and Takeda, H. (1998). Initial anteroposterior pattern of the zebrafish central nervous system is determined by differential competence of the epiblast. *Development* **125,** 1957-66.

Kramer-Zucker, A. G., Wiessner, S., Jensen, A. M., and Drummond, I. A. (2005). Organization of the pronephric filtration apparatus in zebrafish requires Nephrin, Podocin and the FERM domain protein Mosaic eyes. *Dev Biol* **285,** 316-29.

Krauss, S., Concordet, J. P., and Ingham, P. W. (1993). A functionally conserved homolog of the Drosophila segment polarity gene hh is expressed in tissues with polarizing activity in zebrafish embryos. *Cell* **75,** 1431-44.

Kreidberg, J. A., Sariola, H., Loring, J. M., Maeda, M., Pelletier, J., Housman, D., and Jaenisch, R. (1993). WT-1 is required for early kidney development. *Cell* **74,** 679-91.

Krieg, M., Arboleda-Estudillo, Y., Puech, P. H., Kafer, J., Graner, F., Muller, D. J., and Heisenberg, C. P. (2008). Tensile forces govern germ-layer organization in zebrafish. *Nat Cell Biol* **10,** 429-36.

Kubota, F., Murakami, T., Mogi, K., and Yorifuji, H. (2007). Cadherin-6 is required for zebrafish nephrogenesis during early development. *Int J Dev Biol* **51,** 123-9.

Kudoh, T., and Dawid, I. B. (2001). Zebrafish mab21l2 is specifically expressed in the presumptive eye and tectum from early somitogenesis onwards. *Mech Dev* **109,** 95-8.

Kupperman, E., An, S., Osborne, N., Waldron, S., and Stainier, D. Y. (2000). A sphingosine-1-phosphate receptor regulates cell migration during vertebrate heart development. *Nature* **406,** 192-5.

Kuure, S., Vuolteenaho, R., and Vainio, S. (2000). Kidney morphogenesis: cellular and molecular regulation. *Mech Dev* **92,** 31-45.

Kwan, K. M., Fujimoto, E., Grabher, C., Mangum, B. D., Hardy, M. E., Campbell, D. S., Parant, J. M., Yost, H. J., Kanki, J. P., and Chien, C. B. (2007). The Tol2kit: a multisite gateway-based construction kit for Tol2 transposon transgenesis constructs. *Dev Dyn* **236,** 3088-99.

Lametschwandtner, A. (1995). Microvascularization of corpuscles of Stannius in teleost fishes. *Microsc Res Tech* **32,** 104-11.

Langenau, D. M., Feng, H., Berghmans, S., Kanki, J. P., Kutok, J. L., and Look, A. T. (2005). Cre/lox-regulated transgenic zebrafish model with conditional myc-induced T cell acute lymphoblastic leukemia. *Proc Natl Acad Sci U S A* **102,** 6068-73.

Lappi, D. A. (1995). Tumor targeting through fibroblast growth factor receptors. *Semin Cancer Biol* **6,** 279-88.

Lee, S. C., Mietchen, D., Cho, J. H., Kim, Y. S., Kim, C., Hong, K. S., Lee, C., Kang, D., Lee, W., and Cheong, C. (2007). In vivo magnetic resonance microscopy of differentiation in Xenopus laevis embryos from the first cleavage onwards. *Differentiation* **75,** 84-92.

Leiter, E. (1972). Horseshoe kidney: discordance in monozygotic twins. *J Urol* **108,** 683-4.

Leung, C. F., Webb, S. E., and Miller, A. L. (1998). Calcium transients accompany ooplasmic segregation in zebrafish embryos. *Dev Growth Differ* **40,** 313-26.

Li, Y. X., Farrell, M. J., Liu, R., Mohanty, N., and Kirby, M. L. (2000). Double-stranded RNA injection produces null phenotypes in zebrafish. *Dev Biol* **217,** 394-405.

Lian, J., Stewart, C., Puchacz, E., Mackowiak, S., Shalhoub, V., Collart, D., Zambetti, G., and Stein, G. (1989). Structure of the rat osteocalcin gene and regulation of vitamin D-dependent expression. *Proc Natl Acad Sci U S A* **86,** 1143-7.

Liang, P., Jones, C. A., Bisgrove, B. W., Song, L., Glenn, S. T., Yost, H. J., and Gross, K. W. (2004). Genomic characterization and expression analysis of the first nonmammalian renin genes from zebrafish and pufferfish. *Physiol Genomics* **16,** 314-22.

Liao, W., Bisgrove, B. W., Sawyer, H., Hug, B., Bell, B., Peters, K., Grunwald, D. J., and Stainier, D. Y. (1997). The zebrafish gene cloche acts upstream of a flk-1 homologue to regulate endothelial cell differentiation. *Development* **124,** 381-9.

Lin, F., Sepich, D. S., Chen, S., Topczewski, J., Yin, C., Solnica-Krezel, L., and Hamm, H. (2005). Essential roles of G{alpha}12/13 signaling in distinct cell behaviors driving zebrafish convergence and extension gastrulation movements. *J Cell Biol* **169,** 777-87.

Lissemore, J. L., and Starmer, W. T. (1999). Phylogenetic analysis of vertebrate and invertebrate Delta/Serrate/LAG-2 (DSL) proteins. *Mol Phylogenet Evol* **11,** 308-19.

Liu, A., Majumdar, A., Schauerte, H. E., Haffter, P., and Drummond, I. A. (2000). Zebrafish wnt4b expression in the floor plate is altered in sonic hedgehog and gli-2 mutants. *Mech Dev* **91,** 409-13.

Liu, P., Jenkins, N. A., and Copeland, N. G. (2003). A highly efficient recombineering-based method for generating conditional knockout mutations. *Genome Res* **13,** 476-84.

Liu, Q., Xia, Z., Zhong, X., and Case, C. C. (2002). Validated zinc finger protein designs for all 16 GNN DNA triplet targets. *J Biol Chem* **277,** 3850-6.

Logan, C. Y., and Nusse, R. (2004). The Wnt signaling pathway in development and disease. *Annu Rev Cell Dev Biol* **20,** 781-810.

Lonn, U., Lonn, S., Nylen, U., Stenkvist, B., and Vennstrom, B. (1992). Detection and temporal appearance of multiple copies of c-erb-B2 genes in advanced mammary carcinoma using fine needle biopsies and the polymerase chain reaction. *Breast Cancer Res Treat* **23,** 191-200.

Lopez-Sanchez, C., Garcia-Martinez, V., and Schoenwolf, G. C. (2001). Localization of cells of the prospective neural plate, heart and somites within the primitive streak and epiblast of avian embryos at intermediate primitive-streak stages. *Cells Tissues Organs* **169,** 334-46.

Majumdar, A., and Drummond, I. A. (1999). Podocyte differentiation in the absence of endothelial cells as revealed in the zebrafish avascular mutant, cloche. *Dev Genet* **24,** 220-9.

Majumdar, A., and Drummond, I. A. (2000). The zebrafish floating head mutant demonstrates podocytes play an important role in directing glomerular differentiation. *Dev Biol* **222,** 147-57.

Marshall, E. K., JR., and Smith, H. W. (1930). The glomerular development of the vertebrate kidney in relation to habitat. *Biol Bull* **59,** 135-153.

Massague, J. (1998). TGF-beta signal transduction. *Annu Rev Biochem* **67,** 753-91.

Mathieu, J., Griffin, K., Herbomel, P., Dickmeis, T., Strahle, U., Kimelman, D., Rosa, F. M., and Peyrieras, N. (2004). Nodal and Fgf pathways interact through a positive regulatory loop and synergize to maintain mesodermal cell populations. *Development* **131,** 629-41.

Matsui, T., Raya, A., Kawakami, Y., Callol-Massot, C., Capdevila, J., Rodriguez-Esteban, C., and Izpisua Belmonte, J. C. (2005). Noncanonical Wnt signaling regulates midline convergence of organ primordia during zebrafish development. *Genes Dev* **19,** 164-75.

McDermott, A., Gustafsson, M., Elsam, T., Hui, C. C., Emerson, C. P., Jr., and Borycki, A. G. (2005). Gli2 and Gli3 have redundant and context-dependent function in skeletal muscle formation. *Development* **132,** 345-57.

McDevitt, M. A., Hart, R. P., Wong, W. W., and Nevins, J. R. (1986). Sequences capable of restoring poly(A) site function define two distinct downstream elements. *Embo J* **5,** 2907-13.

McFadden, D. G., and Olson, E. N. (2002). Heart development: learning from mistakes. *Curr Opin Genet Dev* **12,** 328-35.

Meng, X., Noyes, M. B., Zhu, L. J., Lawson, N. D., and Wolfe, S. A. (2008). Targeted gene inactivation in zebrafish using engineered zinc-finger nucleases. *Nat Biotechnol* **26,** 695-701.

Michaud, J. L., Rosenquist, T., May, N. R., and Fan, C. M. (1998). Development of neuroendocrine lineages requires the bHLH-PAS transcription factor SIM1. *Genes Dev* **12,** 3264-75.

Minami, N., Suzuki, T., and Tsukamoto, S. (2007). Zygotic gene activation and maternal factors in mammals. *J Reprod Dev* **53,** 707-15.

Mizoguchi, T., Izawa, T., Kuroiwa, A., and Kikuchi, Y. (2006). Fgf signaling negatively regulates Nodal-dependent endoderm induction in zebrafish. *Dev Biol* **300,** 612-22.

Mizuno, T., Shinya, M., and Takeda, H. (1999). Cell and tissue transplantation in zebrafish embryos. *Methods Mol Biol* **127,** 15-28.

Mochizuki, E., Fukuta, K., Tada, T., Harada, T., Watanabe, N., Matsuo, S., Hashimoto, H., Ozato, K., and Wakamatsu, Y. (2005). Fish mesonephric model of polycystic kidney disease in medaka (Oryzias latipes) pc mutant. *Kidney Int* **68,** 23-34.

Moore, G. P. (1975). The RNA polymerase activity of the preimplantation mouse embryo. *J Embryol Exp Morphol* **34,** 291-8.

Moore, M. W., Klein, R. D., Farinas, I., Sauer, H., Armanini, M., Phillips, H., Reichardt, L. F., Ryan, A. M., Carver-Moore, K., and Rosenthal, A. (1996). Renal and neuronal abnormalities in mice lacking GDNF. *Nature* **382,** 76-9.

Moore-Scott, B. A., and Manley, N. R. (2005). Differential expression of Sonic hedgehog along the anterior-posterior axis regulates patterning of pharyngeal pouch endoderm and pharyngeal endoderm-derived organs. *Dev Biol* **278,** 323-35.

Mrowka, C., and Schedl, A. (2000). Wilms' tumor suppressor gene WT1: from structure to renal pathophysiologic features. *J Am Soc Nephrol* **11 Suppl 16,** S106-15.

Mudumana, S. P., Hentschel, D., Liu, Y., Vasilyev, A., and Drummond, I. A. (2008). odd skipped related1 reveals a novel role for endoderm in regulating kidney versus vascular cell fate. *Development* **135,** 3355-67.

Muller, F. (2005). Comparative aspects of alternative laboratory fish models. *Zebrafish* **2,** 47-54.

Mullins, M. C., Hammerschmidt, M., Haffter, P., and Nusslein-Volhard, C. (1994). Large-scale mutagenesis in the zebrafish: in search of genes controlling development in a vertebrate. *Curr Biol* **4,** 189-202.

Myers, D. C., Sepich, D. S., and Solnica-Krezel, L. (2002a). Bmp activity gradient regulates convergent extension during zebrafish gastrulation. *Dev Biol* **243,** 81-98.

Myers, D. C., Sepich, D. S., and Solnica-Krezel, L. (2002b). Convergence and extension in vertebrate gastrulae: cell movements according to or in search of identity? *Trends Genet* **18,** 447-55.

Nakada, T., Westhoff, C. M., Kato, A., and Hirose, S. (2007). Ammonia secretion from fish gill depends on a set of Rh glycoproteins. *Faseb J* **21,** 1067-74.

Nakao, S., Platek, A., Hirano, S., and Takeichi, M. (2008). Contact-dependent promotion of cell migration by the OL-protocadherin-Nap1 interaction. *J Cell Biol* **182,** 395-410.

Nasevicius, A., and Ekker, S. C. (2000). Effective targeted gene 'knockdown' in zebrafish. *Nat Genet* **26,** 216-20.

Nelson, W. J., and Nusse, R. (2004). Convergence of Wnt, beta-catenin, and cadherin pathways. *Science* **303,** 1483-7.

Newport, J., and Kirschner, M. (1982a). A major developmental transition in early Xenopus embryos: I. characterization and timing of cellular changes at the midblastula stage. *Cell* **30,** 675-86.

Newport, J., and Kirschner, M. (1982b). A major developmental transition in early Xenopus embryos: II. Control of the onset of transcription. *Cell* **30,** 687-96.

Nguyen, D. Q., Webber, C., and Ponting, C. P. (2006). Bias of selection on human copy-number variants. *PLoS Genet* **2,** e20.

Nilius, B., Owsianik, G., Voets, T., and Peters, J. A. (2007). Transient receptor potential cation channels in disease. *Physiol Rev* **87,** 165-217.

Nishimura, H., Ogawa, M., and Sawyer, W. H. (1973). Renin-angiotensin system in primitive bony fishes and a holocephalian. *Am J Physiol* **224,** 950-6.

O'Brien, J., Buckley, O., Doody, O., Ward, E., Persaud, T., and Torreggiani, W. (2008). Imaging of horseshoe kidneys and their complications. *J Med Imaging Radiat Oncol* **52,** 216-26.

Oates, A. C., Bruce, A. E., and Ho, R. K. (2000). Too much interference: injection of double-stranded RNA has nonspecific effects in the zebrafish embryo. *Dev Biol* **224,** 20-8.

Obara-Ishihara, T., Kuhlman, J., Niswander, L., and Herzlinger, D. (1999). The surface ectoderm is essential for nephric duct formation in intermediate mesoderm. *Development* **126,** 1103-8.

Ober, E. A., Olofsson, B., Makinen, T., Jin, S. W., Shoji, W., Koh, G. Y., Alitalo, K., and Stainier, D. Y. (2004). Vegfc is required for vascular development and endoderm morphogenesis in zebrafish. *EMBO Rep* **5,** 78-84.

Odenthal, J., Haffter, P., Vogelsang, E., Brand, M., van Eeden, F. J., Furutani-Seiki, M., Granato, M., Hammerschmidt, M., Heisenberg, C. P., Jiang, Y. J., Kane, D. A., Kelsh, R. N., Mullins, M. C., Warga, R. M., Allende, M. L., Weinberg, E. S., and Nusslein-Volhard, C. (1996a). Mutations affecting the formation of the notochord in the zebrafish, Danio rerio. *Development* **123,** 103-15.

Odenthal, J., Rossnagel, K., Haffter, P., Kelsh, R. N., Vogelsang, E., Brand, M., van Eeden, F. J., Furutani-Seiki, M., Granato, M., Hammerschmidt, M., Heisenberg, C. P., Jiang, Y. J., Kane, D. A., Mullins, M. C., and Nusslein-Volhard, C. (1996b). Mutations affecting xanthophore pigmentation in the zebrafish, Danio rerio. *Development* **123,** 391-8.

Oktem, H., Gozil, R., Calguner, E., Bahcelioglu, M., Mutlu, S., Kurkcuoglu, A., Yucel, D., Senol, E., Babus, T., and Kadioglu, D. (2008). Morphometric study of a horseshoe kidney. *Med Princ Pract* **17,** 80-3.

Ornitz, D. M., and Itoh, N. (2001). Fibroblast growth factors. *Genome Biol* **2,** REVIEWS3005.

Osheim, Y. N., Proudfoot, N. J., and Beyer, A. L. (1999). EM visualization of transcription by RNA polymerase II: downstream termination requires a poly(A) signal but not transcript cleavage. *Mol Cell* **3,** 379-87.

Pabo, C. O., Peisach, E., and Grant, R. A. (2001). Design and selection of novel Cys2His2 zinc finger proteins. *Annu Rev Biochem* **70,** 313-40.

Paffett-Lugassy, N., Hsia, N., Fraenkel, P. G., Paw, B., Leshinsky, I., Barut, B., Bahary, N., Caro, J., Handin, R., and Zon, L. I. (2007). Functional conservation of erythropoietin signaling in zebrafish. *Blood* **110,** 2718-26.

Pan, X., Wan, H., Chia, W., Tong, Y., and Gong, Z. (2005). Demonstration of site-directed recombination in transgenic zebrafish using the Cre/loxP system. *Transgenic Res* **14,** 217-23.

Patel, S. R., and Dressler, G. R. (2004). Expression of Pax2 in the intermediate mesoderm is regulated by YY1. *Dev Biol* **267,** 505-16.

Patel, T. V., and Singh, A. K. (2008). Crossed fused ectopia of the kidneys. *Kidney Int* **73,** 662.

Perner, B., Englert, C., and Bollig, F. (2007). The Wilms tumor genes wt1a and wt1b control different steps during formation of the zebrafish pronephros. *Dev Biol* **309,** 87-96.

Pichel, J. G., Shen, L., Sheng, H. Z., Granholm, A. C., Drago, J., Grinberg, A., Lee, E. J., Huang, S. P., Saarma, M., Hoffer, B. J., Sariola, H., and Westphal, H. (1996). Defects in enteric innervation and kidney development in mice lacking GDNF. *Nature* **382,** 73-6.

Piotrowska, K., and Zernicka-Goetz, M. (2002). Early patterning of the mouse embryo--contributions of sperm and egg. *Development* **129,** 5803-13.

Placzek, M. (1995). The role of the notochord and floor plate in inductive interactions. *Curr Opin Genet Dev* **5,** 499-506.

Porteus, M. H., and Carroll, D. (2005). Gene targeting using zinc finger nucleases. *Nat Biotechnol* **23,** 967-73.

Pourquie, O., Fan, C. M., Coltey, M., Hirsinger, E., Watanabe, Y., Breant, C., Francis-West, P., Brickell, P., Tessier-Lavigne, M., and Le Douarin, N. M. (1996). Lateral and axial signals involved in avian somite patterning: a role for BMP4. *Cell* **84,** 461-71.

Prioleau, M. N., Huet, J., Sentenac, A., and Mechali, M. (1994). Competition between chromatin and transcription complex assembly regulates gene expression during early development. *Cell* **77,** 439-49.

Prodocimo, V., and Freire, C. A. (2003). Glomeruli and renal tubules are restricted to the cranial kidney of the adult estuarine Sphoeroides testudineus. *J Fish Biol* **63,** 1258-1265.

Proudfoot, N. J., Furger, A., and Dye, M. J. (2002). Integrating mRNA processing with transcription. *Cell* **108,** 501-12.

Rackley, R. R., Flenniken, A. M., Kuriyan, N. P., Kessler, P. M., Stoler, M. H., and Williams, B. R. (1993). Expression of the Wilms' tumor suppressor gene WT1 during mouse embryogenesis. *Cell Growth Differ* **4,** 1023-31.

Rahman, S., Oberdorf, A., Montecino, M., Tanhauser, S. M., Lian, J. B., Stein, G. S., Laipis, P. J., and Stein, J. L. (1993). Multiple copies of the bone-specific osteocalcin gene in mouse and rat. *Endocrinology* **133,** 3050-3.

Redon, R., Ishikawa, S., Fitch, K. R., Feuk, L., Perry, G. H., Andrews, T. D., Fiegler, H., Shapero, M. H., Carson, A. R., Chen, W., Cho, E. K., Dallaire, S., Freeman, J. L., Gonzalez, J. R., Gratacos, M., Huang, J., Kalaitzopoulos, D., Komura, D., MacDonald, J. R., Marshall, C. R., Mei, R., Montgomery, L., Nishimura, K., Okamura, K., Shen, F., Somerville, M. J., Tchinda, J., Valsesia, A., Woodwark, C., Yang, F., Zhang, J., Zerjal, T., Zhang, J., Armengol, L., Conrad, D. F., Estivill, X., Tyler-Smith, C., Carter, N. P., Aburatani, H., Lee, C., Jones, K. W., Scherer, S. W., and Hurles, M. E. (2006). Global variation in copy number in the human genome. *Nature* **444,** 444-54.

Reimschussel, R. (2001). A fish model of renal regeneration and development. *Ilar J* **42,** 285-91.

Reiter, J. F., Kikuchi, Y., and Stainier, D. Y. (2001). Multiple roles for Gata5 in zebrafish endoderm formation. *Development* **128,** 125-35.

Richardson, M. K., Allen, S. P., Wright, G. M., Raynaud, A., and Hanken, J. (1998). Somite number and vertebrate evolution. *Development* **125,** 151-60.

Rivera, M. N., and Haber, D. A. (2005). Wilms' tumour: connecting tumorigenesis and organ development in the kidney. *Nat Rev Cancer* **5,** 699-712.

Roberts, D. M., Slep, K. C., and Peifer, M. (2007). It takes more than two to tango: Dishevelled polymerization and Wnt signaling. *Nat Struct Mol Biol* **14,** 463-5.

Ross, J. S., Wilson, K. J. W., and Waugh, A. (1996). "Anatomy and physiology in health and illness." Churchill Livingstone, New York ; London.

Rottman, J. B. (2002). The ribonuclease protection assay: a powerful tool for the veterinary pathologist. *Vet Pathol* **39,** 2-9.

Rubinstein, A. L. (2003). Zebrafish: from disease modeling to drug discovery. *Curr Opin Drug Discov Devel* **6,** 218-23.

Ryffel, G. U., Werdien, D., Turan, G., Gerhards, A., Goosses, S., and Senkel, S. (2003). Tagging muscle cell lineages in development and tail regeneration using Cre recombinase in transgenic Xenopus. *Nucleic Acids Res* **31,** e44.

Sadowski, M., Dichtl, B., Hubner, W., and Keller, W. (2003). Independent functions of yeast Pcf11p in pre-mRNA 3' end processing and in transcription termination. *Embo J* **22,** 2167-77.

Sainio, K., Hellstedt, P., Kreidberg, J. A., Saxen, L., and Sariola, H. (1997). Differential regulation of two sets of mesonephric tubules by WT-1. *Development* **124,** 1293-9.

Sainio, K., and Raatikainen-Ahokas, A. (1999). Mesonephric kidney--a stem cell factory? *Int J Dev Biol* **43,** 435-9.

Sakaguchi, T., Kikuchi, Y., Kuroiwa, A., Takeda, H., and Stainier, D. Y. (2006). The yolk syncytial layer regulates myocardial migration by influencing extracellular matrix assembly in zebrafish. *Development* **133,** 4063-72.

Sakai, T. (1985). The structure of the kidney from the freshwater teleost Carassius auratus. *Anat Embryol (Berl)* **171,** 31-9.

Samulski, R. J., Chang, L. S., and Shenk, T. (1989). Helper-free stocks of recombinant adeno-associated viruses: normal integration does not require viral gene expression. *J Virol* **63,** 3822-8.

Sauer, B. (1987). Functional expression of the cre-lox site-specific recombination system in the yeast Saccharomyces cerevisiae. *Mol Cell Biol* **7,** 2087-96.

Saxen, L., Lehtonen, E., Karkinen-Jaaskelainen, M., Nordling, S., and Wartiovaara, J. (1976). Are morphogenetic tissue interactions mediated by transmissible signal substances or through cell contacts? *Nature* **259,** 662-3.

Saxen, L., and Sariola, H. (1987). Early organogenesis of the kidney. *Pediatr Nephrol* **1,** 385-92.

Schafer, M., Rembold, M., Wittbrodt, J., Schartl, M., and Winkler, C. (2005). Medial floor plate formation in zebrafish consists of two phases and requires trunk-derived Midkine-a. *Genes Dev* **19,** 897-902.

Schefe, J. H., Unger, T., and Funke-Kaiser, H. (2008). PLZF and the (pro)renin receptor. *J Mol Med* **86,** 623-7.

Schier, A. F. (2007). The maternal-zygotic transition: death and birth of RNAs. *Science* **316,** 406-7.

Schier, A. F., Neuhauss, S. C., Helde, K. A., Talbot, W. S., and Driever, W. (1997). The one-eyed pinhead gene functions in mesoderm and endoderm formation in zebrafish and interacts with no tail. *Development* **124,** 327-42.

Schier, A. F., and Shen, M. M. (2000). Nodal signalling in vertebrate development. *Nature* **403,** 385-9.

Schmitt, E. A., and Dowling, J. E. (1994). Early eye morphogenesis in the zebrafish, Brachydanio rerio. *J Comp Neurol* **344,** 532-42.

Schoenwolf, G. C. (2001). Cutting, pasting and painting: experimental embryology and neural development. *Nat Rev Neurosci* **2,** 763-71.

Schulte, I., Schlueter, J., Abu-Issa, R., Brand, T., and Manner, J. (2007). Morphological and molecular left-right asymmetries in the development of the proepicardium: a comparative analysis on mouse and chick embryos. *Dev Dyn* **236,** 684-95.

Schultz, R. M. (1993). Regulation of zygotic gene activation in the mouse. *Bioessays* **15,** 531-8.

Sebat, J., Lakshmi, B., Troge, J., Alexander, J., Young, J., Lundin, P., Maner, S., Massa, H., Walker, M., Chi, M., Navin, N., Lucito, R., Healy, J., Hicks, J., Ye, K., Reiner, A., Gilliam, T. C., Trask, B., Patterson, N., Zetterberg, A., and Wigler, M. (2004). Large-scale copy number polymorphism in the human genome. *Science* **305,** 525-8.

Segawa, H., Miyashita, T., Hirate, Y., Higashijima, S., Chino, N., Uyemura, K., Kikuchi, Y., and Okamoto, H. (2001). Functional repression of Islet-2 by disruption of complex with Ldb impairs peripheral axonal outgrowth in embryonic zebrafish. *Neuron* **30,** 423-36.

Sepich, D. S., Calmelet, C., Kiskowski, M., and Solnica-Krezel, L. (2005). Initiation of convergence and extension movements of lateral mesoderm during zebrafish gastrulation. *Dev Dyn* **234,** 279-92.

Sepich, D. S., Myers, D. C., Short, R., Topczewski, J., Marlow, F., and Solnica-Krezel, L. (2000). Role of the zebrafish trilobite locus in gastrulation movements of convergence and extension. *Genesis* **27,** 159-73.

Serluca, F. C., Drummond, I. A., and Fishman, M. C. (2002). Endothelial signaling in kidney morphogenesis: a role for hemodynamic forces. *Curr Biol* **12,** 492-7.

Serluca, F. C., and Fishman, M. C. (2001). Pre-pattern in the pronephric kidney field of zebrafish. *Development* **128,** 2233-41.

Sharp, A. J., Locke, D. P., McGrath, S. D., Cheng, Z., Bailey, J. A., Vallente, R. U., Pertz, L. M., Clark, R. A., Schwartz, S., Segraves, R., Oseroff, V. V., Albertson, D. G., Pinkel, D., and Eichler, E. E. (2005). Segmental duplications and copy-number variation in the human genome. *Am J Hum Genet* **77,** 78-88.

Shawlot, W., and Behringer, R. R. (1995). Requirement for Lim1 in head-organizer function. *Nature* **374,** 425-30.

Shen, M. M., and Schier, A. F. (2000). The EGF-CFC gene family in vertebrate development. *Trends Genet* **16,** 303-9.

Shinya, M., Furutani-Seiki, M., Kuroiwa, A., and Takeda, H. (1999). Mosaic analysis with oep mutant reveals a repressive interaction between floor-plate and non-floor-plate mutant cells in the zebrafish neural tube. *Dev Growth Differ* **41,** 135-42.

Slavkin, H. C., Croissant, R., and Bringas, P., Jr. (1972). Epithelial-mesenchymal interactions during odontogenesis. 3. A simple method for the isolation of matrix vesicles. *J Cell Biol* **53,** 841-9.

Smith, C., and Mackay, S. (1991). Morphological development and fate of the mouse mesonephros. *J Anat* **174,** 171-84.

Smith, J. C., Price, B. M., Green, J. B., Weigel, D., and Herrmann, B. G. (1991). Expression of a Xenopus homolog of Brachyury (T) is an immediate-early response to mesoderm induction. *Cell* **67,** 79-87.

So, P. L., and Danielian, P. S. (1999). Cloning and expression analysis of a mouse gene related to Drosophila odd-skipped. *Mech Dev* **84,** 157-60.

Solnica-Krezel, L. (2005). Conserved patterns of cell movements during vertebrate gastrulation. *Curr Biol* **15,** R213-28.

Solnica-Krezel, L., and Driever, W. (1994). Microtubule arrays of the zebrafish yolk cell: organization and function during epiboly. *Development* **120,** 2443-55.

Solnica-Krezel, L., Schier, A. F., and Driever, W. (1994). Efficient recovery of ENU-induced mutations from the zebrafish germline. *Genetics* **136,** 1401-20.

Srivastava, A., Lusby, E. W., and Berns, K. I. (1983). Nucleotide sequence and organization of the adeno-associated virus 2 genome. *J Virol* **45,** 555-64.

Stainier, D. Y. (2001). Zebrafish genetics and vertebrate heart formation. *Nat Rev Genet* **2,** 39-48.

Stainier, D. Y. (2002). A glimpse into the molecular entrails of endoderm formation. *Genes Dev* **16,** 893-907.

Stainier, D. Y., Fouquet, B., Chen, J. N., Warren, K. S., Weinstein, B. M., Meiler, S. E., Mohideen, M. A., Neuhauss, S. C., Solnica-Krezel, L., Schier, A. F., Zwartkruis, F., Stemple, D. L., Malicki, J., Driever, W., and Fishman, M. C. (1996). Mutations affecting the formation and function of the cardiovascular system in the zebrafish embryo. *Development* **123,** 285-92.

Sternberg, N., and Hamilton, D. (1981). Bacteriophage P1 site-specific recombination. I. Recombination between loxP sites. *J Mol Biol* **150,** 467-86.

Stickney, H. L., Barresi, M. J., and Devoto, S. H. (2000). Somite development in zebrafish. *Dev Dyn* **219,** 287-303.

Stitzel, M. L., and Seydoux, G. (2007). Regulation of the oocyte-to-zygote transition. *Science* **316,** 407-8.

Tada, M., Concha, M. L., and Heisenberg, C. P. (2002). Non-canonical Wnt signalling and regulation of gastrulation movements. *Semin Cell Dev Biol* **13,** 251-60.

Tada, M., and Smith, J. C. (2000). Xwnt11 is a target of Xenopus Brachyury: regulation of gastrulation movements via Dishevelled, but not through the canonical Wnt pathway. *Development* **127,** 2227-38.

Takada, Y., Ye, X., and Simon, S. (2007). The integrins. *Genome Biol* **8,** 215.

Tantravahi, J., Alvira, M., and Falck-Pedersen, E. (1993). Characterization of the mouse beta maj globin transcription termination region: a spacing sequence is required between the poly(A) signal sequence and multiple downstream termination elements. *Mol Cell Biol* **13,** 578-87.

Tena, J. J., Neto, A., de la Calle-Mustienes, E., Bras-Pereira, C., Casares, F., and Gomez-Skarmeta, J. L. (2007). Odd-skipped genes encode repressors that control kidney development. *Dev Biol* **301,** 518-31.

Thiery, J. P. (2003). Epithelial-mesenchymal transitions in development and pathologies. *Curr Opin Cell Biol* **15,** 740-6.

Thisse, B., Pflumio, S., Fürthauer, M., Loppin, B., Heyer, V., Degrave, A., Woehl, R., Lux, A., Steffan, T., Charbonnier, X. Q., and Thisse, C. (2001). Expression of the zebrafish genome during embryogenesis (NIH R01 RR15402). ZFIN Direct Data Submission (http://zfin.org).

Thisse, B., Wright, C. V., and Thisse, C. (2000). Activin- and Nodal-related factors control antero-posterior patterning of the zebrafish embryo. *Nature* **403,** 425-8.

Tiedemann, K., and Egerer, G. (1984). Vascularization and glomerular ultrastructure in the pig mesonephros. *Cell Tissue Res* **238,** 165-75.

Timmer, J., Johnson, J., and Niswander, L. (2001). The use of in ovo electroporation for the rapid analysis of neural-specific murine enhancers. *Genesis* **29,** 123-32.

Tran, D. P., Kim, S. J., Park, N. J., Jew, T. M., and Martinson, H. G. (2001). Mechanism of poly(A) signal transduction to RNA polymerase II in vitro. *Mol Cell Biol* **21,** 7495-508.

Trinh, L. A., and Stainier, D. Y. (2004). Fibronectin regulates epithelial organization during myocardial migration in zebrafish. *Dev Cell* **6,** 371-82.

Trinkaus, J. P. (1992). The midblastula transition, the YSL transition and the onset of gastrulation in Fundulus. *Dev Suppl***,** 75-80.

Trinkaus, J. P. (1993). The yolk syncytial layer of Fundulus: its origin and history and its significance for early embryogenesis. *J Exp Zool* **265,** 258-84.

Trinkaus, J. P. (1996). Ingression during early gastrulation of fundulus. *Dev Biol* **177,** 356-70.

Tsang, T. E., Shawlot, W., Kinder, S. J., Kobayashi, A., Kwan, K. M., Schughart, K., Kania, A., Jessell, T. M., Behringer, R. R., and Tam, P. P. (2000). Lim1 activity is required for intermediate mesoderm differentiation in the mouse embryo. *Dev Biol* **223,** 77-90.

Tuzun, E., Sharp, A. J., Bailey, J. A., Kaul, R., Morrison, V. A., Pertz, L. M., Haugen, E., Hayden, H., Albertson, D., Pinkel, D., Olson, M. V., and Eichler,

E. E. (2005). Fine-scale structural variation of the human genome. *Nat Genet* **37,** 727-32.

Tzahor, E., Kempf, H., Mootoosamy, R. C., Poon, A. C., Abzhanov, A., Tabin, C. J., Dietrich, S., and Lassar, A. B. (2003). Antagonists of Wnt and BMP signaling promote the formation of vertebrate head muscle. *Genes Dev* **17,** 3087-99.

Vainio, S., Heikkila, M., Kispert, A., Chin, N., and McMahon, A. P. (1999). Female development in mammals is regulated by Wnt-4 signalling. *Nature* **397,** 405-9.

van den Brink, G. R. (2007). Hedgehog signaling in development and homeostasis of the gastrointestinal tract. *Physiol Rev* **87,** 1343-75.

Van Duyne, G. D. (2001). A structural view of cre-loxp site-specific recombination. *Annu Rev Biophys Biomol Struct* **30,** 87-104.

Veeman, M. T., Axelrod, J. D., and Moon, R. T. (2003a). A second canon. Functions and mechanisms of beta-catenin-independent Wnt signaling. *Dev Cell* **5,** 367-77.

Veeman, M. T., Slusarski, D. C., Kaykas, A., Louie, S. H., and Moon, R. T. (2003b). Zebrafish prickle, a modulator of noncanonical Wnt/Fz signaling, regulates gastrulation movements. *Curr Biol* **13,** 680-5.

Vihtelic, T. S., Fadool, J. M., Gao, J., Thornton, K. A., Hyde, D. R., and Wistow, G. (2005). Expressed sequence tag analysis of zebrafish eye tissues for NEIBank. *Mol Vis* **11,** 1083-100.

Vize, P. D., Seufert, D. W., Carroll, T. J., and Wallingford, J. B. (1997). Model systems for the study of kidney development: use of the pronephros in the analysis of organ induction and patterning. *Dev Biol* **188,** 189-204.

Vize, P. D., and Smith, H. W. (2004). A Homeric view of kidney evolution: A reprint of H.W. Smith's classic essay with a new introduction. Evolution of the kidney. 1943. *Anat Rec A Discov Mol Cell Evol Biol* **277,** 344-54.

Vogel, W. F., Abdulhussein, R., and Ford, C. E. (2006). Sensing extracellular matrix: an update on discoidin domain receptor function. *Cell Signal* **18,** 1108-16.

Wagner, K. D., Wagner, N., and Schedl, A. (2003). The complex life of WT1. *J Cell Sci* **116,** 1653-8.

Wallingford, J. B., Rowning, B. A., Vogeli, K. M., Rothbacher, U., Fraser, S. E., and Harland, R. M. (2000). Dishevelled controls cell polarity during Xenopus gastrulation. *Nature* **405,** 81-5.

Walsh, P. S., Metzger, D. A., and Higuchi, R. (1991). Chelex 100 as a medium for simple extraction of DNA for PCR-based typing from forensic material. *Biotechniques* **10,** 506-13.

Warga, R. M., and Kimmel, C. B. (1990). Cell movements during epiboly and gastrulation in zebrafish. *Development* **108,** 569-80.

Warga, R. M., and Stainier, D. Y. (2002). The guts of endoderm formation. *Results Probl Cell Differ* **40,** 28-47.

Wargelius, A., Ellingsen, S., and Fjose, A. (1999). Double-stranded RNA induces specific developmental defects in zebrafish embryos. *Biochem Biophys Res Commun* **263,** 156-61.

Warner, A. E., Guthrie, S. C., and Gilula, N. B. (1984). Antibodies to gap-junctional protein selectively disrupt junctional communication in the early amphibian embryo. *Nature* **311,** 127-31.

Warner, C. M., and Versteegh, L. R. (1974). In vivo and in vitro effect of alpha-amanitin on preimplantation mouse embryo RNA polymerase. *Nature* **248,** 678-80.

Wei, Z., Park, K. W., Day, B. N., and Prather, R. S. (2001). Effect of epidermal growth factor on preimplantation development and its receptor expression in porcine embryos. *Mol Reprod Dev* **60,** 457-62.

Weidinger, G., Wolke, U., Koprunner, M., Thisse, C., Thisse, B., and Raz, E. (2002). Regulation of zebrafish primordial germ cell migration by attraction towards an intermediate target. *Development* **129,** 25-36.

Weinberg, E. S., Allende, M. L., Kelly, C. S., Abdelhamid, A., Murakami, T., Andermann, P., Doerre, O. G., Grunwald, D. J., and Riggleman, B. (1996). Developmental regulation of zebrafish MyoD in wild-type, no tail and spadetail embryos. *Development* **122,** 271-80.

Weiss, E. A., Gilmartin, G. M., and Nevins, J. R. (1991). Poly(A) site efficiency reflects the stability of complex formation involving the downstream element. *Embo J* **10,** 215-9.

Westerfield, M. (1995). "The Zebrafish Book." University of Oregon Press, Eugene, Oregon.

Wilson, E. T., Cretekos, C. J., and Helde, K. A. (1995). Cell mixing during early epiboly in the zebrafish embryo. *Dev Genet* **17,** 6-15.

Wingert, R. A., and Davidson, A. J. (2008). The zebrafish pronephros: a model to study nephron segmentation. *Kidney Int* **73,** 1120-7.

Wingert, R. A., Selleck, R., Yu, J., Song, H. D., Chen, Z., Song, A., Zhou, Y., Thisse, B., Thisse, C., McMahon, A. P., and Davidson, A. J. (2007). The cdx genes and retinoic acid control the positioning and segmentation of the zebrafish pronephros. *PLoS Genet* **3,** 1922-38.

Wittbrodt, J., Shima, A., and Schartl, M. (2002). Medaka--a model organism from the far East. *Nat Rev Genet* **3,** 53-64.

Woo, K., and Fraser, S. E. (1997). Specification of the zebrafish nervous system by nonaxial signals. *Science* **277,** 254-7.

Woods, I. G., and Schier, A. F. (2008). Targeted mutagenesis in zebrafish. *Nat Biotechnol* **26,** 650-1.

Wright, D. A., Thibodeau-Beganny, S., Sander, J. D., Winfrey, R. J., Hirsh, A. S., Eichtinger, M., Fu, F., Porteus, M. H., Dobbs, D., Voytas, D. F., and Joung, J. K. (2006). Standardized reagents and protocols for engineering zinc finger nucleases by modular assembly. *Nat Protoc* **1,** 1637-52.

Xiong, J. W., Yu, Q., Zhang, J., and Mably, J. D. (2008). An acyltransferase controls the generation of hematopoietic and endothelial lineages in zebrafish. *Circ Res* **102,** 1057-64.

Yakeishi, A., Saga, T., So, H., Tetsuka, M., Araki, Y., Kobayashi, S., and Yamaki, K. (2007). A case of horseshoe kidney with surplus renal arteries. *Kurume Med J* **54,** 89-93.

Yamagata, K., Yamazaki, T., Yamashita, M., Hara, Y., Ogonuki, N., and Ogura, A. (2005). Noninvasive visualization of molecular events in the mammalian zygote. *Genesis* **43,** 71-9.

Yamamoto, A., Amacher, S. L., Kim, S. H., Geissert, D., Kimmel, C. B., and De Robertis, E. M. (1998). Zebrafish paraxial protocadherin is a downstream target of spadetail involved in morphogenesis of gastrula mesoderm. *Development* **125,** 3389-97.

Yamashita, S., Miyagi, C., Carmany-Rampey, A., Shimizu, T., Fujii, R., Schier, A. F., and Hirano, T. (2002). Stat3 Controls Cell Movements during Zebrafish Gastrulation. *Dev Cell* **2,** 363-75.

Yazaki, I., Dale, B., and Tosti, E. (1999). Functional gap junctions in the early sea urchin embryo are localized to the vegetal pole. *Dev Biol* **212,** 503-10.

Yelick, P. C., Abduljabbar, T. S., and Stashenko, P. (1998). zALK-8, a novel type I serine/threonine kinase receptor, is expressed throughout early zebrafish development. *Dev Dyn* **211,** 352-61.

Yelon, D., Ticho, B., Halpern, M. E., Ruvinsky, I., Ho, R. K., Silver, L. M., and Stainier, D. Y. (2000). The bHLH transcription factor hand2 plays parallel roles in zebrafish heart and pectoral fin development. *Development* **127,** 2573-82.

Yeo, C., and Whitman, M. (2001). Nodal signals to Smads through Cripto-dependent and Cripto-independent mechanisms. *Mol Cell* **7,** 949-57.

Yonaha, M., and Proudfoot, N. J. (2000). Transcriptional termination and coupled polyadenylation in vitro. *Embo J* **19,** 3770-7.

Yoshinaga, K., Kodama, K., Tanii, I., and Toshimori, K. (2002). Morphological study of a horseshoe kidney with special reference to the vascular system. *Anat Sci Int* **77,** 134-9.

Yu, J., McMahon, A. P., and Valerius, M. T. (2004). Recent genetic studies of mouse kidney development. *Curr Opin Genet Dev* **14,** 550-7.

Zagris, N. (2001). Extracellular matrix in development of the early embryo. *Micron* **32,** 427-38.

Zagris, N., Kalantzis, K., and Guialis, A. (1998). Activation of embryonic genome in chick. *Zygote* **6,** 227-31.

Zhang, J., Talbot, W. S., and Schier, A. F. (1998). Positional cloning identifies zebrafish one-eyed pinhead as a permissive EGF-related ligand required during gastrulation. *Cell* **92,** 241-51.

Zhang, Y. W., Zhang, Z. X., Miao, Z. H., and Ding, J. (2008). The telomeric protein TRF2 is critical for the protection of A549 cells from both telomere erosion and DNA double-strand breaks driven by salvicine. *Mol Pharmacol* **73,** 824-32.

Zhang, Z., Fu, J., and Gilmour, D. S. (2005). CTD-dependent dismantling of the RNA polymerase II elongation complex by the pre-mRNA 3'-end processing factor, Pcf11. *Genes Dev* **19,** 1572-80.